LOW COORDINATE LATE TRANSITION METAL PLATFORMS FOR CO_2 AND CO COMPLEXES

A Dissertation
Presented to
The Academic Faculty

by

Kevin Omondi Omolo

In Partial Fulfillment
of the Requirements for the Degree
Doctor of Philosophy in the
School of Chemistry and Biochemistry

Georgia Institute of Technology
May 2019

LOW COORDINATE LATE TRANSITION METAL PLATFORMS

FOR CO_2 AND CO COMPLEXES

Approved by:

Dr. Joseph P. Sadighi, Advisor
School of Chemistry and Biochemistry
Georgia Institute of Technology

Dr. Angus P. Wilkinson
School of Chemistry and Biochemistry
School of Materials Science and Engineering
Georgia Institute of Technology

Dr. Jake D. Soper
School of Chemistry and Biochemistry
Georgia Institute of Technology

Dr. Carsten Sievers
School of Chemical and Biomolecular Engineering
Georgia Institute of Technology

Dr. Stefan France
School of Chemistry and Biochemistry
Georgia Institute of Technology

Date Approved: January 29th, 2019

To my late mom, grandma and grandpa
You all might no longer be with us, but your words, deeds and sacrifices live on. Mom and grandma, the Swahili say goes, ‘Udongo uwahi ungali maji’ and I can only say thank you. I am, because you did.

ACKNOWLEDGEMENTS

This story, my story, would not be possible without the many players who participated in it and helped shape it. And to them all, whether mentioned in here or otherwise, I'm deeply grateful.

In a small village in Kenya, far deep down near Lake Victoria, was born a little boy to a selfless young lady, Caroline Achieng', my mother. My mother, together with my grandma, Joyce Ogola, were my first teachers. And it is under their care and guidance that my first lessons in Chemistry took place. Be it extraction of natural products from plants origin in form of herbal medicines or fermentation of flour for special occasions, they taught it all, and did it fervently. It is them who moulded me into whom I am today. I am equally grateful to my grandpa for not only using his words as powerful tools to validate my dreams, but also taking it upon himself to go with me shopping for the required items for high school admission despite the many other options that were available. The aforementioned all believed in me, and so I did. May they all rest in peace!

To this end I have interacted with many mentors and teachers, with the most recent ones being here at Georgia Tech. I want to thank my research advisor, Professor Joseph Sadighi, without whose support this story would have not come to a conclusion. I'm thankful to him for giving me the opportunity to work in his lab and taking it upon himself to train me in the handling of pyrophoric substances in the initial stages of my career in the lab. I want to thank him for his commitment to students' success and always finding time even when he travels out of the country to check in via e-mail or Skype. Joseph is a very present parent, and this made him very accessible and supportive. I also want to thank him

for his sense of humor like those occasional funny imitations of clips from Monty Python and many others. I thank him and his family for organizing and inviting us to Thanksgiving parties at their house. And the list is endless. It has been a wonderful opportunity to work with him.

I thank my thesis committee members Professor Angus Wilkinson, Professor Jake Soper, Professor Stefan France and Professor Carsten Sievers for their mentorship over the years and their support through this process.

Also, while at Georgia Tech, I have been lucky to interact with some of the most amazing people including professors whose classes I took like Dr. Joseph Sadighi, Dr. Christoph Farhni, Dr. Angus Wilkinson, Dr. Facundo Fernandez, Dr. Jake Soper, Dr. John Zhang, Dr. David Collard and Dr. Leslie Gelbaum and many others. Despite being a big institution, they all made Georgia Tech seem like a small college by how accessible to students they were. I thank them for their willingness to work with students and their level of engagement despite their busy schedules. They all made the transition quite easy for someone coming from a small college like myself.

To all the academic professionals, the support staff and the people who work closely with them all, may they all keep up the great work. I thank them for being a great resource for information to graduate students. For being there to answer the many questions that come along this journey of graduate school. I want to thank Dr. Carrie Shepler and Dr. Kimberly Schurmeier for introducing me into teaching and providing me with the resources I needed to be a successful TA through the CETL course that they manage. I want to thank Dr. Robert Braga and Dr. Amanda Stephens for giving me the opportunity through the

Chemistry and Biochemistry department to serve Georgia Tech students through teaching, and for always reappointing me to CHEM2380 section for the whole period I have been here at Georgia Tech. Teaching with both of them not only gave me an opportunity to develop my communication and management skills, but also enabled me to form networks with a number of students, some of whom might most likely be my colleagues out there in the workplace. I also want to thank Dr. Wes Wynens and Dr. Jeff Davis of Grand Challenges for not only giving me a platform to develop my leadership and group management skills, but also to help students shape their engagement in innovative projects from inception to implementation.

I want to thank Dr. Leslie Gelbaum for the NMR training and responding to my concerns whenever they arose. I thank him for the lively chats we always had and for him always making sure that the NMR machines are in great working conditions. I also thank Dr. Johannes Leisen for the NMR support as well. I thank Mr. David Bostwick and his support team for the timely delivery of mass spectrometry data, especially the ones where the expected ions were observed. I thank Dr. John Bacsa for collecting and analysing the X-ray diffraction data.

I would like to thank my group members, past and present including Brandon Tate, Chelsea Brodley, Nicholas Daugherty, Chris Sato, Yu Cao, and Abraham Jordan. I would like to especially thank Brandon for his patience and willingness to answer my questions when I first joined the lab, and teaching me the many techniques and skills that became handy in helping me get around the lab. I thank Chris Sato for putting together a number of SOPs, putting together a list of chemicals in the vials in the gloveboxes, and for trying to bring some orderliness to how things are done around the lab. I thank Nicholas

Daugherty for the many lively choral sessions we had even though we did not make it to the 'voice' competitions. I thank him for the informative conversations we had on matters religion, politics, family, career and science, all these made the days go by faster. I thank Abe Jordan for his contributions to the group meeting discussions, and helping uphold safety around the lab. I thank Yu Cao (Jady), whom I met on the first day of classes, and from there on our friendship in and out of lab just kept growing. I thank her for being a fun person to work with. Many a times things looked bleak, and frustrations and tears seemed bound to win, but we still managed to celebrate occasions like birthdays. I really appreciate her thoughtfulness. I thank all the undergraduate students who have worked in the lab with us. I would like to especially thank Alyssa DeLucia who joined our lab through Research Experiences for Undergraduates (REU) program in summer 2017 and worked with me on the 'Synthesis and Reactivity Studies of Anionic PNP Complexes.' I thank her for the hard work she put in this project. I would also like to thank Eric Chase Morey for all the work he put in the project, 'Nickel Complexes of Cy-xantphos, Characterization and Application in CO_2 Fixation.'

I thank members of Dr. Soper's lab Chris and Jenn, whose accommodations and willingness to let me use their instruments helped bring this story to completion. I especially want to say thank you to Jenn for helping me acquire the cyclic voltammetry data, and on occasions letting me use their infrared spectrometer. I also thank members of Dr. La Pierre's lab for allowing me to use the infrared spectrometer they have in the glovebox. I want to especially pass my sincere gratitude to Brandon Yik for his willingness to help me acquire the infrared data even on weekends and holidays. I thank John Tillotson

for finding time to help me acquire EPR data and going out of his way to help simulate the data. I'm very grateful for his contribution.

A number of friends, past and present, have helped keep my sanity through graduate school, to them all I am very grateful. From the ones I met on visitation day like Sabiha Runa, Moustafa Ali and others made within the first few days of school like Wei-Ya Chen, Smitha Janardan and Melony Ochieng. The short getaway trips that we took, the friends-giving parties we held, the birthday parties we hosted for each other, the candidacy exam practice talks of each other that we attended and the study groups we formed are part of the most important contributions to this journey that I believe we will forever live to remember. And while other friends might be actors/actresses in this story, others make the story, and when the story is told, they are well-woven in it. I'm grateful to Melony Ochieng for being there to celebrate my wins and to cry over my losses. I thank her for the friendship and for being part of the story. I am forever indebted.

And to get to where I am today, there were many other shoulders I leaned/stood on along the way. Starting with those who taught me as a child, hats off to them. I thank them for teaching me the art of time management, by ensuring that they were up early for those dawn preps, so that I had no excuse but to be on time as well. I thank them for showing quite a passion for the courses they taught and invoking in me the excitement for subjects like Mathematics, English and Science & Agriculture. Because of the hard-work they all put in, I was able to identify an area of study that interested me. When the opportunity to apply my love for Mathematics in the topics of 'Mole concepts' and 'Acids, bases, and salts' arose in High School, I was sold. I must say thank you to my High School teacher Rosemary Abuodha for showing a lot of zeal when teaching the Chemistry class and always

making sure that we understood the concepts well. She helped me realize what areas of science I could get involved in to contribute positively to the societal development. I want to thank my undergraduate professors Dr. Thomas Goodwin, Ambassador Alan Eastham, Dr. David Hales and many others for their mentorship.

I want to especially thank my undergraduate research advisor Dr. Liz Gron, who gave me the first opportunity to have a hands-on experience with independent research. I thank her for teaching me the art of science communication and presentation even to helping me put together a poster presentation for ACS Conference as well as helping me choose my first suit for the occasion. I thank her for the pieces of advice she offered me on graduate school, and the work she put in to support me during the application process, and remaining a caring mentor even after I moved on to graduate school by occasionally checking in on me.

Last but not least, I would like to thank everyone in my family, my uncle, aunts, cousins and all the others not listed here. I want to especially thank my uncle John R. Omolo and his family. I thank him for all the financial support over the years that ensured my ambitions were not just pipe dreams but actually came to fruition. I thank them for the support and sacrifices they have made throughout the years. May every one of them continue to be blessed with good health and the desires of their heart.

Finally, the story has been written, and I am the main player in the script. Up to this point, with the guidance of Almighty God, I have played the many roles in it. There are many more roles to come, and I trust in Him. His providence, love and guidance make me

who I am. My breath, heart and intellect I put in His hands. The next Season begins, and as I write this next part, I say thank you to my creator, for His benevolent love.

Table of Contents

LIST OF TABLES

LIST OF FIGURES

LIST OF SCHEMES

LIST OF SYMBOLS AND ABBREVIATIONS

Å	Ångstrom
atm	atmosphere
ATR	attenuated total reflectance
BF_4	tetrafluoroborate
Bn	benzyl
br	broad
Bu	butyl
t-Bu	*tert*-butyl
C	Celsius
^{o}C	degree(s) Celsius
^{13}C NMR	carbon-13 nuclear magnetic resonance
calcd	calculated
cat.	catalyst
cm	centimeter
ca.	circa (just about)
CCSD	Cambridge Crystallographic Structural Database
COD	1,5-cyclooctadiene
^{o}	degree
δ	delta, chemical shift (relative to tetramethylsilane)
d	day (unit of time)
	doublet (spectra, denoting multiplicity)
d	deuterated

D	deuterium
DCM	dichloromethane
dd	doublet of doublets (spectra)
dt	doublet of triplets (spectra)
DI	deionized
DG	directed metalation group
η	eta
e.g.	*exempli gratia* (for example)
EI	electron ionization
Et	ethyl
et al.	and others
etc.	*et cetera* (and so forth)
Et_2O	diethyl ether
EtOAc	ethyl acetate
EtOH	ethanol
GC	gas chromatography
g	gram
GC-MS	gas chromatography-mass spectrometry
equiv.	equivalent
h	hour
^{1}H NMR	proton nuclear magnetic resonance
HOMO	highest occupied molecular orbital
Hz	Hertz
IR	infrared
K	Kelvin

L	ligand
	liter
LUMO	lowest unoccupied molecular orbital
µ	mu, micro (10^{-6})
µM	micrometer
m	meter
	milli (10^{-3})
	multiplet (spectra)
M	mega
	metal
	molar, or moles per liter
MLC	metal-ligand cooperation
$[M^+]$	molecular ion
m/z	mass-to-charge ratio
Me	methyl
mg	milligram
MHz	megahertz
min	minute
mL	milliliter
mm	millimeter
mmol	millimole
MO	molecular orbital
mol	mole
mol%	mole percent
MS	mass spectrometry

nm	nanometer
NMR	nuclear magnetic resonance
n.r.	no reaction
OAc	acetate
OTf	triflate, trifluoromethanesulfonate
%	percent
π	pi
P	pressure
PCET	proton-coupled electron transfer
^{31}P NMR	phosphorus-31 nuclear magnetic resonance
PF_6	hexafluorophosphate
Ph	phenyl
ppm	parts per million
i-Pr	isopropyl
psi	pounds per square inch
q	quartet (spectra)
r.t.	room temperature
σ	sigma
s	second
	singlet (spectra)
	strong (spectra)
sept	septet (spectra)
sext	sextet (spectra)
Θ	theta, diffraction angle
t	triplet (spectra)

t	tertiary (as in *t*-Bu; and *tert*-butyl)
	time
T	temperature (in degrees Celsius)
T	temperature (in Kelvin)
tdd	triplet of doublets of doublets (spectra)
temp	temperature
tert	tertiary (as in *tert*-butyl; and *t*-Bu)
THF	tetrahydrofuran
TMEDA	*N*,*N*,*N*′,*N*′-tetramethylenediamine
tt	triplet of triplets (spectra)
UV-Vis	Ultraviolet-Visible spectroscopy
λ	wavelength
υ	wavenumber
w	weak (spectra)
w/w	weight per weight
wt	weight
wt%	weight percent
XRD	X-ray diffraction

SUMMARY

Ligands exert a subtle control on the structure and reactivity of transition metal complexes in a way that is not only catalytically relevant but also an important aspect in the coordination chemistry. The ability to design and modify different ligand frameworks has been an important component of synthetic chemistry. This ability has enabled reactivity of complexes to be tuned via steric and electronic modification of the ligands frameworks. In turn, ligands that perform different functions during the catalytic processes have been developed ranging from those that act as place-holders to those that are actively involved. Presented in this thesis is an elaboration of the acridine framework and its application in the study of CO and CO_2 coordination complexes. Starting from acridone, a variety of acridine-based ligands are synthesized, modified to suit different reaction conditions, their respective complexes synthesized and characterized, and their ability to function as an electron reservoir investigated. For comparison, the reactivity of complexes of a wide bite angle ligand, Cy-xantphos, with CO and CO_2 are also presented herein.

Chapter 1 contains a brief description of cooperative catalysis in the activation of small molecules. A discussion on the importance of the metal ligand cooperation in achieving bond-breaking/forming reactions mimicking nature is presented. More focus is placed on the ligand frameworks that store electrons in their π-systems to support reactivity at the metal centers especially for CO_2 activation and reduction. These ligands cooperate with metals in a synergistic manner, and their interplay facilitates chemical processes. A majority of the redox-active ligands used in CO_2 activation contain nitrogen donors in a conjugated π system. A structure-property analysis shows that reactive low-nuclearity

metal complexes are required for activation of small molecules. Due to the stability of these small molecules, they require robust and reactive complexes for their activation. A number of the CO_2 reduction catalysts tend to be pincer-type in nature to provide the robustness that these complexes require. Put together, these observations inform the directions of ligand synthesis strategies, complexes formation and reactivity studies contained in this thesis.

Chapter 2 describes synthesis of substituted acridones from bis(4-*tert*-butylphenyl)amine via directed metalation using in-situ-formed carbamate as a removable directing group, followed by closing of the central six-membered ring using phenyl chloroformate. The substituted acridone can be easily converted to a dibromoacridone, a versatile substrate for a number of reactions. Substitution of the bromides using transition-metal-catalyzed cross-coupling reactions or halogen-metal exchange leads to formation of different ligand frameworks with varying degrees of steric hindrance around the nitrogen donor atom. The reaction of the different acridone ligand frameworks with transition metal precursors to form corresponding complexes did not lead to isolable products. However, the dibromoacridone and some of the *ortho*-functionalized acridones were converted to the corresponding acridines under moderate reaction conditions.

Chapter 3 describes the use of dibromoacridine in synthesis of a rigid terdentate PNP-chloroacridine. The chloro substituent at the 9-position of this ligand makes it vulnerable in low-valent metal complexes due to the possibility of side reactions like oxidative addition. However, the reactivity of this position toward nucleophilic aromatic substitution allows its replacement with nucleophiles such as alkoxy and aryloxy groups to give (MeO)PNP-acridine and (ArO)PNP-acridine respectively. This ligand framework

accepts an electron during reduction to form a radical anionic ligand. The cyclic voltammetry study of the free (ArO)PNP-acridine shows a reversible reduction wave, confirming the redox-activity of the free ligand. The ligands form nickel(II) and cobalt(II) complexes that, after reduction, react with CO_2 and CO to form the respective coordination complexes. Transition metals supported by this ligand framework can therefore participate in redox processes in a chemical reaction while avoiding uncommon oxidation states due to the ligand's ability to function as an electron reservoir.

In pursuit of a catalytic system that transforms CO_2 as a C_1 building unit in C-C bond formation, Chapter 4 describes the synthesis and application of (Cy-xantphos)Ni complexes in CO_2 activation. The reaction of (Cy-xantphos)Ni(0) with CO_2 forms (Cy-xantphos)Ni(CO_2) complex. Comparison of data obtained for this complex with other bidentate nickel-CO_2 complexes shows a possible η^2-binding mode. Further reduction of (Cy-xantphos)Ni(CO_2) in the presence of different Lewis acids, followed by exposure to CO or CO_2, produces a product similar to the independently synthesized (Cy-xantphos)Ni$(CO)_2$ complex.

CHAPTER 1. INTRODUCTION

1.1 Cooperative catalysis in small molecule activation

Activation and conversion of small molecules (N_2, H_2, CO_2, O_2, H_2O etc.) into useful products is an energy-intensive process and requires multi-electron/proton systems.[1] For example, the transition metal-catalyzed water oxidation into dioxygen and hydrogen, which in nature takes place at the oxygen-evolving complex of the photosystem II (PSII), occurs through proton-coupled electron transfer (PCET)[1-2] involving a total of four electrons and protons.[3-12] Nitrogen reduction to two equivalents of ammonia requires a series of six electrons and six protons.[13-14] Similar numbers of protons and electrons are required for CO_2 reduction to methanol.[15] Development of transition metals catalysts to activate these molecules is motivated by observations of how nature carries out some of these reactions.

Reduction of nitrogen to ammonia in nature is catalyzed by nitrogenase which consists of two component metalloproteins, the Fe-protein and the MoFe-protein.[16] These two components work in concert to achieve N_2 reduction with the MoFe-protein acting as the active binding site while the Fe-protein being the redox-active agent that supplies electrons to the active site.[17] Another example is the activation of H_2 by [FeFe] or [NiFe] hydrogenases where H_2 is heterolytically split across the metal-ligand bond (Scheme 1.1).[18-22] The reduction of CO_2 to CO occurs at a square planar nickel center[23-25] that contains a [$NiFe_4S_4$] core (Figure 1.1).[23, 25-30] It has been proposed that the Fe plays a crucial

role in elongation of C-O bond, making it easier to cleave the C-O bond to form Ni(II)-CO fragment.[31] These observations plus many others not listed here inspired development of cooperative multi-metallic catalytic approach to bond-breaking and bond-forming processes.[32-34]

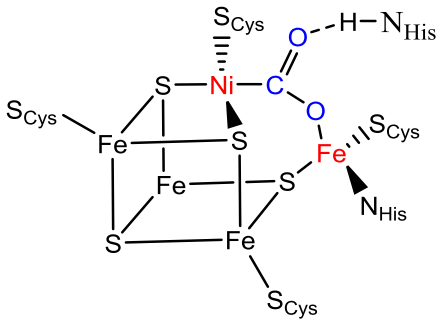

Figure 1.1. Activation of CO_2 at a square planar nickel center in a $[NiFe_4S_4]$ core.

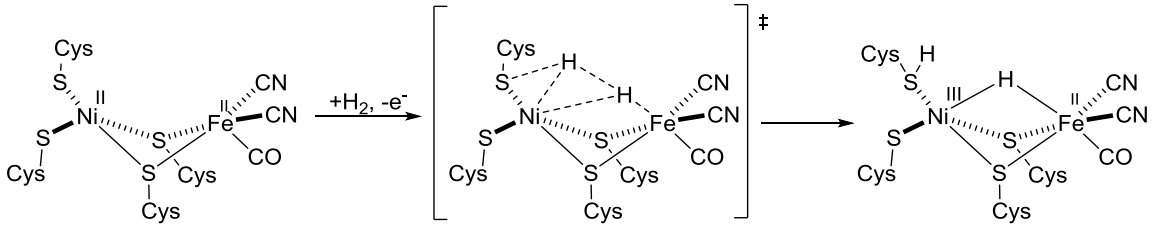

Scheme 1.1. Proposed mechanism of H_2 splitting by [NiFe]-hydrogenase.

An equally important approach is one where the ligands are no longer used as spectators in a reaction, but work in cooperation with transition metals to achieve catalysis. Cooperation between ligand fragments and metals in catalysis is a ubiquitous concept in biological systems. An example is the case of [NiFe]-hydrogenase where an S atom of cysteine helps in the oxidation of H_2 to H^+ as shown in Scheme 1.1 above.[7, 35-38] This cooperation is also represented in redox-active ligands, which can be categorized as either reactive[39] or non-reactive (electron reservoirs) ligands.[40-45] Ability of these ligands to store electrons has successfully facilitated two-electron reactivity of metals that have an intrinsic

tendency to react by one-electron pathways. This has in turn made it possible for these metals to be used in place of noble metals.[40-41, 46-47]

1.2 Activation of CO_2 and effect of ligand framework

In CO_2 reduction, a number of transition metal complexes supported by nitrogen-donor ligands have been used as molecular catalysts.[48-50] Some of the nitrogen-rich donor ligands used include porphyrins,[51-54] polypyridines,[55-58] cyclams, and related unsaturated N_4-macrocycles.[59-64] In the case of complexes bearing polypyridine ligands, evidence suggests that reducing equivalents are stored on the supporting polypyridine ligands during electrocatalytic reduction of CO_2, making these more versatile ligands for molecular catalyst development.[65-68] The electron density is stored at the vicinity of the active site and released only when needed for CO_2 activation.[69-74]

It is suggested that redox non-innocence might have a significant impact on both substrate and product selectivity.[75] Manganese and rhenium tricarbonyl catalysts supported on bipyridyl moieties reduce CO_2 rather than protons in presence of water and/or weak acids.[75-78] An experimental and theoretical study of the complexes made from ligands of pyridine-type or related, with non-innocence behavior suggest that this selectivity originates from the complexes delocalized electronic states.[68]

Previously, a structure-activity relationship study of phosphine-containing palladium pincer electrocatalysts revealed that selectivity for CO_2 reduction was highly sensitive to variations in ligand substituents, donor type (anionic, **1** to neutral, **2**), bite angle (**1**&**2** compared to **3**&**4**) and changes in redox potential of the complexes (Figure 1.2).[33, 79-80] These factors modulate the basicity of the catalytic complexes. For example, for CO_2

activation, at a more reducing potential, high selectivity for CO_2 reduction is achieved resulting into a negative charge on the oxygen atom of the bound CO_2 and a higher basicity than the metal center.[33, 80] CO_2 reduction in the presence of acid using **1** produces only hydrogen.[33] The activity and selectivity of molecular catalysts can be tuned by an informed alteration in their structure.[81-82]

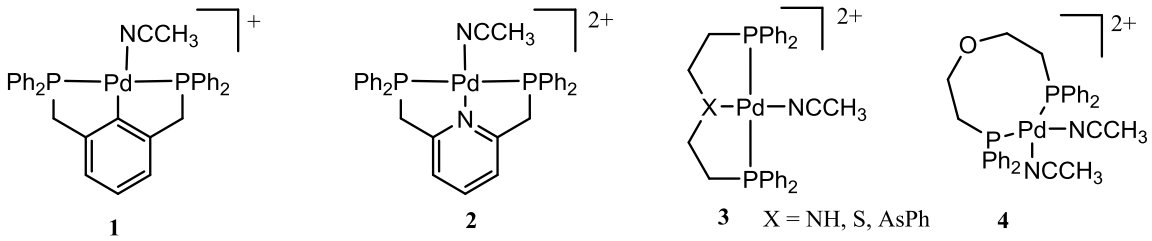

Figure 1.2. Physical alteration in ligand properties.

Due to the high stability of CO_2, its conversion to useful products is chemically challenging, often requiring a series of proton-coupled electron transfer steps to avoid formation of unstable, high energy intermediates.[83-86] The ability of transition metal complexes to coordinate to CO_2 and enable these multi-electron/proton transfer steps put them at the forefront of development of effective activation catalysts.[83] In many cases, low-valent late transition metals are applied in these activation studies since they are very basic and capable of coordinating to a weak ligand like CO_2 through back-bonding.[87]

Since the pioneering work on Ni and Co macrocyclic complexes as potential electrochemical CO_2 reduction catalysts,[59, 88] various metal complexes have been used in this pursuit, many of them based on noble metals.[23, 48-49, 83, 89-93] Coordinatively unsaturated transition metal complexes bearing pincer ligands are a recurring motif.[94-99] However, the cost and toxicity of precious metals continue to drive a search for alternatives within late

first-row transition metals.[46, 100] Molecular catalysts from first-row transition metal complexes based on the terpyridine ligands have showed competition between hydrogen evolution and CO_2 to CO conversion in (90:10, v/v) DMF/H_2O mixtures.[101]

Also, a large number of first-row transition metals engage in single-electron processes.[46-47] Development of ligands that can contribute to the number of electrons available for catalysis either as electron reservoirs or as "redox non-innocent" is quite an appealing approach. When these redox-active ligands are used in conjunction with metals that possess different oxidation states, multi-electron/proton transfer processes are achieved leading to CO_2 reduction to CO or even to methanol.[76-78, 102]

1.3 Low-nuclearity late first-row transition metal complexes and their application in catalysis and coordination chemistry

Small molecule activation often requires large energy inputs and reactive metal centers. The right ligand can both stabilize the metal complexes to give robust catalysts, and tune the geometry and electronic configuration at the metal to achieve the required reactivity. Three-coordinate complexes of transition metals with partially filled d shells have showed unusual reactivity and electronic structure.[103] There are a few examples of three-coordinate d^9 nickel complexes[104-110] in nature. One example is found at the low-coordinate proximal nickel site of the acetyl-coenzyme A synthase (where transformation of methylcobalamin, CO, and coenzyme A into acetyl-coenzyme A takes place).[111-116]A recurring motif in these systems is the presence of geometric constraints and/or rigidity to enforce a T-shaped orientation.

To achieve low nuclearity, a number of nitrogen donor ligands have found widespread applications as either chelating agents or in stabilization of the coordinately unsaturated complexes. Of the different examples of ML_3 complexes reported, a number of them are amido complexes $[M(NR_2)_3]$ with bulky substituents like $SiMe_3$.[117] Others bear mixed ligands like $[M(NR_2)_2L]$ and $[M(NR_2)L_2]$ and most of the structurally characterized complexes are of first row transition metal complexes.[117]

1.4 Concluding Remarks

Despite intensive research in the area of CO_2 activation, there remains work to be done in improving catalyst stability and product selectivity. Where possible, catalysts should also be based on benign, non-toxic and earth-abundant metals instead of the noble ones, for the invention to have practical and economically viable applications. A systematic ligand development based on nitrogen donor atoms, with a rigid ligand backbone, capable of providing vacant substrate binding/activation site while eliminating degradation pathways is of great interest. A tridentate pincer-type ligand that can support a Ni^{2+} in a pseudo square planar geometry with a labile fourth ligand, such as a solvent molecule, would nevertheless allow the ready accessibility of a single equatorial site of the nickel center by a CO_2 molecule for activation.[118]

The following chapters describe the synthesis, modification, characterization, and reactivity studies of (PNP-acridine)-supported nickel and cobalt complexes towards formation of carbonyl complexes and CO_2 activation. This begins with development of a new synthetic procedure that employs CO surrogates for synthesis of acridone as shown in Chapter 2. The acridone is then applied in development of new acridine frameworks in

Chapter 3. A redox-active ligand, PNP-acridine, is used in the synthesis of metal complexes, and modified to arrive at frameworks that are stable in reducing environments. The complexes obtained are characterized and their reactivity tested towards CO_2 activation. Chapter 4 introduces nickel complexes of a wide bite angle Cy-xantphos ligand. These complexes are studied in the formation of carbonyl and CO_2 adducts. The reactivity of the CO_2 complexes is tested in presence of different Lewis acids as well as with hydrogen bond donors.

1.5 REFERENCES

1. Hammes-Schiffer, S., Introduction: Proton-coupled electron transfer. *Chem. Rev.* **2010,** *12*, 6937-6938.

2. Weinberg, D. R.; Gagliardi, C. J.; Hull, J. F.; Murphy, C. F.; Kent, C. A.; Westlake, B. C.; Paul, A.; Ess, D. H.; McCafferty, D. G.; Meyer, T. J., Proton-Coupled Electron Transfer. *Chem. Rev.* **2012,** *112*, 4016-4093.

3. Meyer, T. J.; Huynh, M. H. V., The Remarkable Reactivity of High Oxidation State Ruthenium and Osmium Polypyridyl Complexes. *Inorg. Chem.* **2003,** *42*, 8140-8160.

4. Sala, X.; Romero, I.; Rodríguez, M.; Escriche, L.; Llobet, A., Molecular catalysts that oxidize water to dioxygen. *Angew. Chem. Int. Ed.* **2009,** *48*, 2842-2852.

5. Ferreira, K. N.; Iverson, T. M.; Maghlaoui, K.; Barber, J.; Iwata, S., Architecture of the photosynthetic oxygen-evolving center. *Science* **2004,** *303*, 1831-1838.

6. Rutherford, A.; Boussac, A., Water photolysis in biology. *Science* **2004,** *303*, 1782-1784.

7. Yano, J.; Kern, J.; Sauer, K.; Latimer, M. J.; Pushkar, Y.; Biesiadka, J.; Loll, B.; Saenger, W.; Messinger, J.; Zouni, A., Where water is oxidized to dioxygen: structure of the photosynthetic Mn_4Ca cluster. *Science* **2006,** *314*, 821-825.

8. McEvoy, J. P.; Brudvig, G. W., Water-Splitting Chemistry of Photosystem II. *Chem. Rev.* **2006,** *106*, 4455-4483.

9. Loll, B.; Kern, J.; Saenger, W.; Zouni, A.; Biesiadka, J., Towards complete cofactor arrangement in the 3.0 Å resolution structure of photosystem II. *Nature* **2005,** *438*, 1040.

10. Haumann, M.; Liebisch, P.; Müller, C.; Barra, M.; Grabolle, M.; Dau, H., Photosynthetic O_2 formation tracked by time-resolved X-ray experiments. *Science* **2005,** *310*, 1019-1021.

11. Rosenthal, J.; Nocera, D. G., Role of Proton-Coupled Electron Transfer in O–O Bond Activation. *Acc. Chem. Res.* **2007,** *40*, 543-553.

12. Vigato, P. A.; Tamburini, S.; Fenton, D. E., The activation of small molecules by dinuclear complexes of copper and other metals. *Coord. Chem. Rev.* **1990,** *106*, 25-170.

13. Yandulov, D. V.; Schrock, R. R., Catalytic reduction of dinitrogen to ammonia at a single molybdenum center. *Science* **2003,** *301*, 76-78.

14. Barrière, F., Modeling of the molybdenum center in the nitrogenase FeMo-cofactor. *Coord. Chem. Rev.* **2003,** *236*, 71-89.

15. Rosenthal, J., Progress toward the electrocatalytic production of liquid fuels from carbon dioxide. *Prog. Inorg. Chem.* **2014,** *59*, 299-338.

16. Einsle, O.; Tezcan, F. A.; Andrade, S. L.; Schmid, B.; Yoshida, M.; Howard, J. B.; Rees, D. C., Nitrogenase MoFe-protein at 1.16 Å resolution: a central ligand in the FeMo-cofactor. *Science* **2002,** *297*, 1696-1700.

17. Burgess, B. K.; Lowe, D. J., Mechanism of Molybdenum Nitrogenase. *Chem. Rev.* **1996,** *96*, 2983-3012.

18. Adams, M. W.; Stiefel, E. I., Biological hydrogen production: not so elementary. *Science* **1998,** *282*, 1842-1843.

19. Montet, Y.; Garcin, E.; Volbeda, A.; Hatchikian, C.; Frey, M.; Fontecilla-Camps, J., Structural bases for the catalytic mechanism of NiFe hydrogenase. *Pure. App. Chem.* **1998,** *70*, 25-31.

20. Niu, S.; Hall, M. B., Modeling the active sites in metalloenzymes 5. The heterolytic bond cleavage of H_2 in the [NiFe] hydrogenase of Desulfovibrio gigas by a nucleophilic addition mechanism. *Inorg. chem.* **2001,** *40*, 6201-6203.

21. Hambourger, M.; Gervaldo, M.; Svedruzic, D.; King, P. W.; Gust, D.; Ghirardi, M.; Moore, A. L.; Moore, T. A., [FeFe]-hydrogenase-catalyzed H_2 production in a photoelectrochemical biofuel cell. *J. Am. Chem. Soc.* **2008,** *130*, 2015-2022.

22. Vincent, K. A.; Parkin, A.; Lenz, O.; Albracht, S. P.; Fontecilla-Camps, J. C.; Cammack, R.; Friedrich, B.; Armstrong, F. A., Electrochemical definitions of O_2 sensitivity and oxidative inactivation in hydrogenases. *J. Am. Chem. Soc.* **2005,** *127*, 18179-18189.

23. Appel, A. M.; Bercaw, J. E.; Bocarsly, A. B.; Dobbek, H.; DuBois, D. L.; Dupuis, M.; Ferry, J. G.; Fujita, E.; Hille, R.; Kenis, P. J., Frontiers, opportunities, and challenges in biochemical and chemical catalysis of CO_2 fixation. *Chem. Rev.* **2013,** *113*, 6621-6658.

24. Mondal, B.; Song, J.; Neese, F.; Ye, S., Bio-inspired mechanistic insights into CO_2 reduction. *Curr. Opin. Chem. Bio.* **2015,** *25*, 103-109.

25. Can, M.; Armstrong, F. A.; Ragsdale, S. W., Structure, function, and mechanism of the nickel metalloenzymes, CO dehydrogenase, and acetyl-CoA synthase. *Chem. Rev.* **2014,** *114*, 4149-4174.

26. Doukov, T. I.; Iverson, T. M.; Seravalli, J.; Ragsdale, S. W.; Drennan, C. L., A Ni-Fe-Cu center in a bifunctional carbon monoxide dehydrogenase/acetyl-CoA synthase. *Science* **2002,** *298*, 567-572.

27. Darnault, C.; Volbeda, A.; Kim, E. J.; Legrand, P.; Vernède, X.; Lindahl, P. A.; Fontecilla-Camps, J. C., Ni-Zn-[Fe_4-S_4] and Ni-Ni-[Fe_4-S_4] clusters in closed and open α subunits of acetyl-CoA synthase/carbon monoxide dehydrogenase. *Nat. Struc. Mol. Bio.* **2003,** *10*, 271.

28. Jeoung, J.-H.; Dobbek, H., Carbon dioxide activation at the Ni, Fe-cluster of anaerobic carbon monoxide dehydrogenase. *Science* **2007,** *318*, 1461-1464.

29. Gong, W.; Hao, B.; Wei, Z.; Ferguson, D. J.; Tallant, T.; Krzycki, J. A.; Chan, M. K., Structure of the $\alpha_2\varepsilon_2$ Ni-dependent CO dehydrogenase component of the Methanosarcina barkeri acetyl-CoA decarbonylase/synthase complex. *Proc. Nat. Acad. Sci.* **2008,** *105*, 9558-9563.

30. Fesseler, J.; Jeoung, J. H.; Dobbek, H., How the [$NiFe_4S_4$] cluster of CO dehydrogenase activates CO_2 and NCO^-. *Ang. Chem. Int. Ed.* **2015,** *54*, 8560-8564.

31. Schneck, F.; Ahrens, J.; Finger, M.; Stückl, A. C.; Würtele, C.; Schwarzer, D.; Schneider, S., The elusive abnormal CO_2 insertion enabled by metal-ligand cooperative photochemical selectivity inversion. *Nature Comm.* **2018,** *9*, 1161.

32. Mankad, N. P., Selectivity effects in bimetallic catalysis. *Chem. Eur. J.* **2016,** *22*, 5822-5829.

33. Dubois, D. L., Development of transition metal phosphine complexes as electrocatalysts for CO_2 and CO reduction. *Comments Inorg. Chem.* **1997,** *19*, 307-325.

34. Raebiger, J. W.; Turner, J. W.; Noll, B. C.; Curtis, C. J.; Miedaner, A.; Cox, B.; DuBois, D. L., Electrochemical Reduction of CO_2 to CO Catalyzed by a Bimetallic Palladium Complex. *Organometallics* **2006,** *25*, 3345-3351.

35. Kaim, W.; Schwederski, B., Non-innocent ligands in bioinorganic chemistry—An overview. *Coord. Chem. Rev.* **2010,** *254*, 1580-1588.

36. Palomo, C.; Oiarbide, M.; García, J. M., Current progress in the asymmetric aldol addition reaction. *Chem. Soc. Rev.* **2004,** *33*, 65-75.

37. Parkin, G., Synthetic Analogues Relevant to the Structure and Function of Zinc Enzymes. *Chem. Rev.* **2004,** *104*, 699-768.

38. Weston, J., Mode of Action of Bi- and Trinuclear Zinc Hydrolases and Their Synthetic Analogues. *Chem. Rev.* **2005,** *105*, 2151-2174.

39. Dzik, W. I.; Xu, X.; Zhang, X. P.; Reek, J. N. H.; de Bruin, B., 'Carbene Radicals' in Co^{II}(por)-Catalyzed Olefin Cyclopropanation. *J. Am. Chem. Soc.* **2010,** *132*, 10891-10902.

40. Bouwkamp, M. W.; Bowman, A. C.; Lobkovsky, E.; Chirik, P. J., Iron-Catalyzed [2π + 2π] Cycloaddition of α,ω-Dienes: The Importance of Redox-Active Supporting Ligands. *J. Am. Chem. Soc.* **2006,** *128*, 13340-13341.

41. Sylvester, K. T.; Chirik, P. J., Iron-Catalyzed, Hydrogen-Mediated Reductive Cyclization of 1,6-Enynes and Diynes: Evidence for Bis(imino)pyridine Ligand Participation. *J. Am. Chem. Soc.* **2009,** *131*, 8772-8774.

42. Haneline, M. R.; Heyduk, A. F., C−C Bond-Forming Reductive Elimination from a Zirconium(IV) Redox-Active Ligand Complex. *J. Am. Chem. Soc.* **2006,** *128*, 8410-8411.

43. Blackmore, K. J.; Ziller, J. W.; Heyduk, A. F., "Oxidative Addition" to a Zirconium(IV) Redox-Active Ligand Complex. *Inorg. Chem.* **2005,** *44*, 5559-5561.

44. Stanciu, C.; Jones, M. E.; Fanwick, P. E.; Abu-Omar, M. M., Multi-electron Activation of Dioxygen on Zirconium(IV) to Give an Unprecedented Bisperoxo Complex. *J. Am. Chem. Soc.* **2007,** *129*, 12400-12401.

45. Ketterer, N. A.; Fan, H.; Blackmore, K. J.; Yang, X.; Ziller, J. W.; Baik, M.-H.; Heyduk, A. F., π•−π• Bonding Interactions Generated by Halogen Oxidation of Zirconium(IV) Redox-Active Ligand Complexes. *J. Am. Chem. Soc.* **2008,** *130*, 4364-4374.

46. Chirik, P. J.; Wieghardt, K., Radical ligands confer nobility on base-metal catalysts. *Science* **2010,** *327*, 794-795.

47. Hu, X., Nickel-catalyzed cross coupling of non-activated alkyl halides: a mechanistic perspective. *Chem. Sci.* **2011,** *2*, 1867-1886.

48. Costentin, C.; Robert, M.; Savéant, J.-M., Catalysis of the electrochemical reduction of carbon dioxide. *Chem. Soc. Rev.* **2013,** *42*, 2423-2436.

49. Benson, E. E.; Kubiak, C. P.; Sathrum, A. J.; Smieja, J. M., Electrocatalytic and homogeneous approaches to conversion of CO_2 to liquid fuels. *Chem. Soc. Rev.* **2009,** *38*, 89-99.

50. Schneider, J.; Jia, H.; Muckerman, J. T.; Fujita, E., Thermodynamics and kinetics of CO_2, CO, and H^+ binding to the metal centre of CO_2 reduction catalysts. *Chem. Soc. Rev.* **2012,** *41*, 2036-2051.

51. Takahashi, K.; Hiratsuka, K.; Sasaki, H.; Toshima, S., Electrocatalytic behavior of metal porphyrins in the reduction of carbon dioxide. *Chem. Lett.* **1979,** *8*, 305-308.

52. Atoguchi, T.; Aramata, A.; Kazusaka, A.; Enyo, M., Cobalt(II)–tetraphenylporphyrin–pyridine complex fixed on a glassy carbon electrode and its prominent catalytic activity for reduction of carbon dioxide. *J. Chem. Soc., Chem. Commun.* **1991**, 156-157.

53. Hammouche, M.; Lexa, D.; Momenteau, M.; Saveant, J. M., Chemical catalysis of electrochemical reactions. Homogeneous catalysis of the electrochemical reduction of carbon dioxide by iron("0") porphyrins. Role of the addition of magnesium cations. *J. Am. Chem. Soc.* **1991,** *113*, 8455-8466.

54. Costentin, C.; Drouet, S.; Robert, M.; Savéant, J.-M., A local proton source enhances CO_2 electroreduction to CO by a molecular Fe catalyst. *Science* **2012,** *338*, 90-94.

55. Hawecker, J.; Lehn, J.-M.; Ziessel, R., Electrocatalytic reduction of carbon dioxide mediated by $Re(bipy)(CO)_3Cl$ (bipy= 2, 2′-bipyridine). *J. Chem. Soc., Chem. Commun.* **1984,** 328-330.

56. Sullivan, B. P.; Bolinger, C. M.; Conrad, D.; Vining, W. J.; Meyer, T. J., One-and two-electron pathways in the electrocatalytic reduction of CO_2 by fac-$Re(bpy)(CO)_3Cl$ (bpy= 2, 2′-bipyridine). *J. Chem. Soc., Chem. Commun.* **1985,** 1414-1416.

57. Chen, Z.; Kang, P.; Zhang, M.-T.; Meyer, T. J., Making syngas electrocatalytically using a polypyridyl ruthenium catalyst. *Chem. Commun.* **2014,** *50*, 335-337.

58. Chen, Z.; Chen, C.; Weinberg, D. R.; Kang, P.; Concepcion, J. J.; Harrison, D. P.; Brookhart, M. S.; Meyer, T. J., Electrocatalytic reduction of CO_2 to CO by polypyridyl ruthenium complexes. *Chem. Commun.* **2011,** *47*, 12607-12609.

59. Fisher, B. J.; Eisenberg, R., Electrocatalytic reduction of carbon dioxide by using macrocycles of nickel and cobalt. *J. Am. Chem. Soc.* **1980,** *102*, 7361-7363.

60. Schneider, J.; Jia, H.; Kobiro, K.; Cabelli, D. E.; Muckerman, J. T.; Fujita, E., Nickel(II) macrocycles: highly efficient electrocatalysts for the selective reduction of CO_2 to CO. *Energy Environ. Sci.* **2012,** *5*, 9502-9510.

61. Thoi, V. S.; Kornienko, N.; Margarit, C. G.; Yang, P.; Chang, C. J., Visible-light photoredox catalysis: selective reduction of carbon dioxide to carbon monoxide by a nickel N-heterocyclic carbene–isoquinoline complex. *J. Am. Chem. Soc.* **2013,** *135*, 14413-14424.

62. Beley, M.; Collin, J.-P.; Ruppert, R.; Sauvage, J.-P., Nickel (II)-cyclam: an extremely selective electrocatalyst for reduction of CO_2 in water. *J. Chem. Soc., Chem. Commun.* **1984,** 1315-1316.

63. Beley, M.; Collin, J. P.; Ruppert, R.; Sauvage, J. P., Electrocatalytic reduction of carbon dioxide by nickel cyclam^{2+} in water: study of the factors affecting the efficiency and the selectivity of the process. *J. Am. Chem. Soc.* **1986,** *108*, 7461-7467.

64. Froehlich, J. D.; Kubiak, C. P., Homogeneous CO_2 reduction by Ni(cyclam) at a glassy carbon electrode. *Inorg. Chem.* **2012,** *51*, 3932-3934.

65. Simpson, T. C.; Durand Jr, R. R., Ligand participation in the reduction of CO_2 catalyzed by complexes of 1, 10 *o*-phenanthroline. *Electrochim. Acta* **1988,** *33*, 581-583.

66. Scheiring, T.; Klein, A.; Kaim, W., EPR study of paramagnetic rhenium(I) complexes (bpy>>•>>─>>) $Re(CO)_3X$ relevant to the mechanism of electrocatalytic CO_2 reduction. *J. Chem. Soc., Perkin Trans. 2* **1997,** 2569-2572.

67. Fujita, E.; Muckerman, J. T., Why Is Re−Re Bond Formation/Cleavage in [Re (bpy)$(CO)_3]_2$ Different from That in $[Re(CO)_5]_2$? Experimental and Theoretical Studies on the Dimers and Fragments. *Inorg. Chem.* **2004,** *43*, 7636-7647.

68. Benson, E. E.; Sampson, M. D.; Grice, K. A.; Smieja, J. M.; Froehlich, J. D.; Friebel, D.; Keith, J. A.; Carter, E. A.; Nilsson, A.; Kubiak, C. P., The Electronic States of Rhenium Bipyridyl Electrocatalysts for CO_2 Reduction as Revealed by X-ray Absorption Spectroscopy and Computational Quantum Chemistry. *Angew. Chem.* **2013,** *125*, 4941-4944.

69. Barton Cole, E.; Lakkaraju, P. S.; Rampulla, D. M.; Morris, A. J.; Abelev, E.; Bocarsly, A. B., Using a one-electron shuttle for the multielectron reduction of CO_2 to methanol: kinetic, mechanistic, and structural insights. *J. Am. Chem. Soc.* **2010,** *132*, 11539-11551.

70. Barton, E. E.; Rampulla, D. M.; Bocarsly, A. B., Selective solar-driven reduction of CO_2 to methanol using a catalyzed p-GaP based photoelectrochemical cell. *J. Am. Chem. Soc.* **2008,** *130*, 6342-6344.

71. Keith, J. A.; Carter, E. A., Theoretical insights into pyridinium-based photoelectrocatalytic reduction of CO_2. *J. Am. Chem. Soc.* **2012,** *134*, 7580-7583.

72. Nie, W.; McCrory, C. C., Electrocatalytic CO_2 reduction by a cobalt bis (pyridylmonoimine) complex: effect of acid concentration on catalyst activity and stability. *Chem. Commun.* **2018,** *54*, 1579-1582.

73. Lacy, D. C.; McCrory, C. C.; Peters, J. C., Studies of cobalt-mediated electrocatalytic CO_2 reduction using a redox-active ligand. *Inorg. Chem.* **2014,** *53*, 4980-4988.

74. Chen, L.; Guo, Z.; Wei, X.-G.; Gallenkamp, C.; Bonin, J.; Anxolabéhère-Mallart, E.; Lau, K.-C.; Lau, T.-C.; Robert, M., Molecular catalysis of the electrochemical and photochemical reduction of CO_2 with Earth-abundant metal complexes. Selective production of CO vs HCOOH by switching of the metal center. *J. Am. Chem. Soc.* **2015,** *137*, 10918-10921.

75. Keith, J. A.; Grice, K. A.; Kubiak, C. P.; Carter, E. A., Elucidation of the selectivity of proton-dependent electrocatalytic CO_2 reduction by fac-Re(bpy)$(CO)_3$Cl. *J. Am. Chem. Soc.* **2013,** *135*, 15823-15829.

76. Bourrez, M.; Molton, F.; Chardon-Noblat, S.; Deronzier, A., [Mn(bipyridyl)$(CO)_3$Br]: An abundant metal carbonyl complex as efficient electrocatalyst for CO_2 reduction. *Angew. Chem. Int. Ed.* **2011,** *50*, 9903-9906.

77. Smieja, J. M.; Kubiak, C. P., Re(bipy-tBu)$(CO)_3Cl^-$ improved catalytic activity for reduction of carbon dioxide: IR-spectroelectrochemical and mechanistic studies. *Inorg. Chem.* **2010,** *49*, 9283-9289.

78. Smieja, J. M.; Sampson, M. D.; Grice, K. A.; Benson, E. E.; Froehlich, J. D.; Kubiak, C. P., Manganese as a substitute for rhenium in CO_2 reduction catalysts: The importance of acids. *Inorg. Chem.* **2013,** *52*, 2484-2491.

79. DuBois, D. L.; Miedaner, A.; Haltiwanger, R. C., Electrochemical reduction of carbon dioxide catalyzed by [Pd(triphosphine)(solvent)]$(BF_4)_2$ complexes: synthetic and mechanistic studies. *J. Am. Chem. Soc.* **1991,** *113*, 8753-8764.

80. Therrien, J. A.; Wolf, M. O.; Patrick, B. O., Polyannulated bis (N-heterocyclic carbene)palladium pincer complexes for electrocatalytic CO_2 reduction. *Inorg. Chem.* **2015,** *54*, 11721-11732.

81. Clark, M. L.; Grice, K. A.; Moore, C. E.; Rheingold, A. L.; Kubiak, C. P., Electrocatalytic CO_2 reduction by M(bpy-R)$(CO)_4$ (M= Mo, W; R= H, t Bu) complexes. Electrochemical, spectroscopic, and computational studies and comparison with group 7 catalysts. *Chem. Sci.* **2014,** *5*, 1894-1900.

82. Machan, C. W.; Chabolla, S. A.; Kubiak, C. P., Reductive Disproportionation of Carbon Dioxide by an Alkyl-Functionalized Pyridine Monoimine Re(I) fac-Tricarbonyl Electrocatalyst. *Organometallics* **2015,** *34*, 4678-4683.

83. Qiao, J.; Liu, Y.; Hong, F.; Zhang, J., A review of catalysts for the electroreduction of carbon dioxide to produce low-carbon fuels. *Chem. Soc. Rev.* **2014,** *43*, 631-675.

84. Heinze, K.; Hempel, K.; Beckmann, M., Multielectron Storage and Photo-Induced Electron Transfer in Oligonuclear Complexes Containing Ruthenium(II) Terpyridine and Ferrocene Building Blocks. *Eur. J. Inorg. Chem.* **2006,** *2006*, 2040-2050.

85. Heyduk, A. F.; Macintosh, A. M.; Nocera, D. G., Four-electron photochemistry of dirhodium fluorophosphine compounds. *J. Am. Chem. Soc.* **1999,** *121*, 5023-5032.

86. Rosenthal, J.; Bachman, J.; Dempsey, J. L.; Esswein, A. J.; Gray, T. G.; Hodgkiss, J. M.; Manke, D. R.; Luckett, T. D.; Pistorio, B. J.; Veige, A. S., Oxygen and hydrogen photocatalysis by two-electron mixed-valence coordination compounds. *Coord. Chem. Rev.* **2005,** *249*, 1316-1326.

87. Cokoja, M.; Bruckmeier, C.; Rieger, B.; Herrmann, W. A.; Kuehn, F. E., Transformation of carbon dioxide with homogeneous transition-metal catalysts: a molecular solution to a global challenge? *Angew. Chem. Int. Ed.* **2011,** *50*, 8510-8537.

88. Tinnemans, A.; Koster, T.; Thewissen, D.; Mackor, A., Tetraaza-macrocyclic cobalt (II) and nickel (II) complexes as electron-transfer agents in the photo (electro) chemical and electrochemical reduction of carbon dioxide. *Recueil des Travaux Chimiques des Pays-Bas* **1984,** *103*, 288-295.

89. Savéant, J.-M., Molecular catalysis of electrochemical reactions. Mechanistic aspects. *Chem. Rev.* **2008,** *108*, 2348-2378.

90. Rakowski Dubois, M.; Dubois, D. L., Development of molecular electrocatalysts for CO_2 reduction and H_2 production/oxidation. *Acc. Chem. Res.* **2009,** *42*, 1974-1982.

91. Berardi, S.; Drouet, S.; Francas, L.; Gimbert-Suriñach, C.; Guttentag, M.; Richmond, C.; Stoll, T.; Llobet, A., Molecular artificial photosynthesis. *Chem. Soc. Rev.* **2014,** *43*, 7501-7519.

92. Sahara, G.; Ishitani, O., Efficient photocatalysts for CO_2 reduction. *Inorg. Chem.* **2015,** *54*, 5096-5104.

93. Onishi, N.; Xu, S.; Manaka, Y.; Suna, Y.; Wang, W.-H.; Muckerman, J. T.; Fujita, E.; Himeda, Y., CO_2 hydrogenation catalyzed by iridium complexes with a proton-responsive ligand. *Inorg. Chem.* **2015,** *54*, 5114-5123.

94. Collin, J.; Sauvage, J., Electrochemical reduction of carbon dioxide mediated by molecular catalysts. *Coord. Chem. Rev.* **1989,** *93*, 245-268.

95. Narayanan, R.; McKinnon, M.; Reed, B. R.; Ngo, K. T.; Groysman, S.; Rochford, J., Ambiguous electrocatalytic CO_2 reduction behaviour of a nickel bis(aldimino)pyridine pincer complex. *Dalton Trans.* **2016,** *45*, 15285-15289.

96. Schmeier, T. J.; Dobereiner, G. E.; Crabtree, R. H.; Hazari, N., Secondary coordination sphere interactions facilitate the insertion step in an iridium (III) CO_2 reduction catalyst. *J. Am. Chem. Soc.* **2011,** *133*, 9274-9277.

97. Langer, R.; Diskin-Posner, Y.; Leitus, G.; Shimon, L. J.; Ben-David, Y.; Milstein, D., Low-Pressure Hydrogenation of Carbon Dioxide Catalyzed by an Iron Pincer Complex Exhibiting Noble Metal Activity. *Angew. Chem. Int. Ed.* **2011,** *50*, 9948-9952.

98. Andrade, G. A.; DiMeglio, J. L.; Guardino, E. T.; Yap, G. P.; Rosenthal, J., Synthesis and structure of palladium (II) complexes supported by bis-NHC pincer ligands for the electrochemical activation of CO_2. *Polyhedron* **2017,** *135*, 134-143.

99. Wang, W.-H.; Himeda, Y.; Muckerman, J. T.; Manbeck, G. F.; Fujita, E., CO_2 hydrogenation to formate and methanol as an alternative to photo-and electrochemical CO_2 reduction. *Chem. Rev.* **2015,** *115*, 12936-12973.

100. Bolm, C., A new iron age. *Nature Chem.* **2009,** *1*, 420.

101. Elgrishi, N.; Chambers, M. B.; Artero, V.; Fontecave, M., Terpyridine complexes of first row transition metals and electrochemical reduction of CO_2 to CO. *Phys. Chem. Chem. Phys.* **2014,** *16*, 13635-13644.

102. Machan, C. W.; Sampson, M. D.; Kubiak, C. P., A molecular ruthenium electrocatalyst for the reduction of carbon dioxide to CO and formate. *J. Am. Chem. Soc.* **2015,** *137*, 8564-8571.

103. Cummins, C. C., Three-Coordinate Complexes of "Hard" Ligands: Advances in Synthesis, Structure and Reactivity. *Prog. Inorg. Chem.* **1997**, 685-836.

104. Melenkivitz, R.; Mindiola, D. J.; Hillhouse, G. L., Monomeric phosphido and phosphinidene complexes of nickel. *J. Am. Chem. Soc.* **2002,** *124*, 3846-3847.

105. Mindiola, D. J.; Hillhouse, G. L., Terminal amido and imido complexes of three-coordinate nickel. *J. Am. Chem. Soc.* **2001,** *123*, 4623-4624.

106. Kitiachvili, K. D.; Mindiola, D. J.; Hillhouse, G. L., Preparation of stable alkyl complexes of Ni (I) and their one-electron oxidation to Ni (II) complex cations. *J. Am. Chem. Soc.* **2004,** *126*, 10554-10555.

107. Kogut, E.; Wiencko, H. L.; Zhang, L.; Cordeau, D. E.; Warren, T. H., A Terminal Ni (III)− Imide with Diverse Reactivity Pathways. *J. Am. Chem. Soc.* **2005,** *127*, 11248-11249.

108. Nilges, M. J.; Barefield, E. K.; Belford, R. L.; Davis, P. H., Electronic structure of three-coordinate nickel (I): electron paramagnetic resonance of nickel-doped halobis (triphenylphosphine) copper (I). *J. Am. Chem. Soc.* **1977,** *99*, 755-760.

109. Eckert, N. A.; Dinescu, A.; Cundari, T. R.; Holland, P. L., A T-shaped three-coordinate nickel (I) carbonyl complex and the geometric preferences of three-coordinate d^9 complexes. *Inorg. Chem.* **2005,** *44*, 7702-7704.

110. Yoo, C.; Lee, Y., AT-Shaped Nickel (I) Metalloradical Species. *Angew. Chem. Int. Ed.* **2017,** *56*, 9502-9506.

111. George, S. J.; Seravalli, J.; Ragsdale, S. W., EPR and infrared spectroscopic evidence that a kinetically competent paramagnetic intermediate is formed when acetyl-coenzyme A synthase reacts with CO. *J. Am. Chem. Soc.* **2005,** *127*, 13500-13501.

112. Amara, P.; Volbeda, A.; Fontecilla-Camps, J. C.; Field, M. J., A quantum chemical study of the reaction mechanism of acetyl-coenzyme A synthase. *J. Am. Chem. Soc.* **2005,** *127*, 2776-2784.

113. Webster, C. E.; Darensbourg, M. Y.; Lindahl, P. A.; Hall, M. B., Structures and energetics of models for the active site of acetyl-coenzyme A synthase: Role of distal and proximal metals in catalysis. *J. Am. Chem. Soc.* **2004,** *126*, 3410-3411.

114. Schenker, R. P.; Brunold, T. C., Computational studies on the A cluster of acetyl-coenzyme A synthase: geometric and electronic properties of the NiFeC species and mechanistic implications. *J. Am. Chem. Soc.* **2003,** *125*, 13962-13963.

115. Hegg, E. L., Unraveling the structure and mechanism of acetyl-coenzyme A synthase. *Acc. Chem. Res* **2004,** *37*, 775-783.

116. Drennan, C. L.; Doukov, T. I.; Ragsdale, S. W., The metalloclusters of carbon monoxide dehydrogenase/acetyl-CoA synthase: a story in pictures. *J. Biol. Inorg. Chem.* **2004,** *9*, 511-515.

117. Alvarez, S., Bonding and stereochemistry of three-coordinated transition metal compounds. *Coord. Chem. Rev.* **1999,** *193*, 13-41.

118. Sheng, M.; Jiang, N.; Gustafson, S.; You, B.; Ess, D. H.; Sun, Y., A nickel complex with a biscarbene pincer-type ligand shows high electrocatalytic reduction of CO_2 over H_2O. *Dalton Trans.* **2015,** *44*, 16247-16250.

CHAPTER 2. ACRIDONE SYNTHESIS AND APPLICATION IN COMPLEX FORMATION

2.1 Background

2.1.1 Development of sterically encumbering amido ligands for low nuclearity complexes

Sterically demanding amido ligands have found widespread use in organometallic chemistry and homogeneous catalysis including applications as chelating systems to stabilize low-valent species or to achieve unusual geometries. Diphenylamine can behave as either a terminal or bridging ligand. A common method to achieve unusually low coordination is to use ligands which are so bulky as to preclude either the attachment of further ligands or the attainment of a higher coordination by ligand bridging.[1]

Isolation of transition metal complexes with coordination numbers as low as three has been achieved by employing diphenylamido (Ph_2N^-) and disilylamido $(Me_3Si)_2N^-$ ligands.[1-7] Many early cases of successful synthesis of homoleptic $M(NR_2)_n$ complexes with dialkylamides were limited to the earlier transition metals.[8] Later transition metals showed reluctance to form stable M-NR_2 complexes. This can be rationalized in terms of the bonding properties of $–NR_2$ which acts as both a σ-donor and a π-donor. It therefore forms stronger bonds with earlier transition metals which have vacant d-orbitals of π-symmetry (π-acceptors) than with later transition metals which are electron-rich (π-donors).[8]

To induce mononuclearity, Powers, Lappert, Lee, Girolami and coworkers all used bulky amido ligands to stabilize two-coordinate transition metal complexes of Cr^{II} through Ni^{II}. [9-16] The steric constraints in monodentate 3,6-dimethyl-1,8-diphenylcarbazolido (**2)** and 1,8-dimesityl-3,6-dimethylcarbazolido (**3**) ligands (Figure 2.1 below) enabled their application in the stabilization of highly reactive Group 13 centers.[17-18] Moreover, fused polycyclic ring type ligands have displayed a greater degree of stability under different reaction conditions due to their rigidity and chemical inertness and also offer a variety of avenues for modification to modulate activity and reactivity at the transition metal center. Even though ligands **2** and **3** offered a point of comparison in the study of the differences in electronic properties of amido versus aryl (**1**) ligands, when used in synthesis of complexes of Cr-Co, the resulting complexes were homoleptic (ML_2).[19]

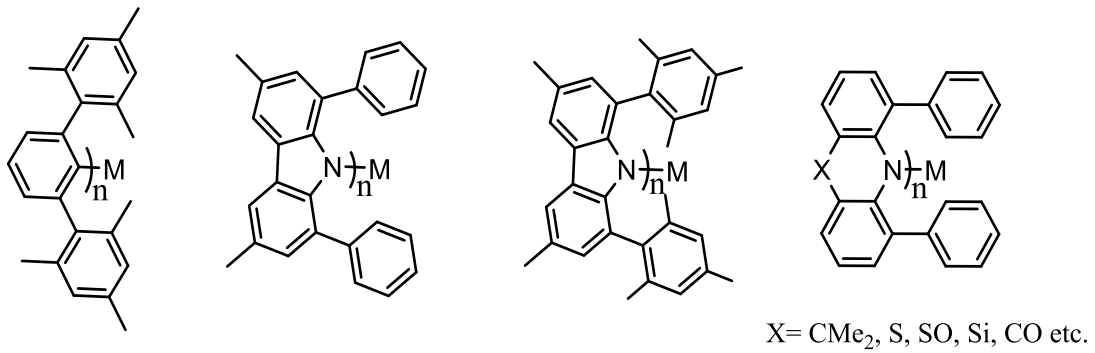

Figure 2.1. Structurally enforced binding pocket protection.

The desire to construct frameworks that can support low-coordinate, especially mononuclear open-shell transition-metal complexes remains to be achieved. The expansion of the carbazole backbone with an atom or combination of atoms like S, Si, -CMe_2, SO, -C=O (**4**, Figure 2.1) would constrain the metal binding pocket and enhance the ability to

achieve low-nuclearity M-NR_2 transition metal complexes. This led to the design of 4,5-substituted acridone-based ligands (**5**, Scheme 2.3).

2.1.2 General applications of acridone and its analogues

Acridone is a biologically active molecule found in an array of natural products, biological probes, pigments, dyes, bioactive molecules, fluorescent labels, and functional materials. The interaction of acridones with their cellular target is very diverse and molecules of this family are broadly applied as antimalarial,[20-21] antifungal,[22] antitumor,[23] anti-inflammatory[24] and antiviral[25-26] agents. Acridone analogues have also shown promising leads in application as chemical therapeutics[27-29] and as treatment measures against multi-drug resistance in cancer cells.[30] Because of its versatile activities, this pharmacologically active moiety has earned the name "privileged structure", and its application in manufacture of the acridone acetic acid sodium salt (Na-AAA), commercially available with a trade name Neovir, reflects its relevance to clinical drug development.[31] Moreover, many acridone-containing molecules exhibit fluorescence in the visible region of the electromagnetic spectrum, making them applicable as fluorescent probes for visualizing their activities in cell cultures or tissue samples.[21, 32-34] For materials development, acridones with extended conjugated systems are promising candidates for organic semiconductors due to their unusual electronic and photo-physical properties.[35] Furthermore, acridones offer fascinating potential catalyst backbones owing to their rigid structure and dentate nitrogen atom.[36-37] Owing to these many applications of acridones and its analogues, development of a facile and efficient method for its synthesis is desirable.

2.1.3 Available synthetic routes to acridone and its analogues

Since the first synthesis of unsubstituted acridone in 1912[38], a number of methods, generally relying on intramolecular six-membered central ring closure as a key step in most employed strategies, have been developed as shown below. Even though numerous cyclization approaches have been investigated, the synthetic routes to obtain the acridone framework can be classified into three main types: (1) C-N coupling;[39-40] (2) acid-promoted cyclization;[41-43] (3) and CO insertion.[44-45] The classical methods to acridone synthesis are paths **a** and **b** on Scheme 2.1.

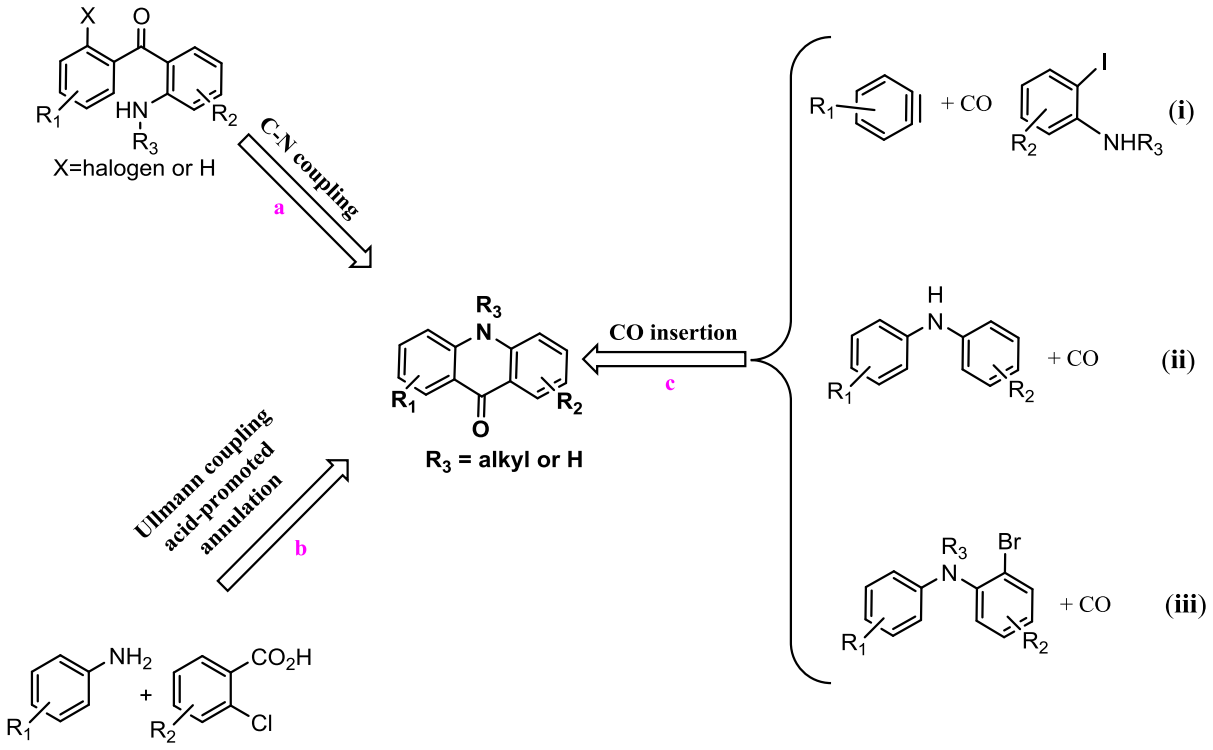

Scheme 2.1. Approaches towards synthesis of acridone and its derivatives.

Reprinted with permission from: Song, J.; Ding, K.; Sun, W.; Wang, S.; Sun, H.; Xiao, K.; Qian, Y.; Liu, C., Synthesis of acridones through palladium-catalyzed carbonylative of 2-Bromo-diarylamines. *Tetrahedron Lett.* **2018**. Copyright 2018. Elsevier Ltd.

Path **a** requires benzophenone substrates like 2-aminobenzophenones or phenyl-(2-phenylaminophenyl)methanone to achieve the C-N coupling reaction.[40] Acid-promoted cyclization (path **b**) includes the use of *N*-phenyl-anthranilic acid or intramolecular nucleophilic substitution of 2-amino-2′-halobenzophenones.[34, 39, 41, 46-49]Although these strategies provide access to substituted acridones, they suffer from drawbacks like relatively harsh and strict reaction conditions, low atom economy, tedious workup procedures and the use of expensive substrates or those that require prior preparation. These disadvantages limit the application of these methods, and the need to develop one-pot intermolecular synthetic approach from readily available starting materials that would exhibit advantages of step economy and high reaction efficiency is still needed.

2.1.4 Synthesis of acridone via CO insertion

With a view to address these challenges, a method that applies CO insertion, path **c**, is more appealing since it utilizes CO as a cheap C_1 source thereby meeting requirements of atom economy, step economy, and green chemistry. These advantages have led to increased interest in developing methods that apply CO insertion for ring closure in acridone synthesis. The first synthetic route to acridones via CO insertion was developed in 2015 by Jiang and coworkers where palladium catalyzed the reaction between aryne generated from silylaryl triflates precursors and *N*-alkyl(aryl)-iodoaniline (Scheme 2.1 (**i**)).[44]A palladium/copper co-catalyzed oxidative carbonylation of diphenylamine (Scheme 2.1 (**ii**)) with the help of an oxidant has also been applied in synthesis of acridone as well.[45] Recently, Song and coworkers reported acridone synthesis via palladium catalyzed carbonylation/C-H activation of 2-bromo-diarylamine.[50]

Over the past three decades, there has been a rising need to develop methodologies that apply CO-free carbonylative procedures that use easy to handle inorganic or organic carbonyl compounds.[51] A number of CO surrogates are known, and transition-metal-catalyzed carbonylation reactions that use CO surrogates as a convenient and safe approach for the synthesis of carbonyl derivatives circumventing the need to use gaseous CO have been investigated.[51-56] We herein report a complementary method for the efficient construction of substituted acridones starting from commercially available bis(4-*tert*-butylphenyl)amine. An *ortho*-directed metalation of the in-situ-formed carbamate followed by the central six-membered ring closure using phenyl chloroformate leads to the formation of the substituted acridone.

2.2 Results and Discussion

2.2.1 New synthesis and characterization of acridone

To arrive at the acridone framework, a nitrogen-based ligand, a synthetic approach that uses carbamate anion as a removable directing group[57-58] was employed. Katritzky and coworkers demonstrated the use of carbon dioxide as an *N*-protecting and a directing group in the regiospecific *ortho*-functionalization of *N*-alkylanilines as shown on Scheme 2.2 below:[59]

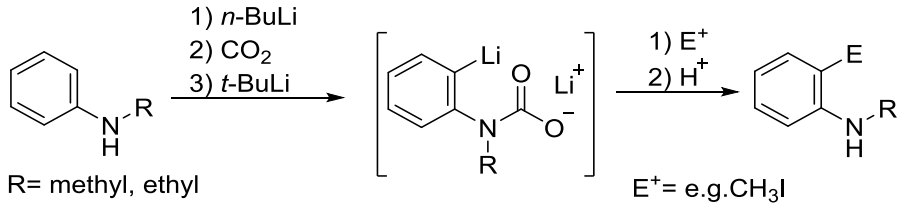

Scheme 2.2. Preparation of *ortho*-substituted *N*-methyl- and *N*-ethyl-aniline.

Starting with the conversion of bis(4-*tert*-butylphenyl)amine to carbamate, we were able to apply directed metalation to achieve symmetric dilithiation. Quenching with phenyl chloroformate led to the formation of 2,7-di-*tert*-butylacridin-9(10*H*)-one in 30% yield (Scheme 2.3).

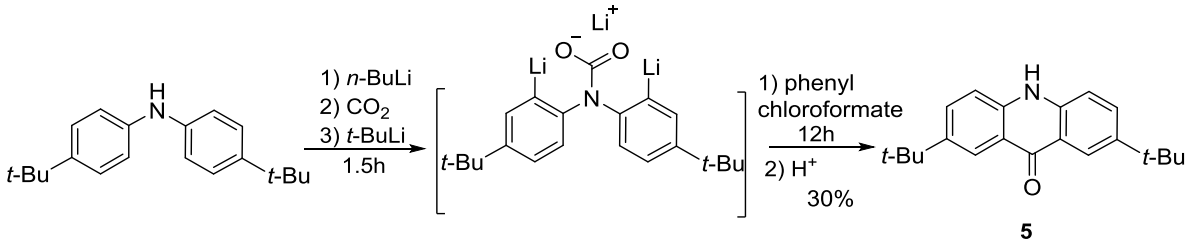

Scheme 2.3. Synthesis of 2,7-di-*tert*-butylacridin-9(10*H*)-one.

The parent acridone (**5**) reacts readily with sodium hydride under reflux to give the deprotonated version as seen from the ^{1}H NMR of its deuterated adduct in Figure 2.9.

2.2.2 Modification of acridone, its coupling products and characterization and complexation studies

With **5** synthesized, either as shown above or via Friedel-Crafts alkylation[60] of the parent acridone (the Friedel-Crafts procedure was used due to the inconsistent yields obtained in scaling up the reaction), we looked to enhance the steric encumbrance around the nitrogen. One way to do this is to turn **5** into a substrate that can undergo coupling reactions, directed metalation, etc. This would mean activating the 4- and 5-positions on the acridone framework.[61] Bromination of 2,7-di-*tert*-butylacridin-9(10*H*)-one (**5**) with bromine in acetic acid produces 4,5-dibromo-2,7-di-*tert*-butylacridin-9(10*H*)-one (**6**) in near-quantitative yield (Scheme 2.4).

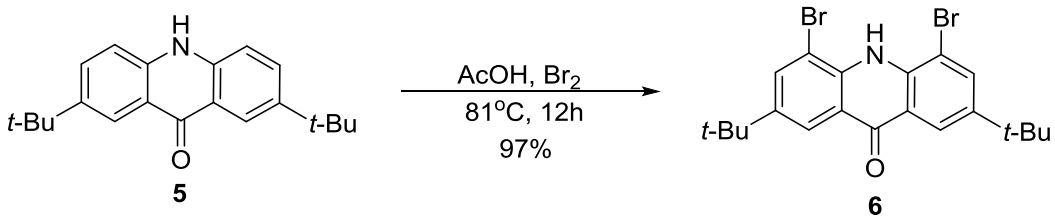

Scheme 2.4. Bromination of 2,7-di-*tert*-butylacridin-9(10*H*)-one.

2.2.2.1 Modification via conversion into chloroacridine

Acridines have attracted a considerable interest due to their unique physical and chemical properties, biological activities, and industrial applications.[62] In industry, acridine and its analogues function as pigments and dyes.[63] Acridine derivatives with extended conjugated systems are expected to be promising candidates for organic semiconductor materials because they have unusual electronic and photophysical properties.[35] Therefore, development of new synthetic methods for construction of various acridine derivatives especially with this backbone that is poised to undergo numerous functionalization reactions is an important step for the chemistry community.

The available synthetic methods include the Brenthsen reaction (this is one of the earliest methods used in the preparation of acridines and entails heating a diphenylamine and a carboxylic acid together with $ZnCl_2$ between 200-270 ^oC for 24 hours),[64-66] cyclization reactions of (2-formyl- or 2-ketophenyl)(phenyl)amines and other methods which include C-H functionalization, dehydrogenation, or metal-catalyzed coupling reactions.[67-71] These methods often require either harsh reaction conditions, such as high temperatures and strongly basic or acidic media, or they require materials that are not readily available. Substrate **6** however undergoes reaction with thionyl chloride to give in

quantitative yields, 4,5-dibromo-2,7-di-*tert*-butyl-9-chloroacridine (**7**) as shown below.[72-73]

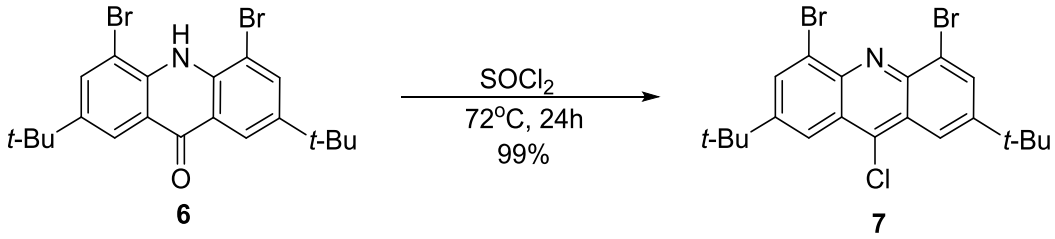

Scheme 2.5. Synthesis of 4,5-dibromo-2,7-di-*tert*-butyl-9-chloroacridine.

Substrate **7** undergoes clean lithium-halogen exchange, making it a suitable candidate for functionalization via electrophilic reactions. After lithium-halogen reaction, treatment with DMF as shown in Scheme 2.6 gives an easily identified product as shown by the singlet resonance in the ^{1}H NMR spectrum at δ 11.61 ppm for the two aldehyde protons (see Figure 2.12).

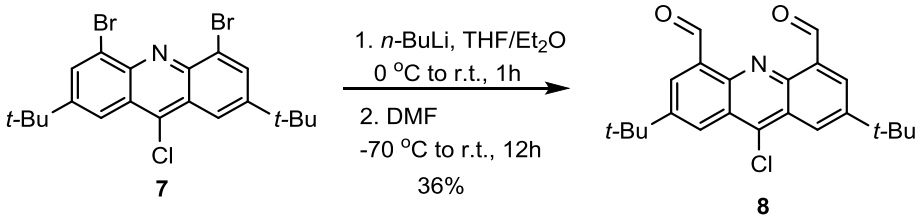

Scheme 2.6. Synthesis of 2,7-di-*tert*-butyl-4,5-dicarboxaldehyde-9-chloroacridine.

Substrate **6** is a versatile synthon that can be converted to different ligand frameworks via functionalization *ortho* to nitrogen using cross-coupling reactions to produce ligands that have a rigid backbone, are sterically hindered and contain a σ-basic nitrogen donor. Alternatively, directed *ortho*-metalation could be applied to arrive at a neutral *N*-donor pyridine-based ligand framework.

2.2.2.2 Modification via *ortho*-functionalization using tolyl groups and complex formation studies

With a view of synthesizing a sterically protected pocket as depicted in **4** in Figure 2.1, we envisioned that installation of *p*-tolyl groups would have a similar effect to the mesityl groups in **1** and **3** (Figure 2.1). To achieve this ligand framework, palladium-catalyzed carbon-carbon[18] bond formation was carried out, as depicted in Scheme 2.7, affording 4,5-di-*p*-tolyl-2,7-di-*tert*-butylacridin-9(10*H*)-one (**9)** in 68% yield. We hypothesized that these groups would align perpendicular to the plane of acridone thus only allowing specific bonding orientation at the nitrogen center and achieving low-nuclearity metal complexes.

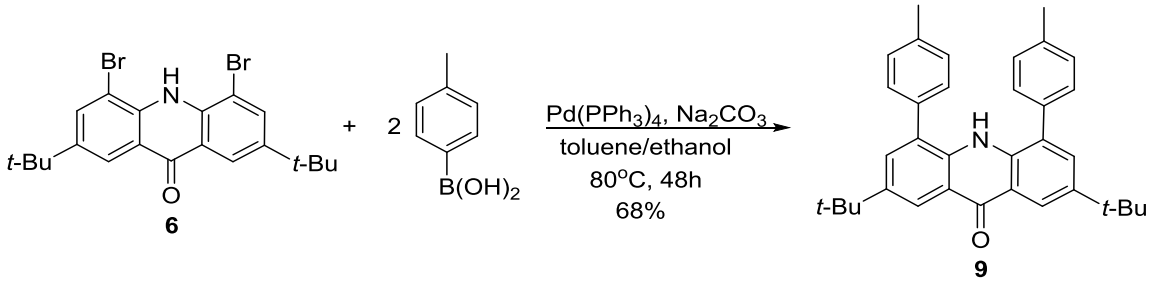

Scheme 2.7. Synthesis of 4,5-di-*p*-tolyl-2,7-di-*tert*-butylacrid-9(10*H*)-one.

The complexes of **2** in Figure 2.1 were synthesized via salt metathesis between the lithium adduct of 3,6-dimethyl-1,8-diphenylcarbazolido and the respective transition metal halides ($CrCl_2$, $MnCl_2$, $FeCl_2(thf)_{1.5}$ or $CoBr_2(DME)$).[19] Gallium complexes of **3** were also synthesized from the treatment of 1,8-dimesityl-3,6-dimethylcarbazolido lithium adduct with $GaCl_3$.[18] With these precedents in mind, we hoped that ligand **9** might behave similarly.

Treatment of **9** with sodium hydride (Scheme 2.8) in THF gave a fluorescent yellow-green solution. Quenching with D_2O, and analysis of the product using ^1H NMR spectroscopy showed the absence of a resonance normally observed at δ 8.30 ppm for the N-*H* moiety, indicating a successful deprotonation (Figure 2.15). When the sodium salt of 4,5-ditolyl-2,7-di-*tert*-butylacridin-9(10*H*)-one was treated with either $CuCl_2$ or $(CuOTf)_2 \bullet C_6H_6$, the resulting products' ^1H NMR spectra showed highly broadened, non-informative resonances typical of paramagnetic products. Attempts to recrystallize the sample led to powdering and reemergence of protio-ligand. This ligand (**9**) however, reacts in the same way as **6** in Scheme 2.5 above to form 4,5-di-*p*-tolyl-2,7-di-*tert*-butyl-9-chloroacridine quantitatively and cleanly as shown in Figure 2.16.

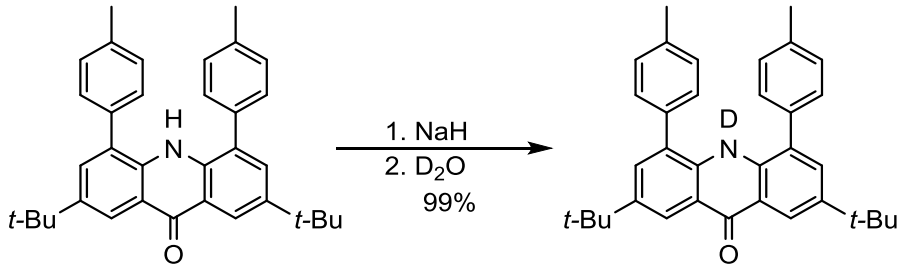

Scheme 2.8. Reaction of 4,5-di-*p*-tolyl-2,7-di-*tert*-butylacrid-9(10*H*)-one with NaH followed by D_2O quench.

2.2.2.3 Modification via *ortho*-functionalization using benzophenone-imine groups and complex formation studies

To enhance the stability of the complexes formed, we increased the number of donor atoms. Using benzophenone imine and **6** under palladium-catalyzed C-N cross-coupling reactions,[74] 2,7-di-*tert*-butyl-4,5-bis(diphenylmethyleneimino)acridin-9(10*H*)-one (**10**) was synthesized in 81% yield (Scheme 2.9).

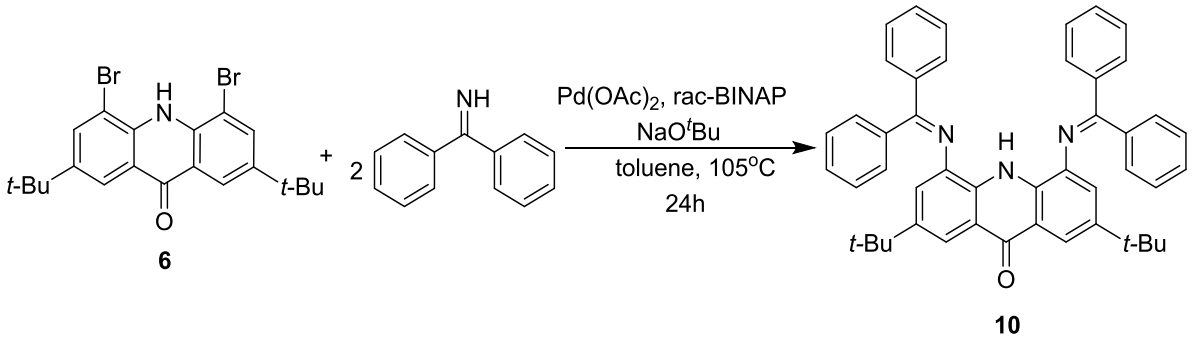

Scheme 2.9. Synthesis of 2,7-di-*tert*-butyl-4,5-bis(diphenylmethyleneimino)acridin-9(10*H*)-one.

An attempt to synthesize a palladium(II) complex of the 2,7-di-*tert*-butyl-4,5-bis(diphenylmethyleneimino)acridin-9(10*H*)-one, by heating the free ligand with palladium(II) acetate, appeared successful as analyzed by ^{1}H NMR spectroscopy (see Figure 2.21) and infrared spectroscopy. The solid-sate structure of crystals obtained from a DCM solution layered with Et_2O at -35 ^{o}C however, revealed only 13% palladation and gave the structure shown in Figure 2.2 below. This structure afforded an insight into the free ligand structure which co-crystallized with it.

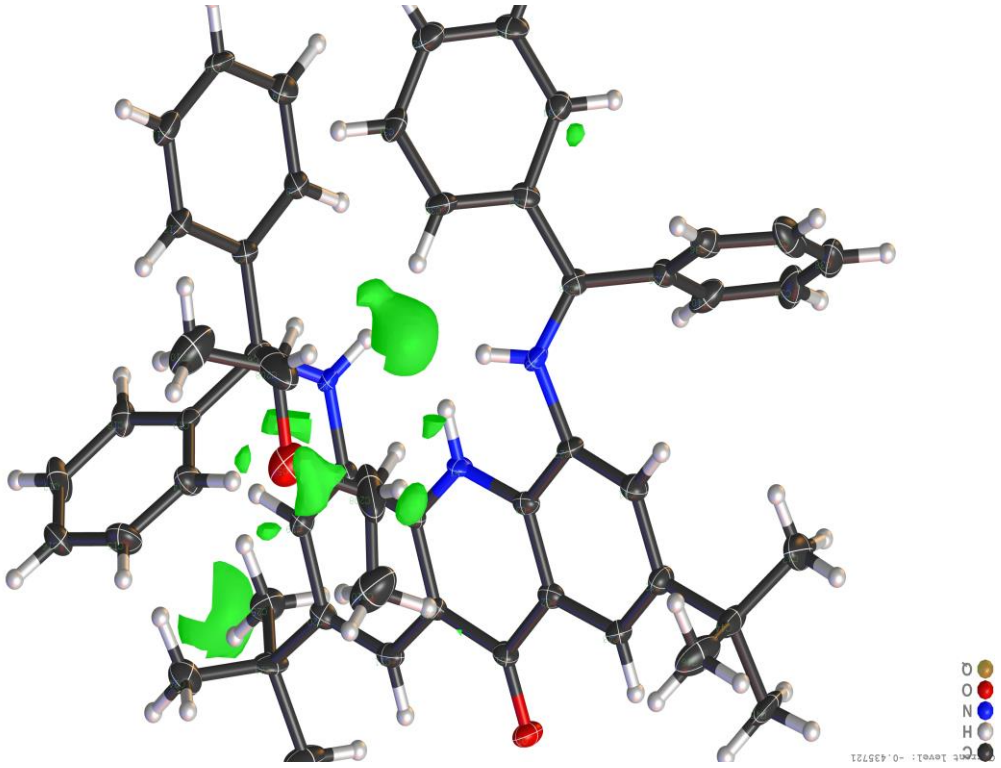

Figure 2.2. Solid-state structure of (**10**)Pd(II) acetate complex shown as 50% probability ellipsoids. (It was not possible to obtain reliable bond metrics due to disorder).

The solid-state analysis of the crystals obtained of the ligand indicate a sterically hindered binding site around the nitrogen atom (Figure 2.3). The N•••N distance is 4.479 Å, putting the H atom *ca.* 2.239 Å from each nitrogen and potentially allowing H-bonding interactions.

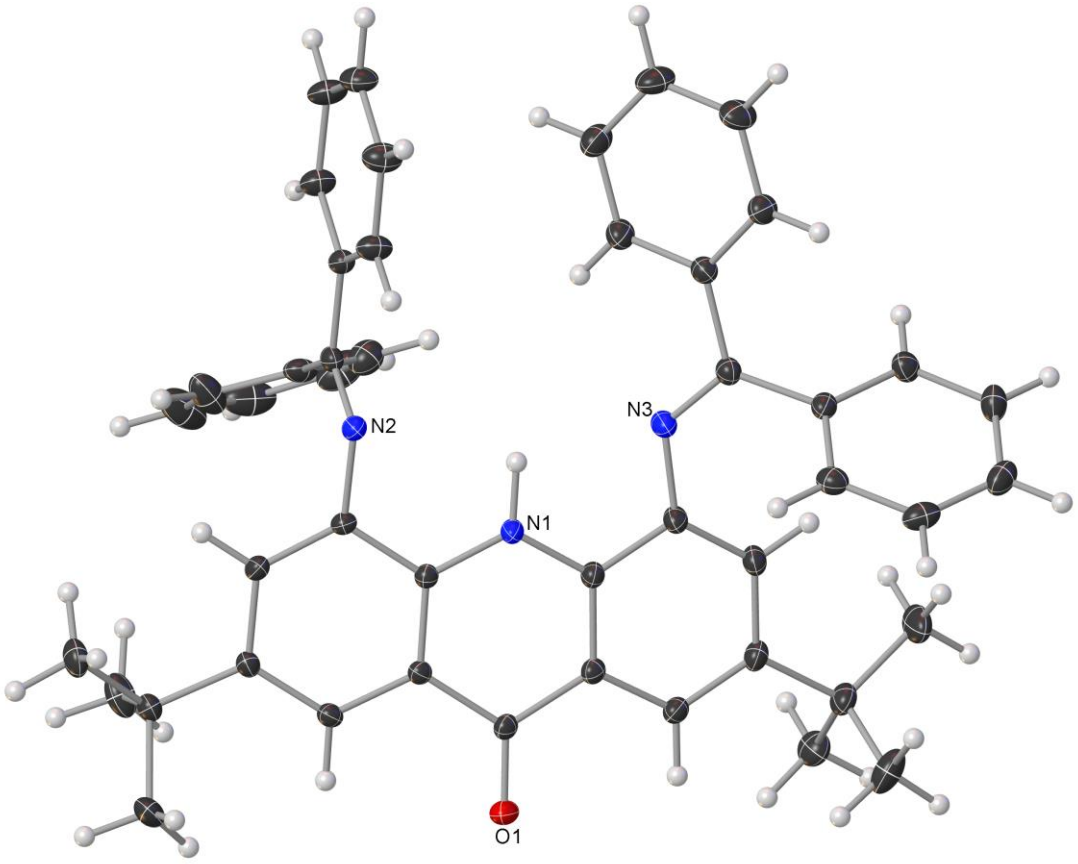

Figure 2.3. Solid-state structure of **10** shown as 50% probability ellipsoids. Selected interatomic distances (Å) and angles (°): C5-N2, 1.421(2); C27-N3, 1.405(3); N2-N3, 4.479; C4-C5-N2, 118.0(4); C3-C27-N3, 114.2(2). N2 and N3 undergo hydrogen bonding with the hydrogen on N1.

Ligand **10** shows an absorption frequency at 3370 cm^{-1} corresponding to the NH stretch in the infrared spectroscopy (Figure 2.4 red trace). The ketone stretch shows up at 1635 cm^{-1}, a slightly lower frequency but comparable to other related structures of similar framework, like 4-pyridone (1642 cm^{-1} for C=O and 3210-2830 cm^{-1} for NH (or OH). The appearance of a well-defined single peak at 3370 cm^{-1} for the NH suggests the predominance of the acridone form over its 9-hydroxyacridine tautomer, in contrast to 4-pyridone which has a more complex pattern in the spectrum in that region as a result of this

effect.[75] When **10** is treated with Me_3Al, complex formation is indicated by the disappearance of the NH absorption as shown by the blue trace in the IR spectrum in Figure 2.4. In the ^1H NMR spectrum (Figure 2.22), there is a new resonance at δ -0.94 ppm in the region where the methyl protons of aluminum attached to an oxygen or nitrogen are expected to appear. The singlet resonance at δ 9.63 ppm in the ^1H NMR spectrum corresponding to N*H* is also gone indicating aluminum complex formation.

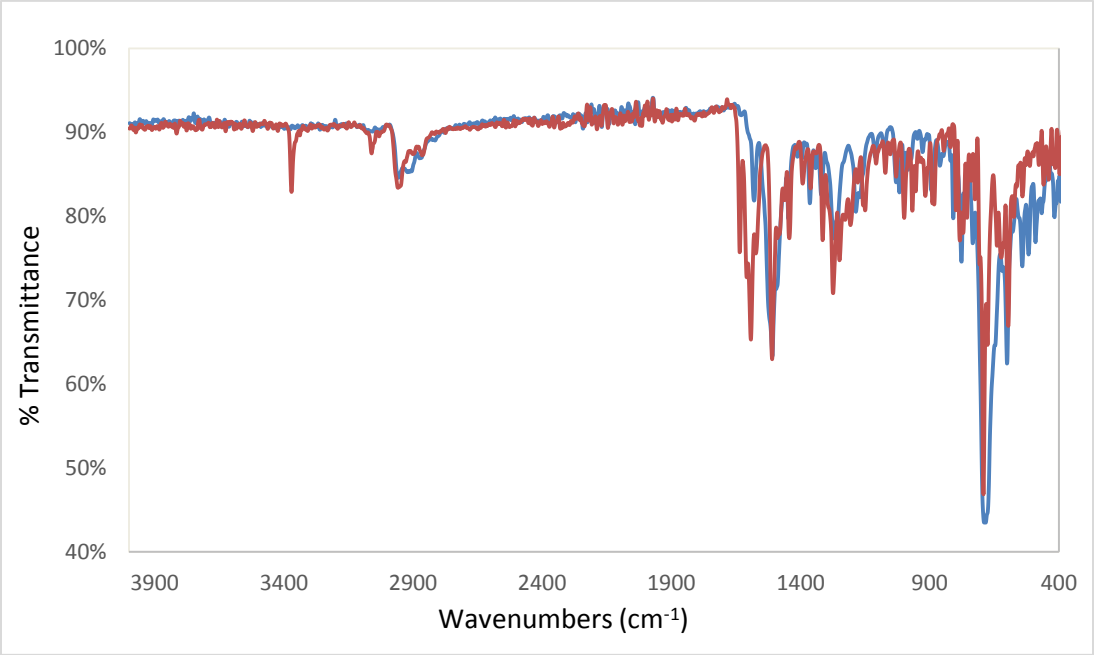

Figure 2.4. IR spectrum of ligand, **10**, before (red) and after (blue) reaction with Me_3Al.

In solution, **10** has a λ_{max} of 430 nm in the UV-Vis spectroscopy and after its reaction with Me_3Al, the absorption is red-shifted to a λ_{max} of 492 nm. The spectroscopic data obtained from the treatment of this ligand with Me_3Al points to the ability of this ligand to interact with group 13 metals and could offer a good comparison with structures **2** and **3** in terms of steric hindrance. However, from the data presented herein, we cannot tell whether the aluminum is *O*- or *N*-bound.

2.2.2.4 Modification via *ortho*-functionalization using morpholine groups and complex formation studies

Ligand frameworks that incorporate electron reservoirs together with proton-channeling pathways could be very useful in the PCET processes that many catalytic processes require. In light of the ease with which the central six-membered ring converts into the acridine framework, we sought to install at the *ortho*-position functional groups bearing oxygen atoms capable of undergoing hydrogen bonding. Using palladium catalyzed C-N cross-coupling reactions, 4,5-dimorpholino-2,7-di-*tert*-butylacridin-9(10*H*)-one (**11**) was synthesized in 56% yield (Scheme 2.10).

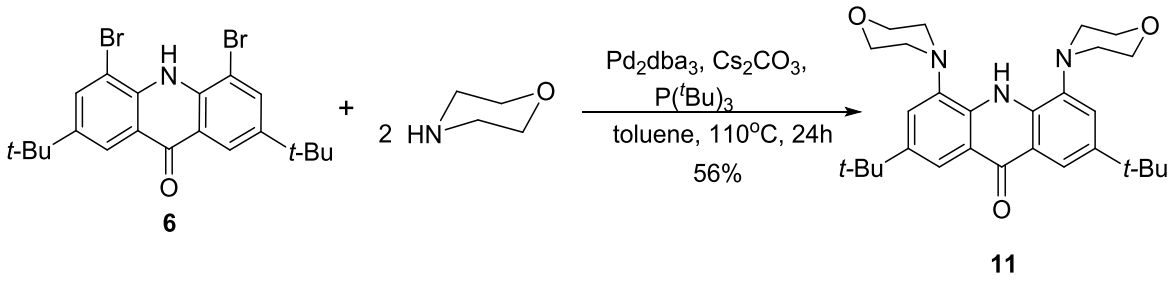

Scheme 2.10. Synthesis of 4,5-dimorpholino-2,7-di-*tert*-butylacridin-9(10*H*)-one.

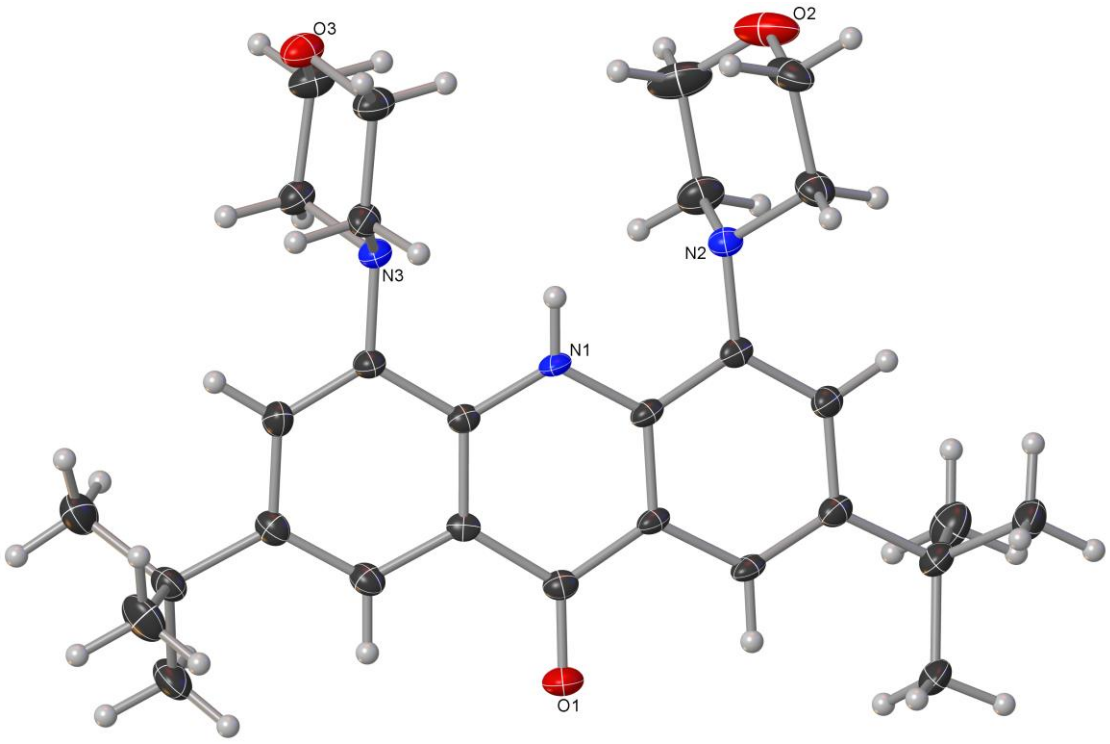

Figure 2.5. Solid-state structure of **11** shown as 50% probability ellipsoids. Selected interatomic distances (Å) and angles (°): C5-N2, 1.428(6); C18-N3, 1.441(6); N2-N3, 4.586; C4-C5-N2, 117.2(4); C3-C1-N3, 116.3(9).

Crystals for X-ray diffraction were obtained from a THF solution layered with hexanes and kept at -35 °C. The solid-state structure of the ligand (Figure 2.5) reveals a wider, less sterically hindered binding pocket as compared to the previous ligands. This pocket was expected to be more amenable to stable metal complex formation if sterics was the problem previously. As with **9**, treatment of **11** with NaH led to deprotonation of the ligand. When the sodium salt of **11** was treated with $CoCl_2$ and the product formed taken for mass spectrometry, a mass of 653 amu was obtained, consistent with $[M^+ + H + 2CH_3CN]$. On the other hand, the reaction of sodium salt of **11** with $CuCl_2$ gave a product of mass 605 amu in the negative mode. This would be consistent with addition of

a methoxide ion from the methanol solvent to the molecular ion during the process of ionization. The free ligand has a λ_{max} of 398 nm in the UV-Vis spectrum, whereas after reaction with $CuCl_2$, peak absorbances at 398 and 673 nm were observed. Attempts at structurally characterizing these products proved unsuccessful. The trimethylaluminum reaction with the ligand leads to similar observations as obtained with **10**, notably the disappearance of the NH stretch at 3357 cm^{-1} (blue trace) in the IR spectrum for the formation of the aluminum complex (red trace) Figure 2.6.

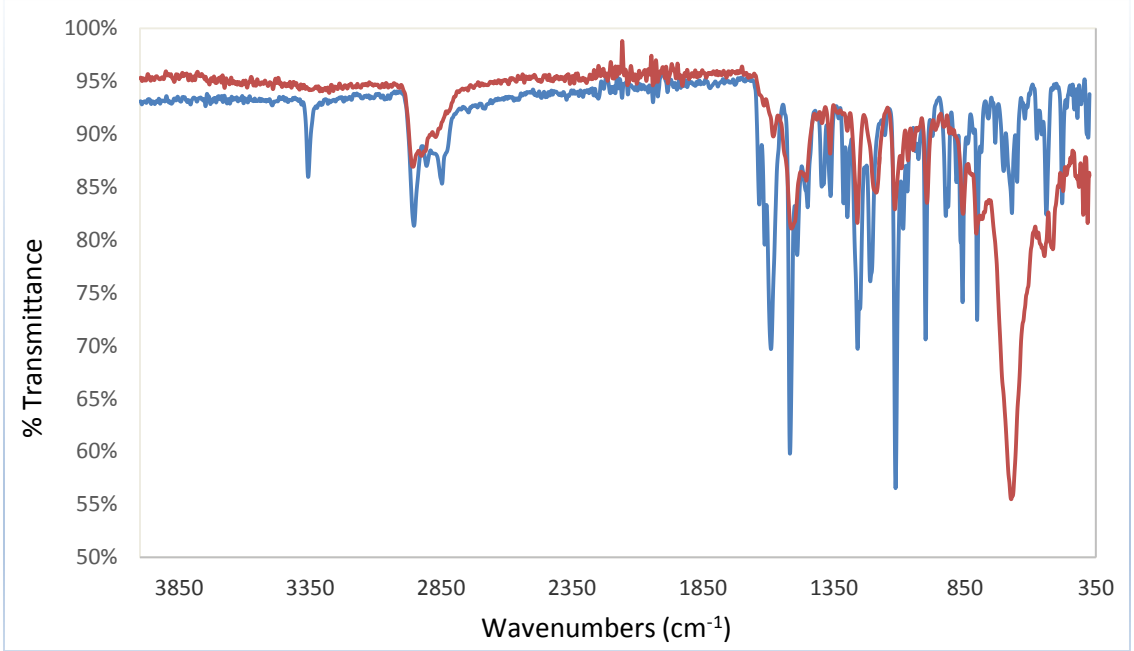

Figure 2.6. IR spectrum of ligand, **11**, before (blue) and after (red) reaction with Me_3Al.

2.3 Concluding Remarks

We have herein shown that through a combination of directed metalation techniques, together with use of CO_2 and CO surrogates, we can synthesize in one pot an acridone bearing tertiary alkyl groups. Modification of this acridone via *ortho*-functionalization either through lithium-halogen exchange or transition-metal-catalyzed

coupling reactions leads to a variety of acridone and acridine frameworks with varying degree of steric hindrance around the nitrogen donor atom.

2.4 Experimental

2.4.1 General Considerations

All reactions, unless otherwise stated, were carried out in an MBraun inert atmosphere (nitrogen) glovebox, or in resealable glassware on a Schlenk line under argon atmosphere. Glassware and magnetic stir bars were dried in a ventilated oven at 160 °C and were allowed to cool under vacuum. Molecular sieves (Alfa Aesar) and Celite (EMD 545) were dried under vacuum for at least twelve hours at 160 °C.

^{1}H NMR spectra were obtained using a Varian Vx 400 MHz or Varian Mercury 300 (300.323 MHz for ^{1}H) spectrometer and ^{13}C NMR spectra were obtained using either Avance IIIHD 500 spectrometer, or Bruker Avance IIIHD 700 spectrometer. ^{1}H and ^{13}C NMR chemical shifts are referenced with respect to solvent signals and are reported relative to tetramethylsilane.[76] Elemental analyses were performed by Atlantic Microlab, Inc. in Norcross, GA. Infrared spectra were collected from neat and liquid samples using a Bruker Alpha-P FT-IR spectrometer equipped with an attenuated total reflection (ATR) platinum diamond reflector accessory. Air and moisture sensitive samples were exposed to air as briefly as possible prior to data collection.

2.4.2 Materials and Methods

Tetrahydrofuran (EMD Millipore Omnisolv), hexanes (EMD Millipore Omnisolv), diethyl ether (EMD Millipore Omnisolv) and toluene (EMD Millipore Omnisolv) were sparged with ultra-high purity argon (NexAir) for 30 min prior to first use, and dried using an MBraun solvent purification system. These solvents were further dried over sodium benzophenone ketyl, degassed by successive freeze–pump–thaw cycles and then transferred under vacuum to an oven-dried resealable flask. Dichloromethane (EMD Millipore Omnisolv), acetonitrile (EMD HPLC) were each stirred over calcium hydride (Alfa Aesar) in a sealed flask for at least twelve hours and degassed by several freeze-pump-thaw cycles, then vacuum-transferred to resealable Schlenk flasks. These solvents were then stored over 3Å molecular sieves (Alfa-Aesar) in the glovebox. Methanol (BDH), acetone (BDH), ethyl acetate (BDH) and hexanes used in benchtop work were used as received.

Dichloromethane-d_2 (Cambridge Isotope Laboratories) and acetonitrile-d_3 were dried by stirring overnight over calcium hydride for at least twelve hours, degassed by several successive freeze–pump–thaw cycles. They were then transferred under vacuum to an oven-dried resealable flasks and stored in the glovebox. Benzene-d_6 and Tetrahydrofuran-d_8 (Cambridge Isotope Laboratories) were dried over sodium benzophenone ketyl, degassed by successive freeze–pump–thaw cycles and transferred under vacuum to an oven-dried resealable flask and stored in the glovebox. D_2O (Cambridge Isotope Laboratories), sodium *tert*-butoxide (TCI America), sodium hydroxide (EMD), anhydrous $MgSO_4$ (AlfaAesar), HCl (BDH), $NaHCO_3$ (BDH), benzophenone

(Alfa-Aesar), calcium hydride (Alfa-Aesar), acetic acid (Alfa-Aesar), nitrogen (NexAir), and argon (both industrial and ultra-high purity grades, NexAir) were used as received.

Sodium hydride (Alfa Aesar), carbon dioxide (NexAir), bis(4-*tert*-butylphenyl)amine (TCI), *n*-BuLi and *t*-BuLi (Sigma Aldrich), phenyl chloroformate (Alfa Aesar), benzophenone-imine (CHEM-IMPEX), bromine (Alfa Aesar), thionyl chloride (Sigma Aldrich), dimethylformamide (EMD), tetrakis(triphenylphosphine)palladium(0) (SREM chemicals), tolylboronic acid (Oakwood Chemicals), (CuOTf).C_6H_6 (Sigma Aldrich), $Pd(OAc)_2$ (STREM), rac-BINAP (Sigma Aldrich), Me_3Al (Sigma Aldrich), morpholine (Fisher Scientific), Pd_2dba_3 (Oxchem), cesium carbonate (Sigma Aldrich), tri-*tert*-butylphosphine (Sigma Aldrich), $CoCl_2$ (Sigma Aldrich), $AlCl_3$ (STREM) were all used as received.

2.4.3 Experimental Procedures

2.4.3.1 2,7-Di-*tert*-butylacridin-9(10*H*)-one

Into a 100-mL Schlenk flask was added bis(4-*tert*-butylphenyl)amine (2.00 g, 7.11 mmol). This was evacuated and refilled with argon and the cycle repeated two more times. Under argon, 12 mL of dry and degassed diethyl ether was added to dissolve. The solution was cooled to -70 °C using dry ice-acetone mixture. A solution of *n*-BuLi in hexanes (2.5 M, 3.2 mL, 7.8 mmol) was added dropwise over 10 min to this solution while stirring. The reaction was further stirred at -70 °C for 1 hour then let to warm up to room temperature for another 1 hour. The solution was degassed in three cycles before being warmed to room temperature. CO_2 was then bubbled into the solution for 10 min. It was stirred at room temperature for 30 min, before being degassed in three cycles then refilled with argon. The reaction mixture was cooled to -70 °C once more, and while stirring, *t*-BuLi in pentane (1.7

M, 8.8 mL, 15 mmol) was added dropwise over 20 min. The cooling bath was changed to -20 °C (ice-salt water) and the reaction mixture kept at this temperature for 1 hour. The reaction was then cooled to -70 °C before addition of phenyl chloroformate (0.89 mL, 7.1 mmol) dropwise. Reaction was left to warm up to room temperature overnight. After 12 hours, it was quenched with 20 mL of distilled water leading to formation of yellow suspension. This was filtered off and dried under vacuum to give 0.235 g of product. To the remaining yellow solution was added 2 mL of distilled water and the mixture heated to 90 °C for about 15 min forming more yellow solid. This was collected via filtration and washed with ~2 mL of chilled water followed by ~2 mL of acetonitrile to give 0.421 g of product leading to a combined yield of 30%. ^{1}H NMR (400 MHz, DMSO) δ (ppm) 11.64 (s, 1H, N*H*), 8.18 (s, 2H, Ar*H*), 7.82 (d, 2H, ortho-Ar*H*), 7.48 (d, 2H, meta-Ar*H*), 1.35 (s, 18H, C(C*H*$_3$)$_3$). ^{13}C NMR (176 MHz, DMSO) δ (ppm) 176.77 (s), 143.11 (s), 138.92 (s), 131.56 (s), 120.77 (s), 119.79 (s), 117.26 (s), 34.29 (s), 31.13 (s). Attempts to scale up the reaction gave inconsistent yields. Therefore, large-scale synthesis was achieved following Friedel-Crafts alkylation method that was published by Yamamoto and Higashibayashi when this project was underway.[60]

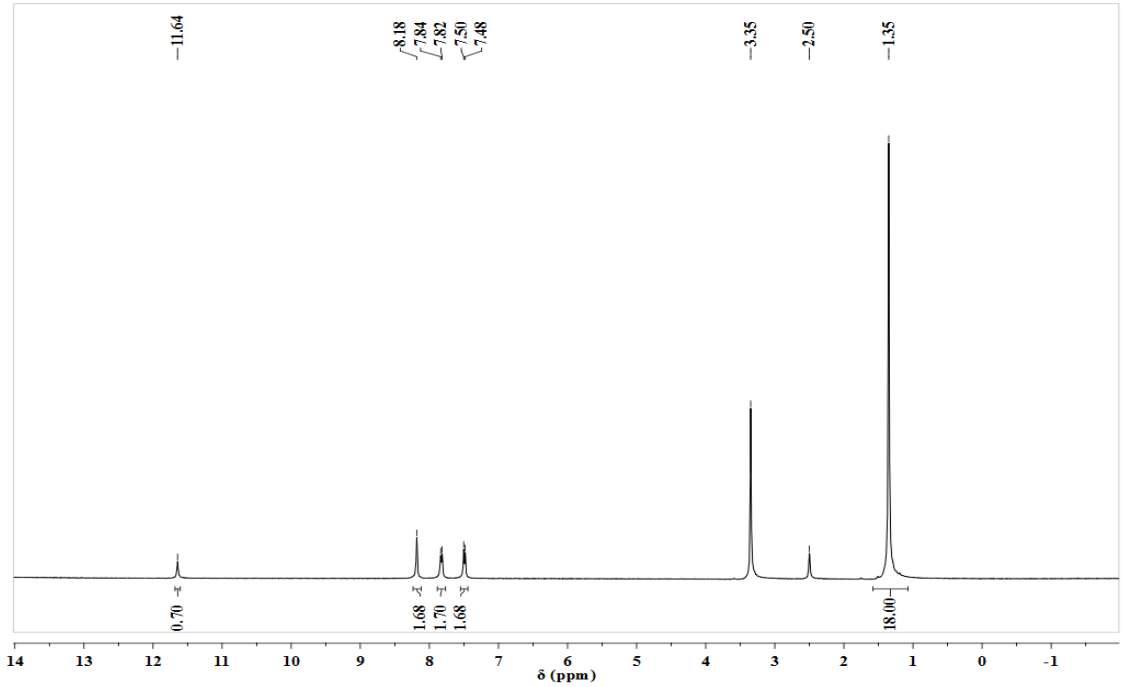

Figure 2.7. ^{1}H NMR spectrum of 2,7-di-*tert*-butylacridin-9(10*H*)-one in DMSO-d_6 solution.

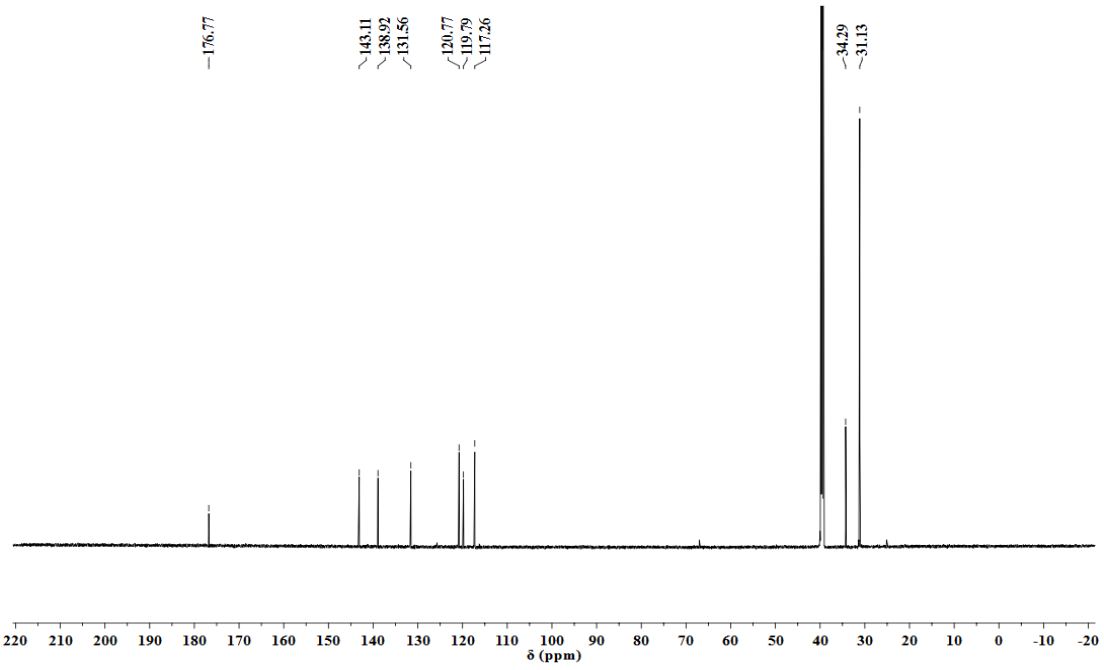

Figure 2.8. ^{13}C NMR spectrum of 2,7-di-*tert*-butylacridin-9(10*H*)-one in DMSO-d_6 solution.

2.4.3.2 2,7-Di-*tert*-butyl-*N*-deuteroacridone

To 2,7-di-*tert*-butylacridin-9(10*H*)-one (0.015 g, 0.048 mmol) in a 50-mL Schlenk flask was added THF (2 mL) followed by sodium hydride (0.006 g, 0.25 mmol) and the mixture brought to stir at 80°C for 6 hours. The greenish-yellow fluorescent solution was quenched with 1 mL of D_2O, then extracted with CH_2Cl_2 (2 mL). The organic mixture was dried using anhydrous $MgSO_4$ then filtered over Celite. The solvent was removed under vacuum to give a yellow solid quantitatively. ^{1}H NMR (400 MHz, DMSO): δ (ppm) 8.12 (d, *J* = 2.9 Hz, 2H), 7.41 (d, *J* = 2.4 Hz, 4H), 1.34 (s, 18H).

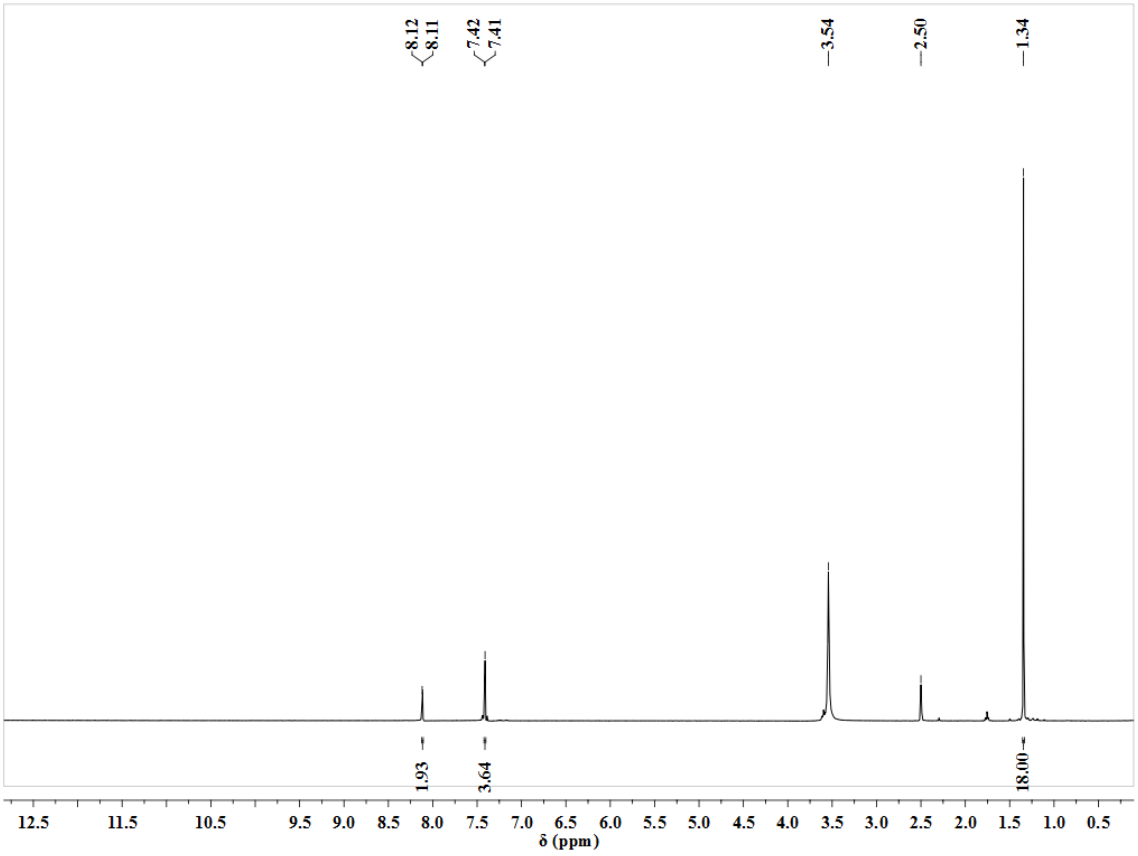

Figure 2.9. ^{1}H NMR spectrum of 2,7-di-*tert*-butyl-*N*-deuteroacridone in DMSO-d_6 solution.

2.4.3.3 4,5-Dibromo-2,7-di-*tert*-butylacridin-9(10*H*)-one

In a 100-mL Schlenk flask, 2,7-di-*tert*-butylacridin-9(10*H*)-one (0.120 g, 0.390 mmol) was dissolved in acetic acid (12 mL). To this yellow solution was added bromine (0.07 mL, 1 mmol) forming a brown solution. It was brought to stir at 81 °C for 24 hours forming a bright yellow suspension. The suspension was cooled in an ice bath before filtering. It was washed with chilled methanol (3 x 5 mL) and air-dried to give light yellow solid (0.177 g, 97%). ^{1}H NMR (400 MHz, CD_2Cl_2): δ (ppm) 10.90 (s, 1H, N*H*), 8.94 (s, 2H, Ar*H*), 8.46 (s, 2H, meta-Ar*H*), 1.49 (s, 18H, C(C*H*$_3$)$_3$).

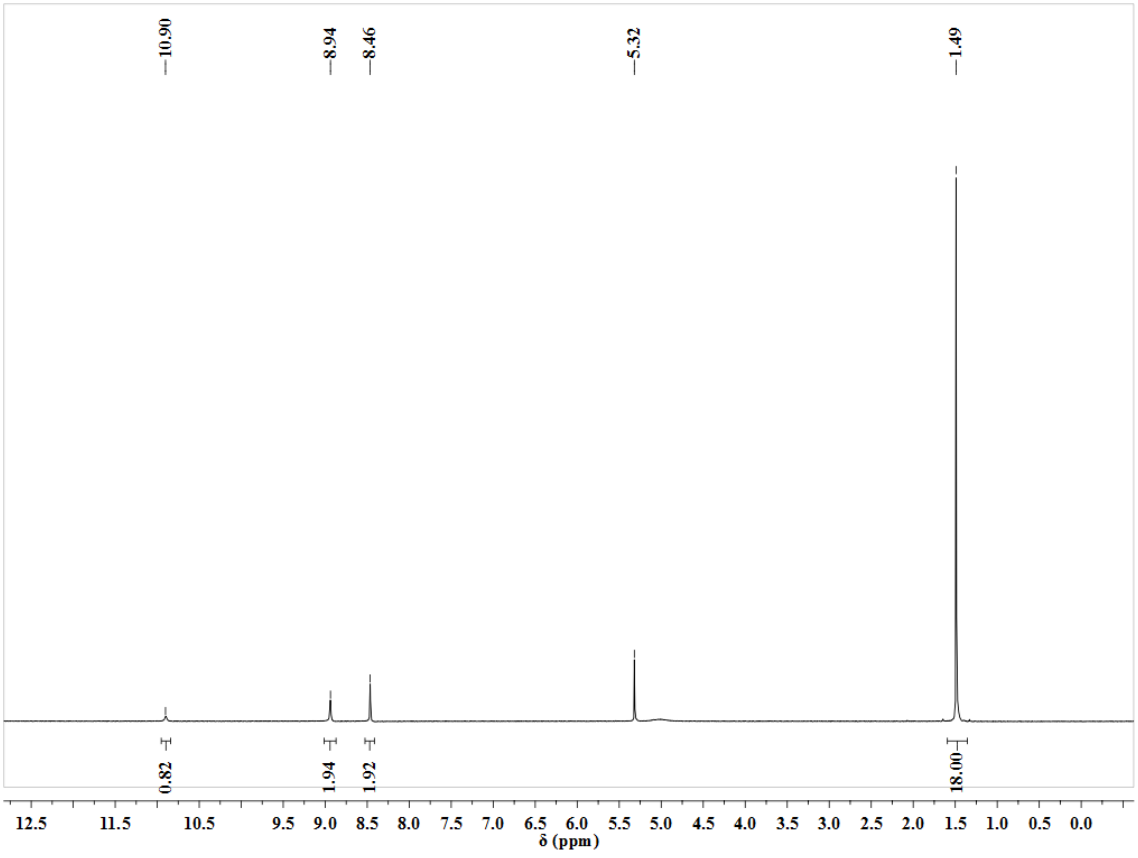

Figure 2.10. ^{1}H NMR spectrum of 4,5-dibromo-2,7-di-*tert*-butylacridin-9(10*H*)-one in CD_2Cl_2 solution.

2.4.3.4 4,5-Di-bromo-2,7-di-*tert*-butyl-9-chloroacridine

To a 500 mL Schlenk flask was added (0.525 g, 1.12 mmol) of 4,5-dibromo-2,7-di-*tert*-butylacridin-9(10*H*)-one. To this, 100 mL of thionyl chloride was added. This yellow solution was brought to stir at 72 ^{o}C for 12 hours after which the solvent was removed under vacuum. The yellow crude solid was taken up in 75 mL of dichloromethane after which it was sequentially washed with 5% ice-cold sodium hydroxide (3 x 20 mL) followed by 20 mL of water. The combined aqueous layers were extracted one more time with 10 mL of CH_2Cl_2. The combined organic phases were dried using anhydrous $MgSO_4$ and filtered over Celite. The solvent was removed under vacuum, leaving a yellow solid. This was washed with cold methanol and the solid filtered and dried under vacuum to give a faint yellow solid (0.536 g, 99%). ^{1}H NMR (400 MHz, $CDCl_3$) δ (ppm) 8.28 (dd, *J* = 7.5, 2.0 Hz, 4H), 1.48 (s, 18H). Anal. Calcd for $C_{21}H_{22}Br_2ClN$: C, 52.15; H, 4.58; N, 2.90. Found: C, 51.33; H, 4.46; N, 2.91.

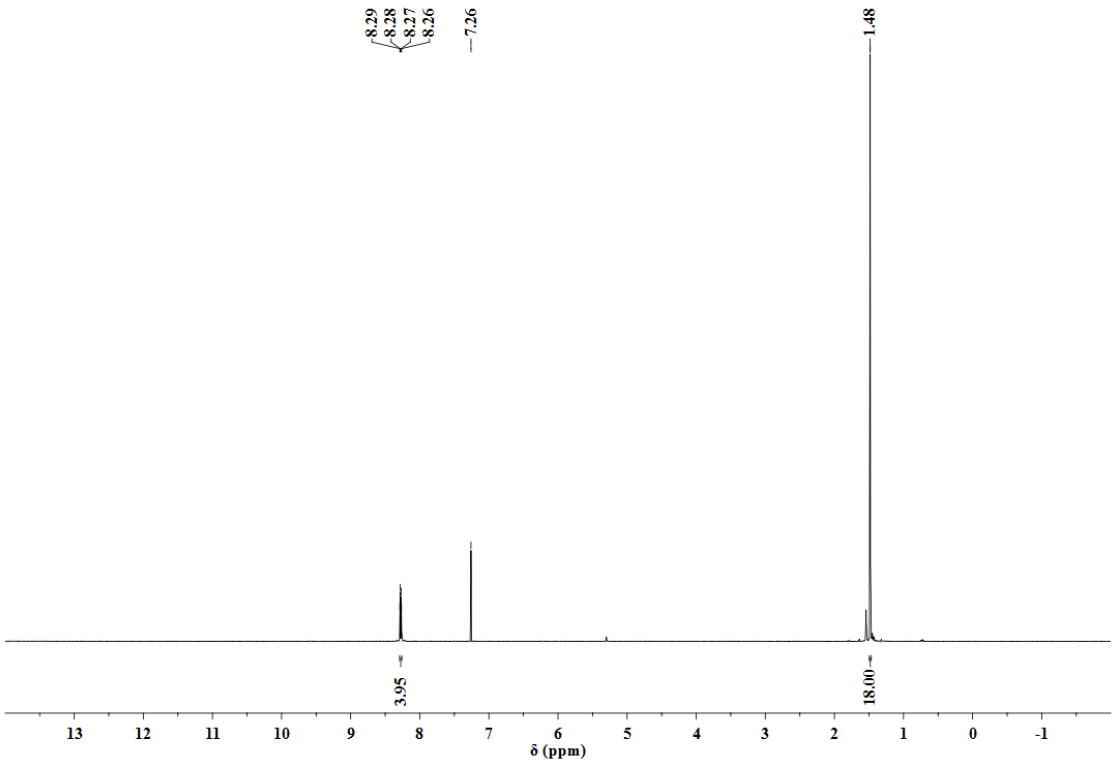

Figure 2.11. ^{1}H NMR spectrum of 4,5-dibromo-2,7-di-*tert*-butyl-9-chloroacridine in $CDCl_3$ solution.

2.4.3.5 2,7-Di-*tert*-butyl-4,5-dicarboxaldehyde-9-chloroacridine

In a 250-mL Schlenk flask was added (0.32 g, 0.66 mmol) of 4,5-dibromo-2,7-di-*tert*-butyl-9-chloroacridine followed by 18 mL of dry and degassed THF. This solution was cooled to 0 °C and *n*-BuLi (2.5 M, 0.5 mL, 1.32 mmol) was added dropwise while stirring. After complete addition, the brown solution was kept at this temperature for 1 hour. It was then cooled to -70 °C, after which (0.4 mL, 4 equiv.) of dry DMF was added with stirring. It was left to warm up to room temperature overnight. The reaction mixture was then cooled to 0 °C, then hydrolyzed using (5mL) of 1M HCl. The light brown solution was diluted with 40 mL of ethyl acetate. It was washed with 2 x 25 mL of 1M NaOH followed by 2 x 25 mL of 1M $NaHCO_3$. The combined aqueous layers were

extracted again with 10 mL of ethyl acetate. The combined organic layer was dried using anhydrous $MgSO_4$, filtered over Celite and solvent removed under vacuum to give a yellowish orange crude product. This was washed with hot hexanes to give an orange solid (0.0921 g, 36%). ^{1}H NMR (300 MHz, $CDCl_3$) δ (ppm) 11.61 (s, 2H), 8.62 (s, 4H), 1.53 (s, 18H).

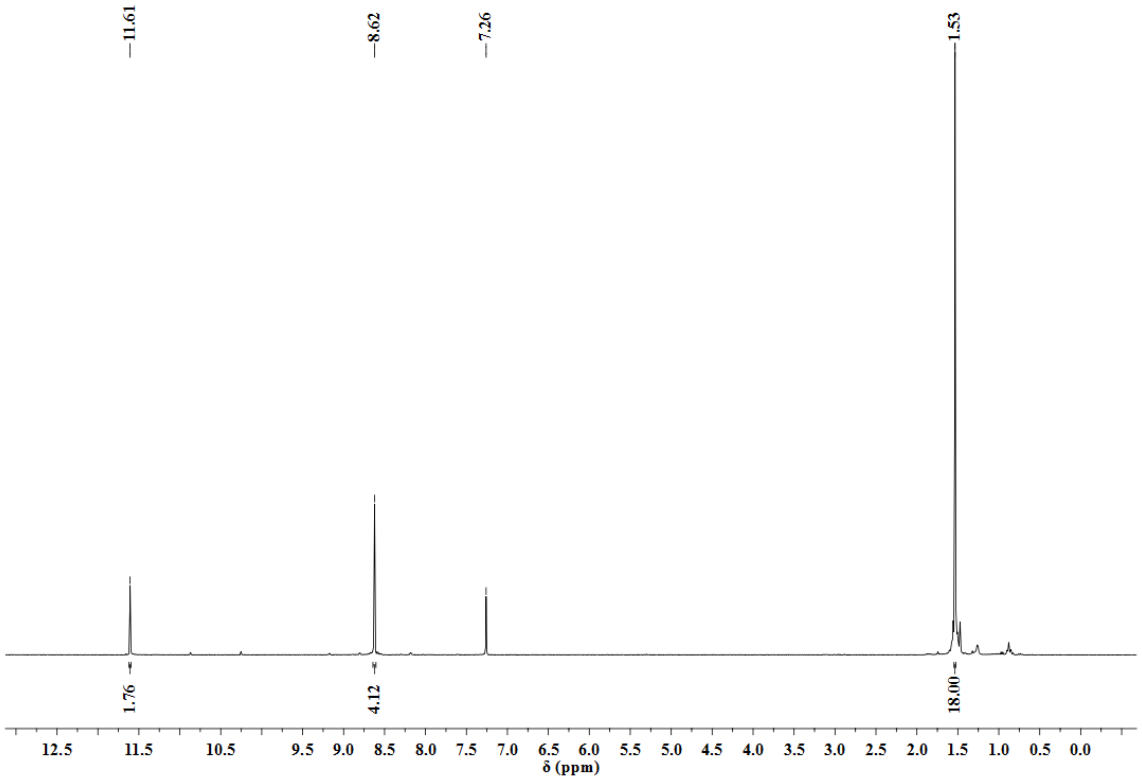

Figure 2.12. ^{1}H NMR spectrum of 2,7-di-*tert*-butyl-4,5-dicarboxaldehyde-9-chloroacridine in $CDCl_3$ solution.

2.4.3.6 4,5-Di-*p*-tolyl-2,7-di-*tert*-butylacridin-9(10*H*)-one

To a 250-mL Schlenk flask were added 4,5-dibromo-2,7-di-*tert*-butylacridin-9(10*H*)-one (0.860 g, 1.85 mmol) and tetrakis(triphenylphosphine)palladium(0) (0.426 g, 0.369 mmol). The flask was evacuated and refilled with argon and the cycle repeated 2 more times. To the stirred mixture was added toluene (100 mL). A solution of *p*-tolylboronic acid (3.78 g, 27.8 mmol) in 22 mL of ethanol was added to the mixture followed by 28 mL of 1 M aqueous sodium carbonate solution. The mixture was then degassed in several cycles before refilling with argon. It was then set to stir at 80 °C for 48 hours. The purple solution was filtered hot, and the filtrate washed with 1M NaOH (2 x 72 mL) followed by 2 x 72 mL of water. The organic layer was dried using anhydrous $MgSO_4$, filtered over Celite and the volatiles removed under vacuum. The crude solid was washed with 10 mL of hot ethanol, filtered and dried to give greenish-yellow solid (0.620 g, 68%). ^{1}H NMR (400 MHz, C_6D_6): δ (ppm) 9.10 (d, 2H, Ar*H*), 8.31 (s, 1H, N*H*), 7.64 (d, 2H, meta-Ar*H*), 6.95 (d, 4H, tol-Ar*H*), 6.84 (d, 4H, tol-Ar*H*), 2.14 (s, tol-C*H*$_3$, 6H), 1.28 (s, 18H, C(C*H*$_3$)$_3$). ^{13}C{^{1}H} NMR (176 MHz, C6D6): δ (ppm) 178.08 (s, C=O), 143.94 (s), 136.97 (s), 135.98 (s), 134.30 (s), 131.01 (s), 129.66 (s), 129.05 (s), 127.98 (s), 127.94 (s), 127.62 (s), 122.79 (s), 121.54 (s), 34.37 (s), 31.12 (s), 20.74 (s). Anal. Calcd for $C_{35}H_{37}NO$: C, 86.20; H, 7.65; N, 2.87. Found: C, 83.94; H, 7.63; N, 2.80.

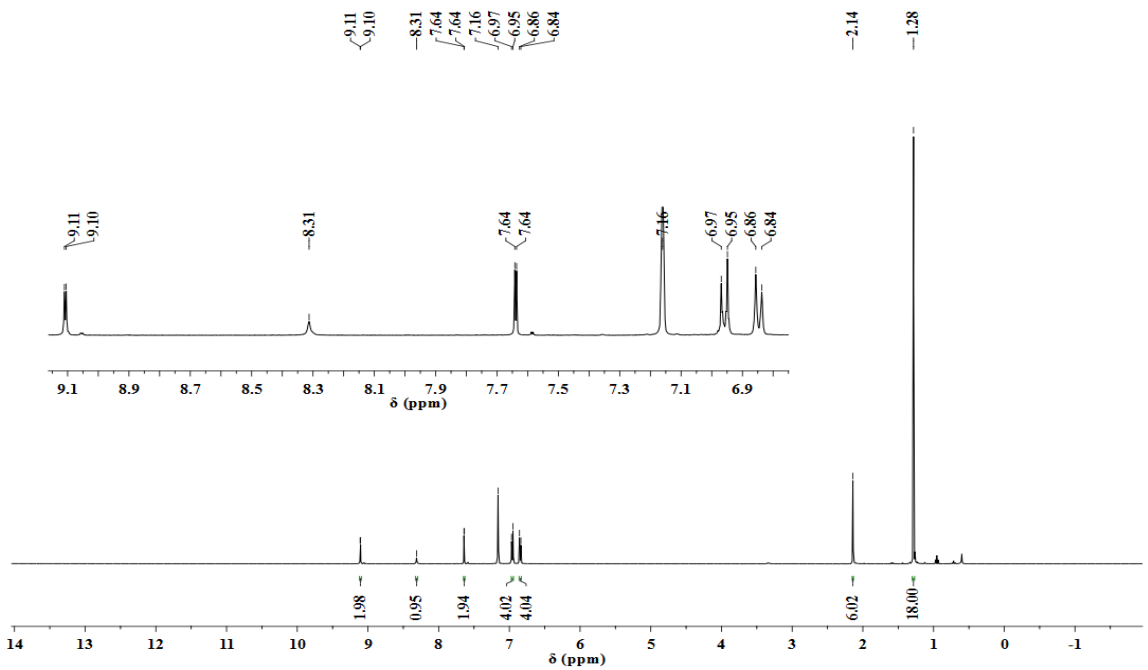

Figure 2.13. ^{1}H NMR spectrum of 4,5-di-*p*-tolyl-2,7-di-*tert*-butylacridin-9(10*H*)-one in C_6D_6 solution.

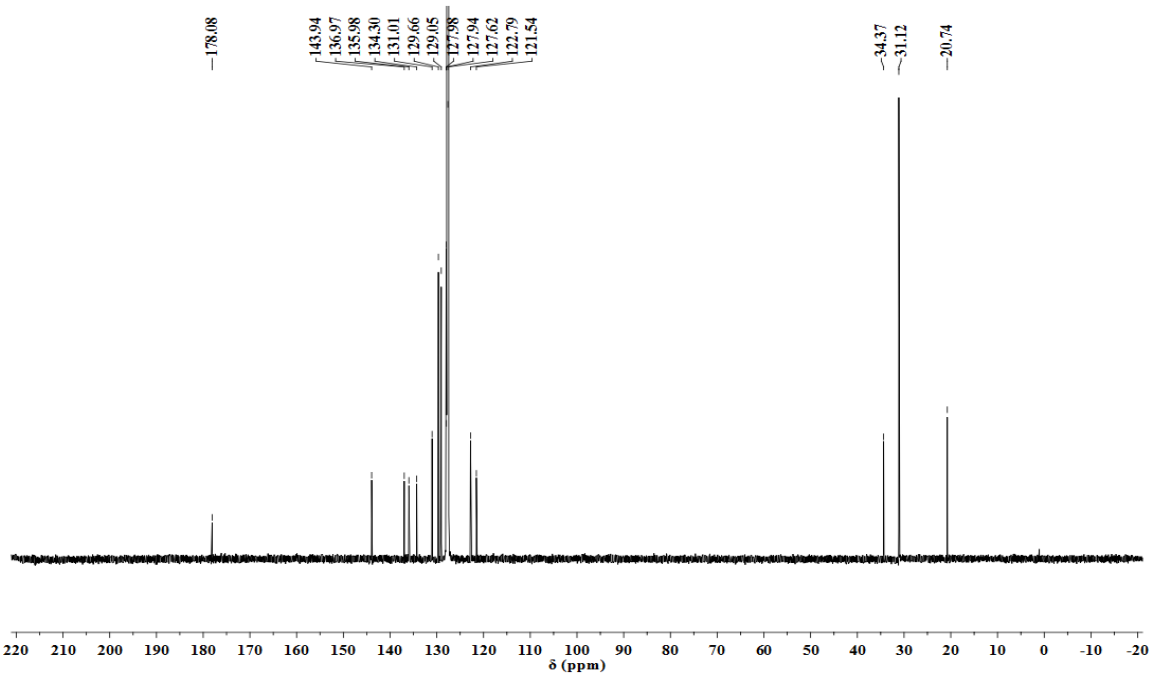

Figure 2.14. ^{13}C NMR spectrum of 4,5-di-*p*-tolyl-2,7-di-*tert*-butylacridin-9(10*H*)-one in C_6D_6 solution.

Deprotonation of 4,5-di-*p*-tolyl-2,7-di-*tert*-butylacridin-9(10*H*)-one and subsequent quenching with D_2O gave the following data. ^{1}H NMR (400 MHz, C_6D_6): δ (ppm) 9.10 (d, 2H, Ar*H*), 7.64 (d, 2H, meta-Ar*H*), 6.95 (d, 4H, tol-Ar*H*), 6.83 (d, 4H, tol-Ar*H*), 2.14 (s, tol-CH_3, 6H), 1.28 (s, 18H, C(CH_3)$_3$).

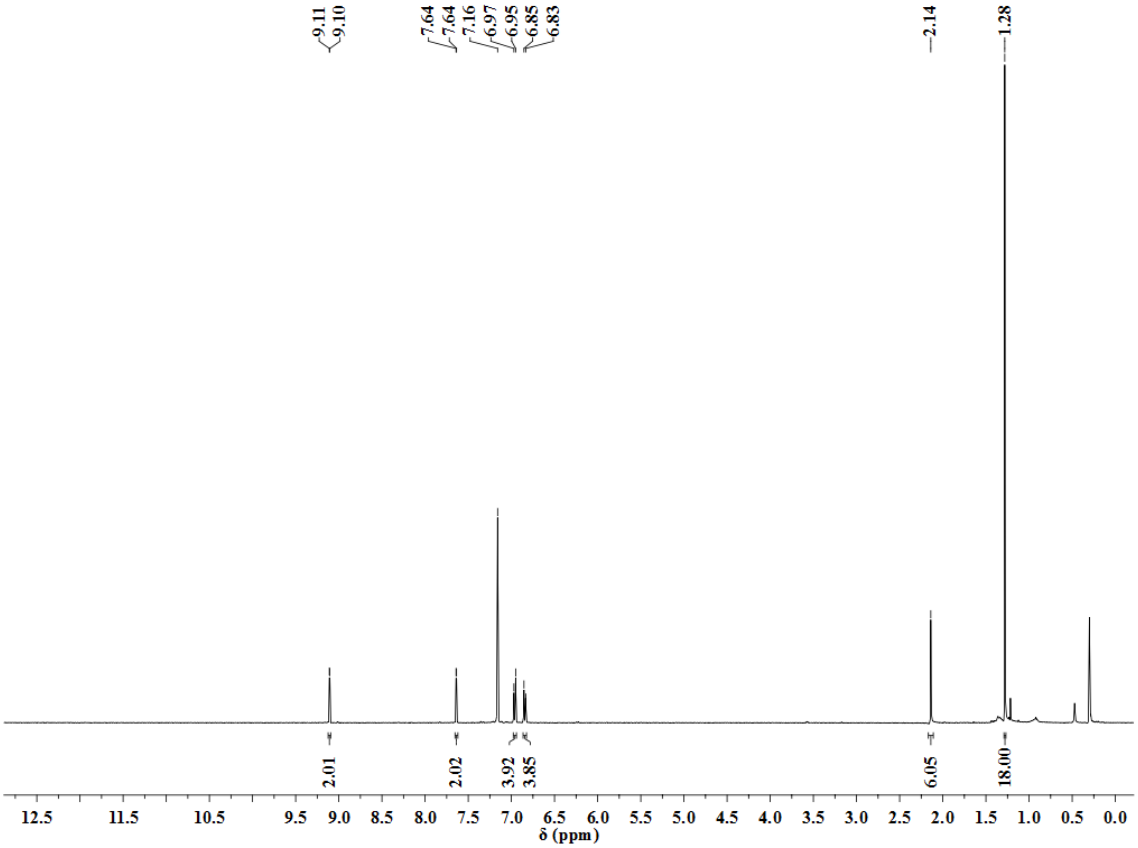

Figure 2.15. ^{1}H NMR spectrum of 4,5-di-*p*-tolyl-2,7-di-*tert*-butylacridin-9(10-*deutero*)-one in C_6D_6 solution.

2.4.3.7 4,5-Di-*p*-tolyl-2,7-di-*tert*-butyl-9-chloroacridine

To a 20-mL vial was added 4,5-di-*p*-tolyl-2,7-di-*tert*-butylacridin-9(10*H*)-one (0.05 g, 0.10 mmol). To this was added 3 mL chloroform, 0.25 mL DMF and 0.24 mL thionyl chloride. This yellow solution was brought to stir at 62 °C for 5 hours after which

the solvent was removed under vacuum. The yellow crude solid was taken up in 2.5 mL of dichloromethane after which it was sequentially washed with 5% ice-cold sodium hydroxide (2 x 2 mL) followed by 2.5 mL of water. The combined aqueous layers were extracted one more time with 2 mL of CH_2Cl_2. The combined organic phases were dried using anhydrous $MgSO_4$ and filtered over Celite. The solvent was removed under vacuum leaving behind a yellow-brown solid. This was washed with cold methanol and the solid filtered and dried under vacuum to give product as a light yellow-brown solid. (0.049 g, 96%). ^{1}H NMR (300 MHz, CD_2Cl_2) δ (ppm) 8.36 (d, *J* = 2.2 Hz, 2H), 7.91 (d, *J* = 2.2 Hz, 2H), 7.57 (d, *J* = 8.0 Hz, 4H), 7.19 (d, *J* = 8.4 Hz, 4H), 2.44 (s, 6H), 1.52 (s, 18H).

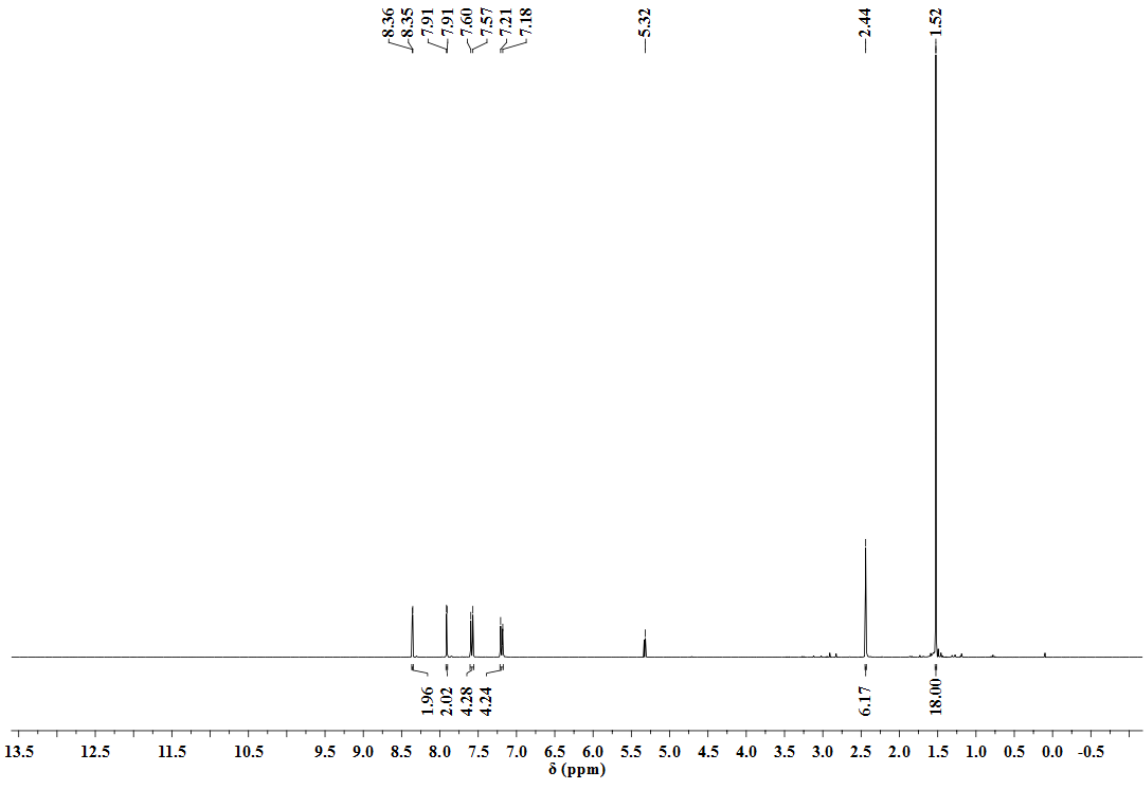

Figure 2.16. ^{1}H NMR spectrum of 4,5-di-*p*-tolyl-2,7-di-*tert*-butyl-9-chloroacridine in CD_2Cl_2 solution.

2.4.3.8 4,5-Dimorpholino-2,7-di-*tert*-butylacridin-9(10*H*)-one

To a 100-mL Schlenk flask under argon was added 4,5-dibromo-2,7-di-*tert*-butylacridin-9(10*H*)-one (0.926 g, 1.99 mmol), morpholine (1.4 mL, 16 mmol), Cs_2CO_3 (1.578g, 4.8 mmol), Pd_2dba_3 (0.282g, 15 mol%), and $P(^tBu)_3$ (75 µL, 15 mol%). To this flask was added 20 mL of dry and degassed toluene after which the mixture was brought to stir at 110 ^oC for 24 h. After cooling down to room temperature, the mixture was washed with 2 x 10 mL of water followed by 10 mL of NaCl solution. The layers were separated, and the aqueous layer was extracted with 15 mL of CH_2Cl_2, which was combined with the organic layer. The combined organic layers were dried using anhydrous $MgSO_4$ and filtered over Celite. The solvent was removed under vacuum. To the crude product was added 2 mL of hot methanol, and the resulting mixture was set to stand at room temperature overnight to recrystallize. The white solid formed was filtered and dried under vacuum to give product as an off-white solid (0.531 g, 56%). ^1H NMR (400 MHz, $CDCl_3$): δ (ppm) 9.78 (s, 1H, N*H*), 8.27 (d, *J* = 2.1 Hz, 2H, Ar*H*), 7.57 (d, *J* = 2.1 Hz, 2H, Ar*H*), 4.04 (s, 8H, morpholino-CH_2), 3.05 (s, 8H, morpholino-CH_2), 1.41 (s, 18H, C(CH_3)$_3$). $^{13}C\{^1H\}$ NMR (176 MHz, CD_2Cl_2): δ (ppm) 178.35 (C=O), 144.03 (s), 140.33 (s), 133.83 (s), 122.49 (s), 121.27 (s), 118.42 (s), 67.91 (s), 53.09 (s), 34.87 (s), 31.20 (s). Anal. Calcd for $C_{29}H_{39}N_3O_3$: C, 72.92; H, 8.23; N, 8.80. Found: C, 71.58; H, 8.00; N, 8.26. ESI-MS (+): 478.3 $[M+H]^+$.

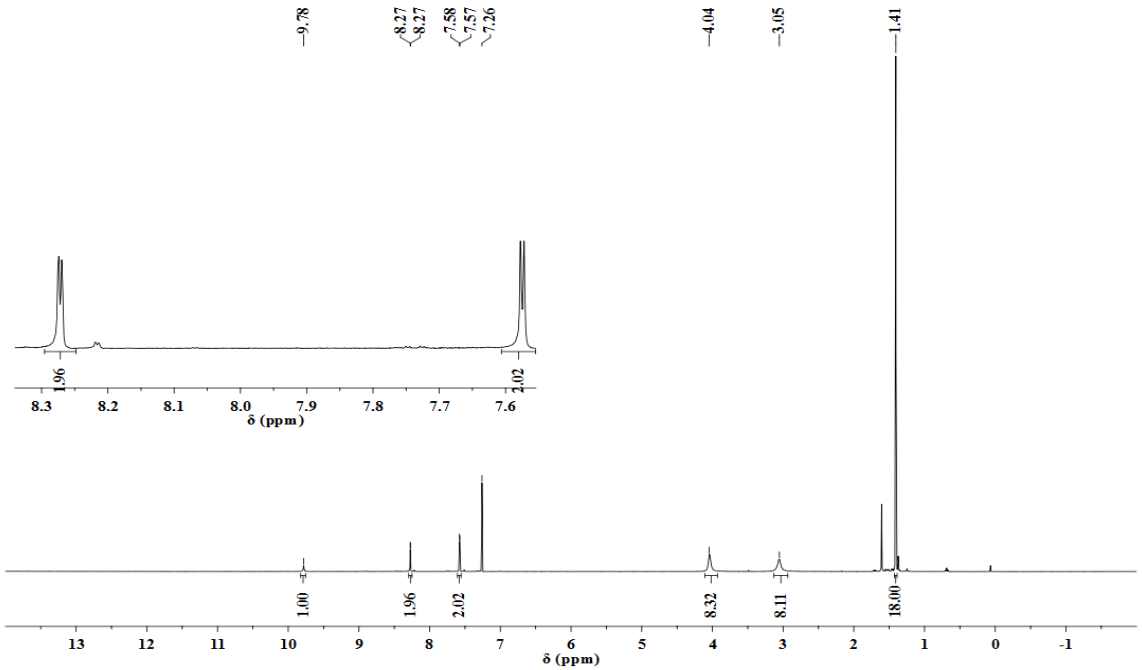

Figure 2.17. ^{1}H NMR spectrum of 4,5-dimorpholino-2,7-di-*tert*-butylacridin-9(10*H*)-one in $CDCl_3$ solution.

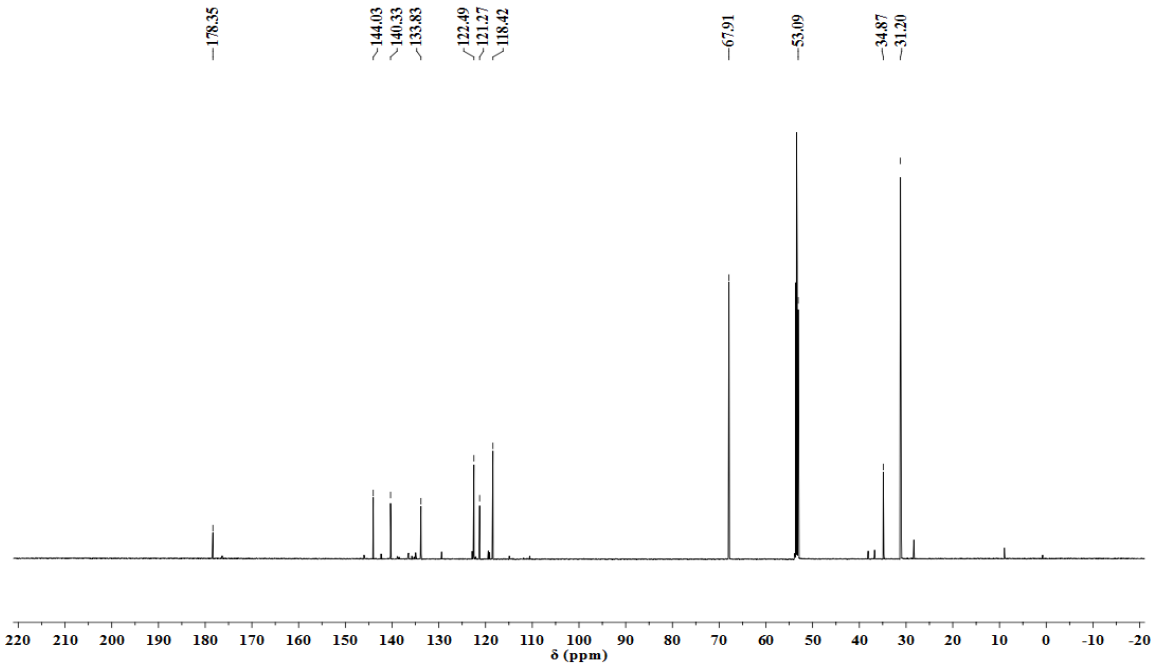

Figure 2.18. ^{13}C NMR spectrum of 4,5-dimorpholino-2,7-di-*tert*-butylacridin-9(10*H*)-one in CD_2Cl_2 solution.

2.4.3.9 2,7-Di-*tert*-butyl-4,5-bis(diphenylmethyleneamino)acridin-9(10*H*)-one

To a 250-mL Schlenk flask under argon was added 4,5-dibromo-2,7-di-*tert*-butylacridin-9(10*H*)-one (1.20 g, 2.58 mmol), benzophenone-imine (0.95 mL, 5.67 mmol), Pd_2dba_3 (0.709 g, 30 mol%), *rac*-BINAP (0.482 g, 30 mol%) and NaO^tBu (0.992 g, 10.32 mmol). To this flask was added 50 mL of dry and degassed toluene, and the resulting mixture was stirred at 105 °C for 24 h. It was then cooled down to room temperature and washed with 2 x 10 mL of water. The combined aqueous layers were extracted with 10 mL of diethyl ether. The combined organics were dried using anhydrous $MgSO_4$ then filtered over Celite to give a greenish-brown solution. The solvent was removed under vacuum to give an oily brown crude product. To this was added hot methanol then cooled down, filtered off and dried under vacuum to give the product as orange solid (1.388 g, 81%). ^{1}H NMR (400 MHz, CD_2Cl_2): δ (ppm) 9.63 (s, 1H, N*H*), 8.03 (s, 2H, acridone-Ar*H*), 7.80 (d, *J* = 7.6 Hz, 2H, bz-imine-Ar*H*), 7.43 (t, *J* = 7.6 Hz, 2H, bz-imine-Ar*H*), 7.35 (d, *J* = 4.0 Hz, 6H, bz-imine-Ar*H*), 7.23 – 7.18 (m, 8H), 6.73 (s, 2H, acridone-Ar*H*), 1.08 (s, 18H, $C(CH_3)_3$). $^{13}C\{^1H\}$ NMR (176 MHz, CD_2Cl_2): δ (ppm) 177.96 (C=O), 169.91 (C=N), 143.12 (s), 138.90 (s), 137.08 (s), 136.05 (s), 133.52 (s), 131.00 (s), 129.10 (s), 129.02 (s), 128.82 (s), 128.54 (s), 128.31 (s), 121.90 (s), 121.06 (s), 117.90 (s), 34.31 (s), 30.81 (s). Anal. Calcd for $C_{47}H_{43}N_3O$: C, 84.78; H, 6.51; N, 6.31. Found: C, 83.58; H, 6.67; N, 6.07. ESI-MS (+): 666.3 $[M+H]^+$.

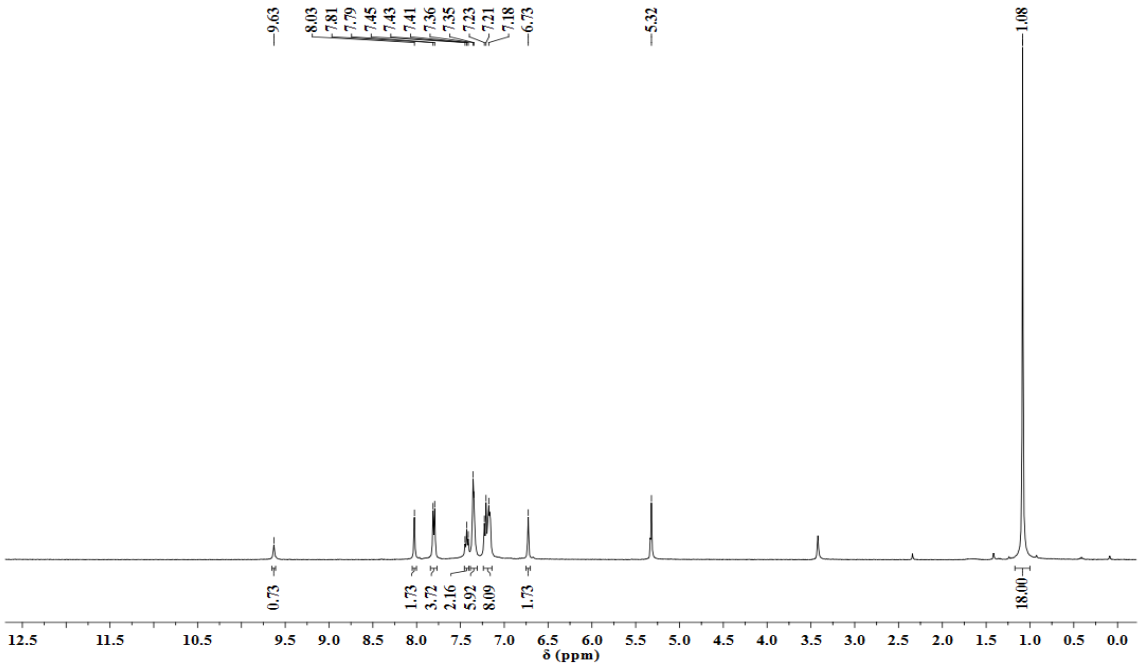

Figure 2.19. ^{1}H NMR spectrum of 4,5-bis(diphenylmethyleneamino)-2,7-di-*tert*-butylacridin-9(10*H*)-one in CD_2Cl_2 solution.

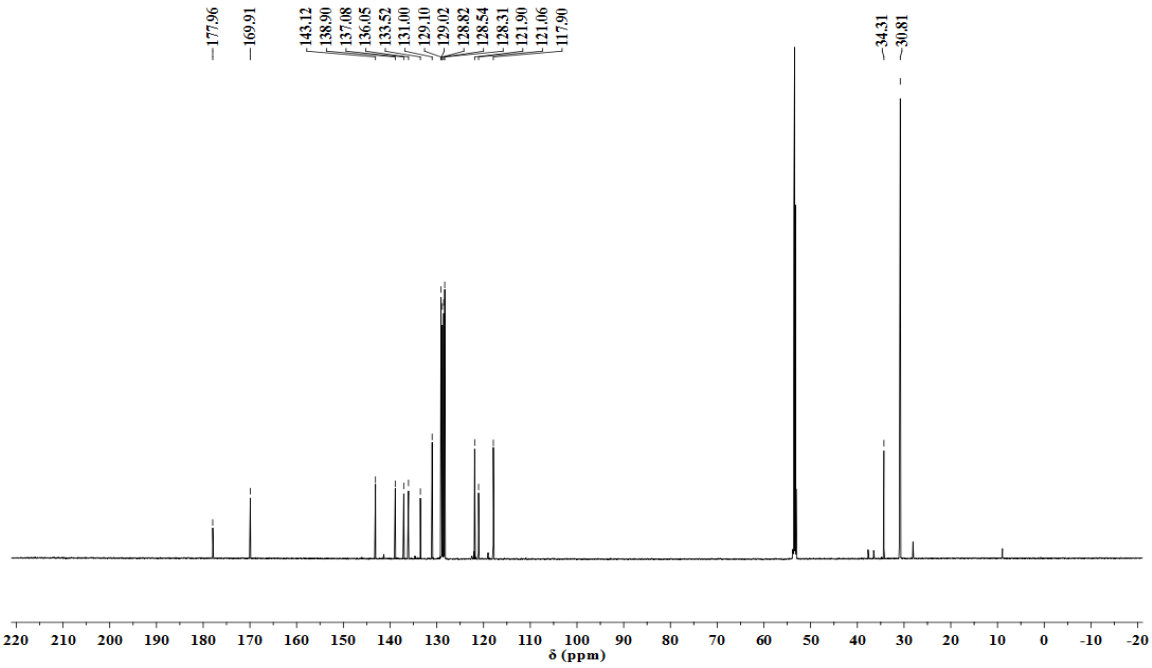

Figure 2.20. ^{13}C NMR spectrum of 4,5-bis(diphenylmethyleneamino)-2,7-di-*tert*-butylacridin-9(10*H*)-one in CD_2Cl_2 solution.

2.4.3.10 [4,5-Bis(diphenylmethyleneamino)-2,7-di-*tert*-butylacridonato]palladium(II) acetate

To a 50-mL Schlenk flask under argon was added 4,5-bis(diphenylmethyleneamino)-2,7-di-*tert*-butylacridin-9(10*H*)-one (0.02 g, 0.03 mmol) together with $Pd(OAc)_2$ (0.007 g, 0.033 mmol) followed by 2 mL of dry toluene. The mixture was brought to stir at reflux for 12 hours leading to a greenish-brown solution. The solvent is removed under vacuum and the product analyzed by ^{1}H NMR (400 MHz, CD_2Cl_2) δ (ppm) 10.14 (s, 1H), 8.17 (d, *J* = 2.0 Hz, 2H), 7.65 (d, *J* = 8 Hz, 2H), 7.55 (t, *J* = 4 Hz, 2H), 7.37 (tt, *J* = 7.6, 1.2 Hz, 2H), 7.23-6.98 (m, 16H), 6.62 (d, *J* = 8 Hz, 2H), 2.31 (s, 3H), 1.95 (s, 3H), 1.11 (s, 18H).

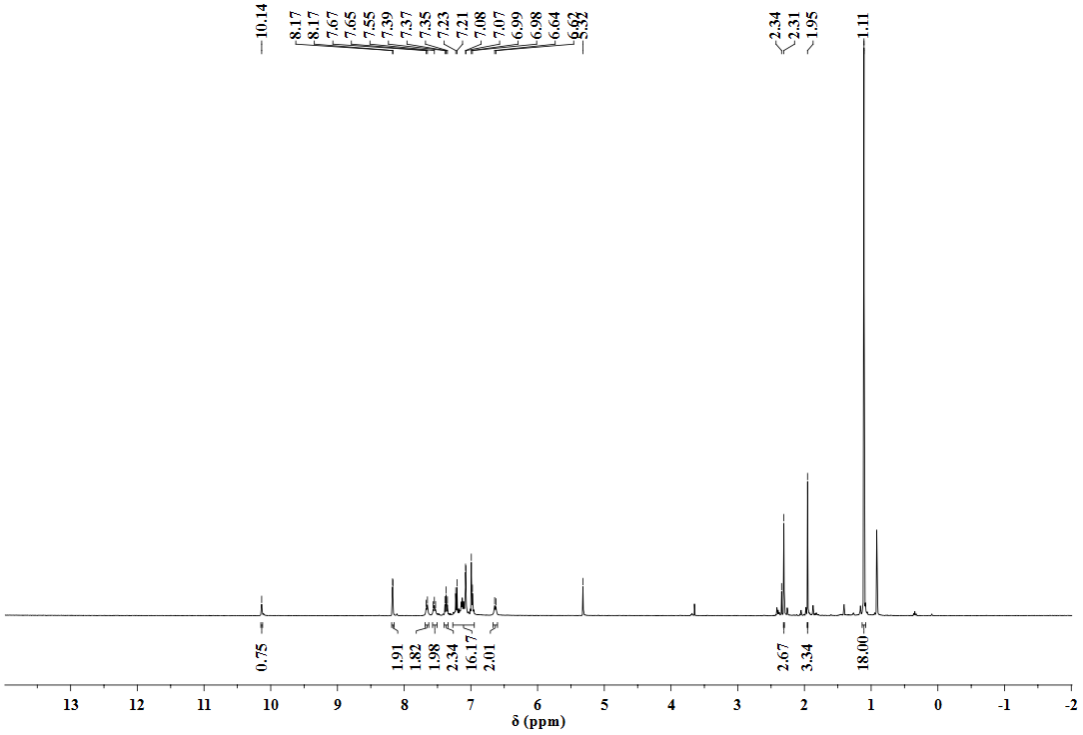

Figure 2.21. ^{1}H NMR spectrum of [4,5-bis(diphenylmethyleneamino)-2,7-di-*tert*-butyl-acridonato]palladium(II) acetate complex in CD_2Cl_2 solution.

2.4.3.11 [4,5-Bis(diphenylmethyleneamino)-2,7-di-*tert*-butylacridonato] dimethylaluminum

To a solution of 4,5-bis(diphenylmethyleneamino)-2,7-di-*tert*-butylacridin-9(10*H*)-one (10 mg, 0.015 mmol) in toluene at 0 °C was added Me_3Al (8 µL, 0.02 mmol) dropwise while stirring. The resulting mixture was stirred at this temperature for 1 hour, then allowed to warm to room temperature for 20 min. Solvent was removed under vacuum, leaving behind a red solid. ^{1}H NMR (400 MHz, CD_2Cl_2) δ (ppm) 8.33 (d, *J* = 1.9 Hz, 2H), 7.60 – 7.55 (m, 6H), 7.46 (d, *J* = 7.3 Hz, 2H), 7.42 – 7.37 (m, 8H), 7.23 (d, *J* = 1.9 Hz, 2H), 7.21 (d, *J* = 6.9 Hz, 4H), 1.08 (s, 18H), -0.93 (s, 6H), -0.94 (s, 10H).

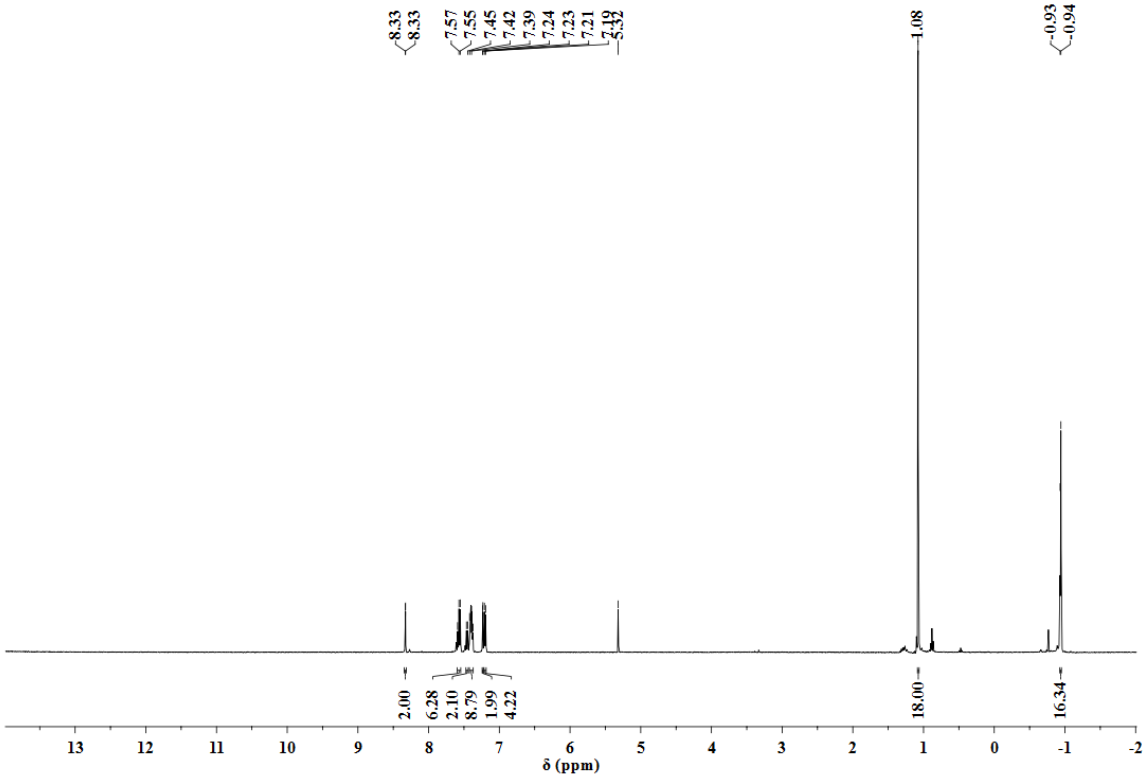

Figure 2.22. ^{1}H NMR spectrum of [4,5-bis(diphenylmethyleneamino)-2,7-di-*tert*-butyl-acridonato]dimethylaluminum complex in CD_2Cl_2 solution.

2.4.4 X-ray Diffraction Studies

A suitable crystal of complex **10** from a DCM solution layered with Et_2O and kept at -35 °C was selected and mounted on a loop on Bruker APEX-II CCD diffractometer using paratone oil. The crystal was kept at 100(2) K during data collection. Using Olex2,[77] the structure was solved with XT[78] structure solution program using Intrinsic Phasing and refined with XL[79] refinement package using Least Squares minimisation.

Crystal Data for $C_{47}H_{43}N_3O$ (*M* =665.84 g/mol), (**10**): monoclinic, space group $P2_1/n$ (no. 14), *a* = 12.8604(14) Å, *b* = 18.361(2) Å, *c* = 15.7943(17) Å, *β* = 106.9562(14)°, *V* = 3567.5(7) Å^3, *Z* = 4, *T* = 100(2) K, μ(MoKα) = 0.074 mm^{-1}, *Dcalc* = 1.240 g/cm^3, 62939 reflections measured (3.492° ≤ 2Θ ≤ 61.06°), 10881 unique (R_{int} = 0.0700, R_{sigma} = 0.0497) which were used in all calculations. The final R_1 was 0.0622 (I > 2σ(I)) and wR_2 was 0.1774 (all data).

A suitable single yellow prism-shaped crystals of complex **11** was selected from a THF solution layered with hexanes at -35 ^oC. The crystal with dimensions 0.25×0.10×0.10 mm^3 was mounted on a loop on a Saxi-CrysAlisPro-abstract goniometer imported SAXI images diffractometer using paratone oil. The crystal was kept at a steady *T*= 100(2) K during data collection.

Data were measured using *w* scans using MoK_a radiation. The total number of runs and images was based on the strategy calculation from the program CrysAlisPro.[77] The maximum resolution that was achieved was *Q* = 24.713° (0.85 Å). Data reduction, scaling and absorption corrections were performed using CrysAlisPro (Rigaku, V1.171.38.41, 2015). The final completeness was 100.00 % out to 24.713° in *Q*. The absorption coefficient

m of this material is 0.077 mm^{-1} at this wavelength (*l* = 0.711Å) and the minimum and maximum transmissions are 0.873 and 1.000.

The structure was solved in the space group $P2_1/c$ (# 14) by the XT using Olex2 as the graphical interface,[77] the structure was solved with XT[78] structure solution program using Intrinsic Phasing solution method and refined with XL[79] refinement package using Least Squares minimisation. All non-hydrogen atoms were refined anisotropically. Hydrogen atom positions were calculated geometrically and refined using the riding model.

Crystal Data. $C_{29}H_{39}N_3O_3$, M_r = 477.63, monoclinic, $P2_1/c$ (No. 14), a = 8.1922(9) Å, b = 22.935(3) Å, c = 14.2034(16) Å, b = 94.712(10)°, a = g = 90°, V = 2659.6(5) $Å^3$, T = 100(2) K, Z = 4, Z' = 1, $m(MoK_a)$ = 0.077 mm^{-1}, 14008 reflections measured, 4540 unique (R_{int} = 0.1711) which were used in all calculations. The final wR_2 was 0.1717 (all data) and R_1 was 0.0966 ($I > 2\sigma(I)$).

2.5 REFERENCES

1. Hope, H.; Olmstead, M. M.; Murray, B. D.; Power, P. P., Syntheses and x-ray structures of the lithium, nickel, and cobalt complexes $[Li(THF)_4][Ni(NPh_2)_3].0.5\ C_7H_8$,$[\{Ni(NPh_2)_2\}_2]$ and $[\{Co(NPh_2)_2\}_2]$: structural characterization of three coordinate first row d^7 and d^8 complexes. *J. Am. Chem. Soc.* **1985,** *107*, 712-713.

2. Olmstead, M. M.; Power, P. P.; Shoner, S. C., Three-coordinate iron complexes: x-ray structural characterization of the iron amide-bridged dimers $[Fe(NR_2)_2]_2$ (R= $SiMe_3$, C_6H_5) and the adduct $Fe[N(SiMe_3)_2]_2(THF)$ and determination of the association energy of the monomer $Fe\{N(SiMe_3)_2\}_2$ in solution. *Inorg. Chem.* **1991,** *30*, 2547-2551.

3. Jilles, J.; Wilberth, J., Chromium (II) amides: synthesis and structures. *J. Chem. Soc., Dalton Trans.* **1993,** 789-797.

4. Murray, B. D.; Power, P. P., Three-coordinate metal amides of manganese (II) and cobalt(II): synthesis and x-ray structure of the first tris (silylamide) of manganese and the x-ray crystal structures of $[M_2(N(SiMe_3)_2)_4]$(M= Mn, Co). *Inorg. Chem.* **1984,** *23*, 4584-4588.

5. Bradley, D. C.; Hursthouse, M. B.; Abdul Malik, K.; Möseler, R., The crystal molecular structure of "bis (hexamethyldisilylamido) manganese". *Transit. Metal Chem.* **1978,** *3*, 253-254.

6. Power, P. P., Some highlights from the development and use of bulky monodentate ligands. *J. Organomet. Chem.* **2004,** *689*, 3904-3919.

7. Eller, P.; Bradley, D.; Hursthouse, M.; Meek, D., Three coordination in metal complexes. *Coord. Chem. Rev.* **1977,** *24*, 1-95.

8. Bradley, D. C.; Chisholm, M. H., Transition-metal dialkylamides and disilylamides. *Acc. Chem. Res.*. **1976,** *9*, 273-280.

9. Chen, H.; Bartlett, R. A.; Olmstead, M. M.; Power, P. P.; Shoner, S. C., Series of two-coordinate and quasi-two-coordinate transition-metal complexes: synthesis, structural, and spectroscopic studies of sterically demanding borylamide ligands-NRBR'$_2$ (R= Ph, R'= Mes, Xyl; R= R'= Mes), their lithium salts, Li(Et$_2$O)$_2$NRBR'$_2$, and their transition-metal derivatives, M(NPhBMes$_2$)$_2$ (M= Cr, Co, Ni), Co(NPhBXyl$_2$)$_2$ and M(NMesBMes$_2$)$_2$ (M= Cr. fwdarw. Ni). *J. Am. Chem. Soc.* **1990,** *112*, 1048-1055.

10. Chen, H.; Bartlett, R. A.; Dias, H. R.; Olmstead, M. M.; Power, P. P., The use of very crowded silylamide ligands-N(SiMe$_n$Ph$_{3-n}$)$_2$ (n= 0, 1, or 2) to synthesize crystalline, two-coordinate, derivatives to manganese(II), iron(II), and cobalt(II) and the free ion [Ph$_3$SiNSiPh$_3$]. *J. Am. Chem. Soc.* **1989,** *111*, 4338-4345.

11. Bartlett, R. A.; Power, P. P., Two-coordinate, nonlinear, crystalline d^6 and d^7 complexes: syntheses and structures of M{N(SiMePh$_2$)$_2$}$_2$, M= Fe or Co. *J. Am. Chem. Soc.* **1987,** *109*, 7563-7564.

12. Bartlett, R. A.; Feng, X.; Olmstead, M. M.; Power, P. P.; Weese, K. J., Synthesis and x-ray structural characterization of the metal borylamide complexes Li(Et$_2$O)$_2$NPhBMes$_2$, (THF)(Et$_2$O)$_2$LiClCo{NPhBMes$_2$}$_2$, and Mn{NMesBMes$_2$}$_2$.3PhMe (Mes= 2, 4, 6-Me$_3$C$_6$H$_2$): Modified amide ligands with poor bridging and. pi.-donor characteristics. *J. Am. Chem. Soc.* **1987,** *109*, 4851-4854.

13. Bartlett, R. A.; Chen, H.; Power, P. P., [M(NMesBMes$_2$)$_2$](M= Cr, Ni): Stable, Distorted, Two-Coordinate d^4 and d^8 Complexes. *Angew. Chem. Int. Ed. Eng.* **1989,** *28*, 316-317.

14. Avent, A. G.; Hitchcock, P. B.; Lappert, M. F.; Sablong, R.; Severn, J. R., Synthesis, structures, characterization, dynamic behavior, and reactions of novel late transition metal(II) 1-azaallyls. *Organometallics* **2004,** *23*, 2591-2600.

15. Au-Yeung, H. Y.; Lam, C. H.; Lam, C.-K.; Wong, W.-Y.; Lee, H. K., Unusual Iron(II) and Cobalt(II) complexes derived from monodentate arylamido Ligands. *Inorg. Chem.* **2007,** *46*, 7695-7697.

16. Reiff, W. M.; Schulz, C. E.; Whangbo, M.-H.; Seo, J. I.; Lee, Y. S.; Potratz, G. R.; Spicer, C. W.; Girolami, G. S., Consequences of a Linear Two-Coordinate Geometry for the Orbital Magnetism and Jahn−Teller Distortion Behavior of the High Spin Iron (II) Complex Fe[N(*t*-Bu)$_2$]$_2$. *J. Am. Chem. Soc.* **2008,** *131*, 404-405.

17. Spitzmesser, S. K.; Gibson, V. C., Dialkylaluminium complexes derived from 1,8-diphenyl-3,6-dimethylcarbazole: a new sterically hindered monodentate ligand system. *J Organomet. Chem.* **2003,** *673*, 95-101.

18. Coombs, N. D.; Stasch, A.; Cowley, A.; Thompson, A. L.; Aldridge, S., Bulky aryl functionalized carbazolyl ligands: amido alternatives to the 2,6-diarylphenyl ligand class? *Dalton Trans.* **2008,** 332-337.

19. Ashley, A. E.; Cowley, A. R.; Green, J. C.; Johnston, D. R.; Watkin, D. J.; Kays, D. L., Synthesis and Characterisation of Low-Coordinate Transition-Metal Complexes Stabilised by Sterically Demanding Carbazolido Ligands. *Eur. J. Inorg. Chem.* **2009,** *2009*, 2547-2552.

20. Kelly, J. X.; Smilkstein, M. J.; Brun, R.; Wittlin, S.; Cooper, R. A.; Lane, K. D.; Janowsky, A.; Johnson, R. A.; Dodean, R. A.; Winter, R., Discovery of dual function acridones as a new antimalarial chemotype. *Nature* **2009,** *459*, 270.

21. Kelly, J. X.; Smilkstein, M. J.; Cooper, R. A.; Lane, K. D.; Johnson, R. A.; Janowsky, A.; Dodean, R. A.; Hinrichs, D. J.; Winter, R.; Riscoe, M., Design, synthesis, and evaluation of 10-*N*-substituted acridones as novel chemosensitizers in Plasmodium falciparum. *Antimicrob. Agents Chemother.* **2007,** *51*, 4133-4140.

22. Rahimizadeh, M.; Pordel, M.; Bakavoli, M.; Bakhtiarpoor, Z.; Orafaie, A., Synthesis of imidazo [4,5-*a*]acridones and imidazo [4,5-*a*]acridines as potential antibacterial agents. *Monatshefte für Chemie-Chemical Monthly* **2009,** *140*, 633.

23. Tabarrini, O.; Cecchetti, V.; Fravolini, A.; Nocentini, G.; Barzi, A.; Sabatini, S.; Miao, H.; Sissi, C., Design and synthesis of modified quinolones as antitumoral acridones. *J. Med. Chem.* **1999,** *42*, 2136-2144.

24. Naidoo, D.; Coombes, P. H.; Mulholland, D. A.; Crouch, N. R.; van den Bergh, A. J., N-Substituted acridone alkaloids from Toddaliopsis bremekampii (Rutaceae: Toddalioideae) of south-central Africa. *Phytochem.* **2005,** *66*, 1724-1728.

25. Manfroni, G.; Paeshuyse, J.; Massari, S.; Zanoli, S.; Gatto, B.; Maga, G.; Tabarrini, O.; Cecchetti, V.; Fravolini, A.; Neyts, J., Inhibition of subgenomic hepatitis C virus RNA replication by acridone derivatives: identification of an NS_3 helicase inhibitor. *J. Med. Chem.* **2009,** *52*, 3354-3365.

26. Goodell, J. R.; Madhok, A. A.; Hiasa, H.; Ferguson, D. M., Synthesis and evaluation of acridine-and acridone-based anti-herpes agents with topoisomerase activity. *Bioorg. Med. Chem.* **2006,** *14*, 5467-5480.

27. Denny, W. A., Acridine derivatives as chemotherapeutic agents. *Curr. Med. Chem.* **2002,** *9*, 1655-1665.

28. Watterson, S. H.; Chen, P.; Zhao, Y.; Gu, H. H.; Dhar, T. M.; Xiao, Z.; Ballentine, S. K.; Shen, Z.; Fleener, C. A.; Rouleau, K. A., Acridone-Based Inhibitors of Inosine 5'-Monophosphate Dehydrogenase: Discovery and SAR Leading to the Identification of *N*-(2-(6-(4-Ethylpiperazin-1-yl)pyridin-3-yl)propan-2-yl)-2-fluoro-9-oxo-9,10-dihydroacridine-3-carboxamide (BMS-566419). *J. Med. Chem.* **2007,** *50*, 3730-3742.

29. Pouli, N.; Marakos, P., Fused xanthone derivatives as antiproliferative agents. *Anti-Cancer Agents Med. Chem. (Formerly Current Medicinal Chemistry-Anti-Cancer Agents)* **2009,** *9*, 77-98.

30. Mayur, Y.; Ahmad, O.; Rajendra Prasad, V.; Purohit, M.; Srinivasulu, N.; Shanta Kumar, S., Synthesis of 2-methyl N10-substituted acridones as selective inhibitors of multidrug resistance (MDR) associated protein in cancer cells. *Med. Chem.* **2008,** *4*, 457-465.

31. Goodrich, S.; Patel, M.; Woydziak, Z. R., Synthesis of a Fluorescent Acridone Using a Grignard Addition, Oxidation, and Nucleophilic Aromatic Substitution Reaction Sequence. *J. Chem. Edu.* **2015,** *92*, 1221-1225.

32. Bahr, N.; Tierney, E.; Reymond, J.-L., Highly photoresistant chemosensors using acridone as fluorescent label. *Tetrahedron Lett.* **1997,** *38*, 1489-1492.

33. Faller, T.; Hutton, K.; Okafo, G.; Gribble, A.; Camilleri, P.; Games, D. E., A novel acridone derivative for the fluorescence tagging and massspectrometric sequencing of peptides. *Chem. Commun.* **1997,** 1529-1530.

34. Woydziak, Z. R.; Fu, L.; Peterson, B. R., Synthesis of fluorinated benzophenones, xanthones, acridones, and thioxanthones by iterative nucleophilic aromatic substitution. *The J. Org. Chem.* **2011,** *77*, 473-481.

35. Zhang, D.; Jiang, X.; Yang, H.; Martinez, A.; Feng, M.; Dong, Z.; Gao, G., Acridine-based macrocyclic fluorescent sensors: self-assembly behavior characterized by crystal structures and a tunable bathochromic-shift in emission induced by $H_2PO_4^-$ via adjusting the ring size and rigidity. *Org. Biomol. Chem.* **2013,** *11*, 3375-3381.

36. Graham, L. A.; Suryadi, J.; West, T. K.; Kucera, G. L.; Bierbach, U., Synthesis, aqueous reactivity, and biological evaluation of carboxylic acid ester-functionalized platinum–acridine hybrid anticancer agents. *J. Med. Chem.* **2012,** *55*, 7817-7827.

37. Ye, X.; Plessow, P. N.; Brinks, M. K.; Schelwies, M.; Schaub, T.; Rominger, F.; Paciello, R.; Limbach, M.; Hofmann, P., Alcohol amination with ammonia catalyzed by an acridine-based ruthenium pincer complex: a mechanistic study. *J. Am. Chem. Soc.* **2014,** *136*, 5923-5929.

38. Allen, C., H and McKee, GHW. *Org. Synth.* **1939,** *19*, 6-9.

39. Gorvin, J. H.; Whalley, D. P., Aromatic nitro-group displacement reactions. Part 1. A novel route to substituted 10-phenylacridones. *J. Chem. Soc., Perkin Trans. 1* **1979**, 1364-1370.

40. Zhou, W.; Liu, Y.; Yang, Y.; Deng, G.-J., Copper-catalyzed intramolecular direct amination of sp^2C–H bonds for the synthesis of *N*-aryl acridones. *Chem. Commun.* **2012,** *48*, 10678-10680.

41. Zhou, W.; Yang, Y.; Liu, Y.; Deng, G.-J., Copper-catalyzed C–C bond cleavage and intramolecular cyclization: an approach toward acridones. *Green Chem.* **2013,** *15*, 76-80.

42. Huang, C.; Yan, S.-J.; Zeng, X.-H.; Sun, B.; Lan, M.-B.; Lin, J., Synthesis and evaluation of the antitumor activity of polyhalo acridone derivatives. *RSC Adv.* **2015,** *5*, 17444-17450.

43. Mohammadi-Khanaposhtani, M.; Shabani, M.; Faizi, M.; Aghaei, I.; Jahani, R.; Sharafi, Z.; Zafarghandi, N. S.; Mahdavi, M.; Akbarzadeh, T.; Emami, S., Design, synthesis, pharmacological evaluation, and docking study of new acridone-based 1, 2, 4-oxadiazoles as potential anticonvulsant agents. *Eur. J. Med. Chem.* **2016,** *112*, 91-98.

44. Feng, M.; Tang, B.; Wang, N.; Xu, H. X.; Jiang, X., Ligand Controlled Regiodivergent C_1 Insertion on Arynes for Construction of Phenanthridinone and Acridone Alkaloids. *Angew. Chem. Int. Ed.* **2015,** *54*, 14960-14964.

45. Wen, J.; Tang, S.; Zhang, F.; Shi, R.; Lei, A., Palladium/Copper Co-catalyzed Oxidative C–H/C–H Carbonylation of Diphenylamines: A Way to Access Acridones. *Org. Lett.* **2016,** *19*, 94-97.

46. Nishio, R.; Wessely, S.; Sugiura, M.; Kobayashi, S., Synthesis of acridone derivatives using polymer-supported palladium and scandium catalysts. *J. Comb. Chem.* **2006,** *8*, 459-461.

47. Stankiewicz-Drogon, A.; Dörner, B.; Erker, T.; Boguszewska-Chachulska, A. M., Synthesis of new acridone derivatives, inhibitors of NS3 helicase, which efficiently and specifically inhibit subgenomic HCV replication. *J. Med. Chem.* **2010,** *53*, 3117-3126.

48. Huang, P. C.; Parthasarathy, K.; Cheng, C. H., Copper-Catalyzed Intramolecular Oxidative C-H Functionalization and C-N Formation of 2-Aminobenzophenones: Unusual Pseudo-1,2-Shift of the Substituent on the Aryl Ring. *Chem. Eur. J.* **2013,** *19*, 460-464.

49. Yu, J.; Yang, H.; Jiang, Y.; Fu, H., Copper-Catalyzed Aerobic Oxidative C-H and C-C Functionalization of 1-[2-(Arylamino)aryl]ethanones Leading to Acridone Derivatives. *Chem. Eur. J.* **2013,** *19*, 4271-4277.

50. Song, J.; Ding, K.; Sun, W.; Wang, S.; Sun, H.; Xiao, K.; Qian, Y.; Liu, C., Synthesis of acridones through palladium-catalyzed carbonylative of 2-Bromo-diarylamines. *Tetrahedron Lett.* **2018**.

51. Gautam, P.; Bhanage, B. M., Recent advances in the transition metal catalyzed carbonylation of alkynes, arenes and aryl halides using CO surrogates. *Catal. Sci. Tech.* **2015,** *5*, 4663-4702.

52. Morimoto, T.; Kakiuchi, K., Evolution of carbonylation catalysis: no need for carbon monoxide. *Angew. Chem. Int. Ed.* **2004,** *43*, 5580-5588.

53. Wu, L.; Liu, Q.; Jackstell, R.; Beller, M., Carbonylations of alkenes with CO surrogates. *Angew. Chem. Int. Ed.* **2014,** *53*, 6310-6320.

54. Kochi, T.; Urano, S.; Seki, H.; Mizushima, E.; Sato, M.; Kakiuchi, F., Ruthenium-catalyzed amino-and alkoxycarbonylations with carbamoyl chlorides and alkyl chloroformates via aromatic C−H bond cleavage. *J. Am. Chem. Soc.* **2009,** *131*, 2792-2793.

55. Furusawa, T.; Morimoto, T.; Oka, N.; Tanimoto, H.; Nishiyama, Y.; Kakiuchi, K., Pd(0)-catalyzed CO Gas-free Carbonylation of 2-Bromobiphenyls with Formaldehyde as a Carbonyl Surrogate through the Cleavage of a C–H Bond. *Chemistry Lett.* **2016,** *45*, 406-408.

56. Liu, Q.; Yuan, K.; Arockiam, P. B.; Franke, R.; Doucet, H.; Jackstell, R.; Beller, M., Regioselective Pd-Catalyzed Methoxycarbonylation of Alkenes Using both Paraformaldehyde and Methanol as CO Surrogates. *Angew. Chem. Int. Ed.* **2015,** *54*, 4493-4497.

57. Katritzky, A. R.; Akutagawa, K., Carbon dioxide: A reagent for the protection of nucleophilic centres and the simultaneous activation of alternative locations to electrophilic attack.: Part I. A new synthetic method for the 2-substitution of 1-unsubstituted indoles. *Tetrahedron Lett.* **1985,** *26*, 5935-5938.

58. Snieckus, V., Directed ortho metalation. Tertiary amide and *O*-carbamate directors in synthetic strategies for polysubstituted aromatics. *Chem. Rev.* **1990,** *90*, 879-933.

59. Katritzky, A. R.; Fan, W.-Q.; Akutagawa, K., Carbon dioxide: a reagent for the simultaneous protection of nucleophilic centres and the activation of alternative locations to electrophilic attack.: Part III1. A new synthetic method for the ortho-subttitution of N-monoalkylanilines. *Tetrahedron* **1986,** *42*, 4027-4034.

60. Yamamoto, K.; Higashibayashi, S., Synthesis of Three-Dimensional Butterfly Slit-Cyclobisazaanthracenes and Hydrazinobisanthenes through One-Step Cyclodimerization and Their Properties. *Chem. Eur. J.* **2016,** *22*, 663-671.

61. Acheson, R.; Robinson, M., 47. The bromination of acridone. *J. Chem. Soc. (Resumed)* **1953**, 232-238.

62. Pang, X.; Lou, Z.; Li, M.; Wen, L.; Chen, C., Tandem Arylation/Friedel–Crafts Reactions of o-Acylanilines with Diaryliodonium Salts: A Modular Synthesis of Acridine Derivatives. *Eur. J. Org. Chem.* **2015,** *2015*, 3361-3369.

63. Geddes, C. D., Optical thin film polymeric sensors for the determination of aqueous chloride, bromide and iodide ions at high pH, based on the quenching of fluorescence of two acridinium dyes. *Dyes and Pigments* **2000,** *45*, 243-251.

64. Bernthsen, A., Zur Kenntniss der Amidine und der Thiamide einbasischer organischer Säuren. *Justus Liebigs Annalen der Chemie* **1878,** *192* (1-2), 1-60.

65. Bernthsen, A., Justw Lleblgs Ann. *Chem., 224* **1884,** *1*.

66. Popp, F. D., Polyphosphoric Acid in the Bernthsen Reaction1. *The J. Org. Chem.* **1962,** *27*, 2658-2659.

67. Su, Q.; Li, P.; He, M.; Wu, Q.; Ye, L.; Mu, Y., Facile synthesis of acridine derivatives by $ZnCl_2$-promoted intramolecular cyclization of o-arylaminophenyl Schiff bases. *Org. Lett.* **2013,** *16*, 18-21.

68. Tsvelikhovsky, D.; Buchwald, S. L., Synthesis of heterocycles via Pd-ligand controlled cyclization of 2-chloro-*N*-(2-vinyl) aniline: preparation of carbazoles, indoles, dibenzazepines, and acridines. *J. Am. Chem. Soc.* **2010,** *132*, 14048-14051.

69. Belmont, P.; Belhadj, T., An Efficient and Simple Aminobenzannulation Reaction: Pyrrolidine as a Trigger for the Synthesis of 1-Amino-acridines. *Org. Lett.* **2005,** *7*, 1793-1795.

70. Lian, Y.; Hummel, J. R.; Bergman, R. G.; Ellman, J. A., Facile synthesis of unsymmetrical acridines and phenazines by a Rh(III)-catalyzed amination/cyclization/aromatization cascade. *J. Am. Chem. Soc.* **2013,** *135*, 12548-12551.

71. Guo, H.-M.; Mao, R.-Z.; Wang, Q.-T.; Niu, H.-Y.; Xie, M.-S.; Qu, G.-R., Pd(II)-catalyzed one-pot, three-step route for the synthesis of unsymmetrical acridines. *Org. Lett.* **2013,** *15*, 5460-5463.

72. Srinivas, V.; Kumara Swamy, K. C., Facile formation of phosphono-acridanes via chloroacridines. *ARKIVOC (Gainesville, FL, U. S.)* **2009,** 31-42.

73. Maurice, H. B.; Phillips, R.; Karodia, N., Design, synthesis and biological evaluation of novel acridine-polyamine conjugates against prostate cancer. *Afr. J. Pharm. Pharmacol.* **2009,** *3*, 602-610.

74. Wolfe, J. P.; Åhman, J.; Sadighi, J. P.; Singer, R. A.; Buchwald, S. L., An ammonia equivalent for the palladium-catalyzed amination of aryl halides and triflates. *Tetrahedron Lett.* **1997,** *38*, 6367-6370.

75. Kharitonova, O.; Panin, D.; Belova, O., Chemistry of Ketoacetals: II. β,β′-Ketodiacetal and β,β′-Hydroxydiacetals in Reactions with Amminia and Amines. *Russ. J. Org. Chem.* **2005,** *41*, 1113-1115.

76. Fulmer, G. R.; Miller, A. J.; Sherden, N. H.; Gottlieb, H. E.; Nudelman, A.; Stoltz, B. M.; Bercaw, J. E.; Goldberg, K. I., NMR chemical shifts of trace impurities: common laboratory solvents, organics, and gases in deuterated solvents relevant to the organometallic chemist. *Organometallics* **2010,** *29*, 2176-2179.

77. Dolomanov, O. V.; Bourhis, L. J.; Gildea, R. J.; Howard, J. A.; Puschmann, H., OLEX2: a complete structure solution, refinement and analysis program. *J. Appl. Crystallogr.* **2009,** *42*, 339-341.

78. Sheldrick, G. M., SHELXT - integrated space-group and crystal-structure determination. *Acta Crystallogr. A Found Adv.* **2015,** *71*, 3-8.

79. Sheldrick, G. M., A short history of SHELX. *Acta Crystallogr., Sect. A: Found. Crystallogr.* **2008,** *64*, 112-122.

CHAPTER 3. NEW SYNTHESIS OF ACRIDINE-BASED LIGANDS, COMPLEX FORMATION, CHARACTERIZATION AND REACTIVITY STUDIES

3.1 Background

Many coordinatively unsaturated transition metal complexes display high reactivity.[1] A number of them have been applied in homogeneous catalysis to achieve novel transformations[2] as well as in activation of inert small molecules like CO, CO_2, H_2, N_2, etc.[3] These highly reactive complexes require a suitable ligand framework that is resistant to rearrangements or degradation during reaction. Pincer ligands[4] have found widespread applications in this aspect.[5-6]

Tridentate pincer ligands bind at the flanking and coplanar sites to the metal center to form stable complexes.[4] Homogeneous catalysts of pincer complexes tend to be chemically and thermally stable, thereby minimizing leaching of the metal during catalytic transformations.[5] The stability, reactivity, and selectivity of these complexes can be tuned by ligand or metal modifications. In light of these capabilities, pincer ligands have especially attracted much attention since they were first used by Shaw[7], van Koten and Noltes.[8] Complexes of PNP pincer ligands were first reported in the late 1960s (amino-based PNP pincer complex)[9] and early 1970s (pyridine-based PNP pincer complex).[10]

3.1.1 PNP pincer ligands design, modification and coordination geometry

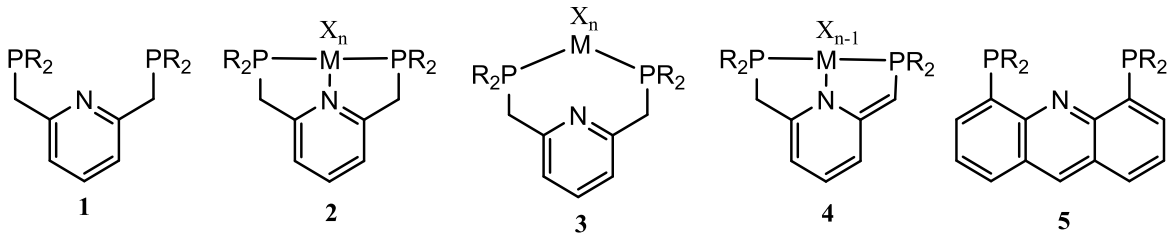

Figure 3.1. Pyridine-based ligands and their coordination geometry.

Neutral tridentate pyridine-based PNP pincer ligands form transition metal complexes that not only possess high reactivity but also offer great flexibility for modification.[11] Some of the examples in this category include 2,6-bis(diphenylphosphinomethyl)pyridine, **1** (Figure 3.1).[12-17] However the methylene groups connecting the phosphorus atoms to the pyridine ring make **1** less rigid and may at times undergo unwanted side-reactions. Binding modes of this ligand include tridentate coordination with a "T-shaped" planar geometry, **2**, and bidentate coordination, **3**.[16] Under basic conditions, complex **2** reacts through elimination of benzylic hydrogen to form a delocalized phosphinomethanide structure, **4**.[17] The phosphorus in these types of complexes are more prone to oxidation than those that do not have a methylene linker. Unlike **1**, "acriphos" **5**,[18] possess a rigid backbone with no benzylic hydrogens, minimizing these possible side-reactions.

A ligand with a rigid backbone should behave differently from those that have flexible backbones. A cobalt complex bearing bis(2-diisopropylphosphino)-4-methylphenylamine (PNP)[19-20] ligand rearranges from a terminal chelating mode to a bridging mode, forming a $[Co_2N_2]$ diamond core resting state. However, it behaves as a

three-coordinate Co(I) synthon, which on treatment with N_2 or CO forms bridging dinitrogen complexes and mono- and di-carbonyl complexes respectively (see Scheme 3.1).[21] Cobalt carbonyl complexes were the first precatalysts used in hydroformylation. One advantage of cobalt is its resistance to poisoning.[22-23] Since the 1998 independent discovery of catalytic application of cobalt-derived pincer complexes based on bis(imino)pyridine by Brookhart, Bennett and Gibson in olefin polymerization,[24-26] a number of cobalt pincer complexes have found wide application in homogenous catalysis including formation of formic acid from CO_2 and H_2.[27-30]

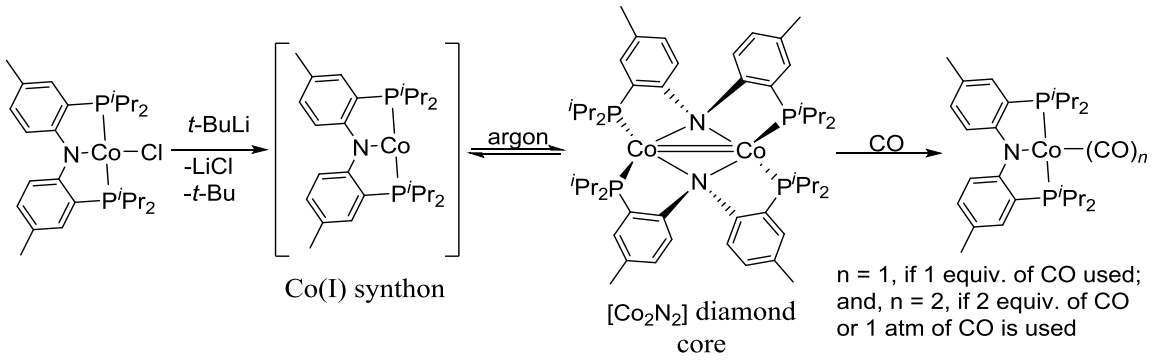

Scheme 3.1. Reorganization of the PNP pincer ligand from a terminal chelating mode to a bridging mode and its reaction with CO.

Many classical examples in homogeneous catalysis involve transformations that occur solely at the metal center while the ligands remain unchanged during the process. However, reactivity in many enzymes involve fine-tuned systems in which the ligand and the metal cooperate to achieve bond activation. Sometimes this metal-ligand cooperation (MLC) leads to chemical modification of both the ligand and the metal. An example is the activation of H_2 by [FeFe] or [NiFe] hydrogenases where H_2 is heterolytically split across the metal-ligand bond without change in metal oxidation state.[31-35] Also, in a MLC through

outer-sphere mechanism like aromatization/dearomatization,[36] the overall oxidation state of the metal remains unchanged. Many complexes of the general framework like **2** with a methylene linker show this type of mechanism. An example is an iridium complex with ^{R}PNP (R =*i*-Pr, *t*-Bu) that activates H_2 and C-H bonds.[37-40]

Metalloenzymes have also showed many reactions that involve ligand-centered redox processes.[41-47] These observations in turn led to a great interest in the study of the behavior of such redox non-innocent (redox-active) ligands and contributed to the development of many effective bio-inspired catalytic transformations.[48-54] Many of the cheaper first-row transition metals are capable of undergoing one-electron transformations that could be very valuable in mediating radical-type reactions. Therefore, ligands that behave as electron reservoirs (reactive or non-reactive)[55-60] have a great potential to expand the applications of these first-row transition metals in organometallic catalysis.[42, 61-62]

There are many examples of first-row transition metal complexes based on redox-active ligands that have showed great catalytic activity.[42] Harry B. Gray and Jonas C. Peters and co-workers developed a highly active cobalt water reduction catalyst based on tetradentate bis(iminopyridine) framework (Figure 3.2 structure **A**).[63] Jonas C. Peters and co-workers also showed that ligand **B** on reduction preferentially reduces CO_2 to CO even in presence of proton donors.[64] The DFT studies on the ligand revealed that it stores reducing equivalents in its structure.[64] Another example by Wieghardt and co-workers is a nickel bis(iminopyridine) pincer (Figure 3.2 structure **C**)[65-66] that was applied by Luca and co-workers in aqueous electrocatalytic H_2 production (Figure 3.3).[67] A computational proposal for this process suggests an energetic accessibility of a PCET step devoid of any redox changes at the Ni^{II} center.[42]

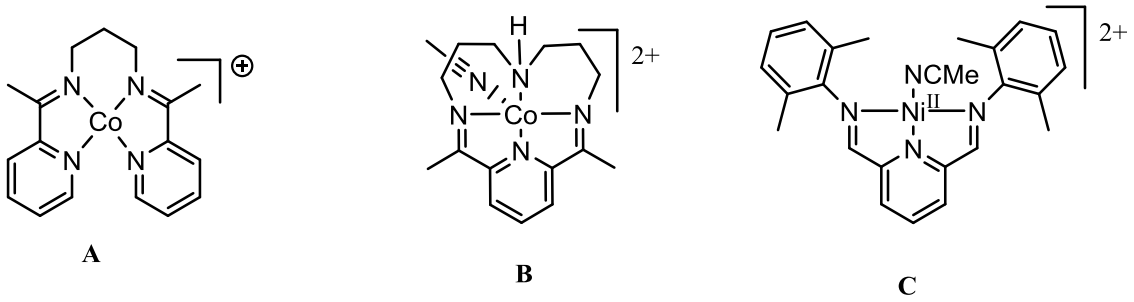

Figure 3.2. Examples of redox-active ligands based on the pyridyl fragment.

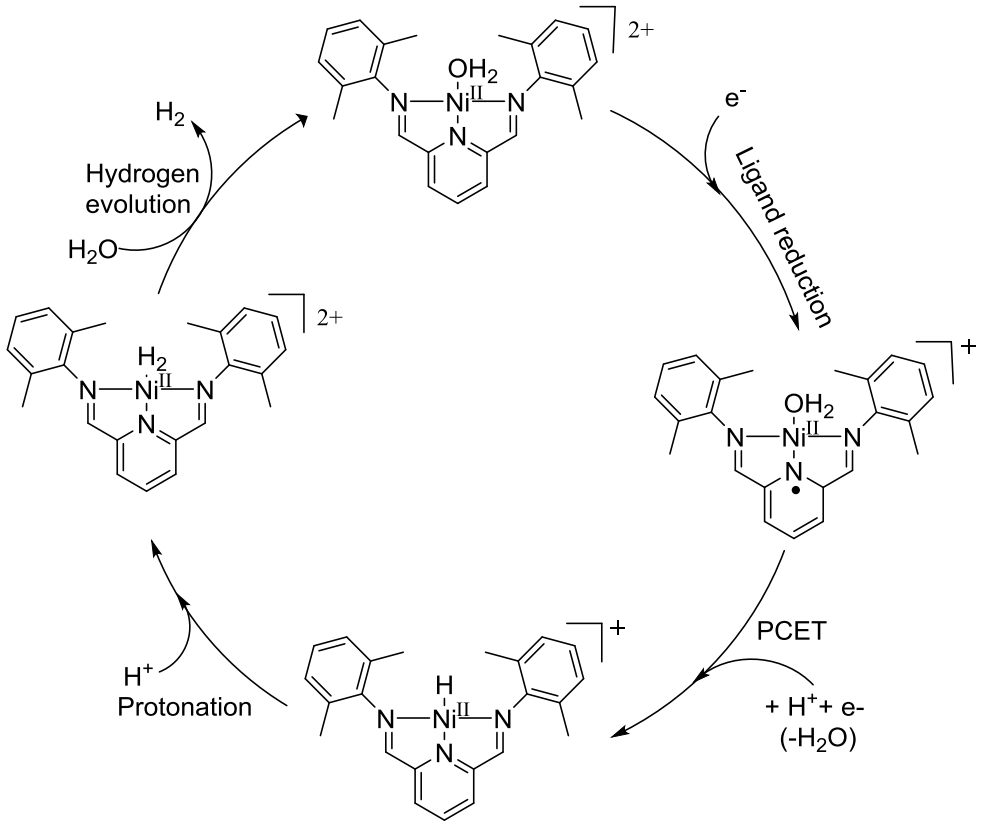

Figure 3.3. A proposed catalytic cycle based on formation Ni^{II}-hydride intermediate.

Another earlier example, that was presented by Soper and co-workers where the metal overall oxidation state remained unchanged, is that of metal-carbon bond formation through oxidative addition on a cobalt(III) center supported by two redox-active amidophenolate ligands.[68] Instead, the two electrons needed for this bond formation is provided through one electron oxidation of each of the redox-active ligands.[68] The

structures **A**, **B** and **C** are just a few of the many examples that exist of ligand frameworks that support redox-active systems. In general, many conjugated C-N ligands like α-diimines, iminepyridines, bypiridines, terpyridines and 2,6-pyridinediimines are considered "non-innocent" since their π systems can easily accept one or more electrons.[61-62]

Ligand-centered reactivity of transition-metal complexes that benefit from either cooperative or redox-active ligands continue to attract much attention in homogeneous catalysis. We were therefore interested in development of a mixed donor ligand built on the pyridine-based six-membered central ring, and studying its ability to act as a one-electron-reducible ligand. Also of interest is the application of complexes of this redox non-innocent ligand in small molecules coordination and activation. The potential of tuning the electronic and steric properties of these pyridine-based ligands without altering their ability to bind to the metal center coupled with hard-soft donor characteristics of the binding atoms, makes these ligands capable of coordinating to a large number of transition metals with varied oxidation states. This in turn extends considerably the importance and applications of these bidentate or polydentate phosphine ligands[69] in homogeneous catalysis.

3.2 Results and Discussion

3.2.1 PNP acridine ligand synthesis, complex formation and characterization

The "acriphos" ligand **5** (R=phenyl) was initially synthesized by Haenel and co-workers from pre-functionalized substrates (2-amino-3-fluorobenzoic acid and 2-fluoroiodobenzene) (Scheme 3.2).[18] This ligand has a rigid tridentate PNP pocket that

prevents the twisting and folding commonly observed with other PNP^R-derived complexes.[18] However, it requires a cumbersome synthetic procedure as well as pre-functionalized substrates. Since its synthesis, the more flexible bis(phosphino)methyl variant has been synthesized by Gunanathan and Milstein.[70-71] Haenel used sodium diphenylphosphide to install the phosphorus moieties. Milstein on the other hand installed bromomethyl groups at 4- and 5-positions of the acridine backbone followed by C-P cross-coupling reaction to make a more flexible flanking arm. Even though these ligands' synthesis is not straightforward, their complexes display great catalytic activities in synthesis of primary amines from alcohols and ammonia as well as in hydroformylation, carbonylation, carboxylation etc.[71-72]

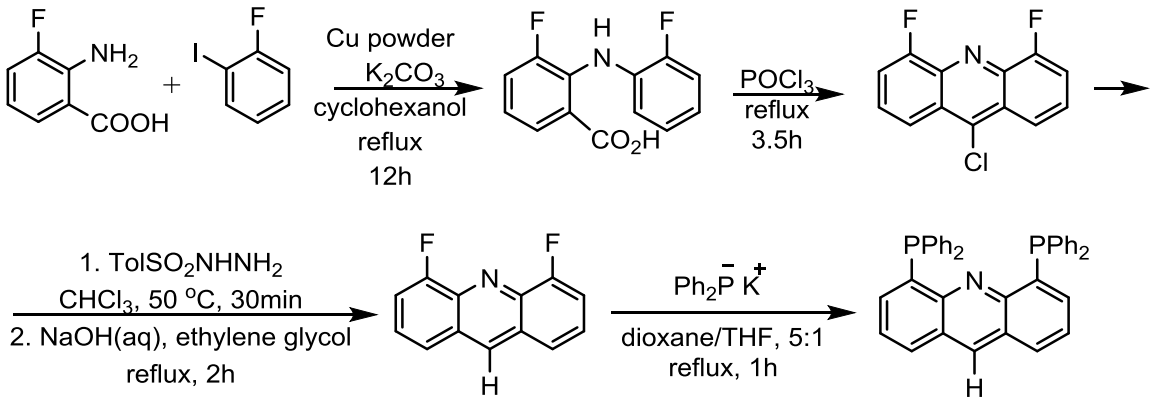

Scheme 3.2. Synthesis of "acriphos" from pre-functionalized substrates.[18]

In order to develop an alternative new synthetic route to the PNP acridine ("acriphos") ligand from the one provided by Haenel and co-workers, an applicable substrate would be 4,5-dibromo-2,7-di-*tert*-butyl-9-chloroacridine which has been shown to undergo a clean dilithiation in the previous Chapter (Scheme 2.6). This substrate is easily obtained from the reaction of 4,5-dibromo-2,7-di-*tert*-butylacridin-9(10*H*)-one with thionyl chloride under reflux. Instead of the fluoro substituents at 4- and 5-positions, this

substrate is bromo-substituted and therefore is expected to react differently from 4,5-difluoro-9-chloroacridine under directed metalation to give a metalated intermediate that can interact with electrophilic alkyl or aryl chlorophosphines to give the desired phosphorus-substituted products.

3.2.1.1 Synthesis of PNP-chloroacridine

For halogen-metal exchange reactions, 4,5-dibromo-2,7-di-*tert*-butyl-9-chloroacridine was treated with *n*-BuLi to give the metalated intermediate, this was then quenched with chlorodiphenylphosphine to afford 2,7-di-*tert*-butyl-9-chloro-4,5-bis(diphenylphosphino)acridine (**6**, ^{acrid}PNP) in 44% yield (Scheme 3.3). This synthetic route makes use of $ClPPh_2$ and circumvents potential issues with unstable phosphide intermediates.

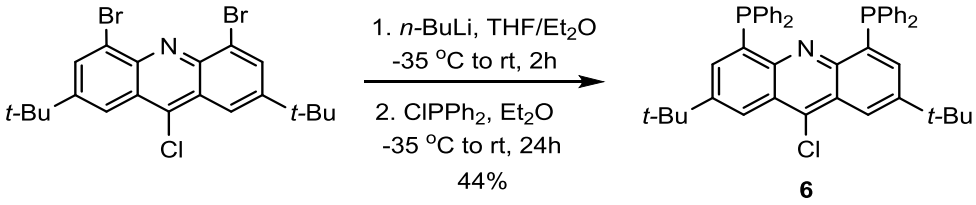

Scheme 3.3. Synthesis of 2,7-di-*tert*-butyl-9-chloro-4,5-bis(diphenylphosphino)acridine.

3.2.1.2 Synthesis of complexes of 2,7-di-*tert*-butyl-9-chloro- 4,5-bis(diphenylphosphino)acridine and their characterization

The efficacy of **6** as a ligand was tested in making complexes of Co, Ni, Pd and Ag. The reaction of **6** with $(PPh_3)_2CoCl_2$ in THF at room temperature overnight gives the corresponding (^{acrid}PNP)$CoCl_2$ complex in 96% yield as green solid (Scheme 3.4).

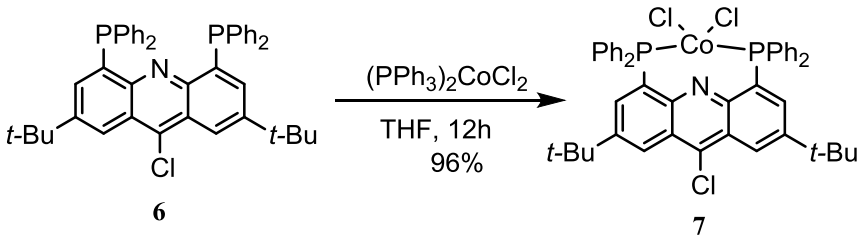

Scheme 3.4. Synthesis of [2,7-di-*tert*-butyl-9-chloro-4,5-bis (diphenylphosphino)acridine]cobalt(II) chloride.

The solid-state analysis of the complex surprisingly revealed a κ^2-coordination mode with the nitrogen unbound (Figure 3.4). Although the Co–N distance of 2.488(2) Å is well within the sum of the two atoms' van der Waals radii, the cobalt lies 0.840 Å above the acridine plane, and the Co1–N1–C9 angle is 155.4(7)° suggesting minimal donation of electron density from nitrogen to cobalt.

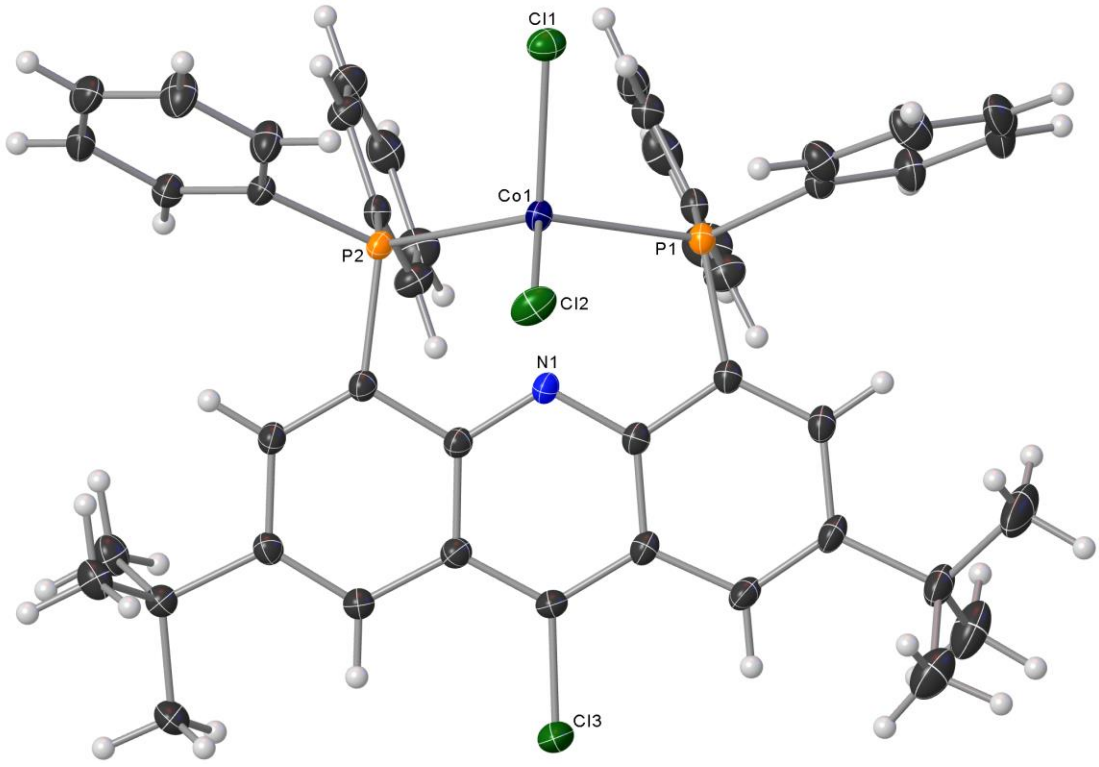

Figure 3.4. Solid-state structure of **7** shown as 50% probability ellipsoids. Selected interatomic distances (Å) and angles (°): N1-Co1, 2.488; Co1-P1, 2.391(9); Co1-P2, 2.411(9); C1-P1, 1.815(3); C4-P2, 1.830(3); P1-Co1-P2, 120.5(2); Cl1-Co1-Cl2, 108.4(9).

When the ligand **6** is treated with $(CH_3CN)_2PdCl_2$ in dichloromethane, it forms a brown solid in 92% yield. Mass spectrometry gives a molecular ion mass that is consistent with the presence of one inner-sphere chloride as depicted by **8** below (Scheme 3.5). The product crystallizes as the tetrachloropalladate(II) salt shown in Figure 3.5.

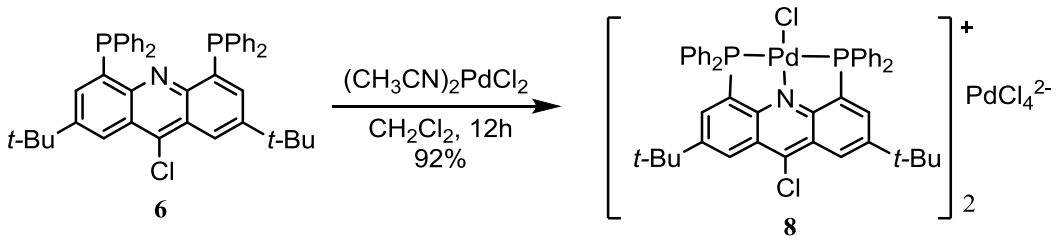

Scheme 3.5. Synthesis of [2,7-di-*tert*-butyl-9-chloro-4,5-bis(diphenylphosphino)acridine]palladium(II) tetrachloropalladate.

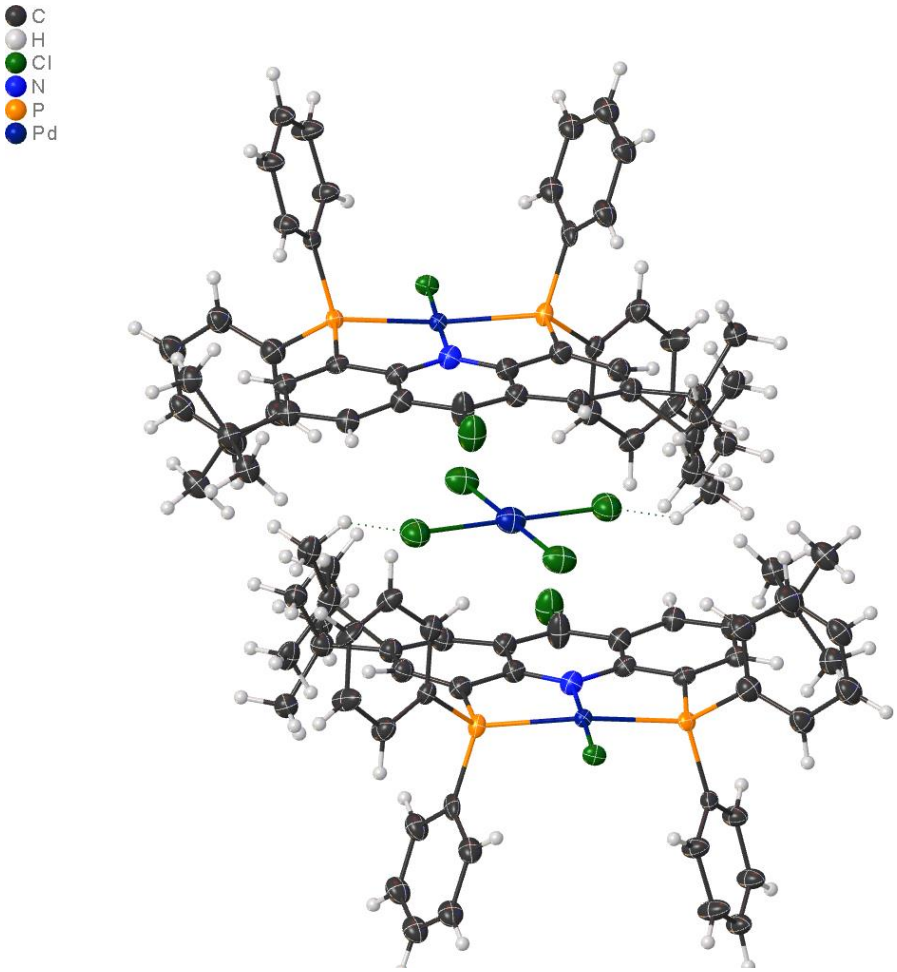

Figure 3.5. Solid-state structure of **8**. (It was not possible to obtain reliable bond metrics due to disorder).

The reaction of **6** with $(PPh_3)_2NiCl_2$ in dichloromethane for 12 hours at room temperature (Scheme 3.6) followed by workup leads to the corresponding complex **9** in

83% yield as a red-purple solid. This crystallizes as a five-coordinate (^{acrid}PNP)$NiCl_2$ as shown in Figure 3.6.

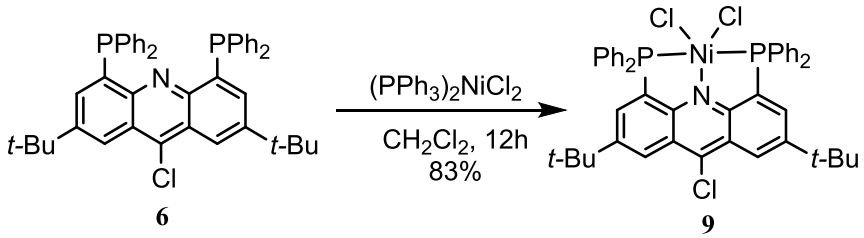

Scheme 3.6. Synthesis of [2,7-di-*tert*-butyl-9-chloro-4,5-bis(diphenylphosphino)-acridine]nickel(II) chloride.

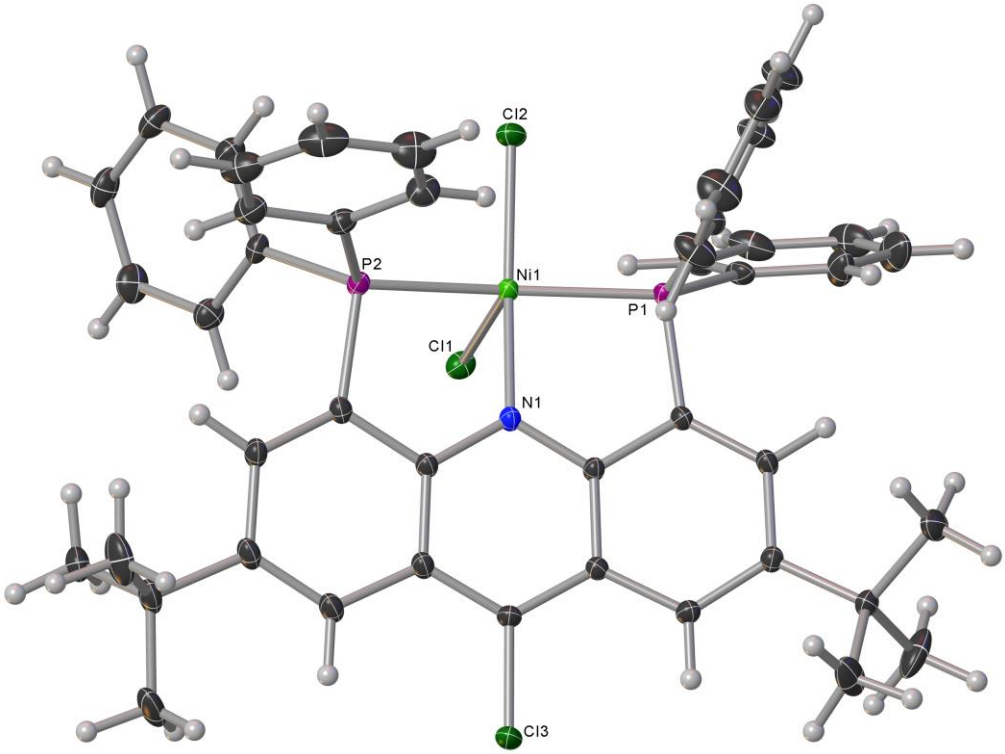

Figure 3.6. Solid-state structure of **9** shown as 50% probability ellipsoids. Selected interatomic distances (Å) and angles (^{o}): N1-Ni1, 1.923; Ni1-P1, 2.178(0); Ni1-P2, 2.190(0); C1-P1, 1.811(2); C4-P2, 1.815(2); P1-Ni1-P2, 159.5(5).

Reactivity studies of (^{acrid}PNP)$NiCl_2$

Reactions of five-coordinate nickel complexes have been studied for different pincer complexes. Hu and coworkers showed alkyl-alkyl Kumada-type coupling of a preformed nickel(II) pincer complex, ([(N_2N)Ni-Cl)].[73] Vicic and coworkers also used a terpyridine ligand in making five coordinate nickel complexes to enable detection of a Ni(III) intermediate formed during cross-coupling reactions.[74] Complex **9** reacts with one equivalent of isopropylmagnesium chloride solution to give a mixture of products. However, when two equivalents of the Grignard are used, it reacts cleanly to form the dialkyl nickel complex (**10**) as shown in Scheme 3.7 below. Attempts to oxidize **10** to induce C-C reductive elimination were unsuccessful, as were attempted insertion reactions of CO_2 or CO.

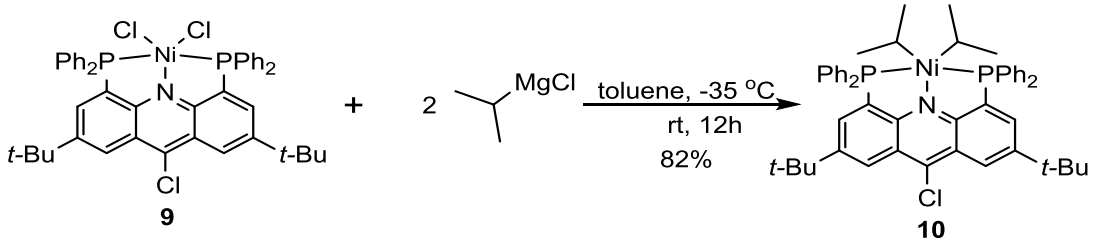

Scheme 3.7. Reaction of (^{acrid}PNP)$NiCl_2$ with Grignard.

3.2.2 Modification of PNP-chloroacridine ligand, complexes formation and characterization

Nickel under reducing conditions can activate aryl chloride bonds for cross-coupling reactions.[75] Low-valent cobalt on the other hand enables C-H/electrophile coupling reactions of aryl chlorides or alkyl chlorides.[76-77] Therefore, anticipating that the chloride at position C-9 would be vulnerable to attack by low-valent species during

reduction experiments, we decided to modify the ligand framework to avoid these side-reactions. One method would be to convert the 9-Cl position in **6** (Scheme 3.3) to 9-H, then use the resulting ligand to make complexes of cobalt and nickel.

3.2.2.1 Synthesis of PNP-acridine ligands

The chloride at the C-9 position activates it and makes the C9 prone to nucleophilic attack. Therefore, treatment with nucleophilic substrates like *p*-toluenesulfonyl hydrazide leads to conversion of 9-Cl to 9-H in two steps[72] as shown in Scheme 3.8 below in good yields; 83% (first step) and 87% (second step). With attempts to expand the class of ligands and alter the donor ability of the ancillary phosphorus groups, we chose to introduce alkyl phosphorus moiety.

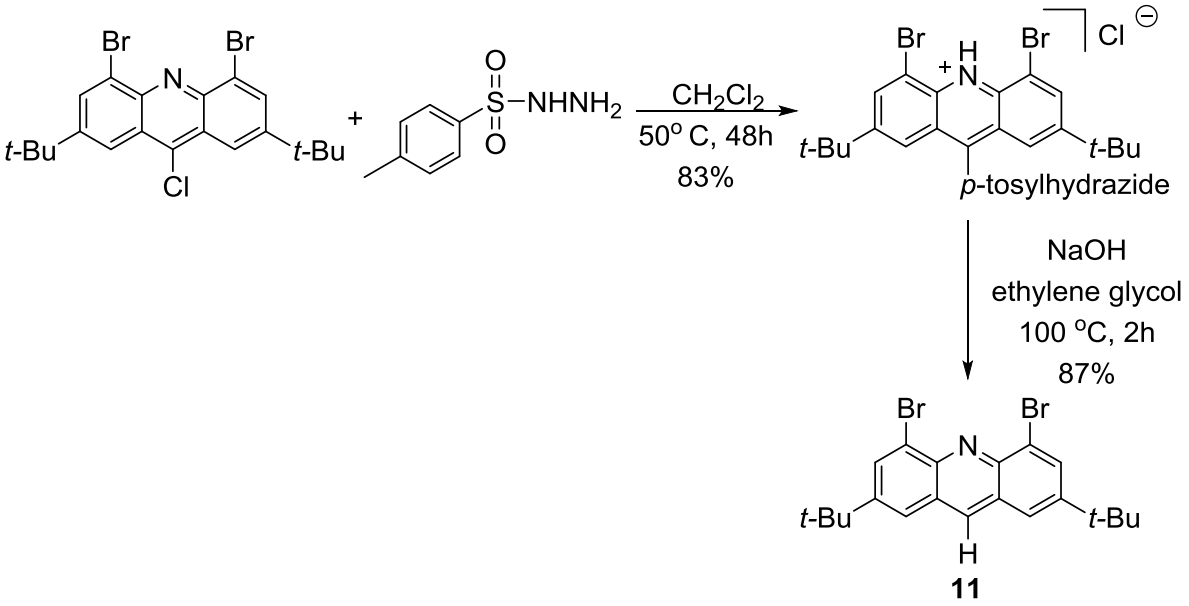

Scheme 3.8. Synthesis of 4,5-dibromo-2,7-di-*tert*-butylacridine.

The reaction of **11** with two equivalents of *n*-BuLi followed by quenching with chlorodiisopropylphosphine led to formation of mixtures **12** and **13** as shown in Scheme

3.9. Acridine has been known to be reactive towards nucleophilic addition at its C-9 position. With reagents like Ph_2PH or Ph_2PLi, acridine reacts as shown in Scheme 3.10 to form the corresponding products **14** and **15**, respectively.[18, 78]

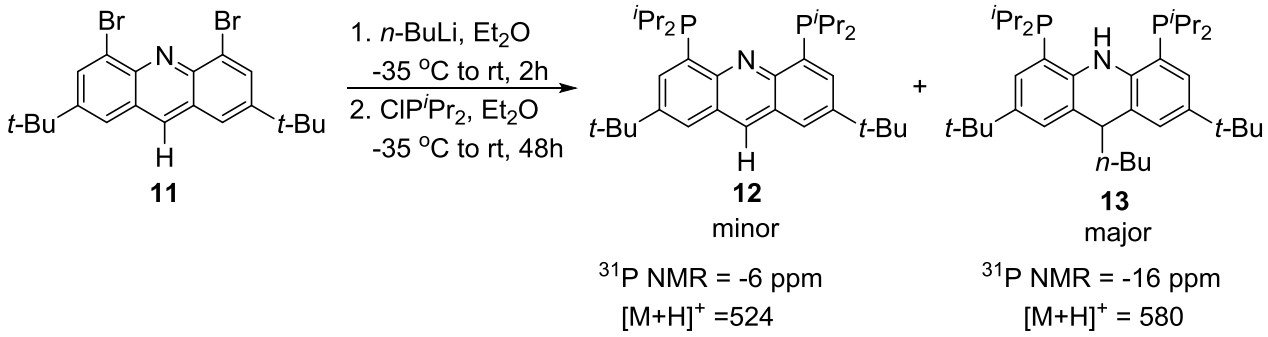

Scheme 3.9. Synthesis of 2,7-di-*tert*-butyl-4,5-bis(diisopropylphosphino)-9-hydroacridine.

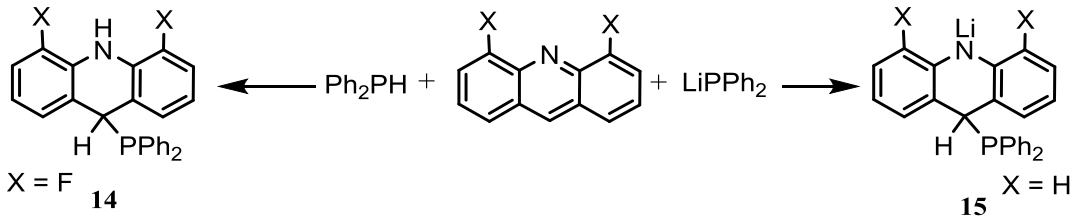

Scheme 3.10. Reactions of 9-hydroacridine at the C-9 position.[18, 78]

However 4,5-di-bromo-2,7-di-*tert*-butyl-9-chloroacridine reacts as shown in Scheme 3.11 below to form **16** in 34% yield.

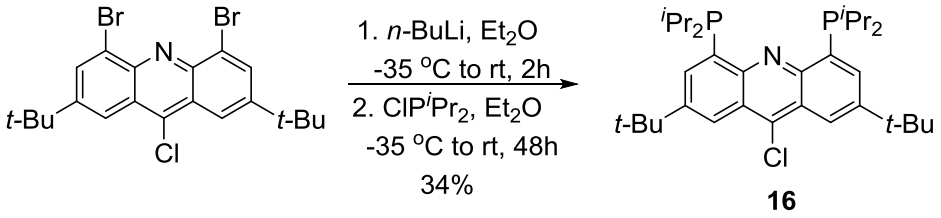

Scheme 3.11. Synthesis of 2,7-di-*tert*-butyl-4,5-bis(diisopropylphosphino)-9-chloroacridine.

3.2.2.2 Synthesis of PNP-9-(alkoxy or aryloxy)acridine ligands

Alternatively, the reaction of 2,7-di-*tert*-butyl-9-chloro-4,5-bis(diphenylphosphino)acridine with oxygen nucleophiles as shown in Scheme 3.12 below would lead to a less reactive C-9 position. With sodium methoxide, the 2,7-di-*tert*-butyl-4,5-bis(diphenylphosphino)-9-methoxyacridine (**17**, (MeO)PNP-acridine) is obtained in 77% yield. With 2,4,6-trimethylphenol, a 58% yield of 2,7-di-*tert*-butyl-4,5-bis(diphenylphosphino)-9-(2,4,6-trimethylphenoxy)acridine (**18**, (ArO)PNP-acridine) is obtained. These two forms of C9-substituted acridines offer different degrees of hindrance about the C-9 position.

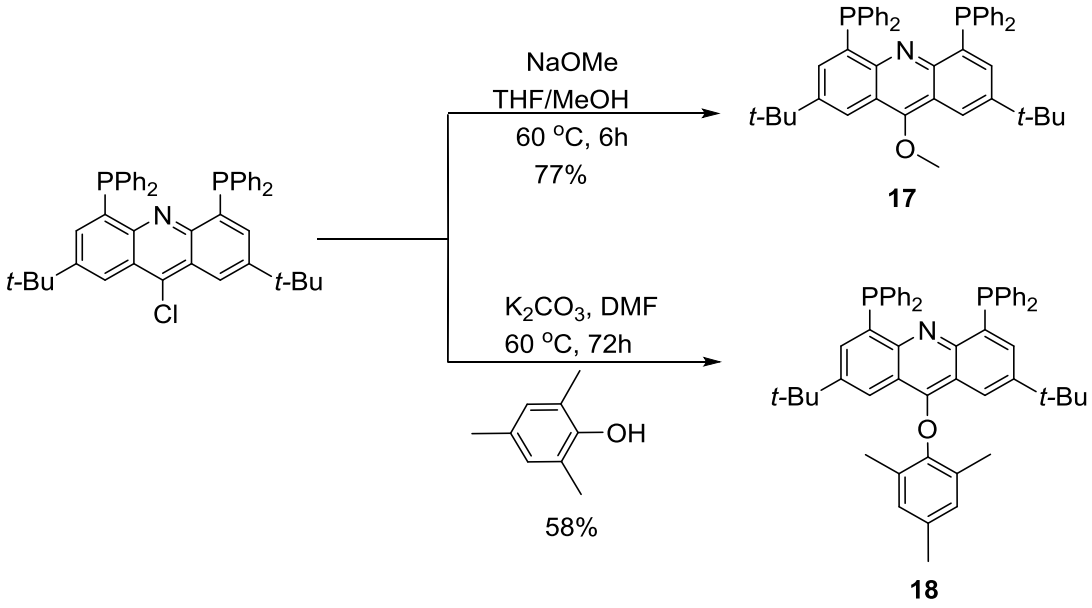

Scheme 3.12. Installation of alkoxy and aryloxy groups at the C-9 position of PNP-9-chloroacridine.

3.2.2.3 Synthesis and reactivity studies of nickel complexes of (MeO)PNP-acridine and (ArO)PNP-acridine ligands

i. Reactivity of [(MeO)PNP-acridine]$NiCl_2$ with CO_2

Reaction between **17** and $(PPh_3)_2NiCl_2$ leads to a slightly unexpected product. The starting ligand (**17**) shows a distinctive singlet resonance in the ^1H NMR spectrum at δ 3.76 ppm from the methoxy protons (red trace, spectrum 1, Figure 3.7). There is however no discernible resonance in the complex ^1H NMR spectrum (black trace, spectrum 2) that results from the methoxy protons when this ligand is treated with $(PPh_3)NiCl_2$ (Figure 3.7). The ^{31}P NMR spectrum shows a shifts from δ -12.49 ppm (free ligand) to δ 19.73 ppm after the complexation reaction. There are distinctive differences in the ^{13}C NMR spectrum before and after complexation reaction as shown in the Figure 3.8 below. A resonance at δ 175.96 ppm in the ^{13}C NMR spectrum of complex (black trace) and lack of a signal in the 60 ppm region for the methoxy carbon as observed with free ligand (red trace) could be indicators of lack of a methoxy group in the complex.

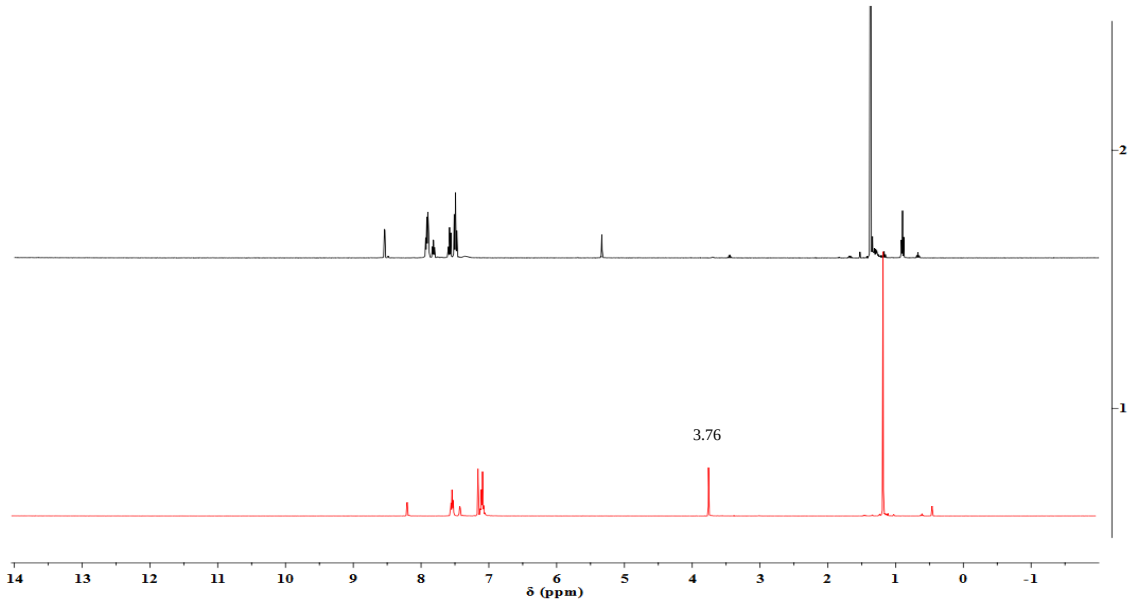

Figure 3.7. Comparison of ^{1}H NMR spectra of ligand, **17** (red trace) in $CDCl_3$ solution and that of [**17**]$NiCl_2$ complex (black trace) in CD_2Cl_2 solution.

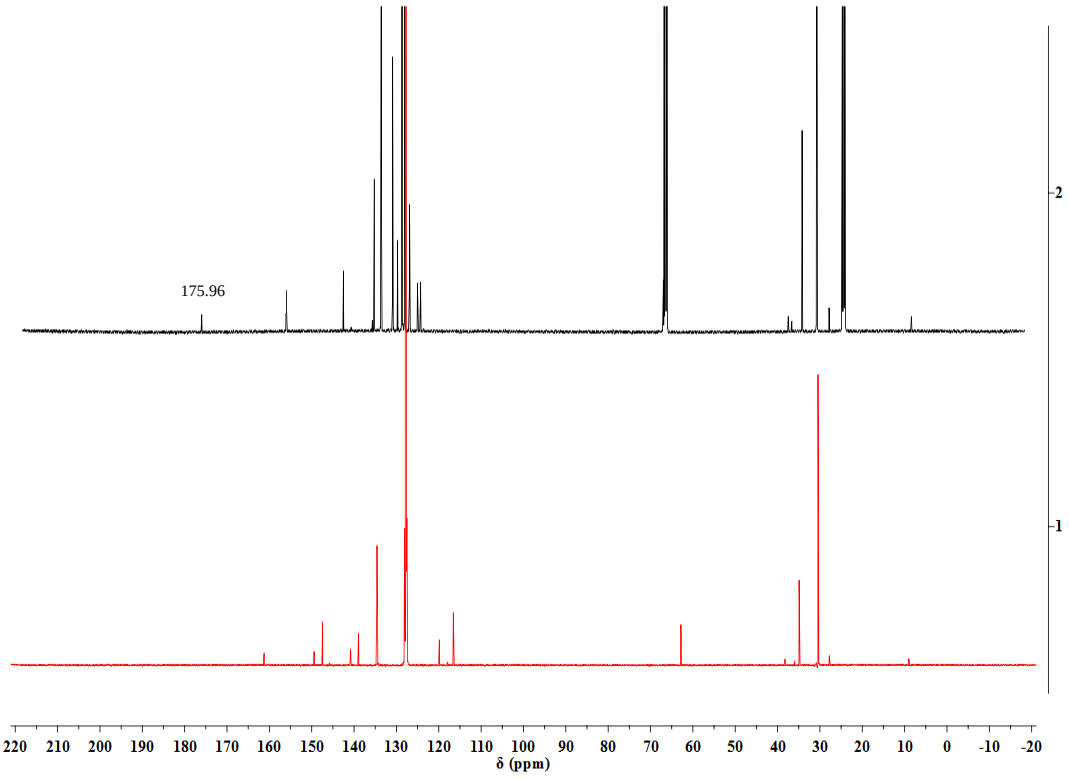

Figure 3.8. Comparison of ^{13}C NMR spectra of ligand, **17** (red trace) in C_6D_6 solution and that of [**17**]$NiCl_2$ complex (black trace).

The mass spectra indicate the presence of the expected product with a molecular ion mass of 782.19 amu [M+Cl]. The spectrum however shows a major peak at M^+ = 767.17 amu. This ion would correspond to a complex formed when the central ring changes to an acridone framework. For CO_2 reduction, a low-valent metal center is needed. Therefore, [**17**]$NiCl_2$ was treated with two equivalents of KC_8 to reduce it to the respective Ni(0) complex. On exposure to CO_2 and analysis by infrared spectroscopy, the infrared spectrum shows two absorptions of equal intensities at 1625 cm^{-1} and 1590 cm^{-1} (Figure 3.9).

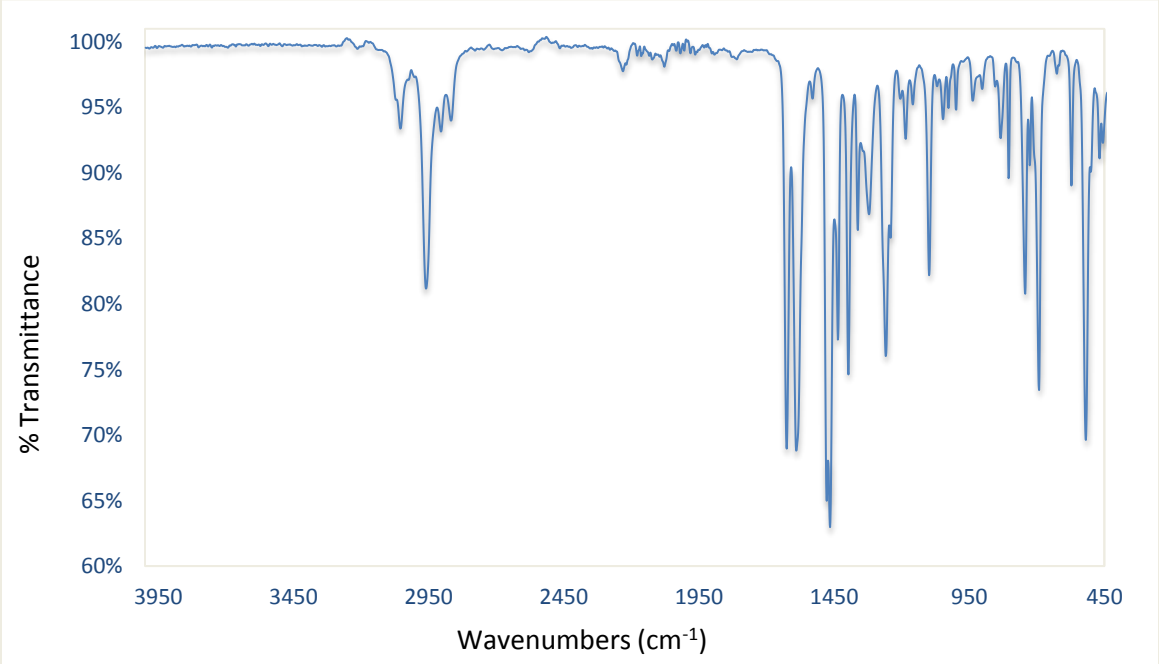

Figure 3.9. IR spectrum of [17]$NiCl_2$ after reduction followed by treatment with CO_2.

With the data we have, we cannot fully understand what is going on in the reaction of **17** with $(PPh_3)_2NiCl_2$ and therefore its application in CO_2 activation would not be informative. Reasoning that with a bulky appendage, access to this position would be minimized, we resorted to synthesis of nickel complex from **18**.

ii. [(ArO)PNP-acridine]$NiCl_2$ and its reaction with CO_2

In dichloromethane, **18** reacts with $(PPh_3)_2NiCl_2$ to give the corresponding complex **19** (Scheme 3.13) in 90% yield with [M+Cl] = 886 amu in the mass spectrometry (Figure 3.10). This complex when reduced with KC_8, forms a paramagnetic species. On exposure to CO_2, the spectra are indistinct, as expected for a paramagnetic species. The spectra obtained after exposure remain so, suggesting that diamagnetic products do not form as observed in the ^1H and ^{31}P NMR spectra.

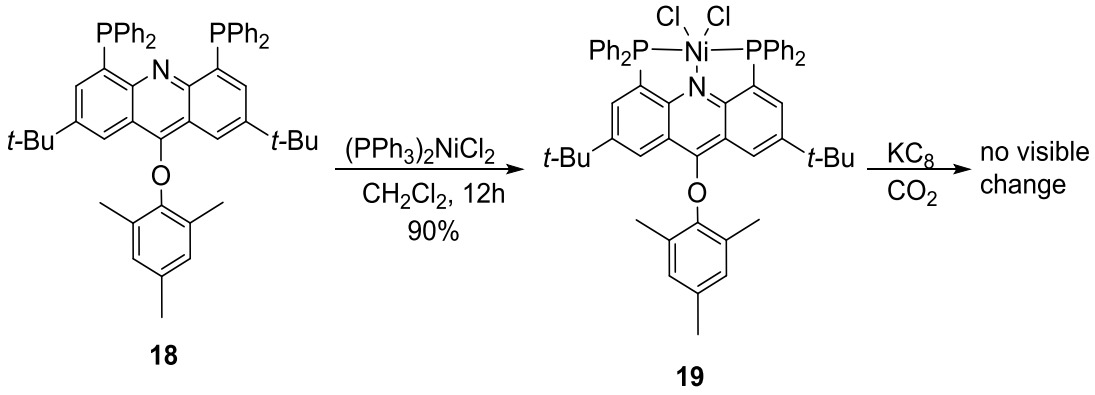

Scheme 3.13. Synthesis of [(ArO)PNP-acridine]$NiCl_2$, its subsequent reduction, and exposure to CO_2.

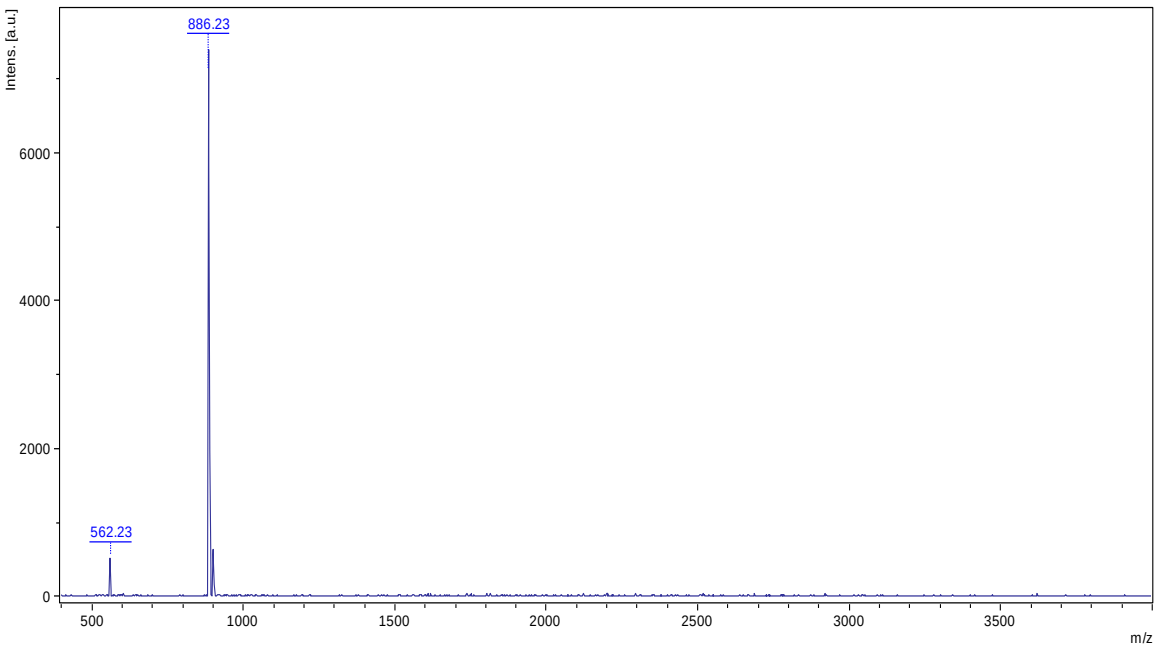

Figure 3.10. Mass spectrum of [(ArO)PNP-acridine]$NiCl_2$.

The infrared spectrum of the complex obtained after the CO_2 reaction shows a broad absorption in the region of 1608-1495 cm^{-1}. Reaction of the reduced species of **19** with $^{13}CO_2$ does not show any coupling between the carbon and the phosphorus in the ^{13}C and ^{31}P NMR spectra. However, there is a broad singlet peak in the ^{13}C NMR spectrum at δ 160.81 ppm that could correspond to carbonate carbon (Figure 3.11).

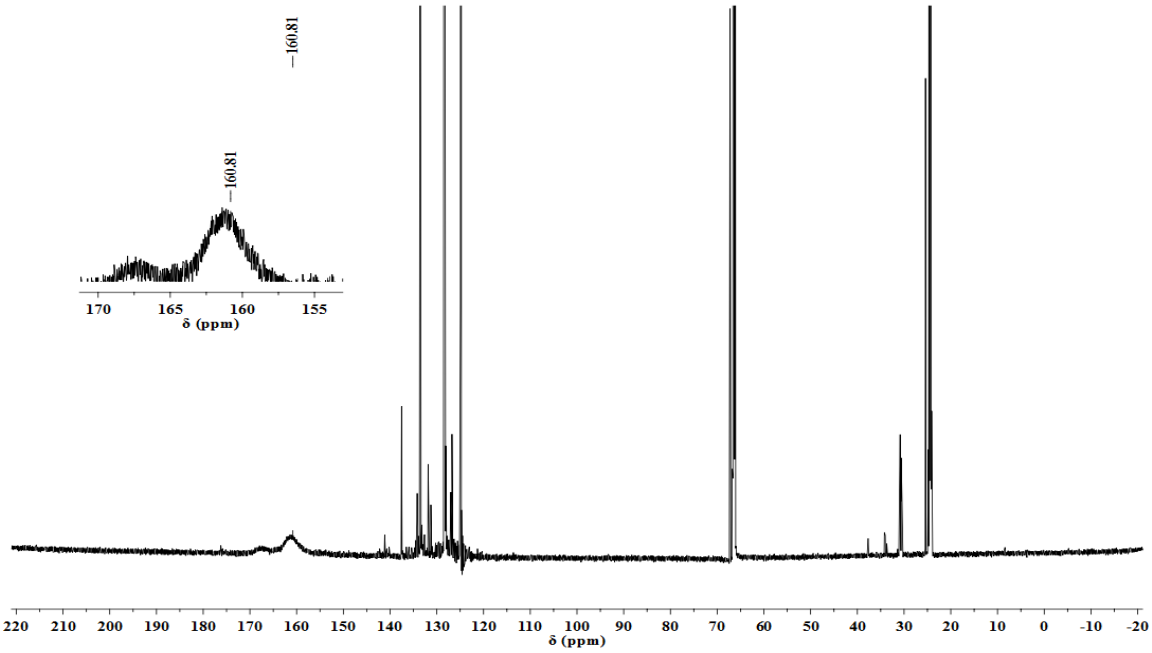

Figure 3.11. ^{13}C NMR of the product of reaction between CO_2 and reduced [(ArO)PNP-acridine]$NiCl_2$.

3.2.2.4 Synthesis and reactivity studies of cobalt complexes of (MeO)PNP-acridine and (ArO)PNP-acridine ligands

i. [(MeO)PNP-acridine]$CoCl_2$ and its reaction with CO

Cobalt complex is formed in 94% yield when **17** reacts with $(PPh_3)_2CoCl_2$ in THF overnight as shown in Scheme 3.14. The product is paramagnetic but its mass spectrometry data gives the mass of expected molecular ion to be 818.21 amu [M+2Cl] while [M+Cl] is 783.23 amu.

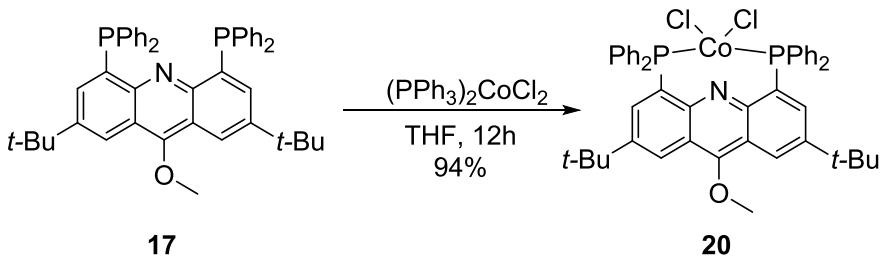

17 **20**

Scheme 3.14. Synthesis of [(MeO)PNP-acridine]$CoCl_2$.

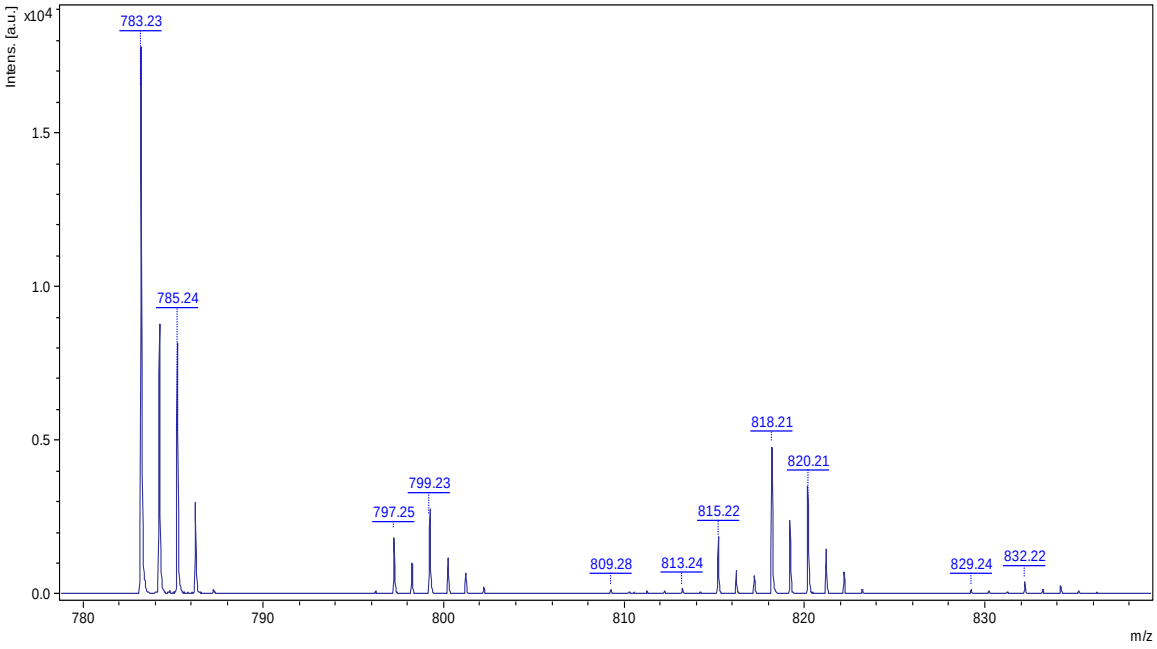

Figure 3.12. Mass spectrum of [(MeO)PNP-acridine]$CoCl_2$.

Reaction of **20** with KC_8 under nitrogen leads to a product which show absorptions at υ = 2025 cm^{-1}, 2081 cm^{-1} in its infrared spectrum (could be a mixture of products hence the two stretches). When Mindiola and co-workers reduced their anionic [(PNP)CoCl] in the presence of dinitrogen, they formed a bridging nitrogen complex with υ_{NN} = 2024 cm^{-1}.[21] It is very likely that one or both of the absorptions might be stretches from bound nitrogen. The resulting reduced species reacts with CO to give a product that has an absorption at 1985 cm^{-1} and 1904 cm^{-1} in the infrared spectrum as shown in Figure 3.13. These values compare closely to the other [(PNP)Co-carbonyl] complexes which were

synthesized by Mindiola and coworkers (υ_{CO}= 1957 cm^{-1}, 1893 cm^{-1})[21] and Caulton and coworkers (υ_{CO}= 1885 cm^{-1}).[79]

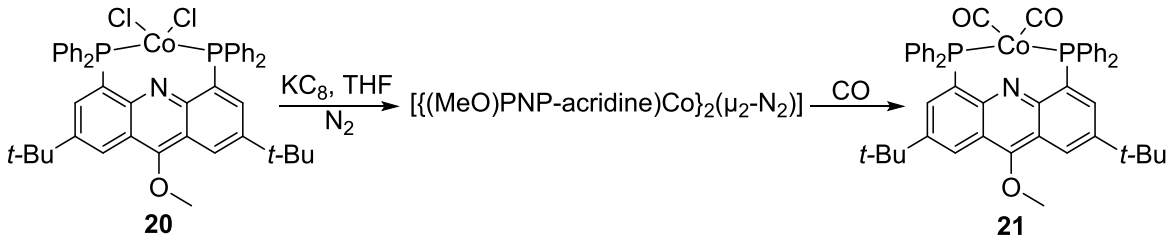

Scheme 3.15. Reduction of [(MeO)PNP-acridine]$CoCl_2$ under N_2 followed by exposure to CO.

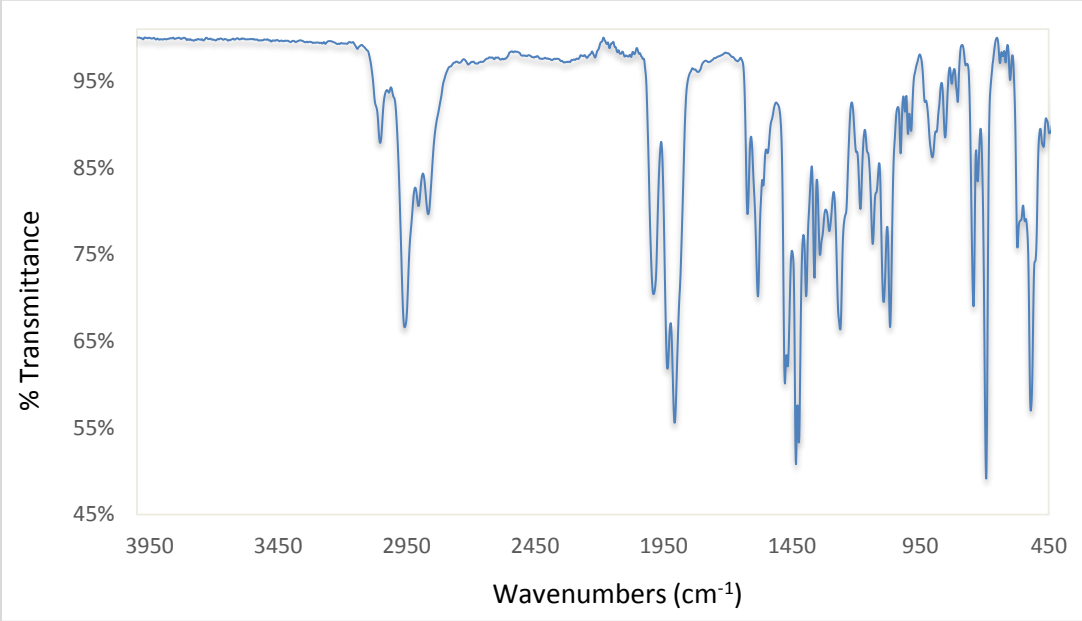

Figure 3.13. Infrared spectrum of [(MeO)PNP-acridine]$CoCl_2$ after reduction and exposure to CO.

ii. [(ArO)PNP-acridine]$CoCl_2$ and its reaction with CO

Reaction of **18** with $(PPh_3)_2CoCl_2$ in THF overnight as shown in Scheme 3.16 leads to formation of the product as an off-green solid in 98% yield. The product is paramagnetic

but its mass spectrometry data gives the mass of molecular ion to be 887.26 amu, [M+Cl] and 922.34 amu, [M+2Cl] (Figure 3.14).

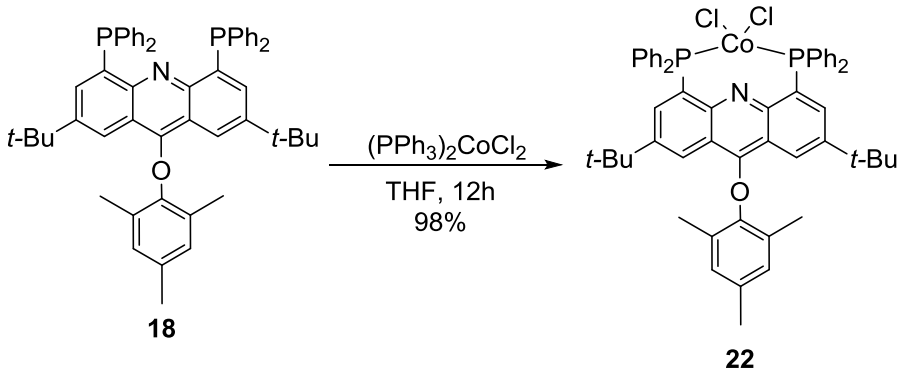

Scheme 3.16. Synthesis of [(ArO)PNP-acridine]$CoCl_2$.

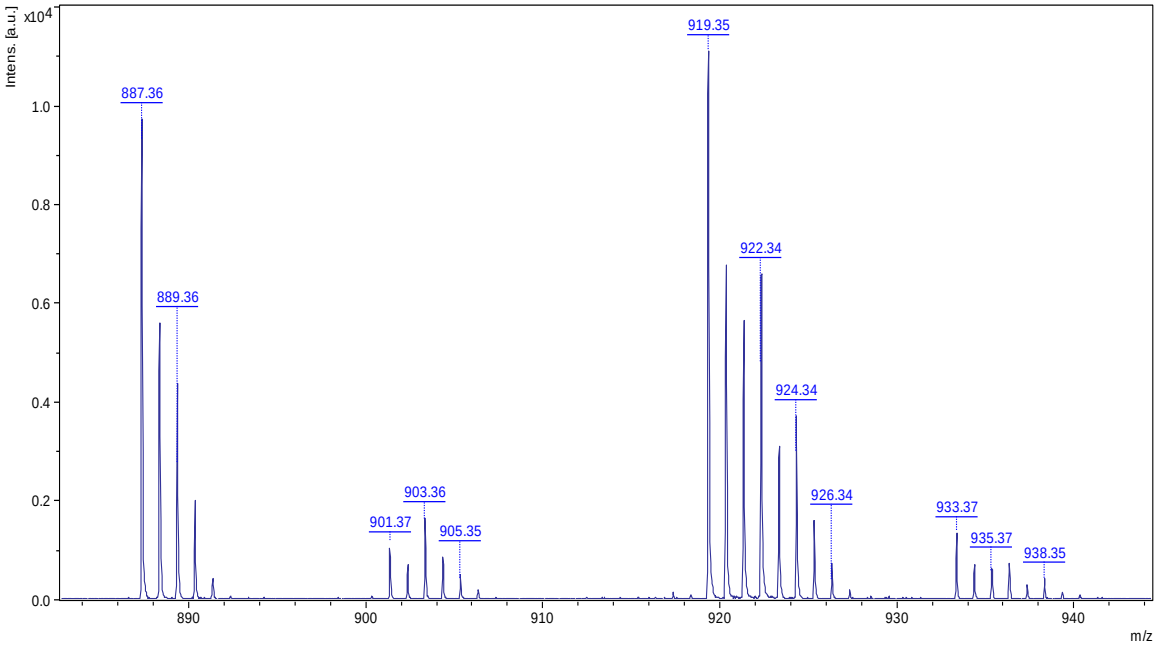

Figure 3.14. Mass spectrum of [(ArO)PNP-acridine]$CoCl_2$.

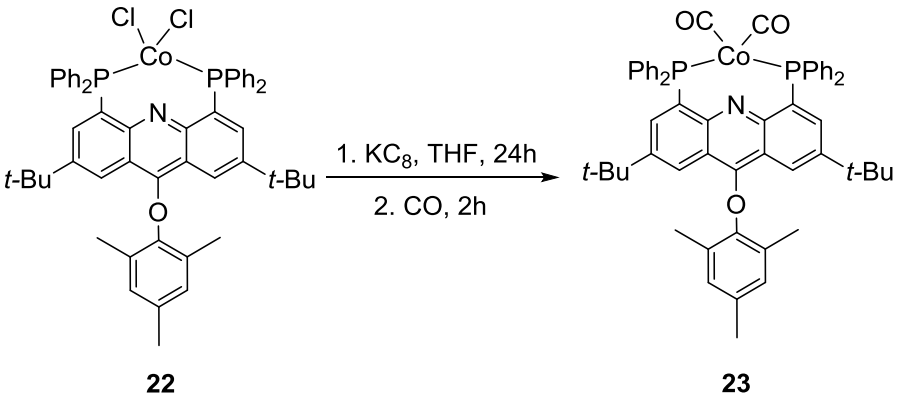

22 **23**

Scheme 3.17. Reduction of [(ArO)PNP-acridine]$CoCl_2$ followed by exposure to CO.

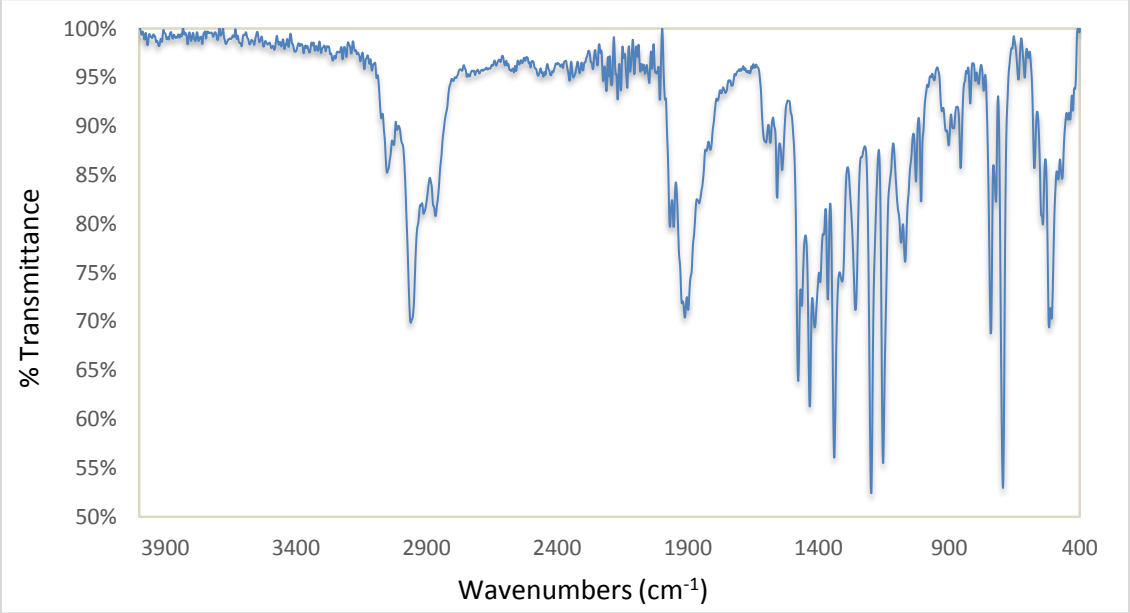

Figure 3.15. Infrared spectrum of [(ArO)PNP-acridine]$CoCl_2$ after reduction and exposure to CO.

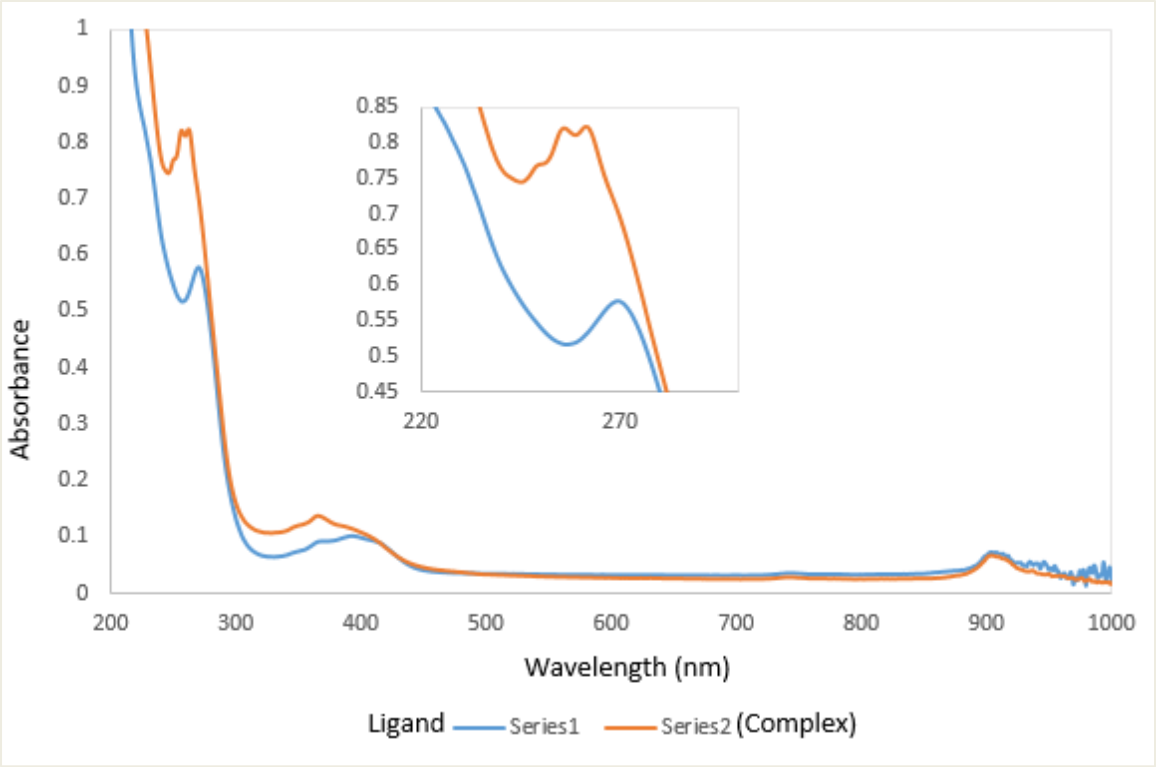

Figure 3.16. UV-visible absorbance of the ligand (**18**) and of [(ArO)PNP-acridine]$Co(CO)_2$.

Reaction of **22** with KC_8 followed by CO leads to a product which gives IR absorption at 1911 cm^{-1} and 1968 cm^{-1} as shown in Figure 3.15. The absorbance of the free ligand features a strong absorption at 270 nm in the UV region potentially due to π to π* transition (Figure 3.16, blue trace). When compared to the carbonyl complex (orange trace), there are more transitions resulting from the complex as can be seen by the presence of peaks at 262 nm, 257 nm and a shoulder one at 250 nm (inset). It is therefore possible that some of these transitions might result from ligand to metal charge transfer (LMCT) processes.

3.2.3 Electrochemical studies of (ArO)PNP-acridine and EPR studies of its radical anion

Treatment of (ArO)PNP-acridine, dissolved in dry THF, with one equivalent of KC_8 leads to an instant color change from yellow to green. The product of this reaction is indeed paramagnetic as confirmed by the broadened resonance in ^{1}H NMR and lack of a signal in ^{31}P NMR. Analysis of the sample by EPR further confirms the presence of unpaired electrons in the ligand. The experimental EPR pattern matches very well with the simulated one (Figure 3.17 and 3.18) and gives a *g*-value of 2.0047.

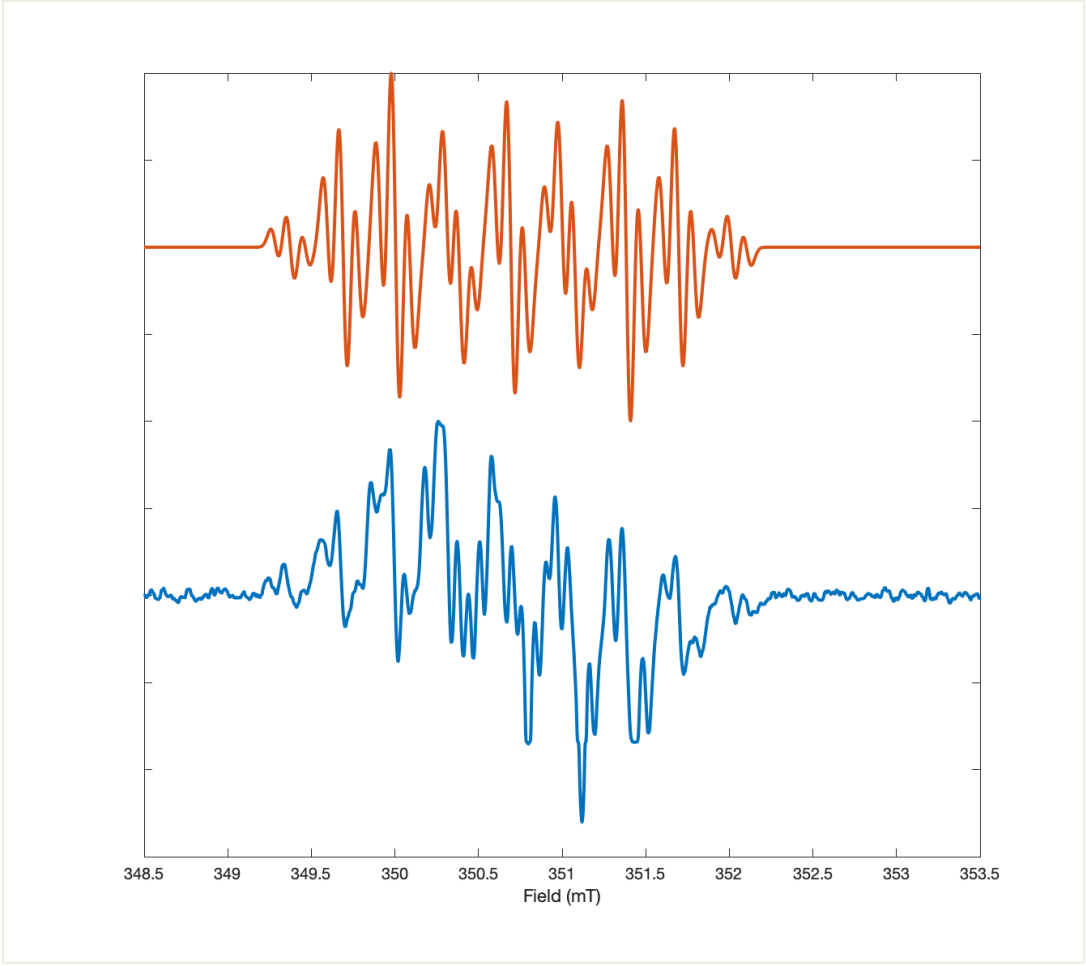

Figure 3.17. Stacked EPR spectra of the ligand ((ArO)PNP-acridine) radical anion; experimental (blue trace) and simulated (orange trace).

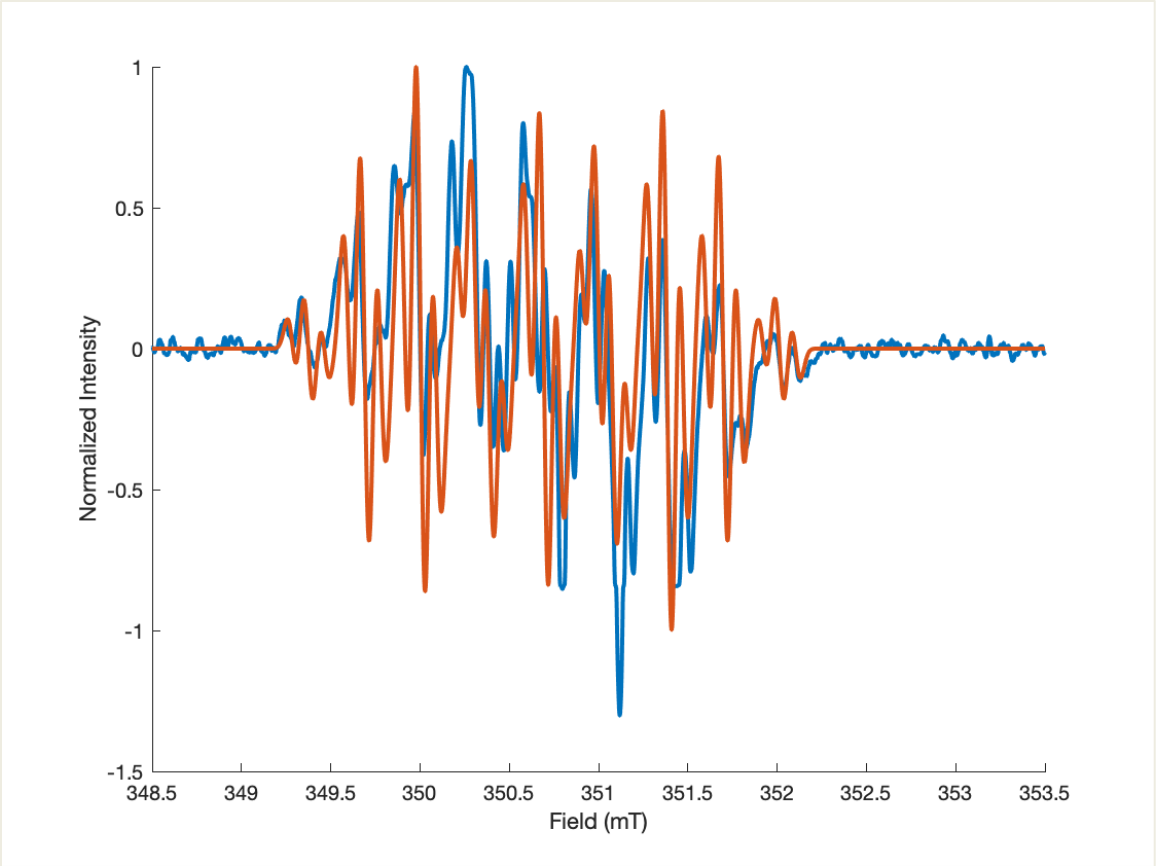

Figure 3.18. Overlaid EPR spectra of the ligand ((ArO)PNP-acridine) radical anion; experimental (blue trace) and simulated (orange trace).

For comparison, a sample of 0.01 g of [(ArO)PNP-acridine]Co(CO)$_2$ in 0.7 mL of dry THF was analyzed by EPR. The EPR pattern obtained is more complicated than the one for the ligand but clearly shows presence of a new paramagnetic species (Figure 3.19). The experimental and the simulated pattern do not match very well; however, the spectra shows species with isotropic best fit *g*-value of 2.0045 and hyperfine coupling constants shown in Table 3.1 below. This *g*-value is almost identical to that obtained for the ligand radical anion.

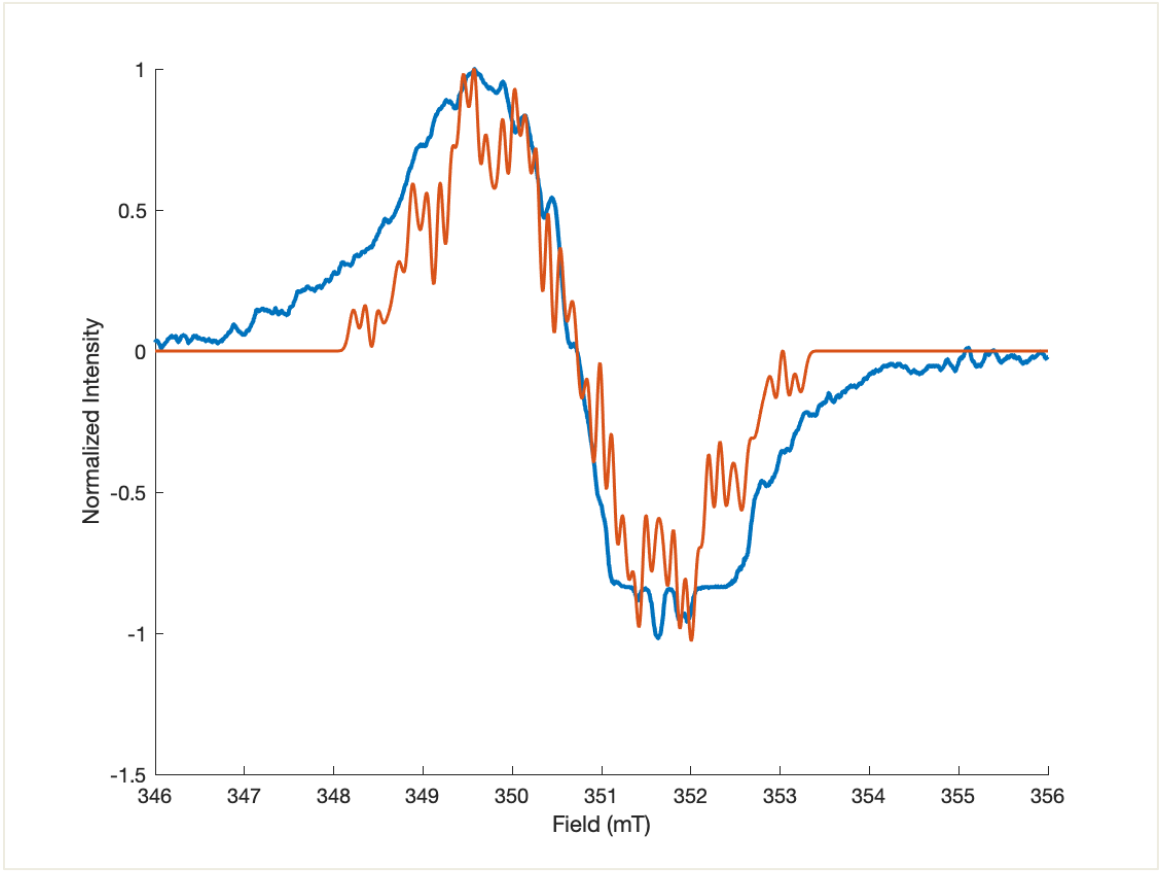

Figure 3.19. Overlaid EPR spectra of [(ArO)PNP-acridine]Co(CO)$_2$ complex; experimental (blue trace) and simulated (orange trace).

Table 3.1. Hyperfine splitting constants for the radical anion ligand and its cobalt complex.

	Hyperfine coupling constants (MHz)				
Complex	A_N	A_P	A_{Ho}	A_{Hp}	A_{Co}
(ArO)PNP-acridine radical	19.34	2.52	8.97	8.69	
[(ArO)PNP-acridine]Co(CO)$_2$	8.36	3.47	14.49	19.77	6.51

Distinguishing between metal- and ligand-centered radicals requires the application of many techniques, of which EPR is one.[80] Spectroscopic features of radical ligands mirror those of free organic radicals e.g. well-resolved EPR signals that are detectable at room temperature, and well-resolved ligand (super)-hyperfine coupling constants close to the *g*-

value of free electron (g_e =2.0023).[81] Metal-centered radical complexes on the other hand generally display much broader spectra as a result of rapid electron-spin relaxation effects.[80-81] Therefore for metal-centered radicals, EPR data acquisition at lower temperatures (<70 K) are preferred, and normally lead to anisotropic spectra.[81] Typical but not always, are the much larger deviations (g >2.1 or g <1.95) of the g-anisotropies of these metalloradicals from g_e compared to those of radical ligand complexes.[81] The g-value and hyperfine constants alone are not sufficient to assign radicals as either metal-centered or ligand-centered. However, more often than not, an observation of sharp and strong EPR spectra of metal complexes in solution at room temperature is usually a strong indication that the unpaired electron is located in a ligand-based orbital with only weak mixing with metal orbitals.[81]

Electrochemical studies

The redox processes of the ligand ((ArO)PNP-acridine) were examined using cyclic voltammetry. The voltammogram of a 10 mM solution of the ligand in CH_2Cl_2 shows a reversible process with an onset of reduction at -2.40 V (relative to Cp_2Fe/Cp_2Fe^+) (Figure 3.19). (The values for the plot are corrected to the mid-point of the redox wave of ferrocenium).

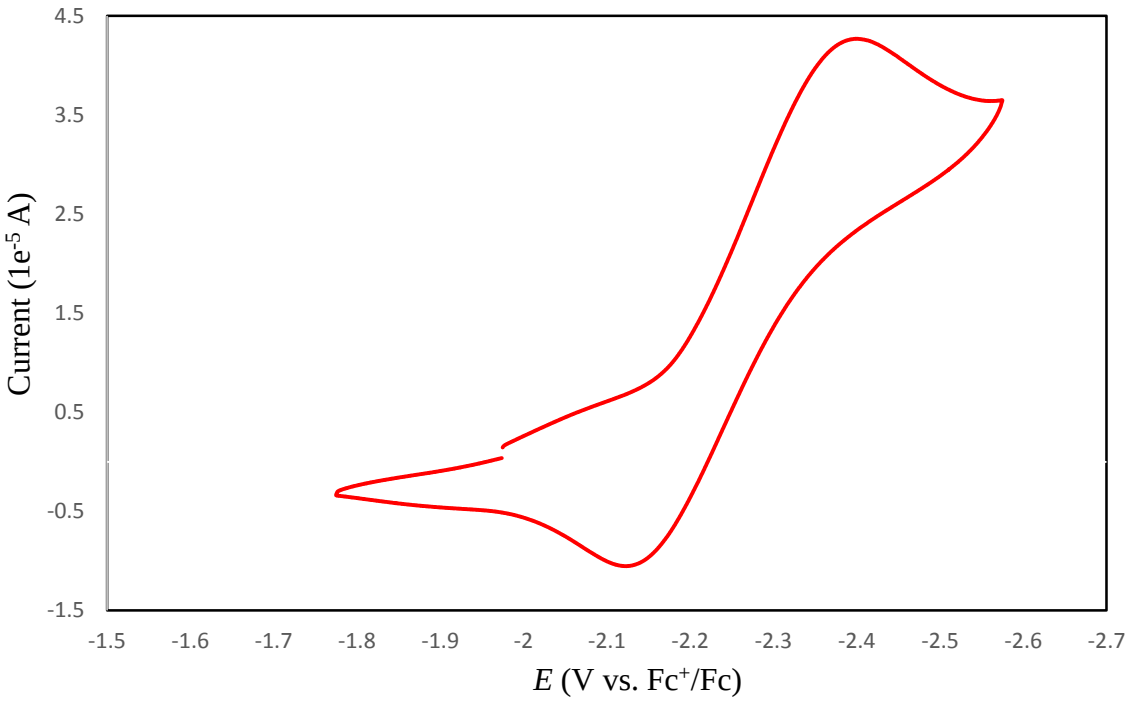

Figure 3.20. Cyclic voltammogram of (ArO)PNP-acridine in CH_2Cl_2.

Conditions: 10 mM solution of ((ArO)PNP-acridine) in CH_2Cl_2, 0.1 M ([*n*-Bu_4N][PF_6]), 1.0 mm Pt electrode, 100 mV/s scan rate. Temperature: 25 ^oC.

3.3 Concluding Remarks

We have herein reported a new synthesis of a rigid tridentate PNP-acridine starting from bis(4-*tert*-butylphenyl)amine or parent acridone that eliminates the requirement of pre-functionalized substrates. We have showed that it is possible to install nucleophiles at the C-9 after the synthesis of PNP-acridine ligand. We have also presented a route for the installation of alkylphosphine moieties on this backbone instead of the known aryl ones. We have applied the ligand to synthesize and characterize different transition metal complexes. Due to the ability of this ligand to support transition metal in different oxidation states, and having been earlier showed to be applicable in a number of catalytic reactions,

this new synthetic route will open a number of opportunities for elaborations and catalytic applications.

3.4 Experimental

3.4.1 General Considerations

All reactions, unless otherwise stated, were carried out in an MBraun inert atmosphere (nitrogen) glovebox, or in a resealable glassware on a Schlenk line under argon atmosphere. Glassware and magnetic stir bars were dried in a ventilated oven at 160 °C and were allowed to cool under vacuum. Molecular sieves (Alfa Aesar) and Celite (EMD 545) were dried under vacuum for at least twelve hours at 160 °C.

^{1}H, ^{31}P spectra were obtained using a Varian Vx 400 MHz or Varian Mercury 300 (300.323 MHz for ^{1}H) spectrometer and ^{13}C, NMR spectra were obtained using either Avance IIIHD 500 spectrometer, or Bruker Avance IIIHD 700 spectrometer. ^{1}H and ^{13}C NMR chemical shifts are referenced with respect to solvent signals and are reported relative to tetramethylsilane.[82] ^{31}P NMR chemical shifts were referenced to 85% H_3PO_4 as an external standard. UV-Vis samples were prepared in the glovebox and transferred into resealable cuvettes and the data acquired using UV-2401 PC recording spectrophotometer. Cyclic voltammetry experiments were performed inside an N_2-filled glovebox in CH_2Cl_2 with 0.1 M ([*n*-Bu_4N][PF_6]) as the supporting electrolyte. The voltammograms were recorded with a CH instrument 620C potentiostat using a 2.5 mm (outer diameter), 1.0 mm (inner diameter) Pt disk working electrode, Ag wire quasi-reference electrode, and a Pt wire auxiliary electrode, at a scan rate of 0.1 V s^{-1}. Reported potentials are referenced to the ferrocenium/ferrocene (Fc^{+}/Fc) redox couple added as an internal standard at the

conclusion of each experiment. Elemental analyses were performed by Atlantic Microlab, Inc. in Norcross, GA. Infrared spectra were collected from neat and liquid samples using a Bruker Alpha-P infrared spectrometer equipped with an attenuated total reflection (ATR) attachment. Since the instrument is inside glovebox, data acquisition for air and moisture sensitive samples were all carried out in the glovebox.

3.4.2 Materials and Methods

Dichloromethane (BDH), diethyl ether (EMD Millipore Omnisolv), hexanes (EMD Millipore Omnisolv), tetrahydrofuran (THF, EMD Millipore Omnisolv), and toluene (EMD Millipore Omnisolv) were sparged with ultra-high purity argon (NexAir) for 30 minutes prior to first use, dried using an MBraun solvent purification system. These solvents were further dried over sodium benzophenone ketyl, transferred under vacuum to an oven-dried sealable flask, and degassed by successive freeze–pump–thaw cycles. Anhydrous benzene (EMD Millipore Drisolv) and anhydrous pentane (EMD Millipore Drisolv), both sealed under a nitrogen atmosphere, were used as received and stored in a glovebox. Acetic acid (Alfa-Aesar), methanol (BDH), acetone (BDH), dichloromethane (BDH) hydrochloric acid (EMD) chloroform (BDH), ethylene glycol (BDH) for benchtop work was used as received. Tap water was purified in a Barnstead International automated still prior to use.

Dichloromethane-d_2 (Cambridge Isotope Labs) and acetonitrile-d_3 (Cambridge Isotope Labs) were dried over excess calcium hydride overnight, vacuum-transferred to an oven-dried sealable flask, and degassed by successive freeze-pump-thaw cycles. Tetrahydrofuran-d_8 (Cambridge Isotope Labs) was dried over sodium benzophenone ketyl,

vacuum-transferred to an oven-dried sealable flask, and degassed by successive freeze-pump-thaw cycles. Deuterium oxide (Cambridge Isotope Labs), chloroform-*d* (Cambridge Isotope Labs), methanol-d_4 (Cambridge Isotope Labs) and methanol-d_1 (Cambridge Isotope Labs) were used as received.

Sodium *tert*-butoxide (TCI America), potassium *tert*-butoxide (Alfa-Aesar), silver trifluoromethanesulfonate (STREM), copper (I) chloride (Alfa-Aesar), *i*-Pr_2MgCl (Sigma Aldrich), *i*-Pr_2PCl (TCI), $ClPPh_2$ (TCI), $(C_6H_5CN)_2PdCl_2$ (STREM), *p*-tosylhydrazide (BTC), $(CH_3CH)_2PdCl_2$ (Sigma Aldrich), $(PPh_3)_2CoCl_2$ (Sigma Aldrich), 2, 4, 6-trimethylphenol (Alfa Aesar), magnesium sulfate (Alfa-Aesar), alumina (EMD), sodium metal (Alfa-Aesar), potassium (Sigma-Aldrich), benzophenone (Alfa-Aesar), calcium hydride (Alfa-Aesar), $^{13}CO_2$ (Cambridge Isotope Labs), hydrogen (Sigma- Aldrich), nitrogen (NexAir), carbon monoxide (GT&S Inc.) and argon (both industrial and ultra-high purity grades, NexAir) were used as received. Carbon dioxide (NexAir) was passed through phosphorus pentoxide (Sigma-Aldrich) to ensure dryness. Diethylzinc (Acros, 1M in hexanes), methylmagnesium bromide (Strem, 3M in diethyl ether) were used as received.

3.4.3 Experimental Procedures

3.4.3.1 2,7-Di-*tert*-butyl-9-chloro-4,5-bis(diphenylphosphino)acridine (**6**)

To a 100-mL Schlenk flask was added (0.42 g, 0.88 mmol) of 4,5-dibromo-2,7-di-*tert*-butyl-9-chloroacridine followed by 40 mL of dry and degassed THF to dissolve. This solution was cooled down to -35 ^oC. A solution of *n*-BuLi in hexanes (2.5 M, 0.74 mL, 1.8 mmol) was added dropwise over 10 min while stirring. This mixture was then stirred at

room temperature for 2 hours after which it was cooled back to -35 ^{o}C. Chlorodiphenylphosphine (0.32 mL, 1.8 mmol) was added all at once. The cooling bath was removed, and the dark brown solution set to stir at room temperature for 24 hours. The solvent was removed under vacuum to give an oily crude product. To this was added 40 mL of dried and degassed dichloromethane then filtered over basic alumina and Celite to give a light brown solution. After solvent removal, the crude product was taken up in 1.5 mL of CH_2Cl_2 followed by addition of 4 mL of chilled ethanol to precipitate the product. The precipitate was filtered and dried to give the product as a light yellow solid (0.126 g, 21%). ^{1}H NMR (400 MHz, CD_2Cl_2) δ (ppm) 8.24 (dd, *J* = 2.0, 0.5 Hz, 2H), 7.30-7.20 (m, 22H), 1.23 (s, 18H). $^{13}C\{^{1}H\}$ NMR (176 MHz, CD_2Cl_2): δ (ppm) 149.85 (C_{Ar}), 148.09 (C_{Ar}), 147.98 (C_{Ar}), 140.66 (t, C_{Ar}), 140.01 (d, C_{Ar}), 138.56 (d, C_{Ar}), 135.77 (C_{Ar}), 134.57 (d, C_{Ar}), 134.50 (d, C_{Ar}), 128.72 (C_{Ar}), 128.55 (C_{Ar}), 128.53 (d, C_{Ar}), 128.51 (C_{Ar}), 124.32 (C_{Ar}), 119.63 (C_{Ar}), 35.71 ($C(CH_3)$), 30.72 ($C(CH_3)$). $^{31}P\{^{1}H\}$ NMR (161 MHz, CD_2Cl_2, 85% H_3PO_4): δ (ppm) -13.83. Anal. Calcd for $C_{45}H_{42}ClNP_2$: C, 77.85; H, 6.10; N, 2.02. Found: C, 77.66; H, 6.02; N, 1.99.

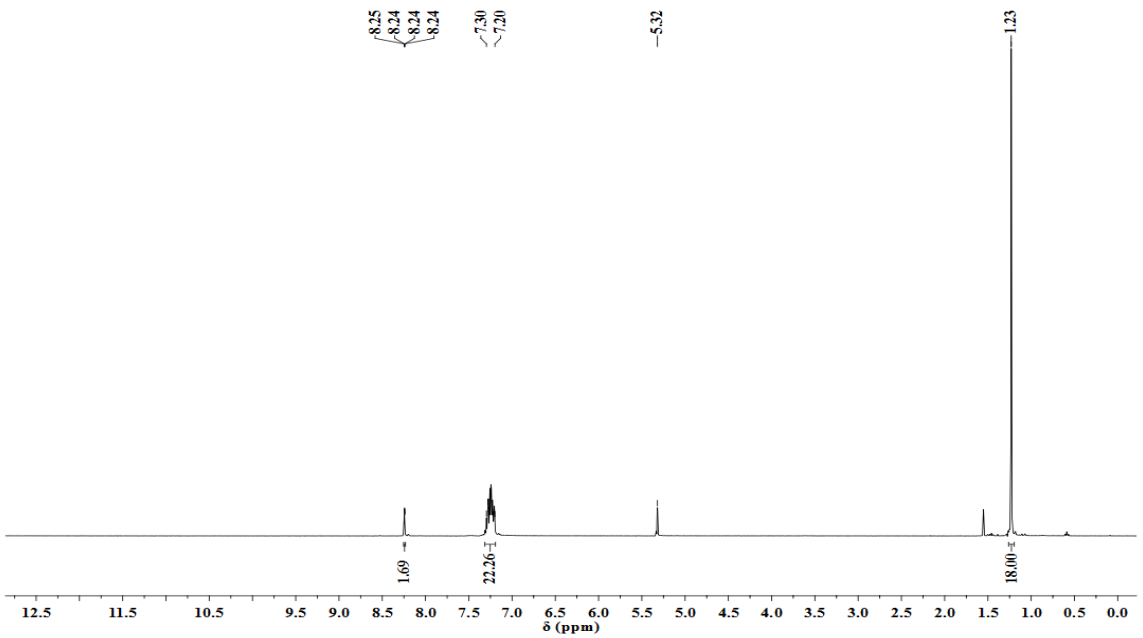

Figure 3.21. ^{1}H NMR spectrum of 2,7-di-*tert*-butyl-9-chloro-4,5-bis(diphenylphosphino)acridine in CD_2Cl_2 solution.

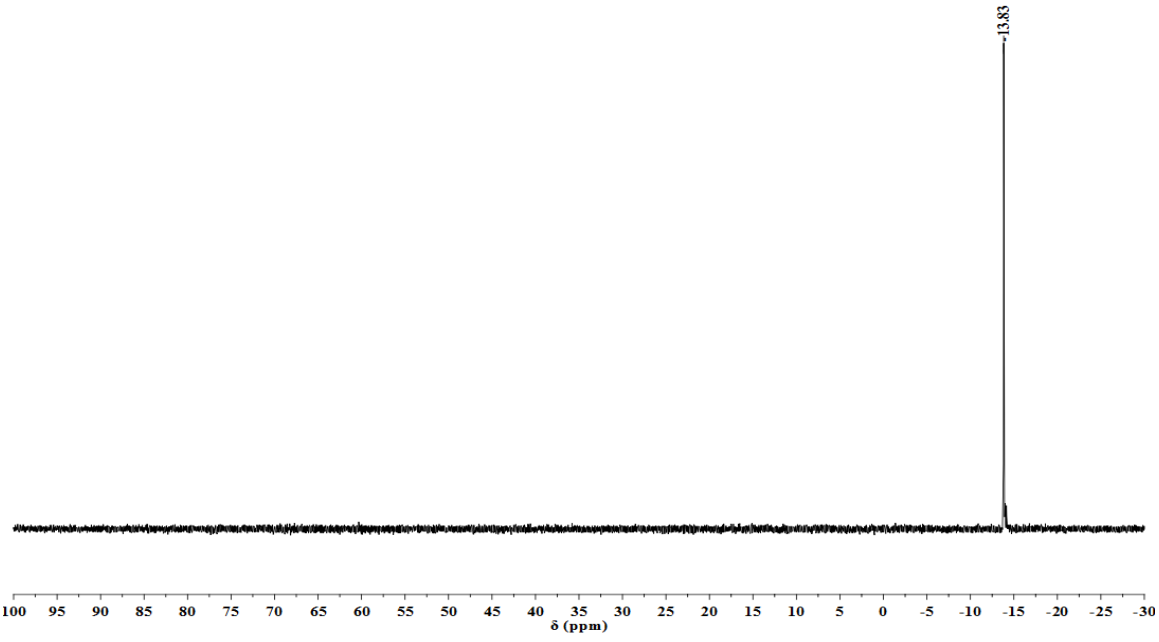

Figure 3.22. ^{31}P NMR spectrum of 2,7-di-*tert*-butyl-9-chloro-4,5-bis(diphenylphosphino)acridine in CD_2Cl_2 solution.

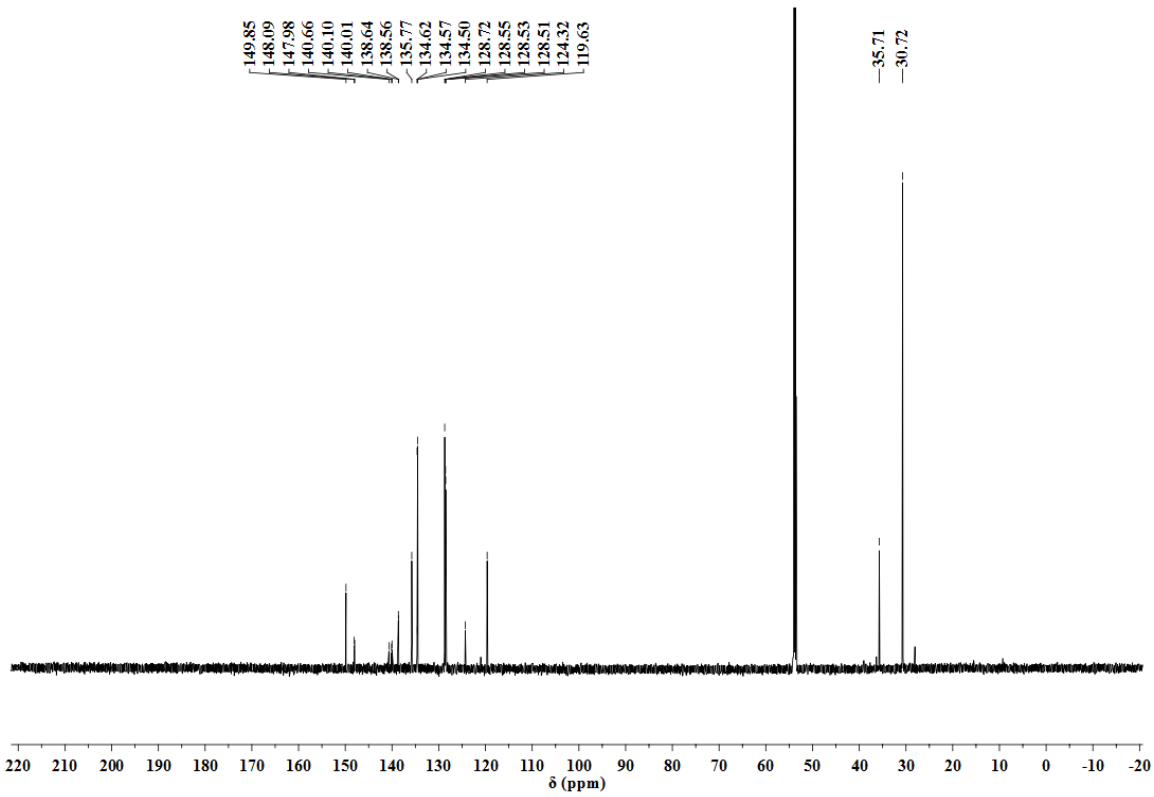

Figure 3.23. ^{13}C NMR spectrum of 2,7-di-*tert*-butyl-9-chloro-4,5-bis(diphenylphosphino)acridine in CD_2Cl_2 solution.

3.4.3.2 2,7-Di-*tert*-butyl-9-methoxy-4,5-bis(diphenylphosphino)acridine (**17**)

To a 100-mL Schlenk flask was added (4.00 mg, 0.174 mmol) of sodium followed by 1 mL of dry and degassed methanol. This was stirred till all the sodium is consumed. A solution of 2,7-di-*tert*-butyl-9-chloro-4,5-bis(diphenylphosphino)acridine (0.014 g, 0.020 mmol) in 1.5 mL of dry and degassed THF was added to the sodium methoxide solution. This mixture was brought to stir at 60 ^oC for 6 hours. The solvent was removed under vacuum leaving behind a yellow crude solid product. The solid was taken up in 2 mL of dichloromethane, to this solution was added 2 mL of H_2O and shaken to form layers then separated. The aqueous layer was extracted two more times with 1.5 mL each of dichloromethane. The combined organic layers were dried using anhydrous $MgSO_4$

and then filtered over Celite. Solvent was removed under vacuum to give a yellow solid. This was washed with 1 mL of cold methanol, filtered off and dried under vacuum to give pure product as a yellow solid (0.0104 g, 77%). ^{1}H NMR (400 MHz, C_6D_6) δ 8.20 (d, *J* = 2.1 Hz, 2H), 7.54 (td, *J* = 7.4, 1.7 Hz, 8H), 7.43 (dd, *J* = 3.5, 2.2 Hz, 2H), 7.08-7.13 (m, 12H), 3.76 (s, 3H), 1.18 (s, 18H). ^{13}C NMR (176 MHz, C_6D_6) δ 161.61 (t), 149.75 (d, *J* = 18.2 Hz), 147.80 (s), 141.18 (d, *J* = 17.4 Hz), 139.30 (d, *J* = 14.6 Hz), 135.02 (s), 134.83 (d, *J* = 20.9 Hz), 128.44 – 128.35 (m), 128.31 (s), 120.23 (s), 116.93 (s), 63.19 (s), 35.29 (s), 30.82 (s). ^{31}P{^{1}H} NMR (161 MHz, C_6D_6, 85% H_3PO_4): δ (ppm) -12.49. Anal. Calcd for $C_{46}H_{45}NOP_2$: C, 80.09; H, 6.58; N, 2.03. Found: C, 79.82; H, 6.75; N, 1.96.

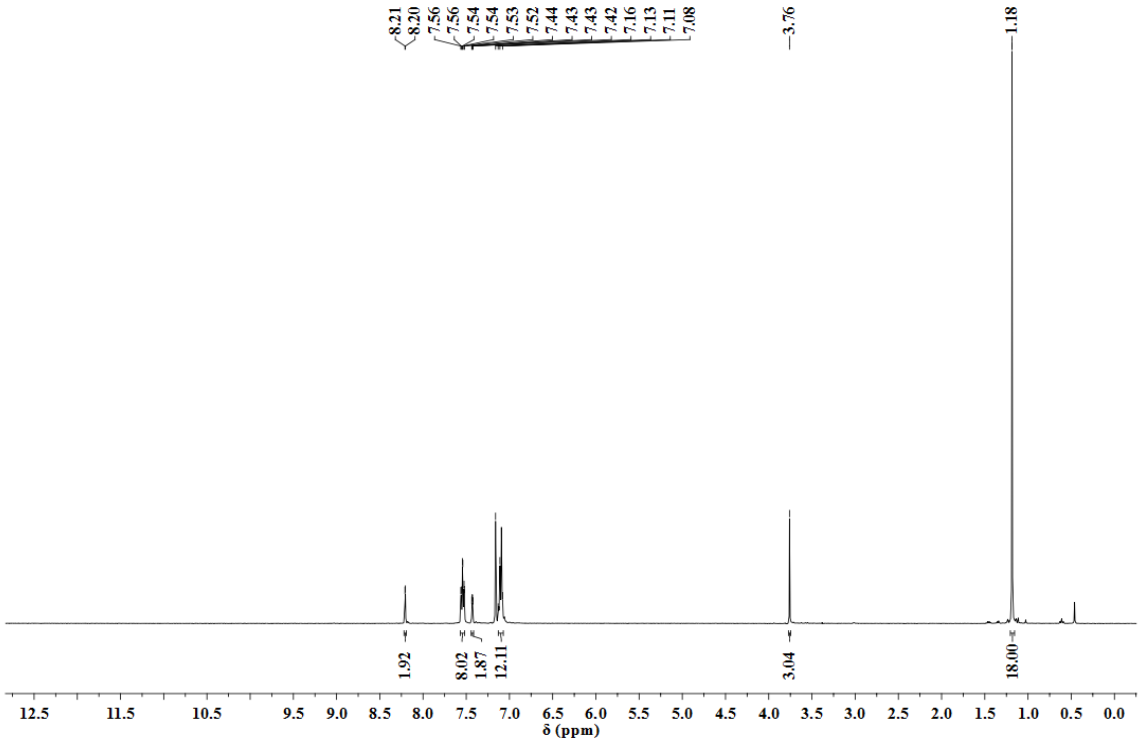

Figure 3.24. ^{1}H NMR spectrum of 2,7-di-*tert*-butyl-9-methoxy-4,5-bis(diphenylphosphino)acridine in C_6D_6 solution.

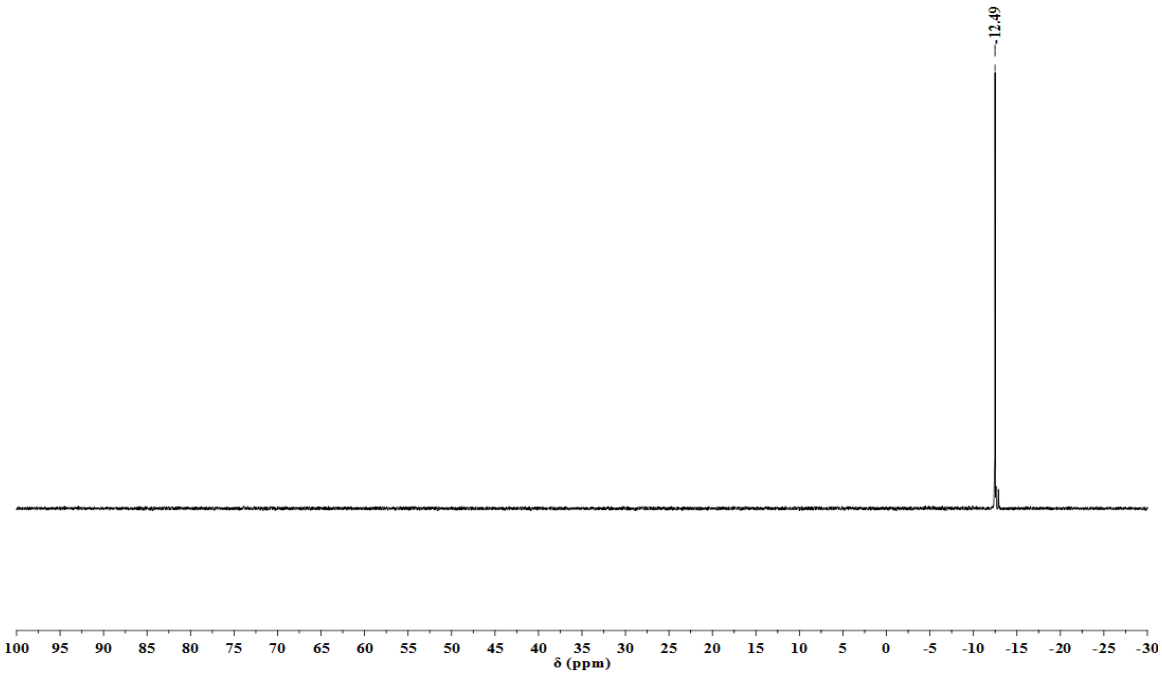

Figure 3.25. ^{31}P NMR spectrum of 2,7-di-*tert*-butyl-9-methoxy-4,5-bis(diphenylphosphino)acridine in C_6D_6 solution.

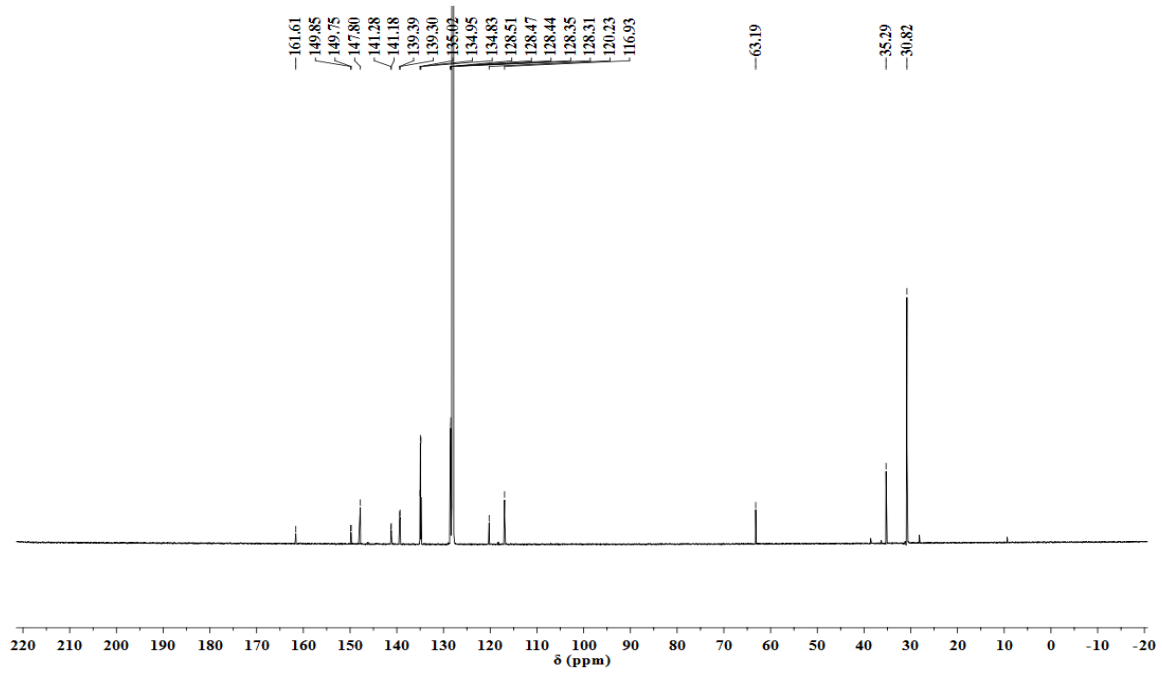

Figure 3.26. ^{13}C NMR spectrum of 2,7-di-*tert*-butyl-9-methoxy-4,5-bis(diphenylphosphino)acridine in C_6D_6 solution.

3.4.3.3 2,7-Di-*tert*-butyl-9-(2,4,6-trimethylphenoxy)-4,5-bis(diphenylphosphino) acridine (**18**)

To a 100-mL Schlenk flask was placed 2,7-di-*tert*-butyl-9-chloro-4,5-bis(diphenylphosphino)acridine, (0.018 g, 0.026 mmol), K_2CO_3 (0.110 g, 0.080 mmol), and 2,4,6-trimethylphenol (0.011 g, 0.081 mmol) followed by 2.5 mL of DMF. The mixture was set to stir at 60 ^oC for 72 hours. The solvent was removed under vacuum, and the crude solid taken up in dichloromethane. It was washed with water and the layers separated, the aqueous layer was extracted two more times with 1.5 mL of water each. The combined organic layers were dried using anhydrous $MgSO_4$ and filtered over Celite. The solvent was removed under vacuum to give a red-orange solid. This was washed with methanol, filtered off and dried under vacuum to give the product as an orange solid (0.012 g, 58%). ^1H NMR (400 MHz, C_6D_6) δ 8.20 (dd, *J* = 2.1, 0.8 Hz, 2H), 7.53 (td, *J* = 7.2, 1.7 Hz, 10H), 7.39 (dd, *J* = 3.5, 2.1 Hz, 2H), 7.13 – 7.05 (m, 14H), 6.67 (s, 2H), 2.09 (s, 3H), 2.01 (s, 6H), 1.06 (s, 18H). ^{13}C NMR (176 MHz, C_6D_6) δ 157.24 (s, C_{Ar}), 153.75 (s, C_{Ar}), 149.15 (d, C_{Ar}), 146.95 (s, C_{Ar}), 140.56 (d, C_{Ar}), 139.15 (d, C_{Ar}), 134.53 (s, C_{Ar}), 134.46 (d, C_{Ar}), 128.70 (s, C_{Ar}), 128.08 (s, C_{Ar}), 127.98 (t, C_{Ar}), 117.56 (s, C_{Ar}), 116.94 (s, C_{Ar}), 34.97 ($C(CH_3)$), 30.41 ($C(CH_3)$), 20.21 (phenoxy(CH_3)), 16.80 (phenoxy(CH_3)). $^{31}P\{^1H\}$ NMR (161 MHz, C_6D_6, 85% H_3PO_4): δ (ppm) -12.17. Anal. Calcd for $C_{54}H_{53}NOP_2$: C, 81.69; H, 6.73; N, 1.76. Found: C, 81.79; H, 6.90; N, 1.78.

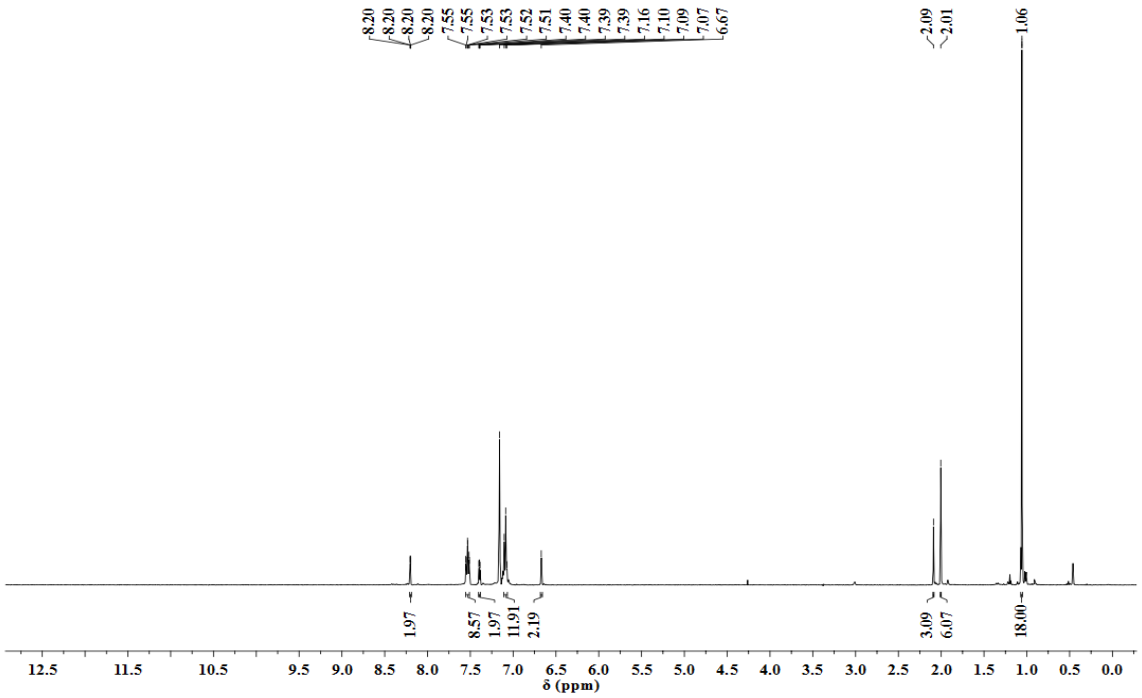

Figure 3.27. ^{1}H NMR spectrum of 2,7-di-*tert*-butyl-9-(2,4,6-trimethylphenoxy)-4,5-bis(diphenylphosphino)acridine in C_6D_6 solution.

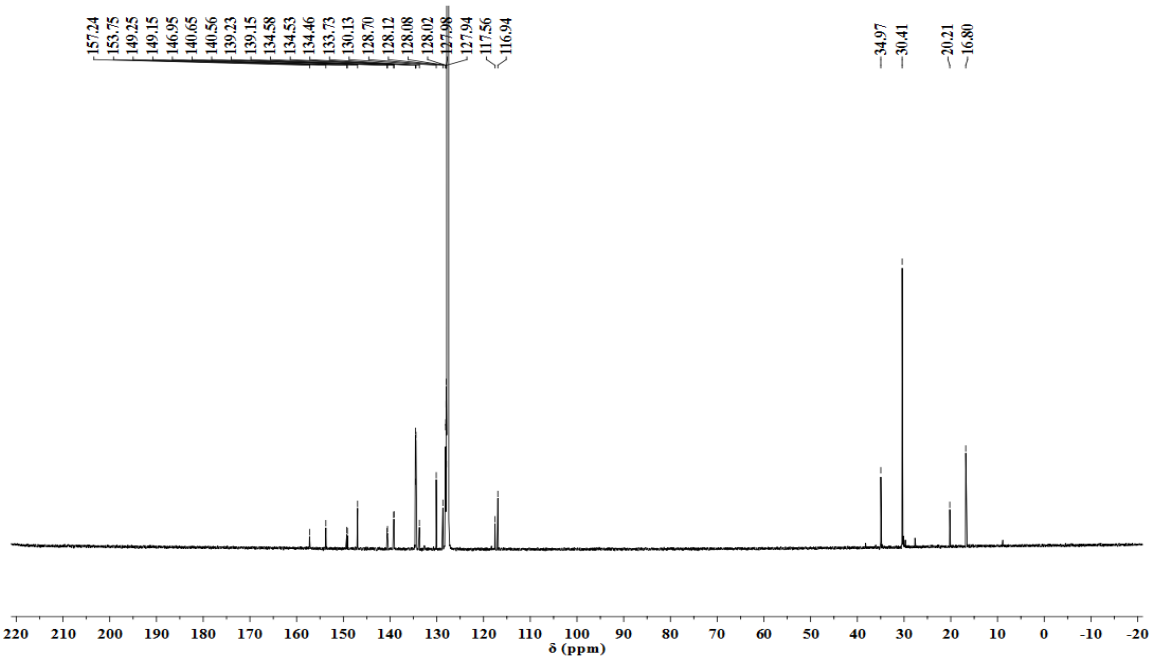

Figure 3.28. ^{13}C NMR spectrum of 2,7-di-*tert*-butyl-9-(2,4,6-trimethylphenoxy)-4,5-bis(diphenylphosphino)acridine in C_6D_6 solution.

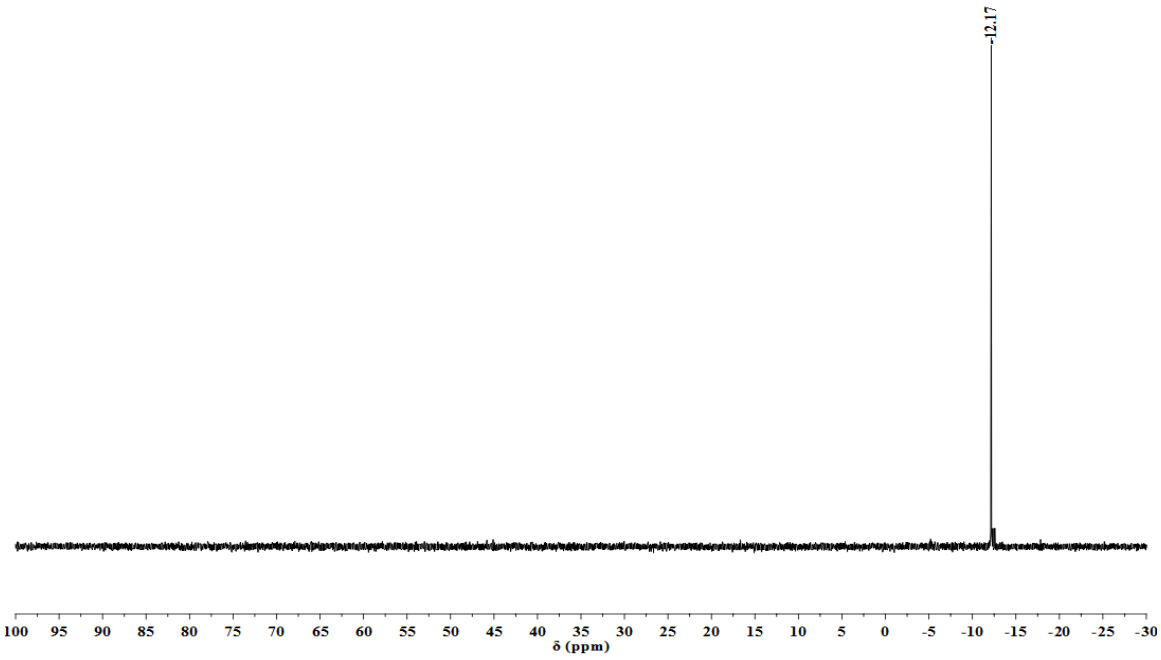

Figure 3.29. ^{31}P NMR spectrum of 2,7-di-*tert*-butyl-9-(2, 4, 6-trimethylphenoxy)-4,5-bis(diphenylphosphino)acridine in C_6D_6.

3.4.3.4 4,5-Dibromo-2,7-di-*tert*-butylacridine (**11**)

In a 250-mL Schlenk flask was placed *p*-tosylhydrazide (0.164 g, 0.883 mmol). This was evacuated and then refilled with argon. To the flask was added 4 mL of chloroform to dissolve then placed in oil bath at 50 ^{o}C. 4,5-dibromo-2,7-di-*tert*-butyl-9-chloroacridine (0.388 g, 0.803 mmol) was dissolved in 5 mL chloroform and this solution was added to the one in the flask at 50 ^{o}C. The mixture was stirred at this temperature for 15 min before setting to stir at room temperature for 12 hours. The solvent was removed under vacuum to give an oily crude, to which was added 2 mL of hexanes to produce product as a yellow precipitate. The precipitate was filtered off, washed with 1.5 mL of cold hexanes and dried under vacuum to give the product as a yellow solid (0.446 g, 83%). The ^{1}H NMR (400 MHz, $CDCl_3$) spectrum of the product showed broadened peaks at δ

(ppm) 10.16, 8.23, 7.81-7.76, 7.38-7.32, 2.45 and 1.42. This 9-(*p*-tosylhydrazide)-4,5-dibromoacridinium chloride salt was suspended in 16 mL of ethylene glycol. To this suspension was added 8 mL of 3.4 M NaOH solution and the mixture stirred at 100 ^{o}C for 2 hours forming a red-brown precipitate. It was cooled down to room temperature then poured into a beaker containing 5 mL ice-cold water. The red precipitate was collected via vacuum filtration and washed with water then dried for some time. This resulting solid was washed with cold methanol to give product as a white solid with some pink taint (0.261 g, 87%). ^{1}H NMR (400 MHz, CD_2Cl_2) δ 8.73 (s, 1H), 8.29 (d, J = 2.0 Hz, 2H), 7.90 (d, J = 2.0 Hz, 2H), 1.46 (s, 18H). ^{13}C NMR (101 MHz, CD_2Cl_2) δ 149.95 (s), 144.80 (s), 137.29 (s), 133.99 (s), 128.02 (s), 125.20 (s), 122.74 (s), 35.43 (s), 30.95 (s). Anal. Calcd for $C_{21}H_{23}Br_2N$: C, 56.15; H, 5.16; Br, 35.57; N, 3.12. Found: C, 56.35; H, 5.24; Br, 35.32; N, 3.07.

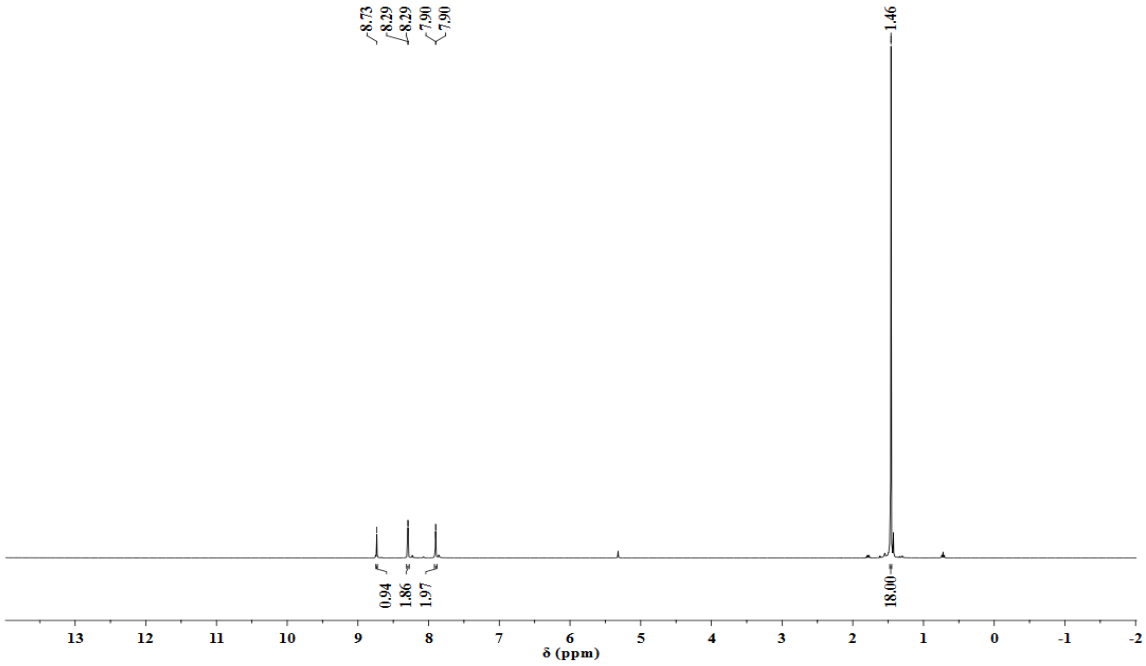

Figure 3.30. ^{1}H NMR spectrum of 4,5-dibromo-2,7-di-*tert*-butylacridine in CD_2Cl_2 solution.

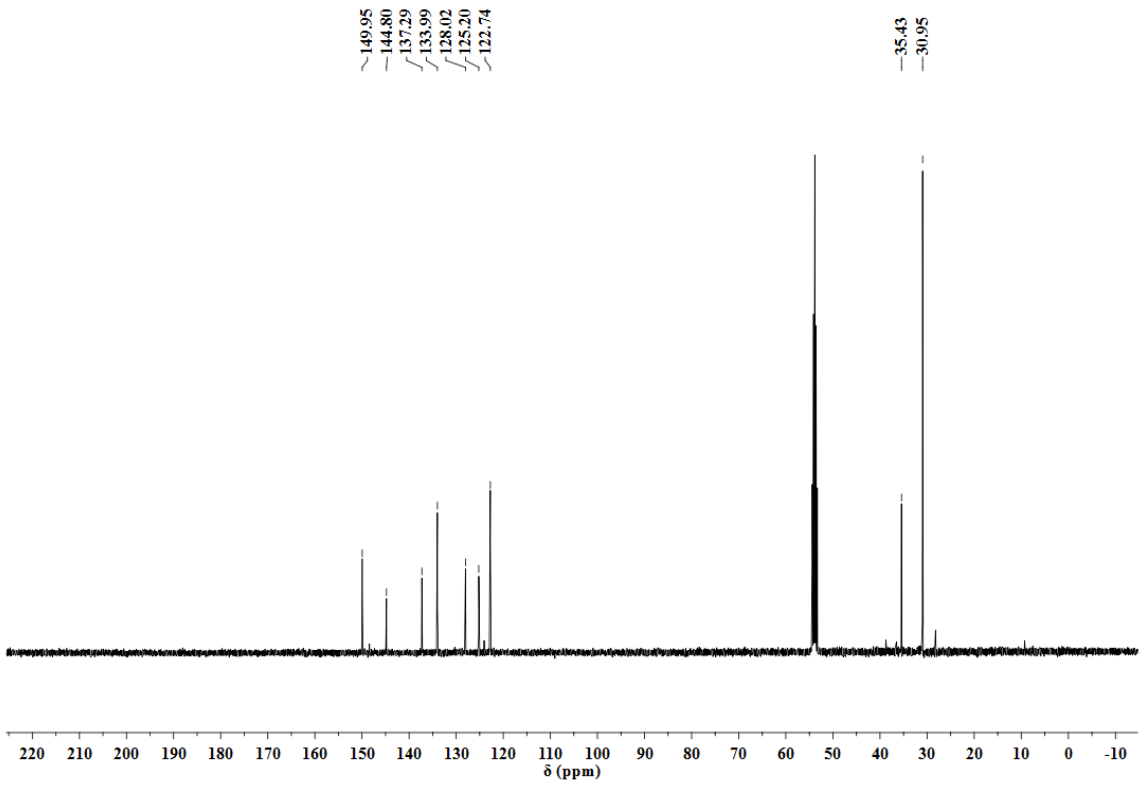

Figure 3.31. ^{13}C NMR spectrum of 4,5-dibromo-2,7-di-*tert*-butylacridine in CD_2Cl_2 solution.

3.4.3.5 2,7-Di-*tert*-butyl-4,5-bis(diisopropylphosphino)acridine

Into a 100-mL Schlenk flask was placed 4,5-dibromo-2,7-di-*tert*-butylacridine (0.374 g, 0.832 mmol) followed by 25 mL of diethyl ether to dissolve. This solution was cooled down to -35 ^oC. A solution of *n*-BuLi in hexanes (2.5 M, 0.7 mL, 1.7 mmol) was added dropwise while stirring. The reaction mixture was let to warm up to room temperature for 2 hours after complete addition. It was then cooled back to -35 ^oC, then (0.26 mL, 1.66 mmol) of chlorodiisopropylphosphine was added all at once. The reaction mixture was stirred at room temperature for 24 hours. An aliquot from this reaction showed only about 30% conversion to the desired product. The reaction was left to stir for another

12 hours after which conversion to the desired product improved to 50%. The solvent was removed under vacuum and the crude product taken up in degassed dichloromethane. It was filtered through a column containing 50:50 silica gel and basic alumina and the yellow second eluent collected. This eluent was evaporated to dryness. The product was precipitated using 1 mL of cold ethanol. This reaction however leads to formation of a mixture of products: 2,7-di-*tert*-butyl-4,5-bis(diisopropylphosphino)acridine (**12**) and 2,7-di-*tert*-butyl-9-(*n*-butyl)-4,5-bis(diisopropylphosphino)-9,10-dihydroacridine (**13**). Data for **12** ^{1}H NMR (400 MHz, CD_2Cl_2) δ (ppm) 8.65 (s, 1H), 8.03 (dd, *J* = 4.4, 2.4 Hz, 2H), 7.84 (d, *J* = 2.0 Hz, 2H), 2.80 (m, 4H), 1.47 (s, 18H), 1.17 (dd, *J* = 13.2, 7.2 Hz, 14H), 0.93 (dd, *J* = 13.2, 6.8 Hz, 14H). ^{31}P{^{1}H} NMR (161 MHz, CD_2Cl_2, 85% H_3PO_4): δ (ppm) -6.01 (The spectrum however has a very poorly resolved baseline). HRMS (ESI): m/z 524.36 [M+H] (Calcd for $C_{33}H_{51}NP_2$: 523.35).

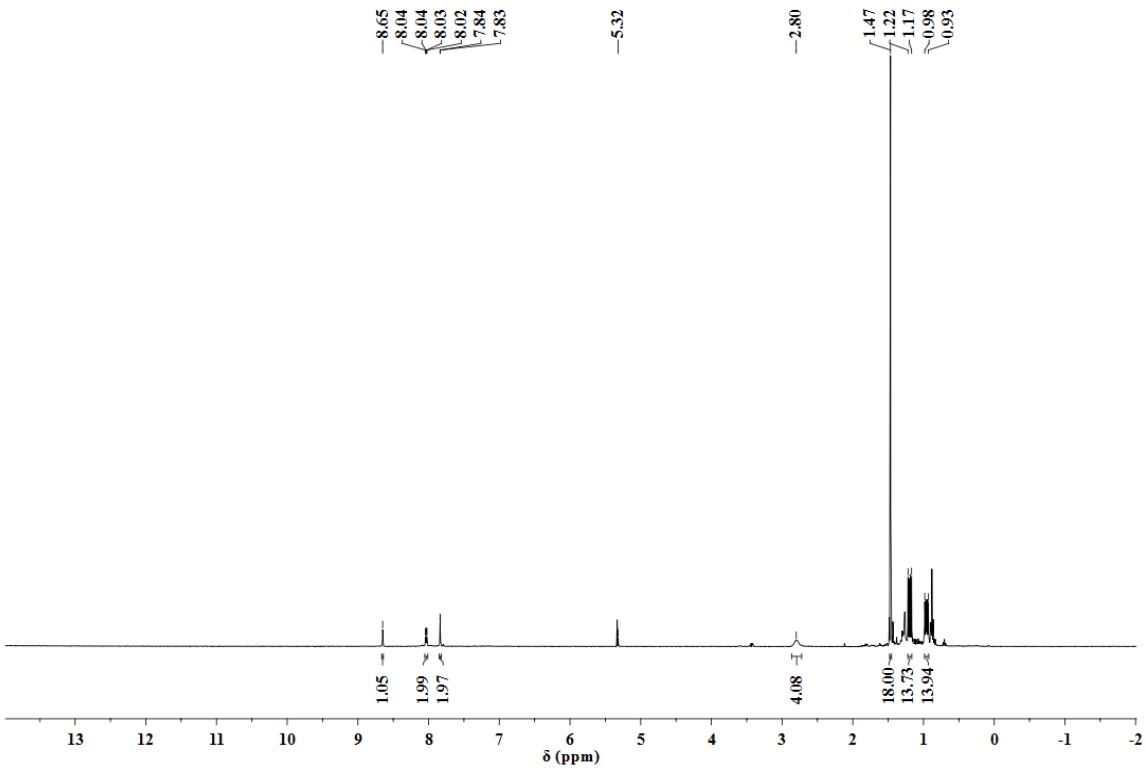

Figure 3.32. ^{1}H NMR spectrum of 2,7-di-*tert*-butyl-4,5-bis(diisopropylphosphino)acridine in CD_2Cl_2 solution.

Data for **13** ^{1}H NMR (400 MHz, CD_2Cl_2) δ (ppm) 8.93 (t, J = 8.8 Hz, 1H), 7.24 – 7.20 (m, 2H), 7.15 (d, J = 2.4 Hz, 2H), 2.28-2.17 (m, 4H), 1.33 (s, 18H), 1.22-1.12 (m, 18H), 1.01-0.91 (m, 17H), 0.80 (t, J = 6.8 Hz, 3H). $^{31}P\{^{1}H\}$ NMR (161 MHz, CD_2Cl_2, 85% H_3PO_4): δ (ppm) -16.02. HRMS (ESI): m/z 580.41 $[M]^+$ (Calcd for $C_{37}H_{61}NP_2$: 581.42).

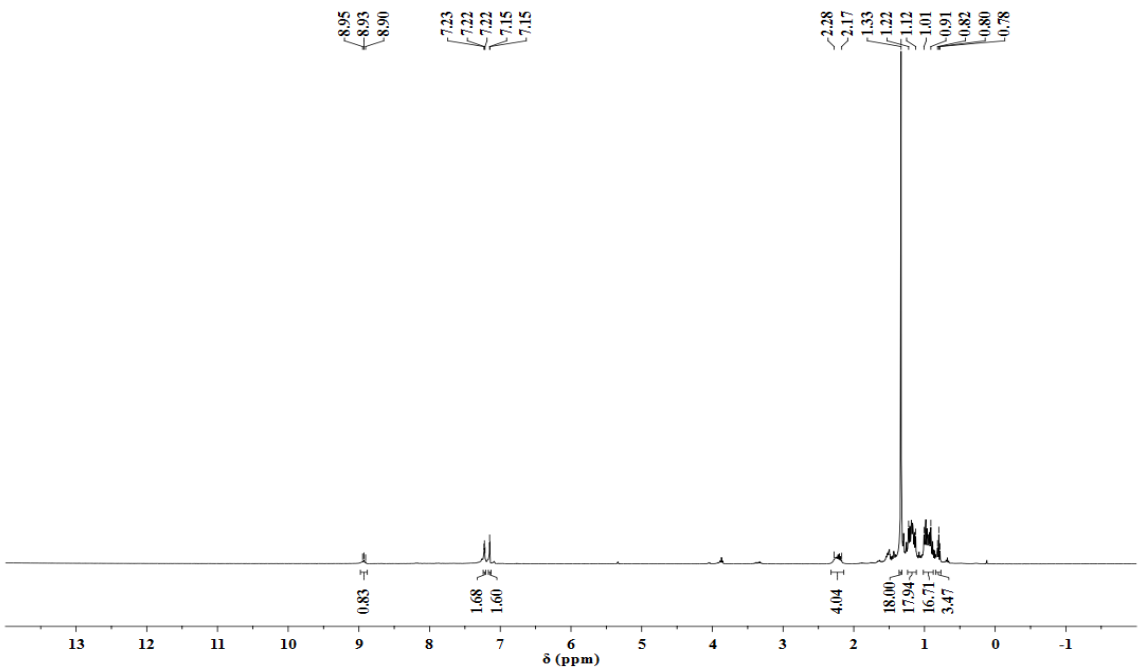

Figure 3.33. ^{1}H NMR spectrum of 2,7-di-*tert*-butyl-9-(*n*-butyl)-4,5-bis(diisopropylphosphino)-9,10-dihydroacridine in CD_2Cl_2 solution.

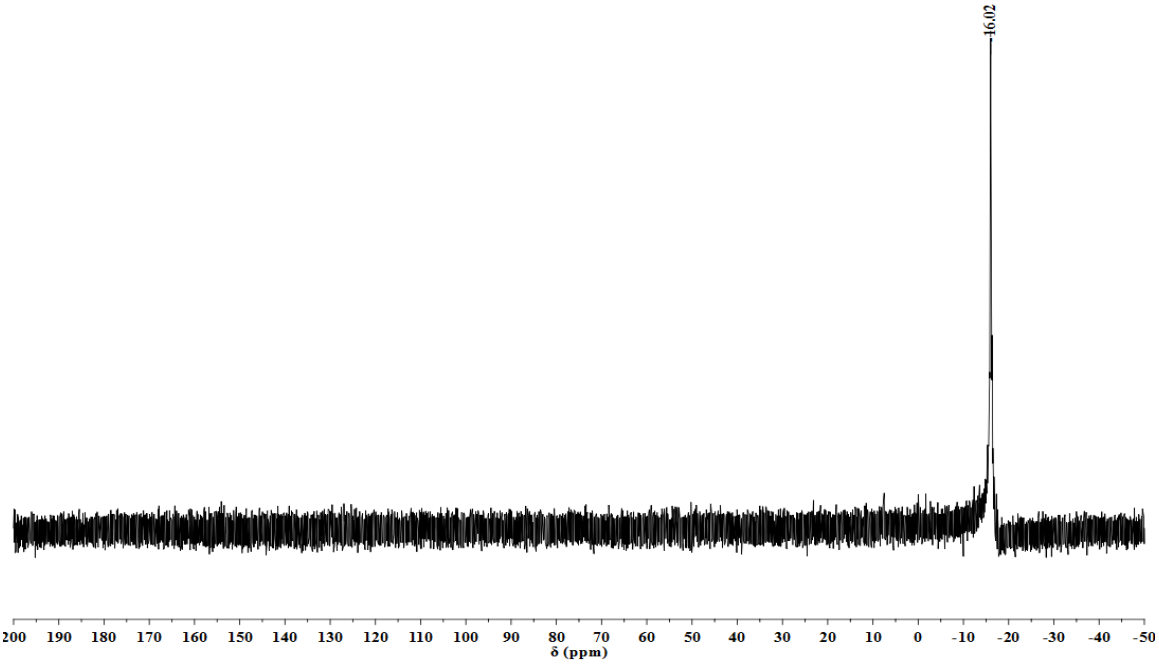

Figure 3.34. ^{31}P NMR spectrum of 2,7-di-*tert*-butyl-9-(*n*-butyl)-4,5-bis(diisopropylphosphino)-9,10-dihydroacridine in CD_2Cl_2 solution.

3.4.3.6 [2,7-Di-*tert*-butyl-9-chloro-4,5-bis(diphenylphosphino)acridine]silver triflate

To a 20-mL scintillation vial, (0.015 g, 0.021 mmol) of 2,7-di-*tert*-butyl-9-chloro-4,5-bis(diphenylphosphino)acridine was dissolved using 0.5 mL of CD_2Cl_2 solution. This solution was added dropwise to another vial containing silver triflate (0.006 g, 0.021 mmol) in 0.5 mL of CD_2Cl_2 solution and stirred for 3 hours. ^1H NMR (400 MHz, CD_2Cl_2) δ (ppm) 8.56 (d, *J* = 2.0 Hz, 2H), 7.75 (td, *J* = 5.6, 2.0 Hz, 4H), 7.63 (td, *J* = 6.0, 1.6 Hz, 8H), 7.46-7.40 (m, 8H), 7.17 (dd, *J* = 10.4, 2.0 Hz, 2H), 1.22 (s, 18H). $^{31}P\{^1H\}$ NMR (161 MHz, CD_2Cl_2, 85% H_3PO_4): δ (ppm) -6.14.

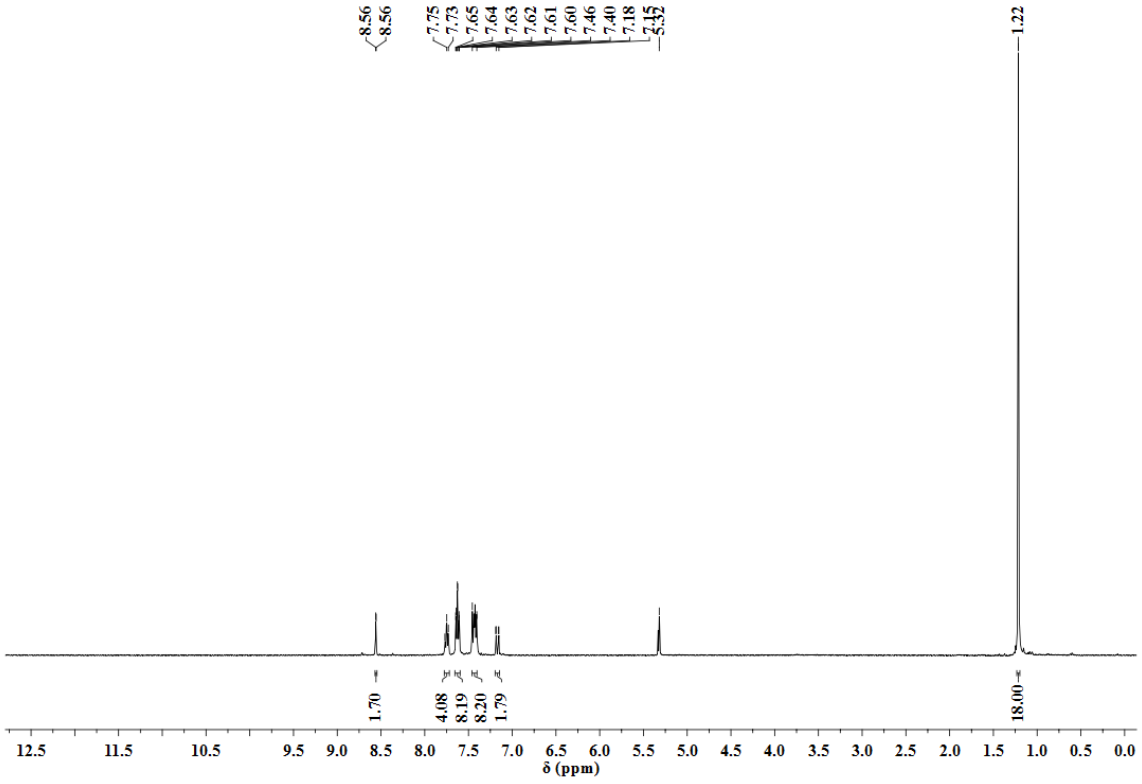

Figure 3.35. ^1H NMR spectrum of [2,7-di-*tert*-butyl-9-chloro-4,5-bis(diphenylphosphino)acridine]silver triflate in CD_2Cl_2 solution.

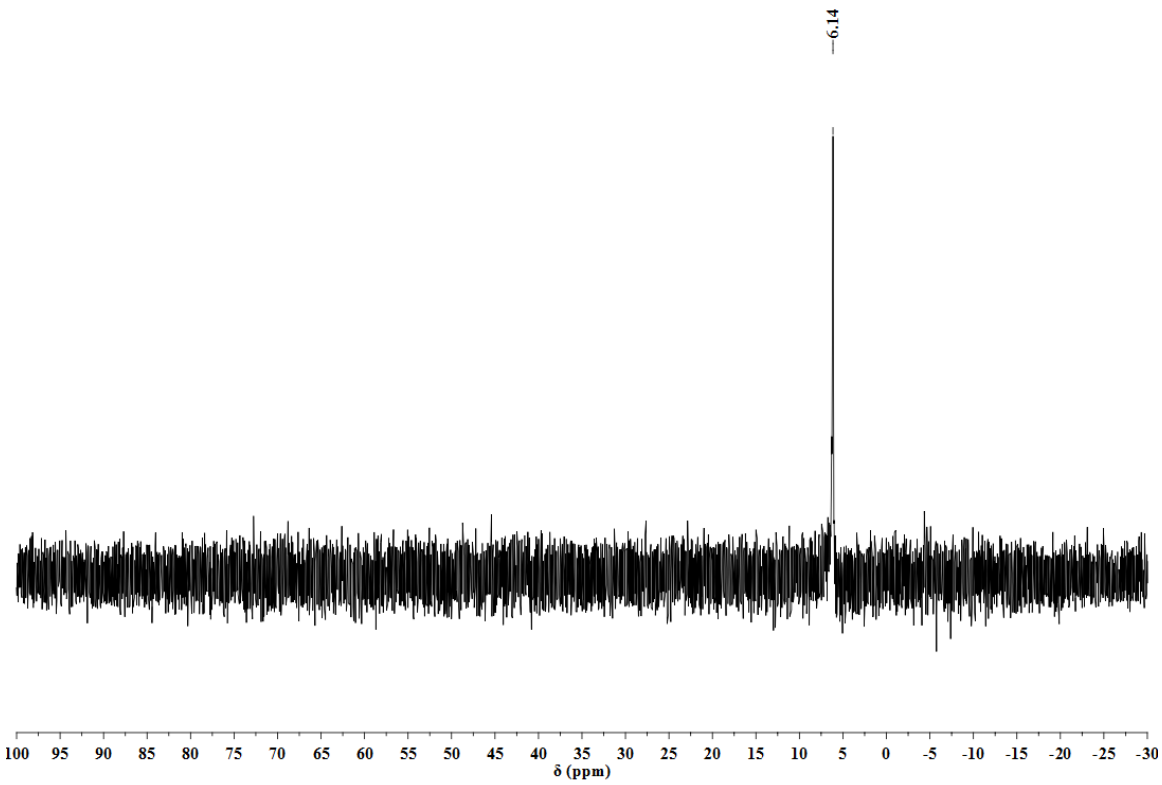

Figure 3.36. ^{31}P NMR spectrum of [2,7-di-*tert*-butyl-9-chloro-4,5-bis(diphenylphosphino)acridine]silver triflate in CD_2Cl_2 solution.

3.4.3.7 [2,7-Di-*tert*-butyl-9-chloro-4,5-bis(diphenylphosphino)acridine]palladium(II) tetrachloropalladate (**8**)

To a 20-mL scintillation vial (0.012 g, 0.014mmol) of 2,7-di-*tert*-butyl-9-chloro-4,5-bis(diphenylphosphino)acridine and (0.006 g, 0.014 mmol) of bis(benzonitrile)palladium(II) chloride were placed. Dichloromethane (1 mL) was added, and the mixture set to stir overnight. The solvent was removed under vacuum to dryness to give a brown-red solid. It was washed with 1 mL of cold methanol give the product as a brown solid (0.011 g, 92% yield). ^1H NMR (400 MHz, CD_2Cl_2) δ (ppm) 8.86 (d, J = 1.7 Hz, 2H), 8.38 (td, J = 5.8, 1.9 Hz, 2H), 7.85 (dd, J = 13.8, 7.2 Hz, 8H), 7.63 (t, J = 7.4 Hz,

4H), 7.55 (t, *J* = 7.5 Hz, 8H), 1.50 (s, 18H). $^{31}P\{^{1}H\}$ NMR (161 MHz, C_6D_6, 85% H_3PO_4): δ (ppm) 32.11.

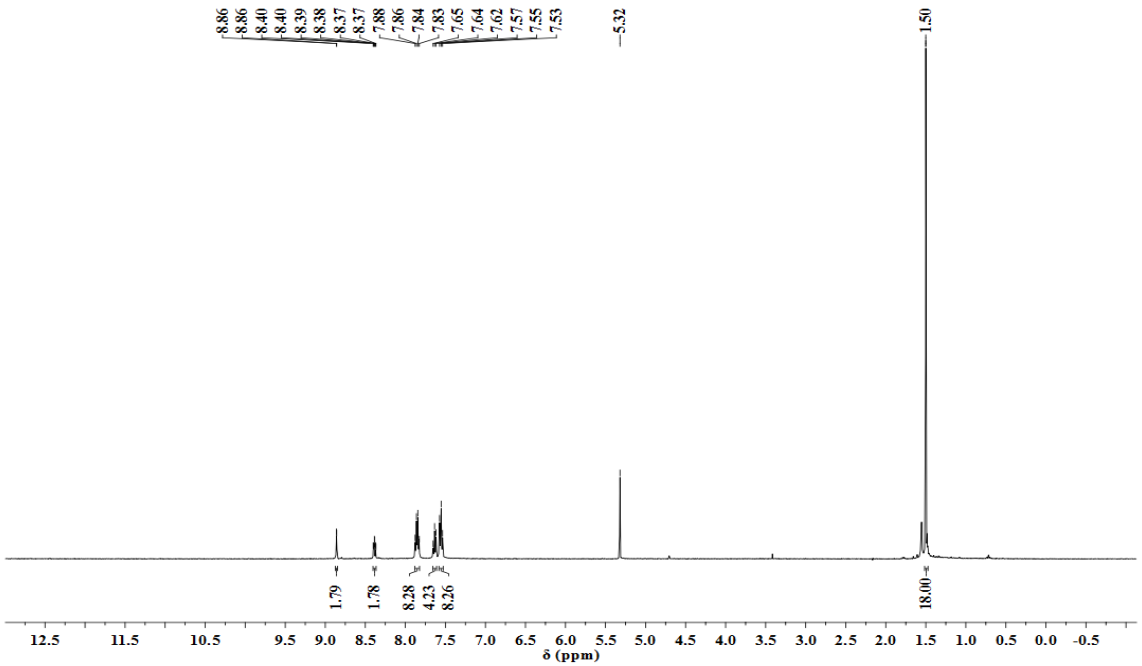

Figure 3.37. ^{1}H NMR spectrum of [2,7-di-*tert*-butyl-9-chloro-4,5-bis(diphenylphosphino)acridine]palladium(II) tetrachloropalladate in CD_2Cl_2 solution.

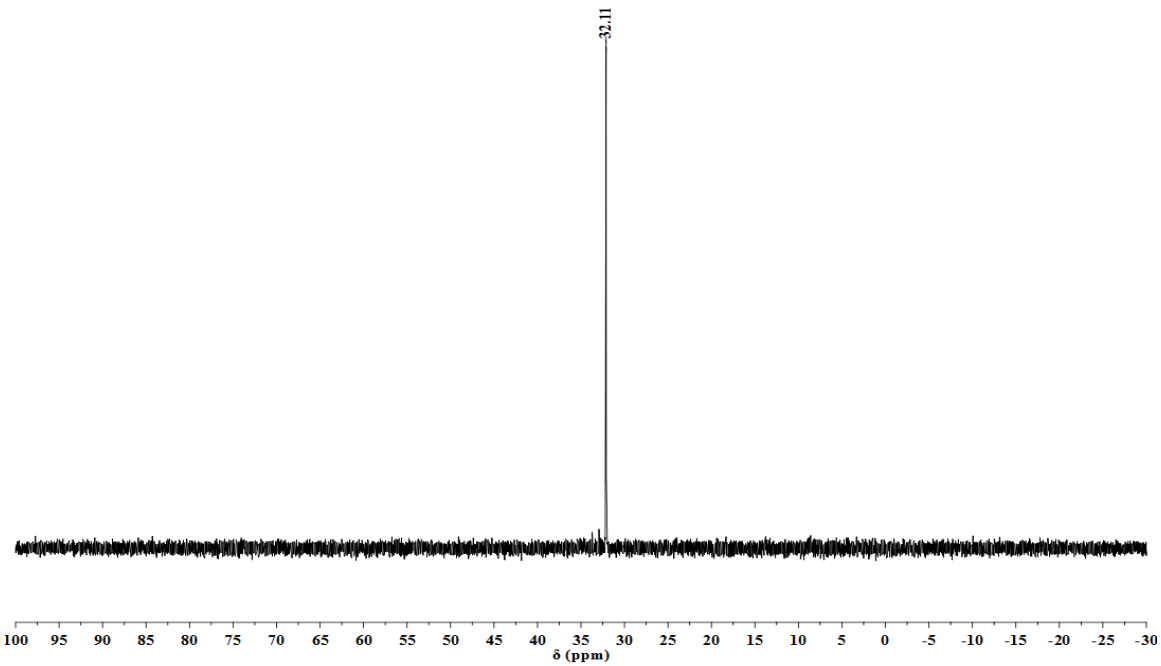

Figure 3.38. ^{31}P NMR spectrum of [2,7-di-*tert*-butyl-9-chloro-4,5-bis(diphenylphosphino)acridine]palladium(II) tetrachloropalladate in CD_2Cl_2 solution.

3.4.3.8 [2,7-Di-*tert*-butyl-9-chloro-4,5-bis(diphenylphosphino)acridine]cobalt(II) chloride (**7**)

Into a 20-mL scintillation vial fitted with a stir-bar (0.016 g, 0.024 mmol) of dichlorobis(triphenylphosphine)cobalt(II) was dissolved using 1 mL of THF. To this was added solution of 2,7-di-*tert*-butyl-9-chloro-4,5-bis(diphenylphosphino)acridine (0.015 g, 0.022 mmol) in 2 mL of THF dropwise while stirring. The reaction was set to stir at room temperature overnight after which solvent was evaporated to dryness. To this crude solid was added cold diethyl ether (2 mL) and then filtered off to give green solid which was further washed with 1.5 mL of cold diethyl ether. The solid was dried under vacuum to give a paramagnetic product (0.017 g, 96%) characterized by mass spectrometry ESI: m/z 787.15 $[M+Cl]^+$ (calcd for $C_{45}H_{42}Cl_2CoNOP_2$: 787.15, and $C_{45}H_{42}Cl_3CoNP_2$: 822.12).

3.4.3.9 [2,7-Di-*tert*-butyl-9-chloro-4,5-bis(diphenylphosphino)acridine]nickel(II) chloride (**9**)

Into a 20-mL scintillation vial, (0.024 g, 0.036 mmol) of dichlorobis(triphenylphosphine)nickel(II) was dissolved using 2 mL of dichloromethane. To this was added solution of 2,7-di-*tert*-butyl-9-chloro-4,5-bis(diphenylphosphino)acridine (0.025 g, 0.036 mmol) in 2 mL of dichloromethane dropwise while stirring. The reaction was set to stir for 12 hours at room temperature. Solvent was evaporated to dryness leaving behind a red solid. To this solid was added cold Et_2O (2 mL), filtered off and dried under vacuum to give a red-purple solid (0.025 g, 84%). ^{1}H NMR (400 MHz, CD_2Cl_2) δ (ppm) 8.59 (d, *J* = 2.0 Hz, 2H), 8.29 (d, *J* = 2.0 Hz, 2H), 8.03 (dt, *J* = 6.8, 1.6 Hz, 8H), 7.57 (tt, *J* = 7.6, 1.2 Hz, 4H), 7.49 (tt, *J* = 7.2, 1.2 Hz, 8H), 1.44 (s, 18H). ^{13}C NMR (176 MHz, CD_2Cl_2) δ (ppm) 152.79 (s), 151.34 (s), 145.37 (s), 139.91 (s), 134.94 (s), 133.59 (s), 132.16 (s), 129.37 (s), 129.01 (s), 127.46 (s), 124.43 (s), 36.05 (s), 30.85 (s). ^{31}P{^{1}H} NMR (161 MHz, C_6D_6, 85% H_3PO_4): δ (ppm) 24.67. Anal. Calcd for $C_{37}H_{27}Cl_2NNiP$: C, 65.61; H, 5.14; N, 1.70. Found: C, 66.10; H, 5.39; N, 1.70.

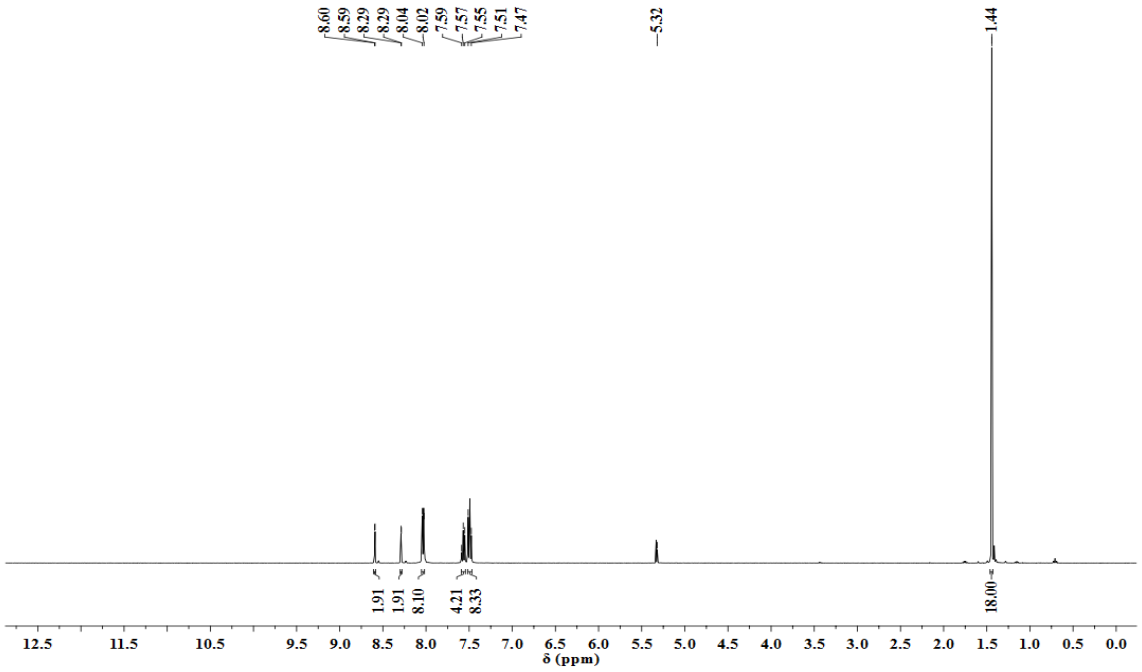

Figure 3.39. ^{1}H NMR spectrum of [2,7-di-*tert*-butyl-9-chloro-4,5-bis(diphenylphosphino)acridine]nickel(II) chloride in CD_2Cl_2 solution.

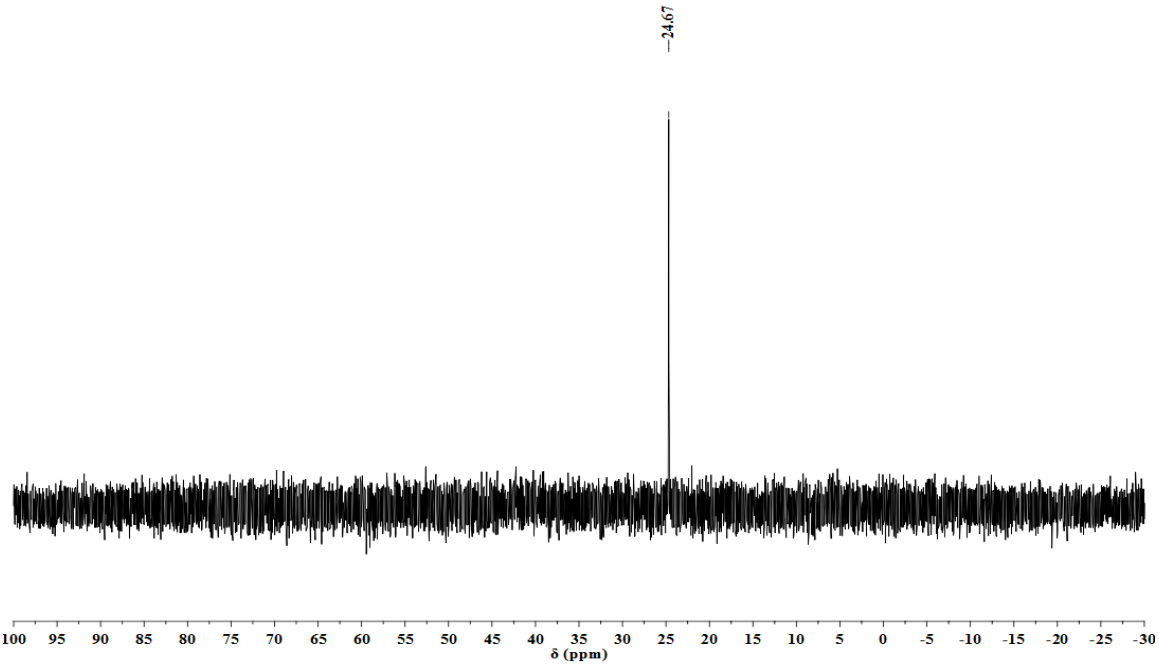

Figure 3.40. ^{31}P NMR spectrum of [2,7-di-*tert*-butyl-9-chloro-4,5-bis(diphenylphosphino)acridine]nickel(II) chloride in $CDCl_3$ solution.

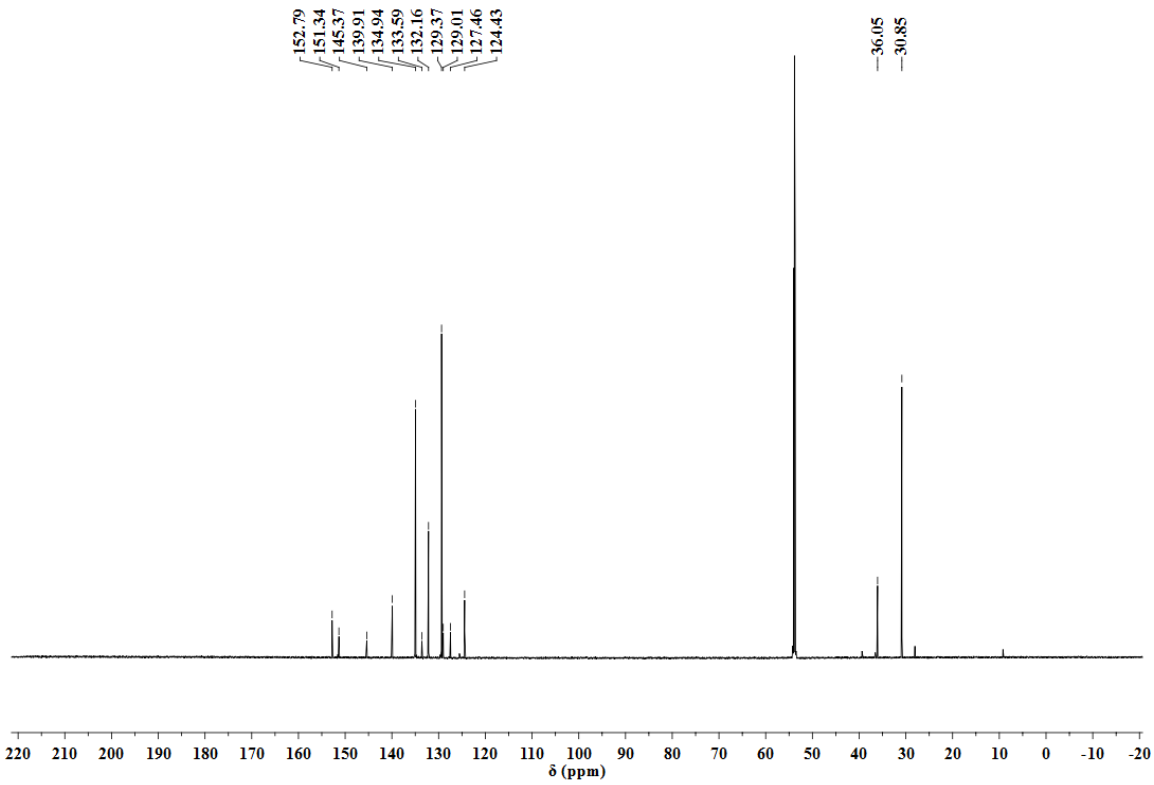

Figure 3.41. ^{13}C NMR spectrum of [2,7-di-*tert*-butyl-9-chloro-4,5-bis(diphenylphosphino)acridine]nickel(II) chloride in CD_2Cl_2 solution.

3.4.3.10 [2,7-Di-*tert*-butyl-9-chloro-4,5-bis(diphenylphosphino)acridine] diisopropylnickel(II) (**10**)

To a scintillation vial was placed (0.059 g, 0.072 mmol) of [2,7-di-*tert*-butyl-9-chloro-4,5-bis(diphenylphosphino)acridine]nickel(II) chloride and dissolved using 2 mL of toluene. Isopropylmagnesium chloride (76 µL, 0.15 mmol) was added to the solution at -35 ^oC while stirring. The reaction mixture was set to stir at room temperature for 12 hours after which the solvent was evaporated to dryness. Cold 1,4-dioxane (1 mL) was added and the resulting suspension filtered off. The filtrate was evaporated to dryness to give product as a purple solid (0.0493 g, 82% yield). ^1H NMR (400 MHz, C_6D_6) δ (ppm) 8.02 (dd, *J* = 12.2, 6.6 Hz, 8H), 7.57 (d, *J* = 1.9 Hz, 2H), 7.30 (dd, *J* = 7.0, 5.0 Hz, 2H), 6.97 (d, *J* = 6.7

Hz, 12H), 2.58 (septet, J = 6.8 Hz 2H), 1.22 (s, 18H), 1.07 (d, J = 6.4 Hz, 6H). $^{31}P\{^{1}H\}$ NMR (161 MHz, C_6D_6, 85% H_3PO_4): δ (ppm) 23.24.

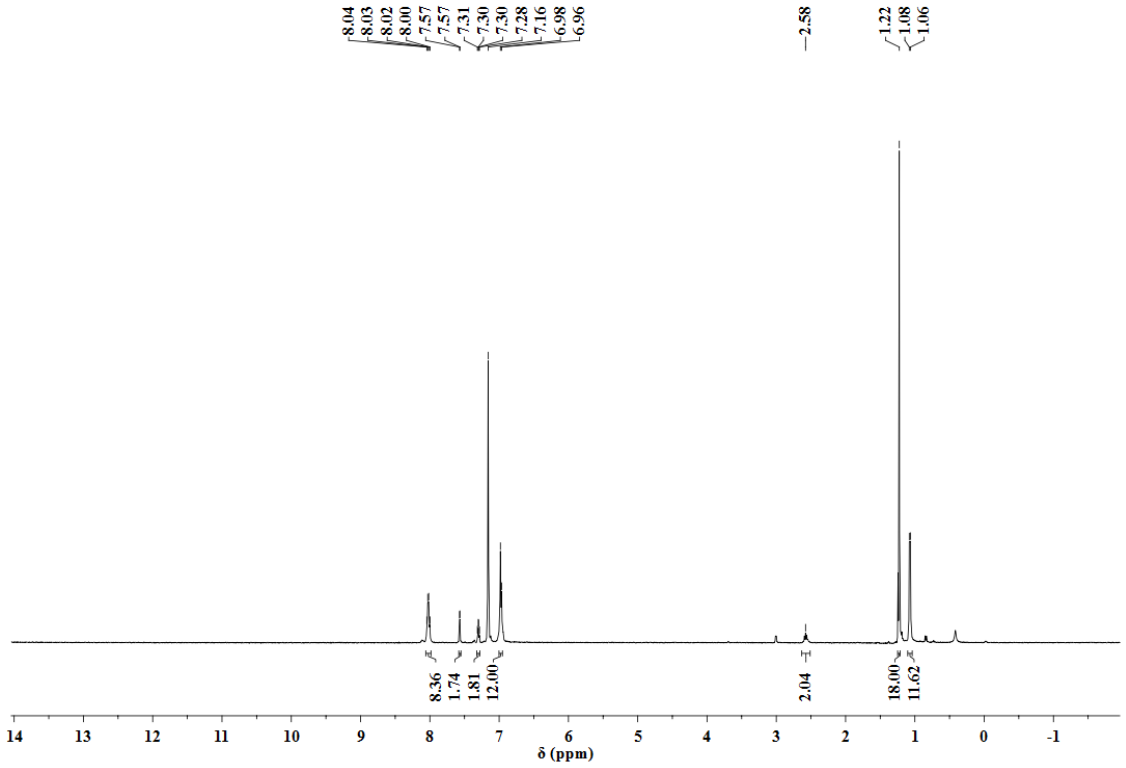

Figure 3.42. ^{1}H NMR spectrum of [2,7-di-*tert*-butyl-9-chloro-4,5-bis(diphenylphosphino)acridine]diisopropylnickel(II) in C_6D_6 solution.

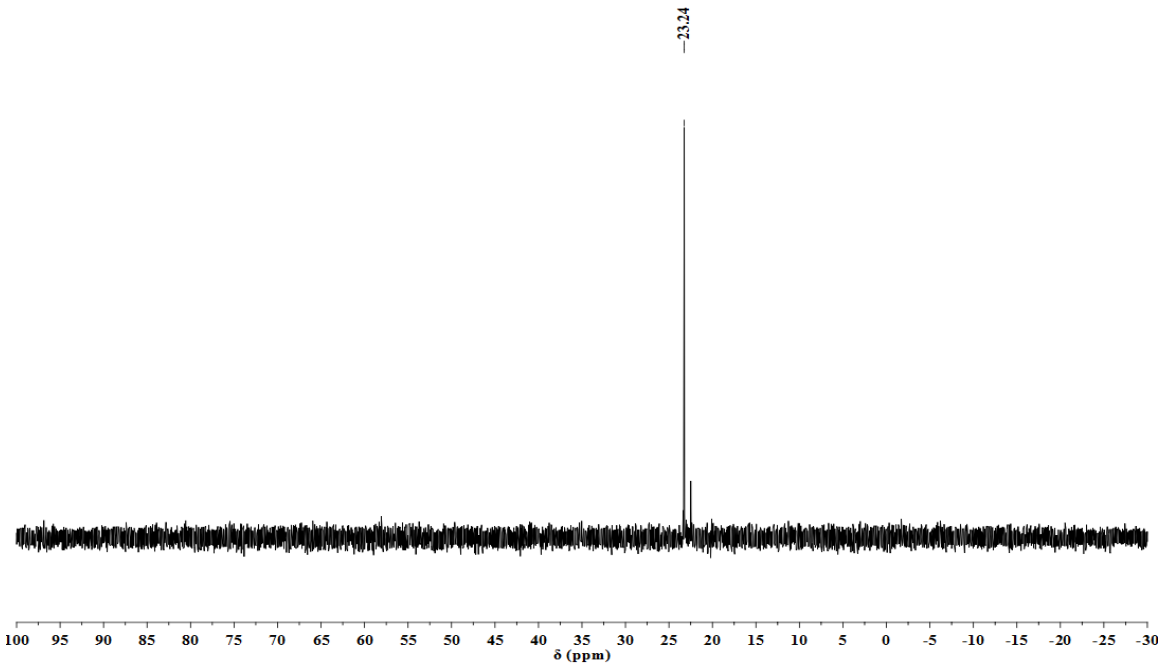

Figure 3.43. ^{31}P NMR of [2,7-di-*tert*-butyl-9-chloro-4,5-bis(diphenylphosphino) acridine]diisopropylnickel(II) in C_6D_6 solution.

3.4.3.11 [2,7-Di-*tert*-butyl-9-methoxy-4,5-bis(diphenylphosphino)acridine] cobalt(II) chloride (**20**)

To a 20-mL scintillation vial was placed 2,7-di-*tert*-butyl-9-methoxy-4,5-bis (diphenylphosphino)acridine (0.045 g, 0.068 mmol) and (0.045 g, 0.068 mmol) of dichlorobis(triphenylphosphine)cobalt(II). To this mixture was added 5 mL of THF and set to stir for 12 hours. The solvent was removed under vacuum to give an off-green solid. Cold Et_2O (2 mL) was added to wash the solid and then it was filtered off. The solid was dried under vacuum to give (0.047 g, 94% yield). It was analyzed by mass spectrum using HRMS (MALDI): m/z 818.21 $[M+Cl_2]^+$ (calcd for $C_{46}H_{45}Cl_2CoNOP_2$: 818.17).

3.4.3.12 [2,7-Di-*tert*-butyl-9-(2,4,6-trimethylphenoxy)-4,5-bis(diphenylphosphino)acridine]cobalt(II) chloride (**22**)

Into a 20-mL scintillation vial was placed 2,7-di-*tert*-butyl-9-(2,4,6-trimethylphenoxy)-4,5-bis(diphenylphosphino)acridine (0.067 g, 0.084 mmol) and (0.055 g, 0.084 mmol) of dichlorobis(triphenylphosphine)cobalt(II). To this was added 7.5 mL of THF and set to stir for 12 hours. The solvent was removed under vacuum to give a light green solid. Cold Et_2O (3 mL) was added to wash the solid and then it was filtered off. The solid was dried under vacuum to give (0.076 g, 97% yield). The product was analyzed by mass spectrum using HRMS (MALDI): m/z 887.36 $[M+Cl]^+$ (calcd for $C_{54}H_{53}ClCoNOP_2$: 887.26 and $C_{54}H_{53}Cl_2CoNOP_2$: 922.23).

3.4.3.13 [2,7-Di-*tert*-butyl-9-(2,4,6-trimethylphenoxy)-4,5-bis(diphenylphosphino)acridine]nickel(II) chloride (**19**)

Into a 20-mL scintillation vial, (0.012 g, 0.015 mmol) of dichlorobis(triphenylphosphine)nickel(II) and 2,7-di-*tert*-butyl-9-(2,4,6-trimethylphenoxy)-4,5-bis(diphenylphosphino)acridine (0.012 g, 0.015 mmol) were added then dissolved using 2 mL of dichloromethane. The reaction mixture was set to stir for 12 hours at room temperature. Solvent was evaporated to dryness leaving behind a reddish-purple solid. To this was added cold Et_2O (1 mL) and the filtered off to give red solid. This was dried under vacuum giving the product (0.014 g, 99%). ^{1}H NMR (400 MHz, THF-d_8) δ (ppm) 8.80 (s, 2H), 8.71 (s, 2H), 7.98 (d, J = 7.4 Hz, 8H), 7.53 (t, J = 7.2 Hz, 8H), 7.18 (t, J = 7.4 Hz, 4H), 7.03 (s, 2H), 2.31 (s, 3H), 2.11 (s, 6H), 1.25 (s, 18H). ^{31}P{^{1}H} NMR (161 MHz, C_6D_6, 85% H_3PO_4): δ (ppm) 23.77.

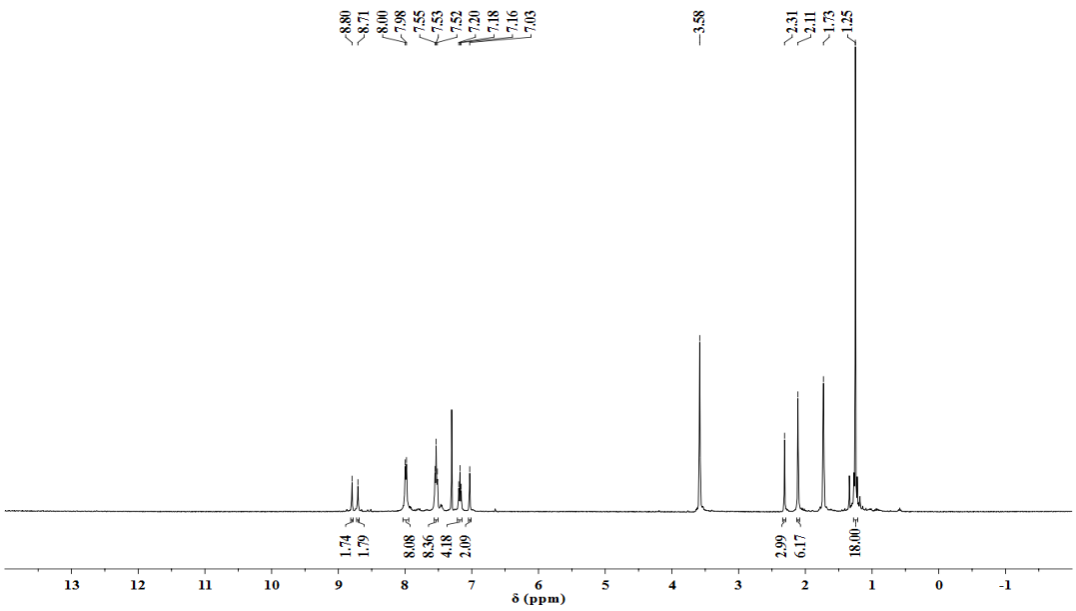

Figure 3.44. ^{1}H NMR spectrum of [2,7-di-*tert*-butyl-9-(2,4,6-trimethylphenoxy)-4,5-bis(diphenylphosphino)acridine]nickel(II) chloride in THF-d_8 solution.

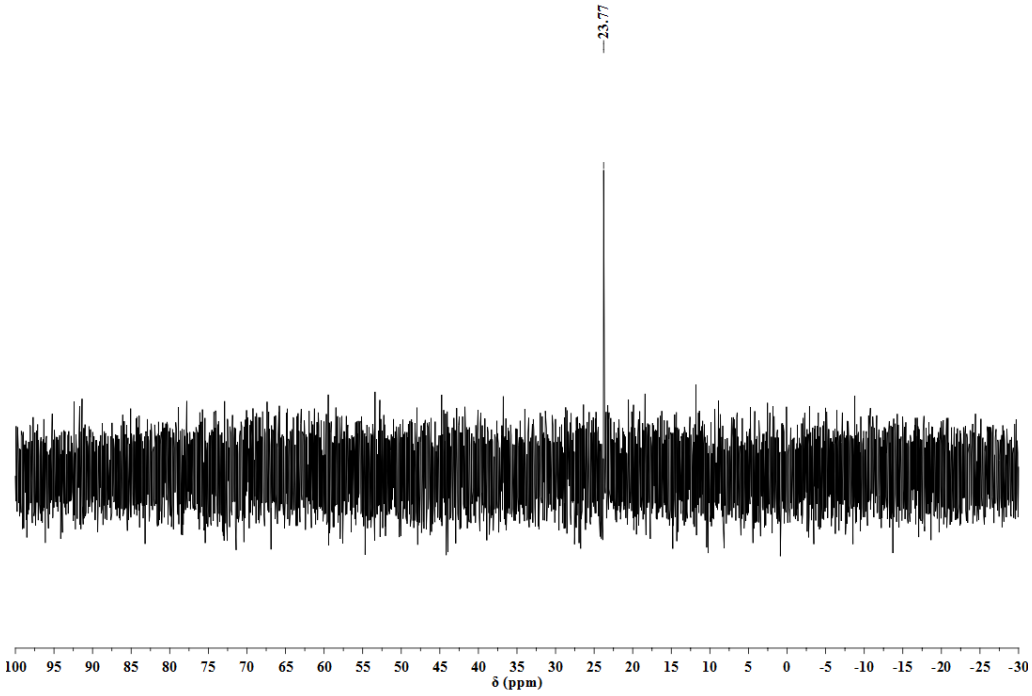

Figure 3.45. ^{31}P NMR spectrum of [2,7-di-*tert*-butyl-9-(2,4,6-trimethylphenoxy)-4,5-bis(diphenylphosphino)acridine]nickel(II) chloride in THF-d_8 solution.

3.4.3.14 Reduction Experiments

A given mass of the complex was weighed into a scintillation vial in the glovebox. To this was added dry and degassed THF to dissolve. Two equivalents of KC_8 synthesized according to literature[83] were dissolve in a given volume of dry and degassed THF. This KC_8 solution was added to the complex solution dropwise while stirring at room temperature. The mixture was left to stir for 12 hours in the glovebox. The mixture was then filtered off over Celite, and the solvent remove under vacuum to get the reduced species as a solid.

3.4.3.15 Reactivity of reduced species with CO_2 and CO

A given mass of the reduced complex species was dissolved in dry and degassed THF-d_8 solution. The solution was then transferred into a J-Young NMR tube. This was then degassed several times through freeze-pump-thaw cycles. Then 1 atm of the respective gas was introduced into the J-Young tube. The sample was agitated for about 30 min and in some cases (reaction of CO_2 with nickel complexes) overnight. The products were analyzed using spectroscopic methods.

3.4.4 X-ray Diffraction Studies

A suitable crystal of complex **7** from a DCM solution layered with Et_2O and kept at -35 ^oC was selected and mounted on a loop on Bruker APEX-II CCD diffractometer using paratone oil. The crystal was kept at 100(2) K during data collection. Using Olex2,[84] the structure was solved with ShelXD[85] structure solution program using Dual Space and refined with the ShelXL[86] refinement package using Least Squares minimisation.

Crystal Data for $C_{46}H_{44}Cl_5CoNP_2$ (*M* =908.94 g/mol), (**7**): monoclinic, space group $P2_1/n$ (no. 14), *a* = 9.6819(5) Å, *b* = 30.4563(14) Å, *c* = 15.0708(9) Å, *β* = 93.805(2)°, *V* = 4434.2(4) $Å^3$, *Z* = 4, *T* = 100(2) K, μ(MoKα) = 0.793 mm^{-1}, *Dcalc* = 1.362 g/cm^3, 77780 reflections measured ($4.424° \leq 2\Theta \leq 60.136°$), 12977 unique ($R_{int}$ = 0.0458, R_{sigma} = 0.0340) which were used in all calculations. The final R_1 was 0.0592 ($I > 2\sigma(I)$) and wR_2 was 0.1358 (all data).

A suitable crystal of complex **9** from a slow evaporation benzene and toluene solution was selected and mounted on a loop on Bruker APEX-II CCD diffractometer using paratone oil. The crystal was kept at 100(2) K during data collection. Using Olex2,[84] the structure was solved with ShelXT[85] structure solution program using Intrinsic Phasing and refined with ShelXL[87] refinement package using Least Squares minimisation.

Crystal Data for $C_{55}H_{53}Cl_3NNiP_2$ (*M* =954.96 g/mol), (**9**): triclinic, space group P-1 (no. 2), *a* = 11.4684(5) Å, *b* = 15.3120(7) Å, *c* = 15.4461(7) Å, *α* = 65.826(2)°, *β* = 83.663(2)°, *γ* = 74.927(2)°, *V* = 2389.38(19) $Å^3$, *Z* = 2, *T* = 100(2) K, μ(MoKα) = 0.679 mm^{-1}, *Dcalc* = 1.327 g/cm^3, 33460 reflections measured ($4.668° \leq 2\Theta \leq 61.016°$), 14477 unique ($R_{int}$ = 0.0470, R_{sigma} = 0.0715) which were used in all calculations. The final R_1 was 0.0490 ($I > 2\sigma(I)$) and wR_2 was 0.1076 (all data).

3.4.5 EPR Experiments

Samples for EPR measurements were prepared under N_2 atmosphere in the glovebox. The radical anion of (ArO)PNP-acridine was generated by reducing 0.01 g of the ligand using 1 equivalent of KC_8 (0.002 g) in 1 mL of THF. The mixture was filtered over Celite and dried under vacuum. Into a vial, 0.005 g of this product was dissolved in

300 µL of dry THF and transferred to an EPR tube and sealed in the glovebox. Into another vial, 0.01 g of [(ArO)PNP-acridine]Co(CO)$_2$ was dissolved in 0.7 mL of dry THF and transferred to an EPR tube then sealed. The X-band continuous wave (CW) EPR measurements were performed on a Bruker EMX spectrometer with 9.839 GHz at 298 K for both samples. Simulation data were obtained using EasySpin (available at www.easyspin.org) package for Matlab 2018a using the garlic method.[88]

3.5 REFERENCES

1. Benito-Garagorri, D.; Lagoja, I.; Veiros, L. F.; Kirchner, K. A., Reactivity of coordinatively unsaturated iron complexes towards carbon monoxide: to bind or not to bind? *Dalton Trans.* **2011,** *40*, 4778-4792.

2. Ittel, S. D.; Johnson, L. K.; Brookhart, M., Late-metal catalysts for ethylene homo- and copolymerization. *Chem. Rev.* **2000,** *100*, 1169-1204.

3. Cummins, C. C., Three-Coordinate Complexes of "Hard" Ligands: Advances in Synthesis, Structure and Reactivity. *Prog. Inorg. Chem.* **1997**, 685-836.

4. van Koten, G., Tuning the reactivity of metals held in a rigid ligand environment. *Pure Appl. Chem.* **1989,** *61*, 1681-1694.

5. Lawrence, M. A.; Green, K.-A.; Nelson, P. N.; Lorraine, S. C., Pincer ligands—Tunable, versatile and applicable. *Polyhedron* **2018,** *143*, 11-27.

6. Werkmeister, S.; Neumann, J.; Junge, K.; Beller, M., Pincer-Type Complexes for Catalytic (De)Hydrogenation and Transfer (De)Hydrogenation Reactions: Recent Progress. *Chem. Eur. J.* **2015,** *21*, 12226-12250.

7. Moulton, C. J.; Shaw, B. L., Transition metal–carbon bonds. Part XLII. Complexes of nickel, palladium, platinum, rhodium and iridium with the tridentate ligand 2,6-bis[(di-t-butylphosphino)methyl]phenyl. *J. Chem. Soc., Dalton Trans.* **1976,** 1020-1024.

8. van Koten, G.; Timmer, K.; Noltes, J. G.; Spek, A. L., A novel type of Pt–C interaction and a model for the final stage in reductive elimination processes involving C–C coupling at Pt; synthesis and molecular geometry of [1,N,N′-η-2,6-bis{(dimethylamino)methyl}toluene]iodoplatinum(II) tetrafluoroborate. *J. Chem. Soc., Chem. Commun.* **1978,** 250-252.

9. Sacconi, L.; Bertini, I., Five-coordinate nickel(II) complexes with nitrogen-phosphorus and nitrogen-arsenic tetradentate ligands. *J. Am. Chem. Soc.* **1967,** *89*, 2235-2236.

10. Dahlhoff, W.; Dick, T.; Ford, G.; Nelson, S., Iron(II), cobalt(II) and nickel(II) complexes of phosphorus-nitrogen ligands. *J. Inorg. Nucl. Chem.* **1971,** *33*, 1799-1811.

11. van der Vlugt, J. I.; Reek, J. N., Neutral Tridentate PNP Ligands and Their Hybrid Analogues: Versatile Non-Innocent Scaffolds for Homogeneous Catalysis. *Angew. Chem. Int. Ed.* **2009,** *48*, 8832-8846.

12. Dahlhoff, W.; Nelson, S., Studies on the magnetic cross-over in five-co-ordinate complexes of iron(II), cobalt(II), and nickel(II). Part II. *J. Chem. Soc. A: Inorganic, Physical, Theoretical* **1971**, 2184-2190.

13. Barloy, L.; Ku, S. Y.; Osborn, J. A.; De Clan, A.; Fischer, J., Synthesis and structure of new 2,6-(diphenylphosphinomethyl)pyridine ruthenium(II) complexes. *Polyhedron* **1997,** *16*, 291-295.

14. Hahn, C.; Sieler, J.; Taube, R., Complex Catalysis, XLIX On the Coordination of Olefins and Secondary Amines at the Cationic [2,6-Bis(diphenylphosphanylmethyl) pyridine]rhodium(I) Fragment $[Rh(PNP)]^+$-Synthesis and Characterization of [Rh(PNP)(L)]X (L= Ethylene, Styrene, HNR_2; X= BF_4, PF_6, CF_3SO_3). *Chem. Ber.* **1997,** *130*, 939-945.

15. Jia, G.; Lee, H. M.; Williams, I. D.; Lau, C. P.; Chen, Y., Synthesis, Characterization, and Acidity Properties of $[MCl(H_2)(L)(PMP)]BF_4$ (M= Ru, L= PPh_3, CO; M= Os, L= PPh_3; PMP= 2,6-$(Ph_2PCH_2)_2C_5H_3N$). *Organometallics* **1997,** *16*, 3941-3949.

16. Giannoccaro, P.; Vasapollo, G.; Sacco, A., Homogeneous catalysis of the water-gas shift reaction using 2,6-bis (diphenylphosphinomethyl)pyridine complexes of nickel. *J. Chem. Soc., Chem. Commun.* **1980,** 1136-1137.

17. Sacco, A.; Vasapollo, G.; Nobile, C. F.; Piergiovanni, A.; Pellinghelli, M. A.; Lanfranchi, M., Syntheses and structures of 2-diphenylphosphinomethylenide-6-diphenylphosphinomethylenepyridine complexes of palladium(II) and platinum(II); crystal structures of [PtCl{2-$(CHPPH_2)$-6-(CH_2PPh_2)pyridine}] and [Pd(COOMe)2-$(CHPPh_2)$-6-(CH_2PPh_2)pyridine]. *J. Organomet. Chem.* **1988,** *356*, 397-409.

18. Hillebrand, S.; Bartkowska, B.; Bruckmann, J.; Krüger, C.; Haenel, M. W., 4,5-bis (diphenylphosphino)acridine: A new type of tridentate phosphorus-nitrogen-phosphorus ligands. *Tetrahedron Lett.* **1998,** *39*, 813-816.

19. Ozerov, O. V.; Guo, C.; Papkov, V. A.; Foxman, B. M., Facile Oxidative Addition of N−C and N−H Bonds to Monovalent Rhodium and Iridium. *J. Am. Chem. Soc.* **2004,** *126*, 4792-4793.

20. Fan, L.; Foxman, B. M.; Ozerov, O. V., N− H Cleavage as a Route to Palladium Complexes of a New PNP Pincer Ligand. *Organometallics* **2004,** *23*, 326-328.

21. Fout, A. R.; Basuli, F.; Fan, H.; Tomaszewski, J.; Huffman, J. C.; Baik, M. H.; Mindiola, D. J., A Co_2N_2 Diamond-Core Resting State of Cobalt(I): A Three-Coordinate CoI Synthon Invoking an Unusual Pincer-Type Rearrangement. *Angew. Chem.* **2006,** *118*, 3369-3373.

22. Franke, R.; Selent, D.; Börner, A., Applied hydroformylation. *Chem. Rev.* **2012,** *112*, 5675-5732.

23. Pruchnik, F., Organometallic chemistry of the transition metals. Plenum Press, New York: 1990.

24. Small, B. L.; Brookhart, M., Iron-based catalysts with exceptionally high activities and selectivities for oligomerization of ethylene to linear α-olefins. *J. Am. Chem. Soc.* **1998,** *120*, 7143-7144.

25. Small, B. L.; Brookhart, M.; Bennett, A. M., Highly active iron and cobalt catalysts for the polymerization of ethylene. *J. Am. Chem. Soc.* **1998,** *120*, 4049-4050.

26. Britovsek, G. J.; Gibson, V. C.; McTavish, S. J.; Solan, G. A.; White, A. J.; Williams, D. J.; Kimberley, B. S.; Maddox, P. J., Novel olefin polymerization catalysts based on iron and cobalt. *Chem. Commun.* **1998,** 849-850.

27. Gibson, V.; Solan, G., Catalysis Without Precious Metals. *Wiley-VCH, Weinheim* **2010,** *111*, l.

28. Junge, K.; Papa, V.; Beller, M., Cobalt-Pincer Complexes in Catalysis. *Chemistry* **2019,** *25*, 122-143.

29. Spentzos, A. Z.; Barnes, C. L.; Bernskoetter, W. H., Effective Pincer Cobalt Precatalysts for Lewis Acid Assisted CO_2 Hydrogenation. *Inorg. Chem.* **2016,** *55*, 8225-8233.

30. Mills, M. R.; Barnes, C. L.; Bernskoetter, W. H., Influences of Bifunctional PNP-Pincer Ligands on Low Valent Cobalt Complexes Relevant to CO_2 Hydrogenation. *Inorg. Chem.* **2018,** *57*, 1590-1597.

31. Adams, M. W.; Stiefel, E. I., Biological hydrogen production: not so elementary. *Science* **1998,** *282*, 1842-1843.

32. Montet, Y.; Garcin, E.; Volbeda, A.; Hatchikian, C.; Frey, M.; Fontecilla-Camps, J., Structural bases for the catalytic mechanism of NiFe hydrogenase. *Pure Appl. Chem.* **1998,** *70*, 25-31.

33. Niu, S.; Hall, M. B., Modeling the active sites in metalloenzymes 5. The heterolytic bond cleavage of H_2 in the [NiFe]hydrogenase of Desulfovibrio gigas by a nucleophilic addition mechanism. *Inorg. Chem.* **2001,** *40*, 6201-6203.

34. Hambourger, M.; Gervaldo, M.; Svedruzic, D.; King, P. W.; Gust, D.; Ghirardi, M.; Moore, A. L.; Moore, T. A., [FeFe]-hydrogenase-catalyzed H2 production in a photoelectrochemical biofuel cell. *J. Am. Chem. Soc.* **2008,** *130*, 2015-2022.

35. Vincent, K. A.; Parkin, A.; Lenz, O.; Albracht, S. P.; Fontecilla-Camps, J. C.; Cammack, R.; Friedrich, B.; Armstrong, F. A., Electrochemical definitions of O2 sensitivity and oxidative inactivation in hydrogenases. *J. Am. Chem. Soc.* **2005,** *127*, 18179-18189.

36. Khusnutdinova, J. R.; Milstein, D., Metal–ligand cooperation. *Angew. Chem. Int. Ed.* **2015,** *54*, 12236-12273.

37. Ben-Ari, E.; Leitus, G.; Shimon, L. J.; Milstein, D., Metal− Ligand Cooperation in C−H and H_2 Activation by an Electron-Rich PNP Ir(I) System: Facile Ligand Dearomatization−Aromatization as Key Steps. *J. Am. Chem. Soc.* **2006,** *128*, 15390-15391.

38. Feller, M.; Karton, A.; Leitus, G.; Martin, J. M.; Milstein, D., Selective sp^3C−H Activation of Ketones at the β Position by Ir(I). Origin of Regioselectivity and Water Effect. *J. Am. Chem. Soc.* **2006,** *128*, 12400-12401.

39. Gunanathan, C.; Milstein, D., Metal–ligand cooperation by aromatization–dearomatization: a new paradigm in bond activation and "Green" catalysis. *Acc. Chem. Res.* **2011,** *44*, 588-602.

40. Schwartsburd, L.; Iron, M. A.; Konstantinovski, L.; Diskin-Posner, Y.; Leitus, G.; Shimon, L. J.; Milstein, D., Synthesis and Reactivity of an Iridium(I) Acetonyl PNP Complex. Experimental and Computational Study of Metal−Ligand Cooperation in H−H and C−H Bond Activation via Reversible Ligand Dearomatization. *Organometallics* **2010,** *29*, 3817-3827.

41. Lyaskovskyy, V.; de Bruin, B., Redox non-innocent ligands: versatile new tools to control catalytic reactions. *Acs Catal.* **2012,** *2*, 270-279.

42. Luca, O. R.; Crabtree, R. H., Redox-active ligands in catalysis. *Chem. Soc. Rev.* **2013,** *42*, 1440-1459.

43. Praneeth, V. K.; Ringenberg, M. R.; Ward, T. R., Redox-Active Ligands in Catalysis. *Angew. Chem. Int. Ed.* **2012,** *51*, 10228-10234.

44. Dzik, W. I.; van der Vlugt, J. I.; Reek, J. N.; de Bruin, B., Ligands that store and release electrons during catalysis. *Angew. Chem. Int. Ed.* **2011,** *50*, 3356-3358.

45. Dzik, W. I.; Zhang, X. P.; de Bruin, B., Redox noninnocence of carbene ligands: carbene radicals in (catalytic) C−C bond formation. *Inorg. Chem.* **2011,** *50*, 9896-9903.

46. de Bruin, B.; Hetterscheid, D. G., Paramagnetic (alkene)Rh and (alkene)Ir complexes: metal or ligand radicals? *Eur. J. Inorg. Chem.* **2007,** *2007*, 211-230.

47. Boyer, J. L.; Rochford, J.; Tsai, M.-K.; Muckerman, J. T.; Fujita, E., Ruthenium complexes with non-innocent ligands: electron distribution and implications for catalysis. *Coordination Chem. Rev.* **2010,** *254*, 309-330.

48. Kaim, W.; Schwederski, B., Non-innocent ligands in bioinorganic chemistry—An overview. *Coord. Chem. Rev.* **2010,** *254*, 1580-1588.

49. Stubbe, J.; Van Der Donk, W. A., Protein radicals in enzyme catalysis. *Chem. Rev.* **1998,** *98*, 705-762.

50. Sono, M.; Roach, M. P.; Coulter, E. D.; Dawson, J. H., Heme-containing oxygenases. *Chem. Rev.* **1996,** *96*, 2841-2888.

51. Bigi, M. A.; Reed, S. A.; White, M. C., Diverting non-haem iron catalysed aliphatic C–H hydroxylations towards desaturations. *Nature Chem.* **2011,** *3*, 216.

52. Lu, H.; Subbarayan, V.; Tao, J.; Zhang, X. P., Cobalt(II)-Catalyzed Intermolecular Benzylic C−H Amination with 2,2,2-Trichloroethoxycarbonyl Azide ($TrocN_3$). *Organometallics* **2009,** *29*, 389-393.

53. Gao, G.-Y.; Jones, J. E.; Vyas, R.; Harden, J. D.; Zhang, X. P., Cobalt-catalyzed aziridination with diphenylphosphoryl azide (DPPA): Direct synthesis of N-phosphorus-substituted aziridines from alkenes. *J. Org. Chem.* **2006,** *71*, 6655-6658.

54. Subbarayan, V.; Ruppel, J. V.; Zhu, S.; Perman, J. A.; Zhang, X. P., Highly asymmetric cobalt-catalyzed aziridination of alkenes with trichloroethoxysulfonyl azide ($TcesN_3$). *Chem. Commun.* **2009,** 4266-4268.

55. Bouwkamp, M. W.; Bowman, A. C.; Lobkovsky, E.; Chirik, P. J., Iron-Catalyzed [2π + 2π] Cycloaddition of α,ω-Dienes: The Importance of Redox-Active Supporting Ligands. *J. Am. Chem. Soc.* **2006,** *128*, 13340-13341.

56. Sylvester, K. T.; Chirik, P. J., Iron-Catalyzed, Hydrogen-Mediated Reductive Cyclization of 1,6-Enynes and Diynes: Evidence for Bis(imino)pyridine Ligand Participation. *J. Am. Chem. Soc.* **2009,** *131*, 8772-8774.

57. Stanciu, C.; Jones, M. E.; Fanwick, P. E.; Abu-Omar, M. M., Multi-electron Activation of Dioxygen on Zirconium(IV) to Give an Unprecedented Bisperoxo Complex. *J. Am. Chem. Soc.* **2007,** *129*, 12400-12401.

58. Blackmore, K. J.; Ziller, J. W.; Heyduk, A. F., "Oxidative Addition" to a Zirconium(IV) Redox-Active Ligand Complex. *Inorg. Chem.* **2005,** *44*, 5559-5561.

59. Haneline, M. R.; Heyduk, A. F., C−C Bond-Forming Reductive Elimination from a Zirconium(IV) Redox-Active Ligand Complex. *J. Am. Chem. Soc.* **2006,** *128*, 8410-8411.

60. Ketterer, N. A.; Fan, H.; Blackmore, K. J.; Yang, X.; Ziller, J. W.; Baik, M.-H.; Heyduk, A. F., π•−π• Bonding Interactions Generated by Halogen Oxidation of Zirconium(IV) Redox-Active Ligand Complexes. *J. Am. Chem. Soc.* **2008,** *130*, 4364-4374.

61. Gibson, V. C.; Redshaw, C.; Solan, G. A., Bis (imino) pyridines: surprisingly reactive ligands and a gateway to new families of catalysts. *Chem. Rev.* **2007,** *107*, 1745-1776.

62. Knijnenburg, Q.; Gambarotta, S.; Budzelaar, P. H., Ligand-centred reactivity in diiminepyridine complexes. *Dalton Trans.* **2006,** 5442-5448.

63. Stubbert, B. D.; Peters, J. C.; Gray, H. B., Rapid water reduction to H_2 catalyzed by a cobalt bis(iminopyridine) complex. *J. Chem. Soc.* **2011,** *133*, 18070-18073.

64. Lacy, D. C.; McCrory, C. C.; Peters, J. C., Studies of cobalt-mediated electrocatalytic CO_2 reduction using a redox-active ligand. *Inorg. Chem.* **2014,** *53*, 4980-4988.

65. Budzelaar, P. H.; de Bruin, B.; Gal, A. W.; Wieghardt, K.; van Lenthe, J. H., Metal-to-Ligand Electron Transfer in Diiminopyridine Complexes of Mn−Zn. A Theoretical Study. *Inorg. Chem.* **2001,** *40*, 4649-4655.

66. de Bruin, B.; Bill, E.; Bothe, E.; Weyhermüller, T.; Wieghardt, K., Molecular and Electronic Structures of Bis(pyridine-2,6-diimine) metal Complexes $[ML_2](PF_6)$ n (n= 0, 1, 2, 3; M= Mn, Fe, Co, Ni, Cu, Zn). *Inorg. Chem.* **2000,** *39*, 2936-2947.

67. Luca, O. R.; Konezny, S. J.; Blakemore, J. D.; Colosi, D. M.; Saha, S.; Brudvig, G. W.; Batista, V. S.; Crabtree, R. H., A tridentate Ni pincer for aqueous electrocatalytic hydrogen production. *New J. Chem.* **2012,** *36*, 1149-1152.

68. Smith, A. L.; Hardcastle, K. I.; Soper, J. D., Redox-active ligand-mediated oxidative addition and reductive elimination at square planar cobalt(III): multielectron reactions for cross-coupling. *J. Am. Chem. Soc.* **2010,** *132*, 14358-14360.

69. Mayer, H. A.; Kaska, W. C., Stereochemical control of transition metal complexes by polyphosphine ligands. *Chem. Rev.* **1994,** *94*, 1239-1272.

70. Chiron, J.; Galy, J.-P., Reactivity of the acridine ring: One-pot regioselective single and double bromomethylation of acridine and some derivatives. *Synlett.* **2003,** *2003*, 2349-2350.

71. Gunanathan, C.; Milstein, D., Selective synthesis of primary amines directly from alcohols and ammonia. *Angew. Chem. Int. Ed.* **2008,** *47*, 8661-8664.

72. Haenel, M. W.; Hillebrand, S., Catalysts made from transition metal compounds and 4,5-diphosphinoacridine-ligands. Google Patents: 2001.

73. Breitenfeld, J.; Ruiz, J.; Wodrich, M. D.; Hu, X., Bimetallic oxidative addition involving radical intermediates in nickel-catalyzed alkyl–alkyl Kumada coupling reactions. *J. Am. Chem. Soc.* **2013,** *135*, 12004-12012.

74. Zhang, C.-P.; Wang, H.; Klein, A.; Biewer, C.; Stirnat, K.; Yamaguchi, Y.; Xu, L.; Gomez-Benitez, V.; Vicic, D. A., A five-coordinate nickel(II) fluoroalkyl complex as a precursor to a spectroscopically detectable Ni(III) species. *J. Am. Chem. Soc.* **2013,** *135*, 8141-8144.

75. Colon, I.; Kelsey, D. R., Coupling of aryl chlorides by nickel and reducing metals. *The J. Org. Chem.* **1986,** *51*, 2627-2637.

76. Gosmini, C.; Moncomble, A., Cobalt-Catalyzed Cross-Coupling Reactions of Aryl Halides. *Isr. J. Chem.* **2010,** *50*, 568-576.

77. Gao, K.; Yoshikai, N., Low-valent cobalt catalysis: new opportunities for C–H functionalization. *Acc. Chem. Res.* **2014,** *47*, 1208-1219.

78. Issleib, K.; Brüsehaber, L., Alkali-Phosphorverbindungen und ihr reaktives Verhalten XXIII: 9.10-Dihydroacridyl-und 9-Acridyl-diorgano-phosphine. *Zeitschrift für Naturforschung B* **1965,** *20*, 181-182.

79. Ingleson, M. J.; Pink, M.; Fan, H.; Caulton, K. G., Exploring the reactivity of four-coordinate PNPCoX with access to three-coordinate spin triplet PNPCo. *Inorg. Chem.* **2007,** *46*, 10321-10334.

80. Suarez, A. I. O.; Lyaskovskyy, V.; Reek, J. N.; van der Vlugt, J. I.; de Bruin, B., Complexes with Nitrogen-Centered Radical Ligands: Classification, Spectroscopic Features, Reactivity, and Catalytic Applications. *Angew. Chem. Int. Ed.* **2013,** *52*, 12510-12529.

81. De Bruin, B.; Hetterscheid, D. G.; Koekkoek, A. J.; Gruetzmacher, H., The organometallic chemistry of Rh-, Ir-, Pd-, and Pt-based radicals: higher valent species. *Prog. Inorg. Chem.* **2007,** *55*, 247-354.

82. Fulmer, G. R.; Miller, A. J.; Sherden, N. H.; Gottlieb, H. E.; Nudelman, A.; Stoltz, B. M.; Bercaw, J. E.; Goldberg, K. I., NMR chemical shifts of trace impurities: common laboratory solvents, organics, and gases in deuterated solvents relevant to the organometallic chemist. *Organometallics* **2010,** *29*, 2176-2179.

83. Weitz, I. S.; Rabinovitz, M., The application of C_8K for organic synthesis: reduction of substituted naphthalenes. *J. Chem. Soc., Perkin Trans. 1* **1993,** 117-120.

84. Dolomanov, O. V.; Bourhis, L. J.; Gildea, R. J.; Howard, J. A.; Puschmann, H., OLEX2: a complete structure solution, refinement and analysis program. *J. Appl. Crystallogr.* **2009,** *42*, 339-341.

85. Sheldrick, G. M., SHELXT - integrated space-group and crystal-structure determination. *Acta Crystallogr. A Found Adv* **2015,** *71*, 3-8.

86. Sheldrick, G. M., A short history of SHELX. *Acta Crystallogr., Sect. A: Found. Crystallogr.* **2008,** *64*, 112-122.

87. Sheldrick, G. M., Crystal structure refinement with SHELXL. *Acta Crystallogr. C Struct. Chem.* **2015,** *71*, 3-8.

88. Stoll, S.; Schweiger, A.; EasySpin, a comprehensive software package for spectral simulation and analysis in EPR. *J. Magn. Reson.* **2006**, 178, 42-55.

CHAPTER 4. NICKEL COMPLEXES OF CY-XANTPHOS, CHARACTERIZATION, AND APPLICATION IN CO_2 FIXATION

4.1 Background

4.1.1 Industrial applications of CO_2 and its catalytic transformations using transition metal complexes

CO_2 exists in abundant quantity as a byproduct of energy generation.[1] Its use as renewable, non-toxic C_1 building block is a very attractive goal for synthetic chemistry on a laboratory and industrial scale.[1-3] Currently, CO_2 is used in the chemical industry for production of urea, salicyclic acid, cyclic carbonates, and polypropylene carbonates.[4] Its reduction to CO[5-10], methane or methanol[11] are still far less implemented due to the energy barriers that need to be overcome.[12] This has led to increased interest in designing catalytic processes that use CO_2 in C-C bond formation, which when achieved could have positive ramifications on efforts towards carbon management.[13-22] But that process has to be able to overcome the kinetic and thermodynamic stability of CO_2 by providing reactive intermediates that can attack the low-energy CO_2 molecule while achieving high selectivity for the desired product.[2]

CO_2 reacts with different transition metals through either its electrophilic carbon, its two equivalent C-O π bonds or its nucleophilic oxygen.[12] As such, it is capable of forming a variety of coordination complexes,[15, 23-27] with the most common binding modes being **1** and **2**.[12]

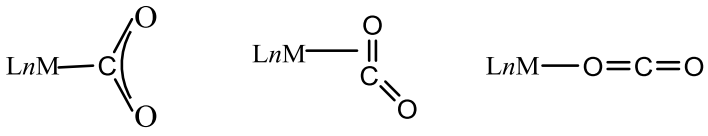

1 **2** **3**

Figure 4.1. Possible coordination modes of CO_2 to transition-metal complexes.

4.1.2 Biological activation of CO_2 at a nickel center and the role of a Lewis acid in the process

Biological reduction of CO_2 to CO (a primary industrial C_1 source) takes place efficiently at a square planar nickel center,[3, 28-29] where nickel(0) has been proposed to be responsible for the CO_2 uptake.[30] X-ray crystallography revealed the active site to contain a $[NiFe_4S_4]$ core[3, 29-34] where CO_2 is proposed to bind forming Ni-COO-Fe and subsequent protonation cleaves C-O bond leaving behind a Ni(II)-CO fragment.[35] As such the coordination of CO_2 and CO at nickel centers supported by pincer ligands to enforce a square planar geometry is of interest, and has been widely explored[35-45] even though the exact mechanistic details remain debatable.[46-48]

Lee and co-workers recently showed that addition of CO_2 to nickel(0) supported by 4,5-bis(diisopropylphosphino)-2,7,9,9-tetramethyl-9H-acridin-10-ide (^{acri}PNP)[45] in the presence of Na^+ leads to formation of LNi-COONa. As in Ni-COO-Fe, the addition of two equivalents of H^+ leads to formation of LNi-CO complex, (^{acri}PNP-Ni(II)CO) (see Scheme 4.1).[45]

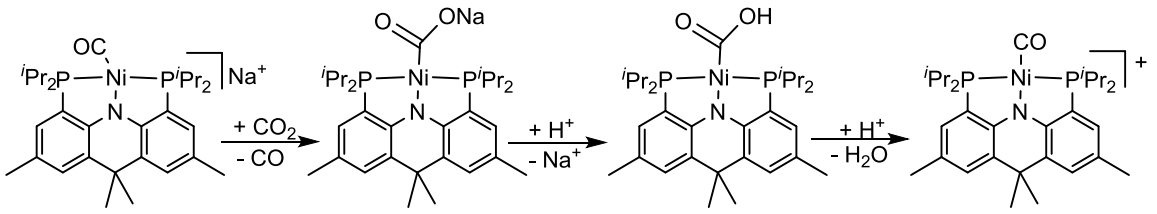

Scheme 4.1. Activation of CO_2 at a nickel center and subsequent reaction with H^+.

4.1.3 Ligand architecture and effects on CO_2 binding modes

The groups of Aresta, and later Hillhouse, demonstrated η^2-CO_2 binding modes at low-valent nickel species when two phosphorus donors were present in their complexes $(PCy_3)_2Ni(\eta^2\text{-}CO_2)$ (**I**)[49] and (dtbpe)Ni(η^2-CO_2) (**II**)[50] respectively (see Figure 4.2). Many four-coordinate Ni(0) species tend to form η^1-CO_2 complexes in which the C-O bonds possess a greater degree of single bond character.[37, 44] The bonds are thus elongated and readily interacts with Lewis acids, making them easier to cleave during reduction processes and favoring the formation of carbonyl complexes.[37] We were however interested in reducing the metal center in $LNi(CO_2)$ in an η^2-binding mode followed by insertion of CO_2 or CO without cleavage of the C-O bond in $LNi(CO_2)$. We envisioned that use of a ligand framework such as that based on Xantphos would enable synthesis of η^2-CO_2 complexes.

Figure 4.2. η^2-CO_2 binding modes at low-valent nickel species.

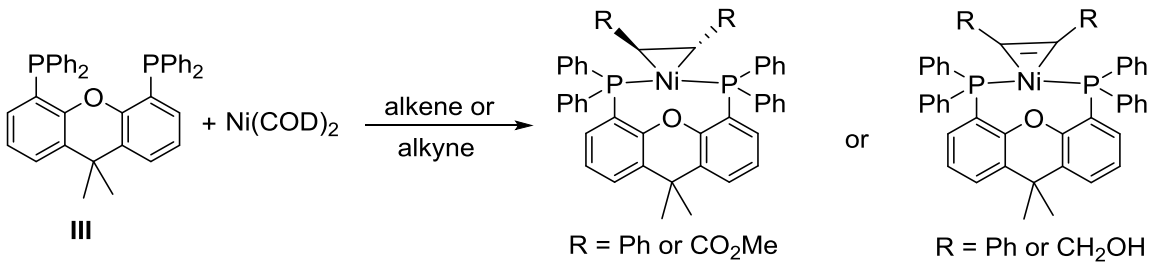

Scheme 4.2. Xantphos[51-52] Ni π-complexes obtained from reaction of $Ni(COD)_2$, Xantphos and 2 equiv. of alkenes or alkynes.[61]

Xantphos ligands (structure **III**, Scheme 4.2) [51-52] are phosphorus-based chelates with a semirigid backbone, and normally bind to metals via the two phosphorus donors. These ligands have a wide bite angle and have been used in a number of nickel-catalyzed reactions including hydrocyanation,[53-56] alkylcyanation,[57] cross coupling,[58] conversion of ethylene into 1-butene[59] and cycloaddition.[60] With the evidence for Xantphos-based Ni-π complexes (see Scheme 4.2 above),[61] we hoped that (Cy-xantphos)Ni(0) would form η^2-CO_2 complexes that are stable enough as to enable transformation of CO_2 as C_1 source. To investigate this possibility, low-valent Cy-xantphos nickel complexes were synthesized and their reactivity with CO_2 under different conditions tested.

4.2 Results and Discussions

4.2.1 Synthesis and characterization of (Cy-xantphos)nickel complexes

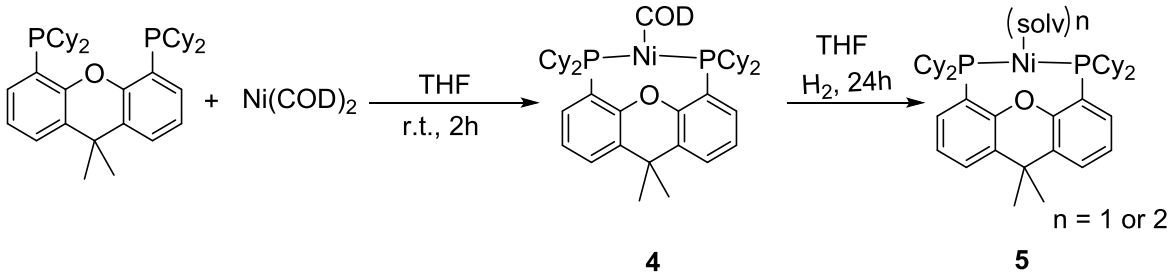

Scheme 4.3. Synthesis of (Cy-xantphos)Ni(0) using $Ni(COD)_2$.

Route 1: Cy-xantphos reacts with $Ni(COD)_2$ (where COD is 1,5-cyclooctadiene) to form (Cy-xantphos)Ni(COD) complex (**4**) with liberation of free COD as seen from the ^{1}H NMR with resonances at δ 5.58 and 2.22 ppm. Hydrogenation of the resulting complex shows a decrease in the intensity of free COD resonances in the ^{1}H NMR spectrum, to form what is presumed to be a solvent-bound (Cy-xantphos)Ni(0) complex (**5**) (Scheme 4.3).

Route 2: Treatment of Cy-xantphos with $(PPh_3)_2NiCl_2$ leads to formation of a purple solid identified as (Cy-xantphos)$NiCl_2$, (**6**) through spectroscopic as well as solid-state analysis. Reduction of this nickel(II) complex using KC_8 produces the low-valent complex **5**.

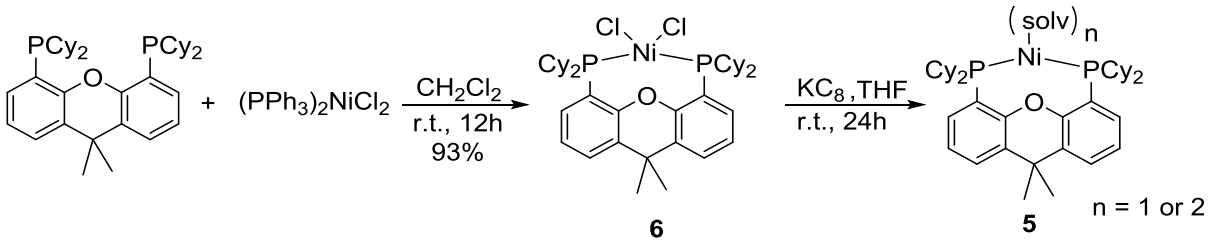

Scheme 4.4. Synthesis of (Cy-xantphos)Ni(0) via reduction of (Cy-xantphos)Ni(II).

Crystal structure obtained from a dichloromethane solution of **6** (Figure 4.3) layered with diethyl ether and kept at -35 ^{o}C reveals a four-coordinate (Cy-xantphos)$NiCl_2$ with P-Ni bond of about 2.351 Å. The bonds are long enough that the Ni is held *ca.* 2.982 Å above oxygen at an angle of 118.7(7)^{o}.

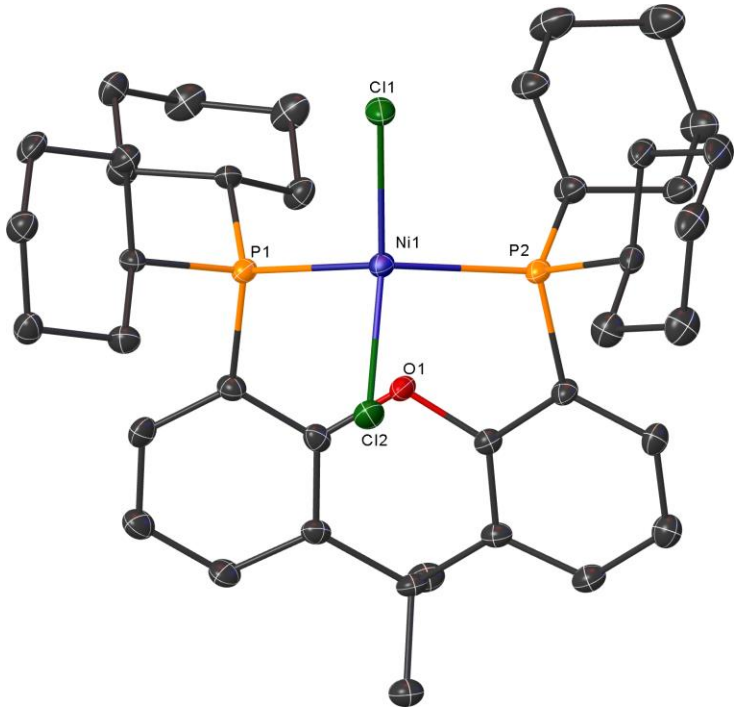

Figure 4.3. Solid-state structure of **6** shown as 50% probability ellipsoids.

H atoms omitted for clarity with selected interatomic distances (Å) and angles (^{o}): O1-Ni1, 2.982; Ni1-P1, 2.345(6); Ni1-P2, 2.356(1); C25-P1, 1.828(3); C32-P2, 1.826(2); P1-Ni1-P2, 118.7(7); P1-Ni1-Cl1, 98.1(4); P1-Ni1-Cl2, 103.1(4); P2-Ni1-Cl1, 101.6(3); P2-Ni1-Cl2, 100.5(8).

4.2.2 Application of Cy-xantphos nickel complexes in CO_2 activation

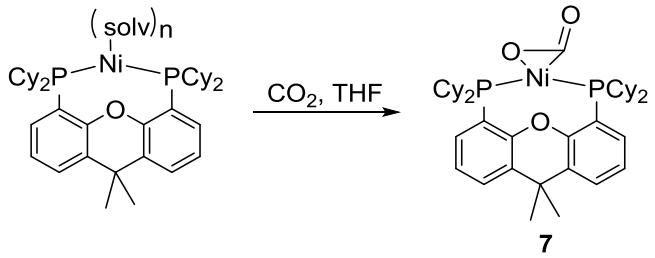

Scheme 4.5. Synthesis of (Cy-xantphos)Ni(CO_2).

Reaction of **5** with CO_2 led to an immediate color change from either dark brown (**route 1**) or red-brown (**route 2**) to brownish-yellow. Analysis of this product by FTIR shows an absorption at 1742 cm^{-1} in the infrared spectrum which could be resulting from the C=O stretch of the (Cy-xantphos)Ni(CO_2) complex (Figure 4.4). This absorption is close to that observed by Aresta and co-workers for their side-on bound CO_2 in $(PCy_3)_2Ni(\eta^2\text{-}CO_2)$[49]and that of Hillhouse and co-workers in (dtbpe)Ni(η^2-CO_2)[50] at 1741 cm^{-1} and 1724 cm^{-1} respectively. These values are slightly higher compared to those observed for tridentate ligands that normally participate in η^1 binding modes (Table 4.1 below).

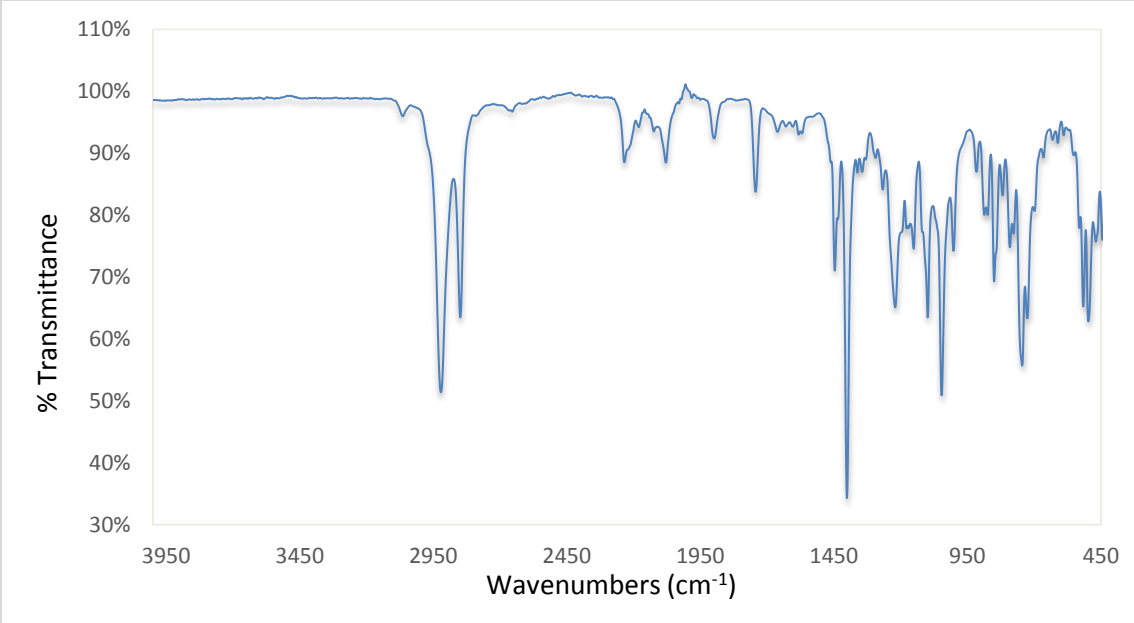

Figure 4.4. IR of (Cy-xantphos)Ni(CO_2) (film).

There is another stretch in the IR at 1896 cm^{-1} (Figure 4.4) from the reaction of CO_2 with the (Cy-xantphos)Ni(0) obtained through reduction of (Cy-xantphos)$NiCl_2$ by KC_8 which is suspected to be that of CO. This could result from further reduction of CO_2 in (Cy-xantphos)Ni(CO_2).

Table 4.1. Comparison of selected physical parameters between PNP and POP nickel CO_2 complexes.

Complex	υ_{CO2} (cm^{-1})	C-O (Å)
$(PCy_3)_2Ni(CO_2)$ (**1**)[49]	1741	1.22, 1.17
(dtbpe)Ni(CO_2) (**2**)[50]	1724	1.200(3), 1.266(3)
$(PP^{Me}P)Ni(CO_2)$ (**3**)[44]	1682	1.218(2), 1,252(2)
$(PP^{Me}P)Ni(COOB(C_6F_5)_3)$ (**4**)[44]	1631	1.223(4), 1.340(4)
(Cy-xantphos)Ni(CO_2) (**5**)	1742	

Table 2 also shows how spectroscopic data and bond lengths relate to the degree of CO_2 activation. Both **1**, **2** and **5** have fairly high absorption frequencies in the infrared

spectrum compared to **3** and **4.** The two C-O bond lengths for each complex 1-3 are fairly close, but the effect of a Lewis acid in elongating the C-O bond is evident in **4**. The presence of borane in **4** causes the bond lengths to differ by ~0.12 Å, a clear indication that one of the C=O bonds has developed more of a single bond character.

4.2.3 Confirmatory test for Ni-CO_2 complex formation using $^{13}CO_2$ experiment

Under reaction conditions similar to those used with natural abundance CO_2, (Cy-xantphos)Ni(0) was treated with $^{13}CO_2$. The data obtained from this experiment points to a successful synthesis of (Cy-xantphos)Ni($^{13}CO_2$). In the ^{13}C NMR spectrum, there is a triplet resonance at δ 157.26 ppm with a coupling constant of 9.5 Hz, while in the ^{31}P NMR spectrum, a single doublet resonance is observed at δ 14.67 ppm with a coupling constant of 9.6 Hz as well. The FTIR data shows a shift in absorption from 1742 cm^{-1} to 1697 cm^{-1} in the infrared spectrum (Figure 4.5). Studies on $(PCy_3)_2Ni$ ($^{13}CO_2$) showed infrared absorption shifts from 1741 cm^{-1} to 1696 cm^{-1} and a resonance at δ 159.28 ppm in the ^{13}C NMR.[15, 62-63] This data strongly suggests formation of nickel CO_2 adducts from the reaction of CO_2 with low-valent Cy-xantphos nickel species.

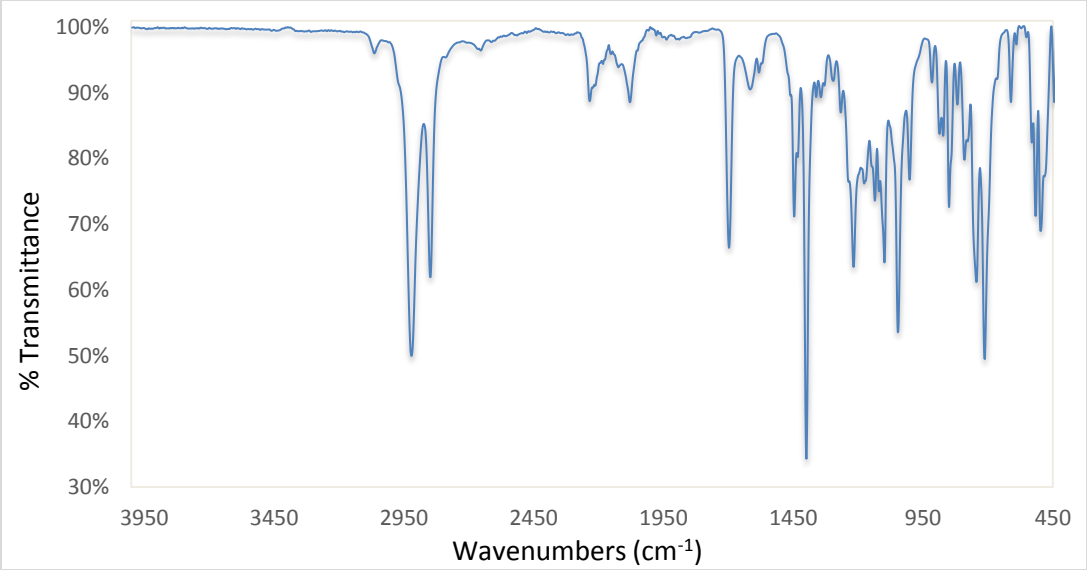

Figure 4.5. IR of (Cy-Xantphos)Ni($^{13}CO_2$) (film).

The results could not prove whether there was formation of NiCO adducts in the course of the reaction. However, literature precedents show that the interaction of transition metal complexes with CO_2 leads to disproportionation into carbonato and carbonyl complexes.[64-65] In the reaction of Ni(dcpe) (dcpe = 1,2-bis(dicyclohexylphosphino)ethane) with CO_2, Mastrorilli and co-workers observed formation a strong band at 1741 cm^{-1} together with a weak band at 1898 cm^{-1}.[66] After further studies, they assigned the absorption at 1898 cm^{-1} to the carbonyl carbon stretch in (dcpe)NiCO. In our case, it is very likely that the band at 1896 cm^{-1} results from (Cy-Xantphos)Ni(CO).

4.2.4 Synthesis of Cy-xantphos nickel dicarbonyl via CO_2 displacement

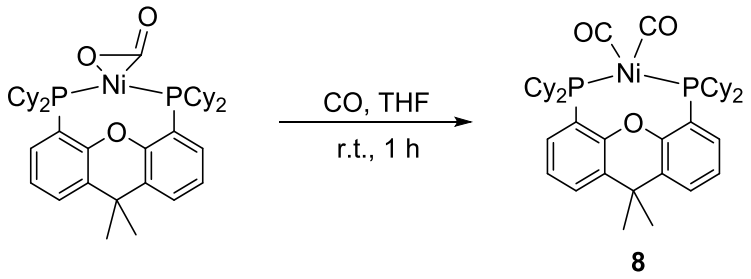

8

Scheme 4.6. Synthesis of (Cy-xantphos)Ni$(CO)_2$.

The reaction of (Cy-Xantphos)Ni(CO_2) with CO at room temperature leads to formation of (Cy-Xantphos)Ni(CO) complex (Scheme 4.6). The obtained complex shows two strong absorptions at 1981 cm^{-1} and 1913 cm^{-1} in the infrared spectrum which must be originating from the two inequivalent carbonyls (Figure 4.7). The complex also gives a triplet resonance at δ 201.92 ppm with a coupling constant of 6.5 Hz in the ^{13}C NMR spectrum. The solid state structure reveals C-O bond of length of 1.18(3) Å on average, compared to (1.128 Å for C-O triple bond in CO) and (1.162 Å for C-O double bond in CO_2).[67] The nickel is held 0.967 Å above the cy-xantphos plane at a Ni1-O1-C3 angle of 146.0(4)°. These observations compare well with other previously reported nickel carbonyl complexes of terdentate pincer ligands (Table 4.2).

Table 4.2. Comparison of selected physical parameters between PNP and POP nickel carbonyl complexes.

Complex	υ_{CO} (cm^{-1})	C-O (Å)	Ni-C (Å)
{(^{acri}PNP)Ni(CO)}$^-$ (**1**)[45]	1828	1.18(1)	1.77(1)
(^{acri}PNP)Ni(CO) (**2**)[45]	1931	1.14(9)	1.76(5)
(**Cy-xantphos**)**Ni**(**CO**)$_2$ (**3**)	1981, 1913	1.18(1), 1.18(4)	1.75(9), 1.73(5)

Data from this independently synthesized Cy-xantphos nickel carbonyl complex will be an important point of reference for the reduction products of (Cy-xantphos)Ni(CO_2).

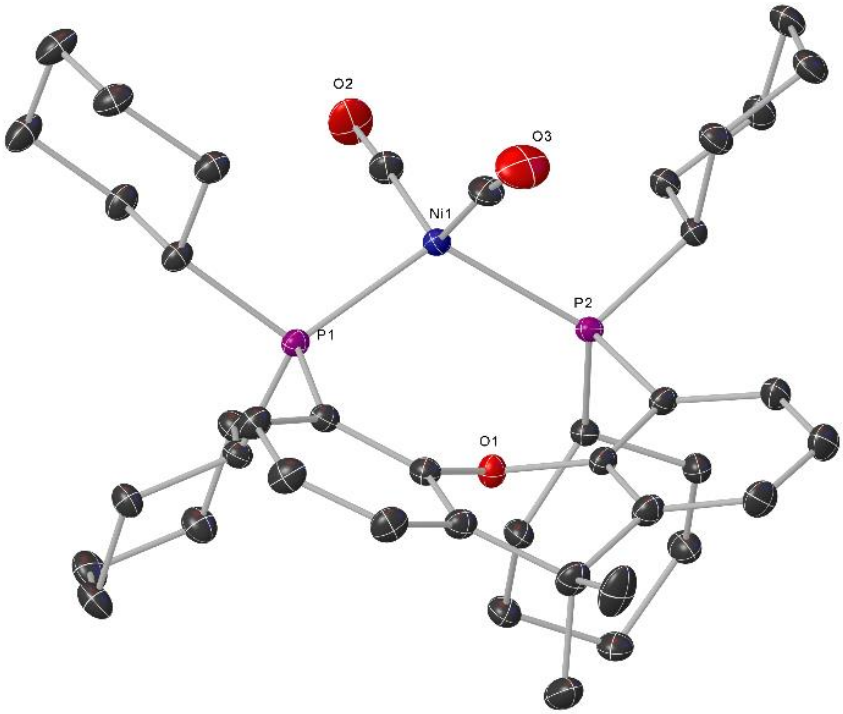

Figure 4.6. Solid-state structure of (Cy-xantphos)Ni$(CO)_2$ shown as 50% probability ellipsoids. H atoms are omitted for clarity. Selected interatomic distances (Å) and angles (^{o}): O1-Ni1, 3.175; Ni1-P1, 2.259(7); Ni1-P2, 2.258(2); C10-P1, 1.837(6); C6-P2, 1.841(2); C40-O2, 1.181(4); C41-O3, 1.184(4); P1-Ni1-P2, 118.6(3); P1-Ni1-C40, 106.2(9); P1-Ni1-C41, 99.5(4); P2-Ni1-C40, 107.3(6); P2-Ni1-C41, 98.4(0).

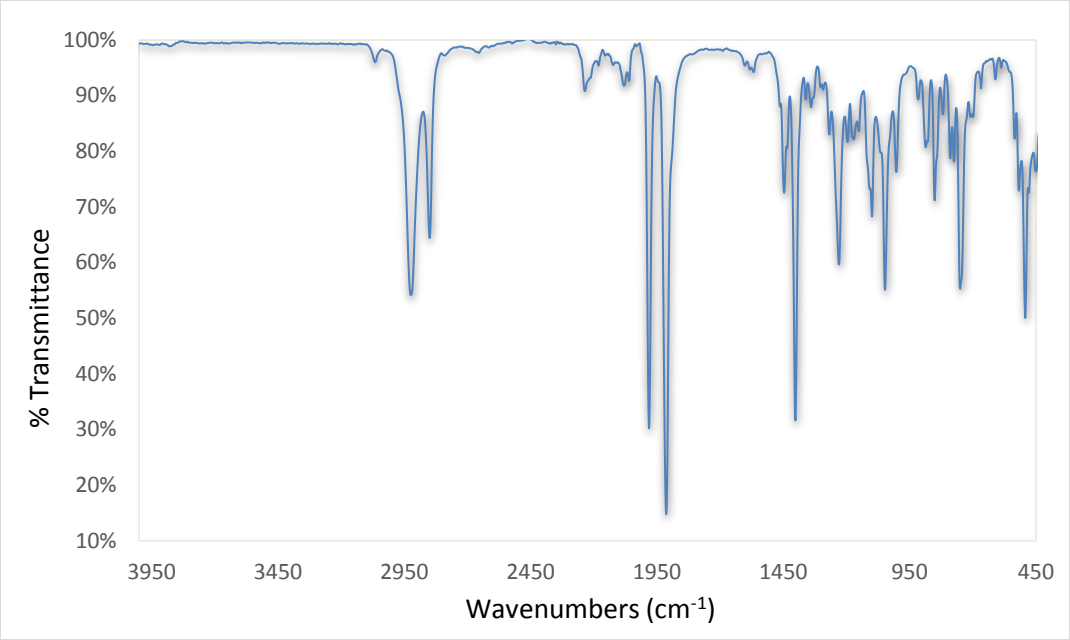

Figure 4.7. IR of (Cy-Xantphos)Ni(CO)$_2$ (film).

4.2.5 Manipulation of (Cy-xantphos)Ni(CO$_2$) adduct

Selectivity remains a key issue in CO_2 functionalization to higher value products. As such, the products obtained from CO_2 reduction range from oxalic acid (1-electron), carbon monoxide or formic acid (2-electron), formaldehyde (4-electron), and methanol (6-electron) all the way to hydrocarbons.[3] Partial reduction of CO_2 produces CO, an attractive target as it remains the primary C_1 building block.

The presence of internal dipoles along the C=O bonds in CO_2 gives it the ambiphilic character. This character enables bifunctional activation of CO_2, and nature takes advantage of this in which the low-valent (nucleophilic) nickel sites attacks the electrophilic carbon of CO_2 while the oxygen is stabilized by a Lewis acid, Fe.[30, 68] In trying to mimic nature, the past 30 years has seen development of transition-metal complexes for CO_2 activation and catalytic reduction based on this observation.[69-71] Our interest in

investigating whether a Lewis acid stabilized (Cy-xantphos)Ni(CO_2) would undergo further reduction at the nickel center and allow CO or CO_2 insertion led to the following studies.

4.2.5.1 Reduction of (Cy-xantphos)Ni($^{13}CO_2$) with KC_8 in presence of magnesium triflate

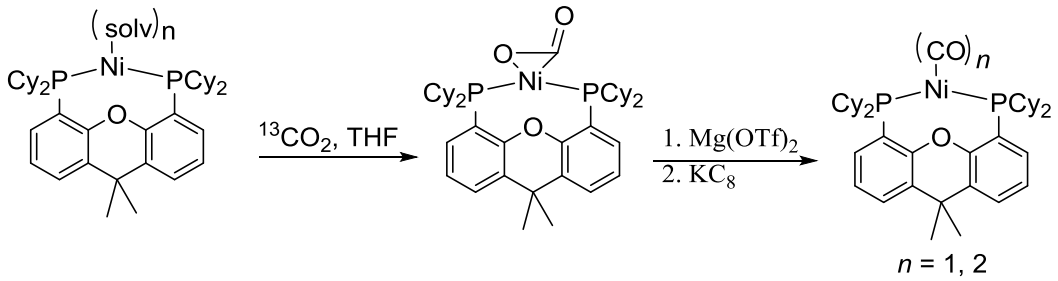

Scheme 4.7. Reduction of (Cy-xantphos)Ni($^{13}CO_2$) in presence of $Mg(OTf)_2$.

There is no change in the ^{31}P and ^{13}C NMR spectra when magnesium triflate is added to the (Cy-xantphos)Ni($^{13}CO_2$) complex. But on addition of one equivalent of KC_8 to this complex, a new product that has a triplet resonance at δ 199.84 ppm with a coupling of 29.9 Hz in the ^{13}C NMR spectrum was formed (Figure 4.8). Compared to the independently synthesized (Cy-xantphos)Ni($CO)_2$, this peak would correspond to a carbonyl carbon. It is therefore within reason to expect that the one equivalent of reducing agent intended to reduce the nickel center instead was consumed in the reduction of some of the bound CO_2. The triplet resonance at δ 157.97 ppm in the spectrum is originally from the carbon of (Cy-xantphos)Ni($^{13}CO_2$) but it is significantly reduced in intensity (see Figure 4.16). Reduction of (Cy-xantphos)Ni($^{13}CO_2$) using sodium naphthalenide solution leads to the same observation.

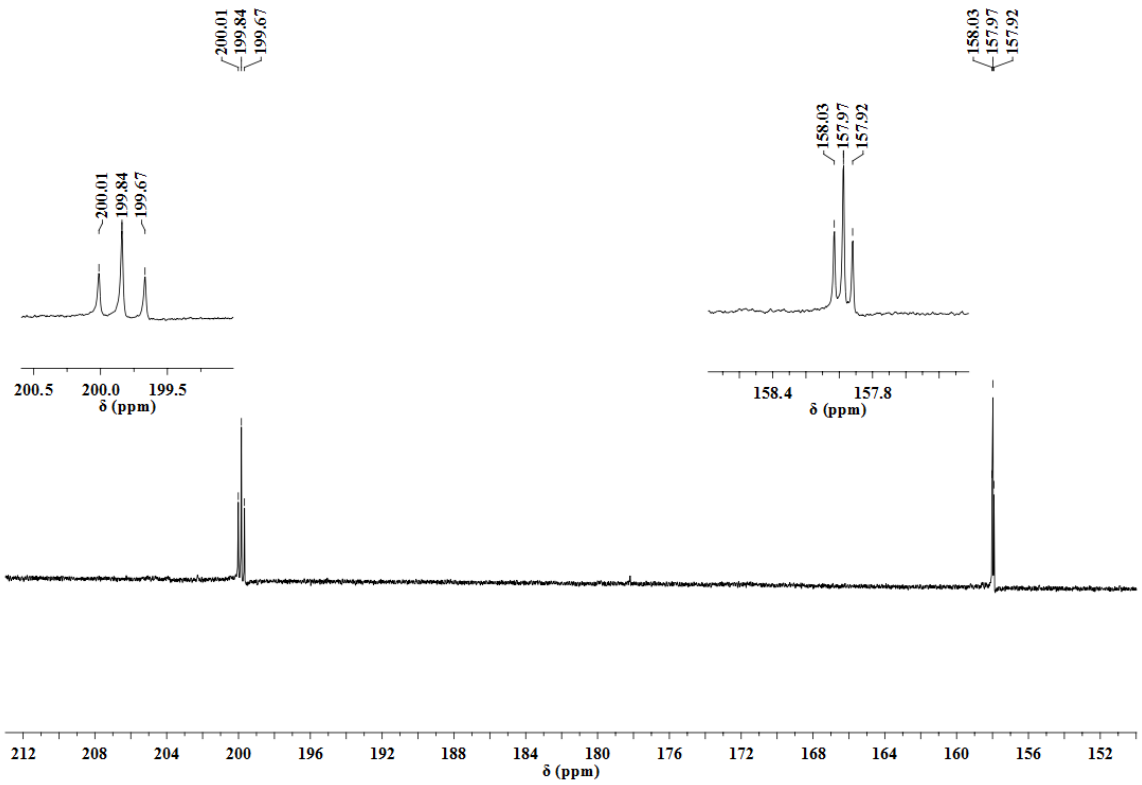

Figure 4.8. A portion of ^{13}C NMR spectrum of the product formed from the reduction of (Cy-xantphos)Ni($^{13}CO_2$) in presence of $Mg(OTf)_2$.

4.2.5.2 Reaction of (Cy-xantphos)Ni($^{13}CO_2$) with amidinium salt followed by reduction

i. Preparation of amidine salt[72]

Reaction between *N*,*N*-dicyclohexylcarbodiimide and phenyllithium forms a lithium amidinate complex, which on hydrolysis with a weakly acidic solution, leads to formation of **9** (Scheme 4.8). The complex reacts with ethereal tetrafluoroboric acid to give the amidinium tetrafluoroborate salt **10** (amidinium-BF_4). This is expected to be a possible hydrogen bond donor compound capable of interacting with the (Cy-xantphos)Ni(CO_2).

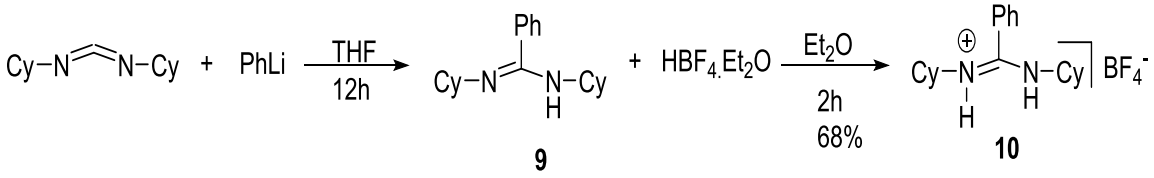

Scheme 4.8. Synthesis of amidinium-BF_4 salt.

ii. Reduction of (Cy-xantphos)Ni($^{13}CO_2$) in the presence of amidinium-BF_4 salt

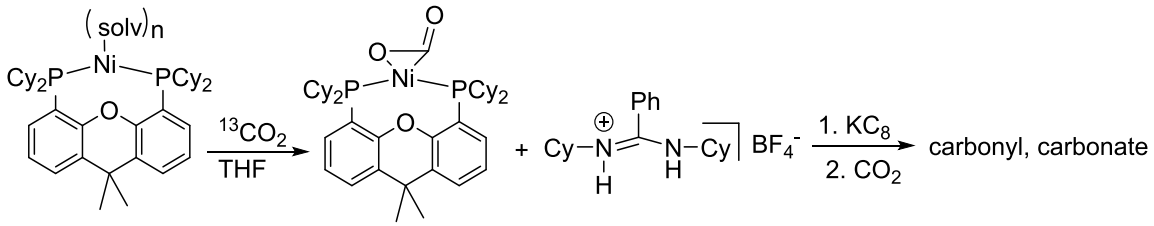

Scheme 4.9. Reduction of (Cy-xantphos)Ni($^{13}CO_2$) in presence of amidinium-BF_4 followed by CO_2 addition.

On treatment of (Cy-xantphos)Ni($^{13}CO_2$) with the amidinium salt (Scheme 4.9) followed by reduction with KC_8 then exposure to CO_2, the ^{31}P NMR spectrum shows a singlet resonance at δ 15.92 ppm instead of the initial doublet obtained for $Ni^{13}CO_2$ adduct. The ^{13}C NMR spectrum gives a major broad singlet resonance at δ 171.35 ppm instead of the earlier recorded triplet at δ 159.21 ppm for (Cy-xantphos)Ni($^{13}CO_2$) as shown in Figure 4.9 below. On standing for 24 hours, the triplet resonance at δ 200.24 ppm intensifies and the ^{31}P NMR spectrum shows multiple peaks. The IR spectrum of the resulting product shows no N-H stretch as seen in IR spectrum of the amidinium-BF_4 salt before the reaction.

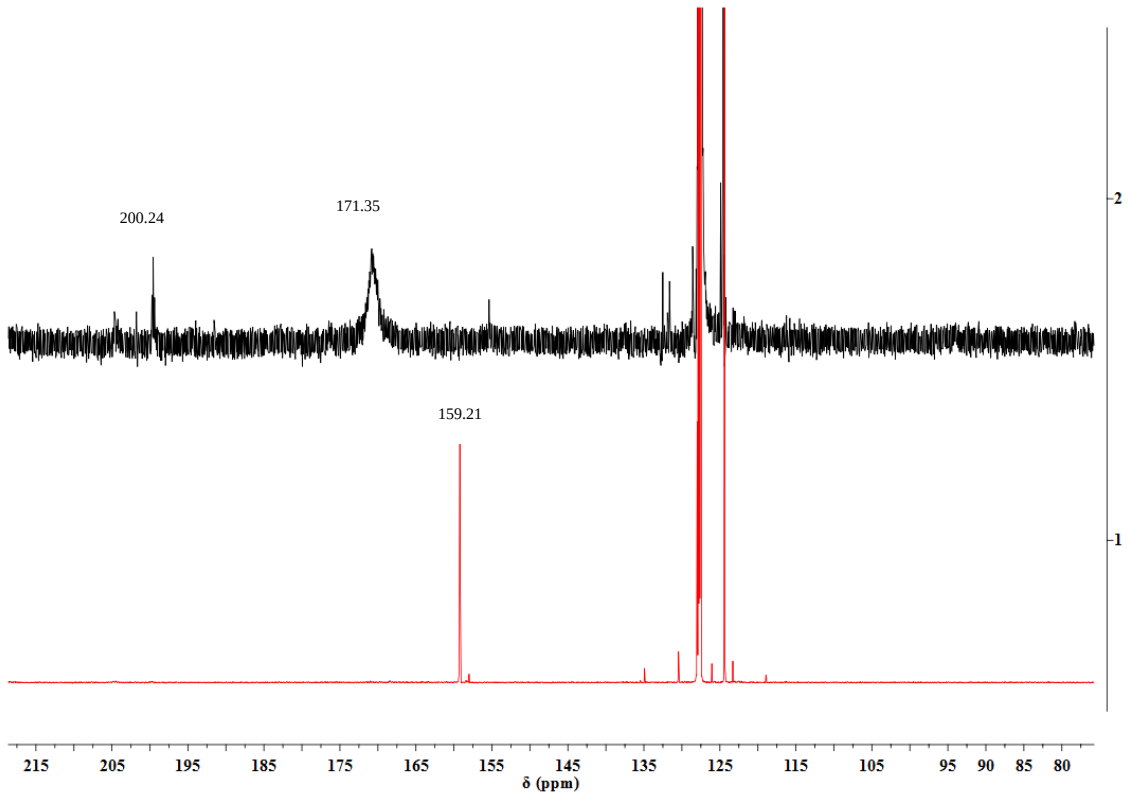

Figure 4.9. ^{13}C NMR spectrum of (Cy-xantphos)Ni($^{13}CO_2$) before (1) and after (2) reduction in presence of amidinium-BF_4 salt.

Previously, complexes of CO_2 in η^2-binding mode similar to those obtained by Aresta[49] and Hillhouse[50] were shown to add another molecule of CO_2 in a head-to-tail fashion to form a dimer of CO_2 (Figure 4.10) prior to reductive disproportionation to give CO and CO_3^{2-}.[69, 73-75]

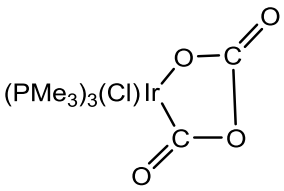

Figure 4.10. An iridium CO_2 dimer.

Besides disproportionation, the application of amidinium-BF_4 in this reaction could provide a bifunctional system that works to initiate the attack of the bound CO_2 by H^+ followed by reduction to give monocarbonyl complex and water as a byproduct.[63, 76]

The ^{13}C NMR can often be used to identify the CO_2 complexes especially when isotopically labeled CO_2 is employed in their synthesis. [Ni(dcpe)][CO_3] and [Ni(dcpp)(η^2-CO_2)] (dcpp = 1,3-bis(dicyclohexylphosphino)propane) exhibit nearly identical chemical shifts for the central carbon at δ 166.2 ppm and 164.2 ppm respectively, but the carbonate appears as a singlet while the CO_2 complex exhibits coupling.[66] In the reaction of low-valent Ni(dcpe) with $^{13}CO_2$, Mastrorilli and co-workers observed formation of a triplet resonance at δ 204.1 ppm which they ascribed to monocarbonyl species Ni(dcpe)(^{13}CO) and the singlet resonance at δ 166.2 ppm to Ni(dcpe)(CO_3).[66] Comparably, in the reaction of (Cy-xantphos)Ni($^{13}CO_2$) with KC_8 in presence of amidinium-BF_4, the newly formed broad singlet at δ 171.35 ppm can be ascribed to a carbonate carbon. The triplet resonance at δ 200.24 ppm observed in the ^{13}C NMR can be assigned to the carbonyl carbon of (Cy-xantphos)Ni($^{13}CO)_2$. This resonance is nearly identical to that obtained for the independently synthesized (Cy-xantphos)Ni($^{13}CO)_2$ at δ 201.92 ppm.

4.3 Concluding Remarks

We have herein synthesized and characterized (Cy-xantphos)Ni(II) complex. We have showed that when reduced, this complex binds both the CO and CO_2 molecules. The carbonyl complex shows two strong inequivalent absorptions in the infrared at fairly high CO vibrational frequencies (υ_{CO}= 1981, 1913 cm^{-1}). Coupled with the fairly short C-O bond

length for a transition metal bound CO (1.183 Å), there seems to be a weak back-donation from Ni center to CO π* orbitals.

The interaction between a transition metal bound CO_2 with a Lewis acid seems to have an overall effect of C-O bond elongation as shown in **4** Table 4.1. This make it easier to cleave the C-O bond during the subsequent reduction step to form the respective carbonyl complexes. It is possible that a similar effect is experienced when (Cy-xantphos)Ni(CO_2) is treated with Lewis acids. Reduction of (Cy-xantphos)Ni(CO_2) in presence of Mg^{2+} ions forms mainly a carbonyl product as seen in the ^{13}C NMR spectrum. The same observations are made, albeit not cleanly, when the reduction of (Cy-xantphos)Ni(CO_2) is carried out in presence of hydrogen bond donor, amidinium-BF_4 salt.

4.4 Experimental

4.4.1 General Considerations

All reactions, unless otherwise stated, were carried out in an MBraun inert atmosphere (nitrogen) glovebox, or in a resealable glassware on a Schlenk line under argon atmosphere. Glassware and magnetic stir bars were dried in a ventilated oven at 160 °C and were allowed to cool under vacuum. Molecular sieves (Alfa Aesar) and Celite (EMD 545) were dried under vacuum for at least twelve hours at 160°C.

^{1}H, ^{31}P spectra were obtained using a Varian Vx 400 MHz or Varian Mercury 300 (300.323 MHz for ^{1}H) spectrometer and ^{13}C, NMR spectra were obtained using either Avance IIIHD 500 spectrometer, or Bruker Avance IIIHD 700 spectrometer. ^{1}H and ^{13}C NMR chemical shifts are referenced with respect to solvent signals and are reported relative

to tetramethylsilane.[77] ^{31}P NMR chemical shifts were referenced to 85% H_3PO_4 as an external standard. Elemental analyses were performed by Atlantic Microlab, Inc. in Norcross, GA. Infrared spectra were collected from neat and liquid samples using a Bruker Alpha-P infrared spectrometer equipped with an attenuated total reflection (ATR) attachment. Since the instrument is inside glovebox, data acquisition for air and moisture sensitive samples were all carried out in the glovebox.

4.4.2 Materials and Methods

Dichloromethane (BDH), diethyl ether (EMD Millipore Omnisolv), hexanes (EMD Millipore Omnisolv), tetrahydrofuran (THF, EMD Millipore Omnisolv), and toluene (EMD Millipore Omnisolv) were sparged with ultra-high purity argon (NexAir) for 30 minutes prior to first use, dried using an MBraun solvent purification system. These solvents were further dried over sodium benzophenone ketyl, transferred under vacuum to an oven-dried sealable flask, and degassed by successive freeze–pump–thaw cycles. Anhydrous benzene (EMD Millipore Drisolv) and anhydrous pentane (EMD Millipore Drisolv), both sealed under a nitrogen atmosphere, were used as received and stored in a glovebox. Methanol (BDH), acetone (BDH), dichloromethane (BDH) hydrochloric acid (EMD) for benchtop work were used as received. Tap water was purified in a Barnstead International automated still prior to use.

Dichloromethane-d_2 (Cambridge Isotope Labs) and acetonitrile-d_3 (Cambridge Isotope Labs) were dried over excess calcium hydride overnight, vacuum-transferred to an oven-dried sealable flask, and degassed by successive freeze-pump-thaw cycles. Tetrahydrofuran-d_8 (Cambridge Isotope Labs), benzene-d_6 were dried over sodium

benzophenone ketyl, vacuum-transferred to an oven-dried sealable flask, and degassed by successive freeze-pump-thaw cycles. Deuterium oxide (Cambridge Isotope Labs), chloroform-*d* (Cambridge Isotope Labs), methanol-d_4 (Cambridge Isotope Labs) and methanol-d_1 (Cambridge Isotope Labs) were used as received.

Sodium *tert*-butoxide (TCI America), potassium *tert*-butoxide (Alfa-Aesar), magnesium sulfate (Alfa-Aesar), alumina (EMD), sodium metal (Alfa-Aesar), benzophenone (Alfa-Aesar), calcium hydride (Alfa-Aesar), $^{13}CO_2$ (Cambridge Isotope Labs), hydrogen (Sigma- Aldrich), nitrogen (NexAir), carbon monoxide (GT&S Inc.) and argon (both industrial and ultra-high purity grades, NexAir) were used as received. Natural abundance carbon dioxide (NexAir) was passed through phosphorus pentoxide (Sigma-Aldrich) to ensure dryness. $Ni(COD)_2$ (Strem), magnesium triflate (Strem), dicyclohexylcarbodiimide (Sigma Aldrich), phenyllithium (Sigma Aldrich), trifluoroboric acid ether complex (Sigma Aldrich), Cy-xantphos (Matrix Scientific) were all used as received.

4.4.3 Experimental Procedures

4.4.3.1 4,5-Bis(dicyclohexylphosphino)-9,9-dimethylxanthene nickel(II) dichloride or (Cy-xantphos)$NiCl_2$ (**6**)

To a 20-mL scintillation vial was added 4,5-bis(dicyclohexylphosphino)-9,9-dimethylxanthene (Cy-xantphos) (0.042 g, 0.066 mmol) and dichlorobis(triphenyl-phosphine)nickel(II) (0.043 g, 0.066 mmol). To this was added 5 mL of dry and degassed dichloromethane to dissolve, giving a blue solution. It was stirred for 12 hours after which solvent was removed under vacuum to give pinkish-blue solid. To this crude was added 2

mL of cold diethyl ether and filtered off, rinsed with 1.5 mL of cold diethyl ether and the resulting pink solid dried under vacuum to give (0.045 g, 93%). ^{1}H NMR (300 MHz, CD_2Cl_2) δ (ppm) 10.62 (s, br, 4H), 8.50 (s, br, 4H), 5.41 (s, br, 4H), 3.10 – 0.95 (m, 50H). ^{31}P NMR (161 MHz, THF-*d*$_8$, 85% H_3PO_4): δ (ppm) (br, s, 12.04. Anal. Calcd for $C_{39}H_{56}Cl_2NiOP_2$: C, 63.96; H, 7.71. Found: C, 63.70; H, 7.71.

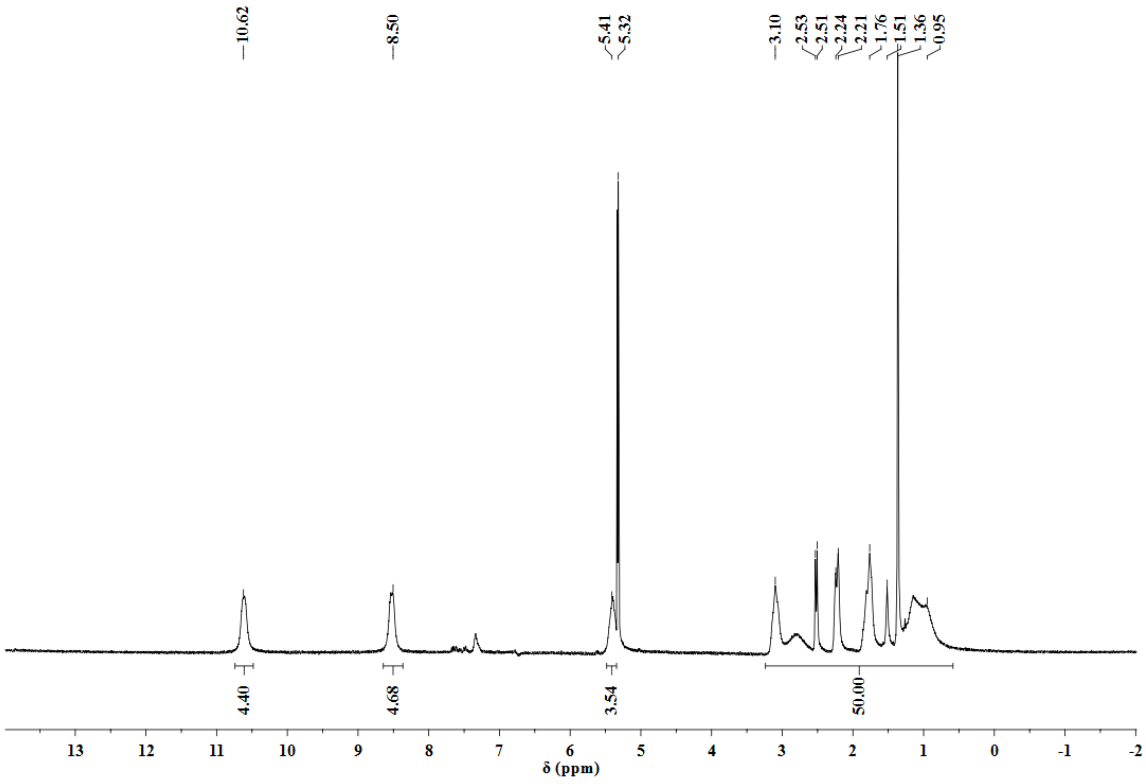

Figure 4.11. ^{1}H NMR spectrum of (Cy-xantphos)$NiCl_2$ in CD_2Cl_2 solution.

4.4.3.2 [4,5-Bis(dicyclohexylphosphino)-9,9-dimethylxanthene]nickel(0) (**5**)

Method A. To 4,5-bis(dicyclohexylphosphino)-9,9-dimethylxanthene (0.024 g, 0.041 mmol) in a 20-mL scintillation vial was added 2 mL of dry and degassed THF to dissolve. To another vial fitted with a stir-bar was added $Ni(COD)_2$ (0.014 g, 0.051 mmol) followed by 1.5 mL of THF to dissolve. This ligand solution was added dropwise over 5

min to the nickel solution while stirring, leading to formation of brown solution. Stirring was continued at room temperature for 2 hours. The solution was concentrated to about 1 mL then transferred to a J-young NMR tube. This was degassed by freeze-pump-thaw cycles and then 1 atm of hydrogen added. The mixture was agitated for 24 hours at room temperature leading to a decrease in the intensity of free COD.

Method B. To [4,5-bis(dicyclohexylphosphino)-9,9-dimethylxanthene]nickel(II) chloride (0.022 g, 0.027 mmol) in a 20-mL scintillation vial fitted with a stir-bar in a glovebox was added 2 mL of dry and degassed THF to dissolve. Into another vial was added KC_8 (0.007 g, 0.055 mmol) followed by 1 mL of THF. This solution of KC_8 was added dropwise to the THF solution of the complex over 5 min while stirring. The reaction was left to stir at room temperature for 18 hours after which it was filtered over Celite to give dark red solution. The solvent was removed under vacuum to give the product as a red solid. ^{1}H NMR (300 MHz, C_6D_6) δ (ppm) 7.27 (d, *J* = 7.5 Hz, 2H), 7.05 (d, *J* = 6.8 Hz, 2H), 6.96 (t, *J* = 7.5 Hz, 2H), 2.22 (s, 6H), 1.90 – 1.28 (m, 44H). ^{13}C NMR (176 MHz, C_6D_6) δ (ppm) 157.82 (t, *J* = 6.0 Hz), 135.07 (s), 129.34 (s), 128.22 (s), 127.98 (s), 124.14 (s), 123.33 (t, *J* = 6.3 Hz), 122.73 (s), 36.75 (t, *J* = 9.8 Hz), 36.03 (s), 35.41 (s), 29.18 (s), 29.09 (s), 27.96 (s), 27.57 (s), 27.18 (s), 26.56 (s), 23.57 (s). ^{31}P NMR (161 MHz, THF-d_8, 85% H_3PO_4): δ (ppm) 7.52.

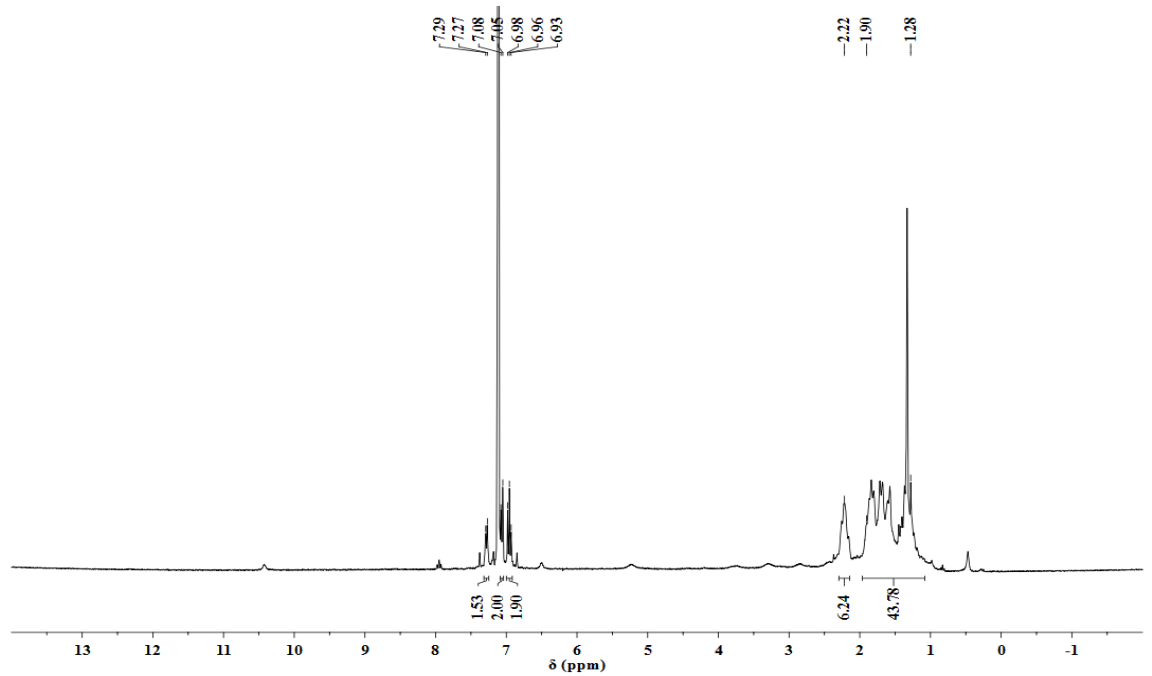

Figure 4.12. ^{1}H NMR spectrum of (Cy-xantphos)Ni(0) in C_6D_6 solution.

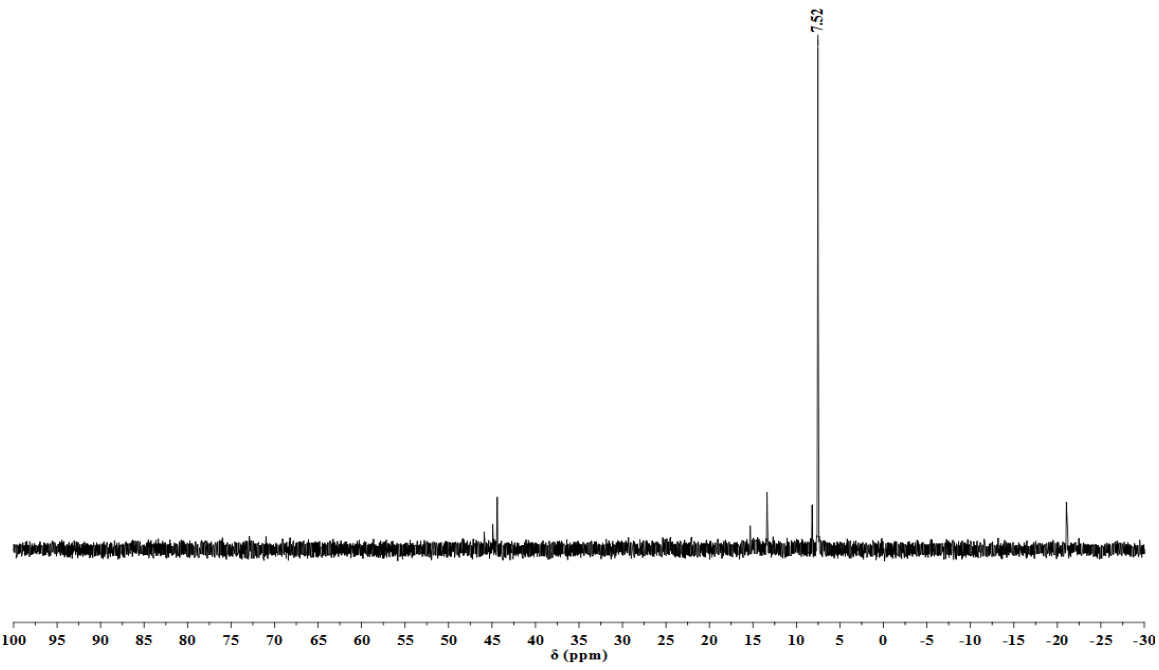

Figure 4.13. ^{31}P NMR spectrum of (Cy-xantphos)Ni(0) complex in THF-d_8 solution.

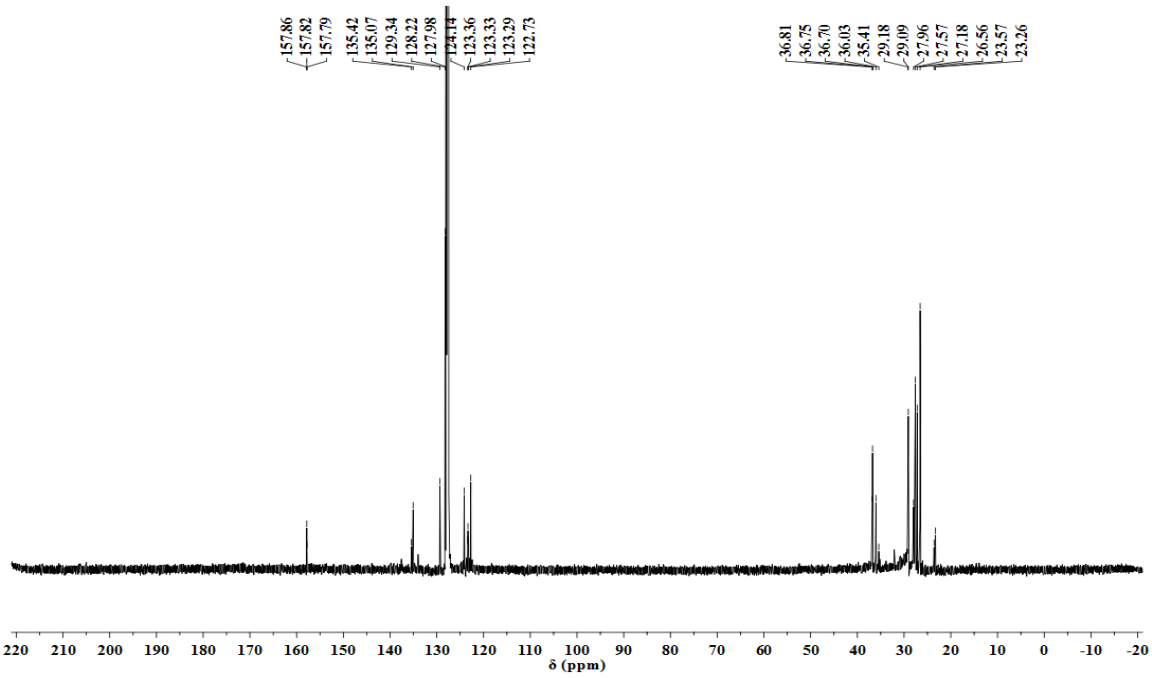

Figure 4.14. ^{13}C NMR spectrum of (Cy-xantphos)Ni(0) in C_6D_6 solution.

4.4.3.3 <u>(Cy-xantphos)Ni(CO_2) (**7**)</u>

The (Cy-xantphos)Ni(0) complex was taken up in THF-d_8 solution and transferred to a J-Young tube and degassed severally. CO_2 was then introduced into this tube and the sample taken for NMR after one hour. ^1H NMR (400 MHz, THF-d_8): δ (ppm) 7.50 (2H, d), 7.41 (2H, br d), 7.18 (t, 2H), 2.38 (10H, pseudo-d), 1.16-1.69 (51H, m). ^{13}C NMR (176 MHz, C_6D_6) δ 159.32 ($NiCO_2$, t, J = 7.4, Hz), 157.96 (t, J = 5.9 Hz), 134.85 (s), 130.46 (s), 128.22 (s), 126.04 (s), 124.38 (s), 123.27 (s), 119.00 (t, J = 9.5 Hz), 35.92 (s), 33.35 (t, J = 10.9 Hz), 29.88 (s), 28.65 (s), 27.95 (s), 27.37 (s), 27.09 (t, J = 6.7 Hz), 26.89 (t, J = 4.2 Hz), 26.28 (s). ^{31}P NMR (161 MHz, THF-d_8, 85% H_3PO_4): δ (ppm) 14.70. IR (film) cm^{-1}: 3067, 2921, 2849, 2234, 2079, 1900, 1742, 1446, 1400, 1219, 1098, 1047, 744, 495.

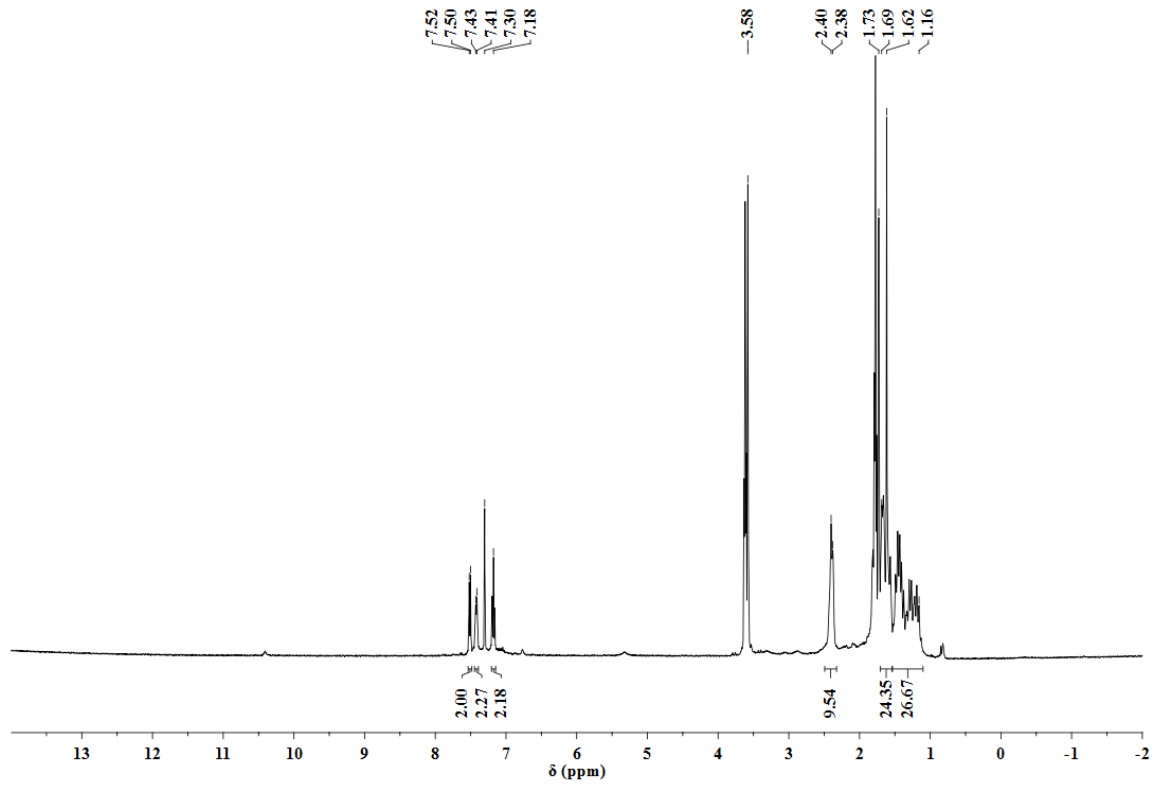

Figure 4.15. ^{1}H NMR spectrum of (Cy-xantphos)Ni(CO_2) in THF-d_8 solution.

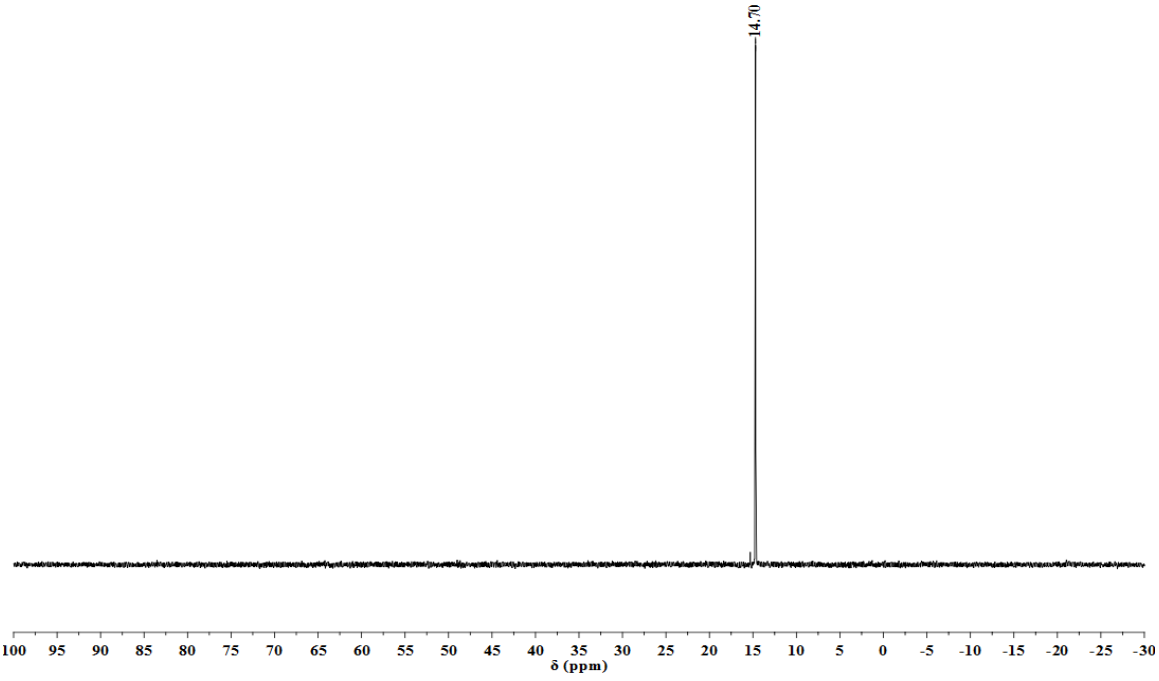

Figure 4.16. ^{31}P NMR spectrum of (Cy-xantphos)Ni(CO_2) in THF-d_8 solution.

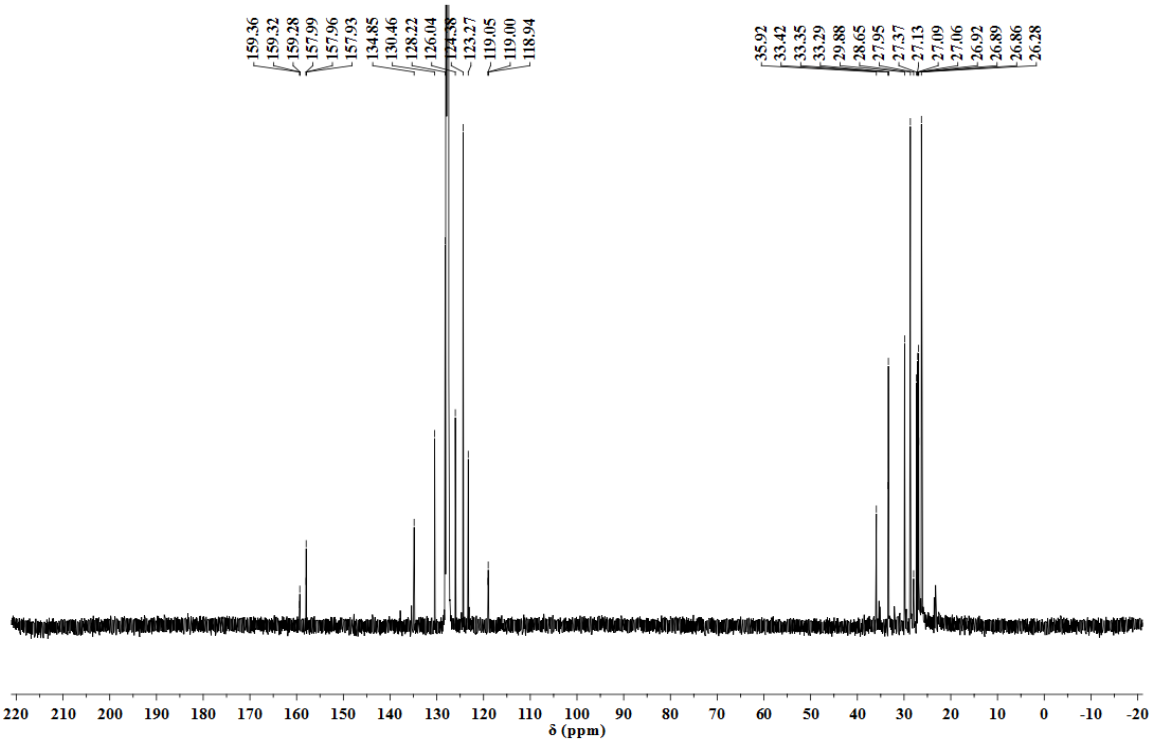

Figure 4.17. ^{13}C NMR spectrum of (Cy-xantphos)Ni(CO_2) in C_6D_6 solution.

4.4.3.4 (Cy-xantphos)Ni($^{13}CO_2$)

(Cy-xantphos)Ni(0) was dissolved in THF-d_8 solution and transferred to a J-Young tube. This was degassed by freeze-pump-thaw cycles after which 1 atm of $^{13}CO_2$ was added into the tube leading to an immediate color change from red to brown. The sample was analyzed by IR and NMR. $^{13}C\{^1H\}$ NMR (176 MHz, THF-d_8): δ (ppm) 159.19 (t, J = 5.6 Hz), 158.05 (Ni-$^{13}CO_2$, t, J = 9.6 Hz), 136.48 (C_{Ar}), 131.14 (C_{Ar}), 128.84 (C_{Ar}), 126.80 (C_{Ar}), 125.68 ($^{13}CO_2$), 123.96(C_{Ar}), 118.62 (C_{Ar}), 68.03 (C_{CH2}), 37.12 (C_{CH2}), 33.83 (t, C_{CH2}), 30.56 (C_{CH3}), 29.35 (C_{CH2}), 27.83 (t, C_{CH2}), 27.15 (C_{CH2}), 26.19 (C_{CH2}). $^{31}P\{^1H\}$ NMR (161 MHz, THF-d_8, 85% H_3PO_4): δ (ppm) 14.67 (d, J = 9.6 Hz). IR (film) cm^{-1}: 3065, 2921, 2847, 2234, 2079, 1697, 1616, 1446, 1398, 1047, 711, 495.

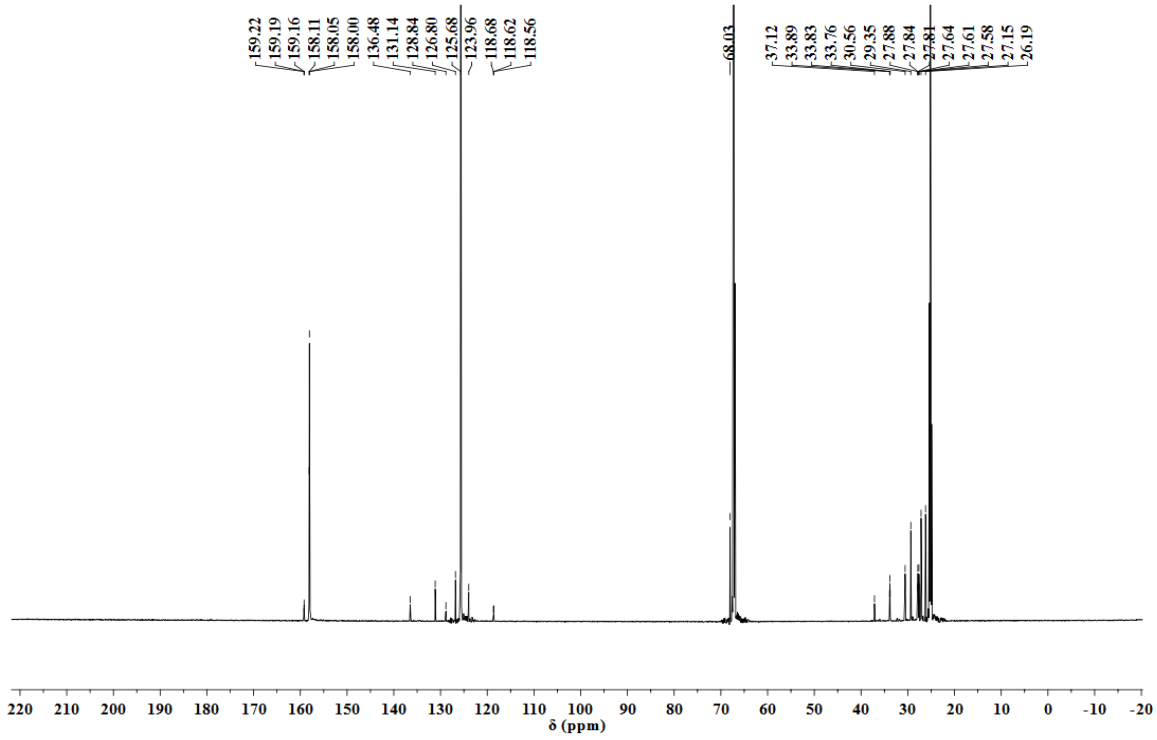

Figure 4.18. ^{13}C NMR spectrum of (Cy-xantphos)Ni($^{13}CO_2$) in THF-d_8 solution.

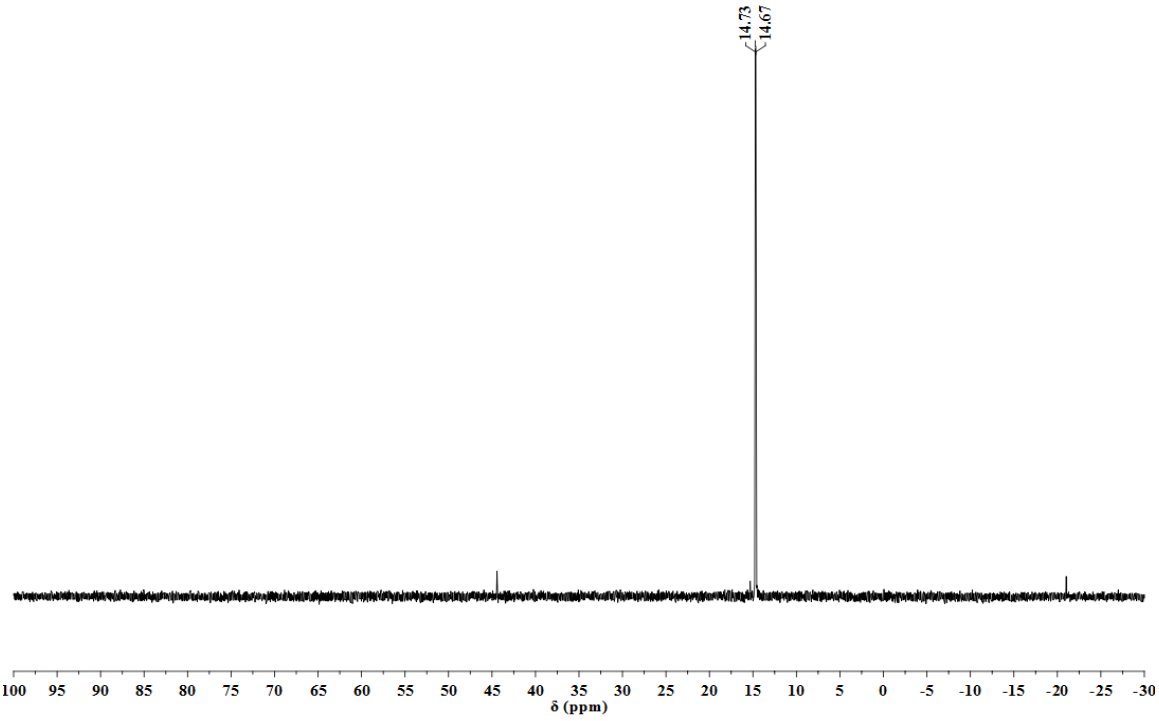

Figure 4.19. ^{31}P NMR spectrum of (Cy-xantphos)Ni($^{13}CO_2$) in THF-d_8 solution.

4.4.3.5 [4,5-Bis(dicyclohexylphosphino)-9,9-dimethylxanthene]nickel carbonyl (**8**)

(Cy-xantphos)Ni(0) was taken up in 1 mL of C_6D_6 and transferred to a J-Young tube. This was degassed severally using freeze-pump-thaw cycles. CO (1 atm) was then introduced into this tube and the sample analyzed by IR and NMR after 2 hours. ^{1}H NMR (700 MHz, C_6D_6) δ (ppm) 7.28 (d, *J* = 7.0 Hz, 2H), 7.11 (d, *J* = 7.7 Hz, 2H), 7.00 (t, *J* = 7.7 Hz, 2H), 2.25 (t, *J* = 11.8 Hz, 4H), 2.15 (d, *J* = 11.9 Hz, 4H), 2.07 (d, *J* = 12.6 Hz, 4H), 1.76 (dd, *J* = 23.1, 10.5 Hz, 16H), 1.61 (d, *J* = 12.6 Hz, 4H), 1.27 (m, 18H), 1.17 (t, *J* = 12.6 Hz, 4H). ^{13}C NMR (176 MHz, C_6D_6) δ (ppm) 201.92 (t, *J* = 6.5 Hz), 156.14 (t, *J* = 5.1 Hz), 145.48 (s), 134.20 (s), 128.99 (s), 128.24 (s), 127.98 (d, *J* = 7.3 Hz), 125.04 (s), 122.60 (s), 36.60 (t, *J* = 8.8 Hz), 35.77 (s), 29.20 (s), 28.16 (s), 27.69 (d, *J* = 2.5 Hz), 27.59 (t, *J* = 5.1 Hz), 27.40 (t, *J* = 5.1 Hz), 26.45 (s), 23.67 (s). ^{31}P{^{1}H} NMR (161 MHz, THF-*d*$_8$, 85% H_3PO_4): δ (ppm) 15.91. IR (film) cm^{-1}: 3065, 2923, 2849, 2236, 2081, 1981, 1913, 1446, 1400, 1230, 1047, 750, 491.

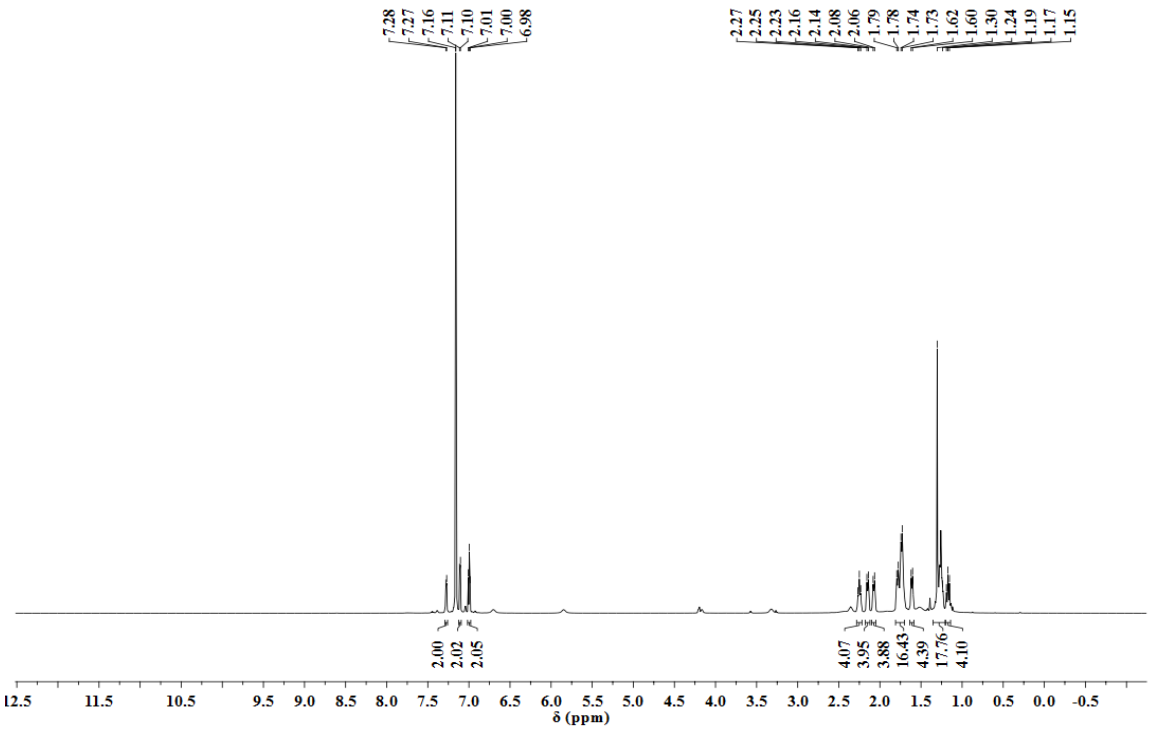

Figure 4.20. ^{1}H NMR spectrum of (Cy-xantphos)Ni-$(CO)_2$ in C_6D_6 solution.

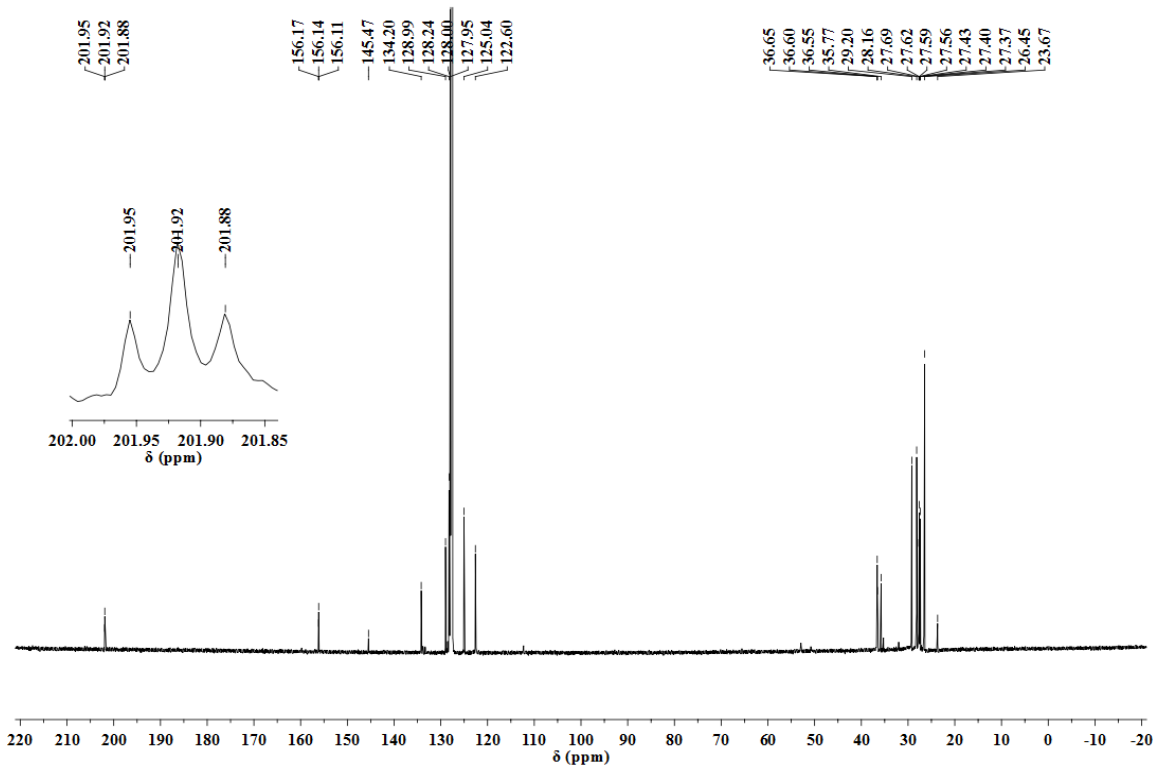

Figure 4.21. ^{13}C NMR spectrum of (Cy-xantphos-Ni-$(CO)_2$ in C_6D_6 solution.

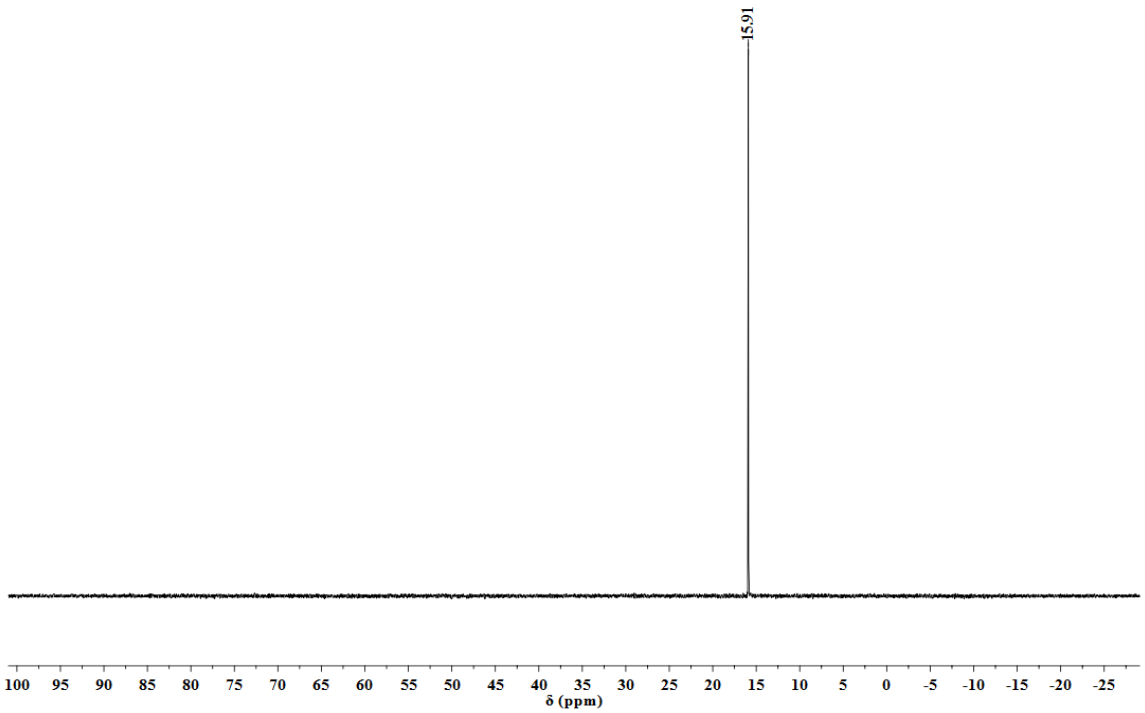

Figure 4.22. ^{31}P NMR spectrum of (Cy-xantphos)Ni-$(CO)_2$ in C_6D_6 solution.

4.4.3.6 Synthesis of amidinium-BF_4 salt (**10**)

Into a 250-mL Schlenk flask was added dicyclohexylcarbodiimide (2.00 g, 9.69 mmol). To this was added 30 mL of diethyl ether to dissolve. The solution was cooled using ice-water bath then phenyllithium in di-*n*-butylether (1.8 M, 27 mL, 0.05 mol) added dropwise over 20 minutes while stirring. After complete addition, the cooling bath was removed and the mixture stirred at room temperature for 16 hours. It was then diluted with 50 mL of cold 0.1 M HCl(aq), and then extracted 3 x 100 mL with Et_2O. The ether extracts were washed with 50 mL of water. The combined organic extracts were dried using anhydrous MgSO4, and filtered over Celite. The solvent was evaporated to dryness under vacuum for several hours to give a light brown oily product. Into a Strauss flask was added (1.00 g, 3.52 mmol) of this product and dissolved using 10 mL of Et_2O. It was then cooled

in ice-water bath. To this cold solution was added (0.85 mL, 3.52 mmol) of ethereal tetrafluoroboric acid. The cooling bath was removed and the mixture stirred for 2 hours at room temperature. The resulting white precipitate was filtered off and dried under vacuum. It was dissolved in 1.5 mL of dichloromethane then layered with 2 mL of Et_2O and set to recrystallize at -35°C overnight. The resulting clear crystals were filtered off and dried under vacuum to give a white solid (0.683 g, 68%). ^{1}H NMR (700 MHz, THF) δ (ppm) 8.40 (d, *J* = 55.3 Hz, 2H), 7.70-7.58 (m, 5H), 4.09-4.04 (m, 1H), 3.09-3.03 (m, 1H), 2.11 (d, *J* = 11.2 Hz, 2H), 1.88 – 1.82 (m, 2H), 1.76 (d, *J* = 11.2 Hz, 2H), 1.71-1.66 (m, 6H), 1.47-1.42 (m, 2H), 1.31-1.26 (m, 2H), 1.21-1.12 (m, 2H), 1.03-0.95 (m, 2H). ^{13}C NMR (176 MHz, THF) δ (ppm) 162.94 (s), 132.54 (s), 130.43 (d, *J* = 6.8 Hz), 129.96 (s), 128.39 (s), 127.94 (s), 57.24 (s), 52.04 (s), 32.69 (s), 32.53 (s), 26.06 (s), 25.80 (s). IR (film) cm^{-1}: 3301 (NH), 3036, 2931, 2859, 1631 (C=N), 1577, 1057, 703.

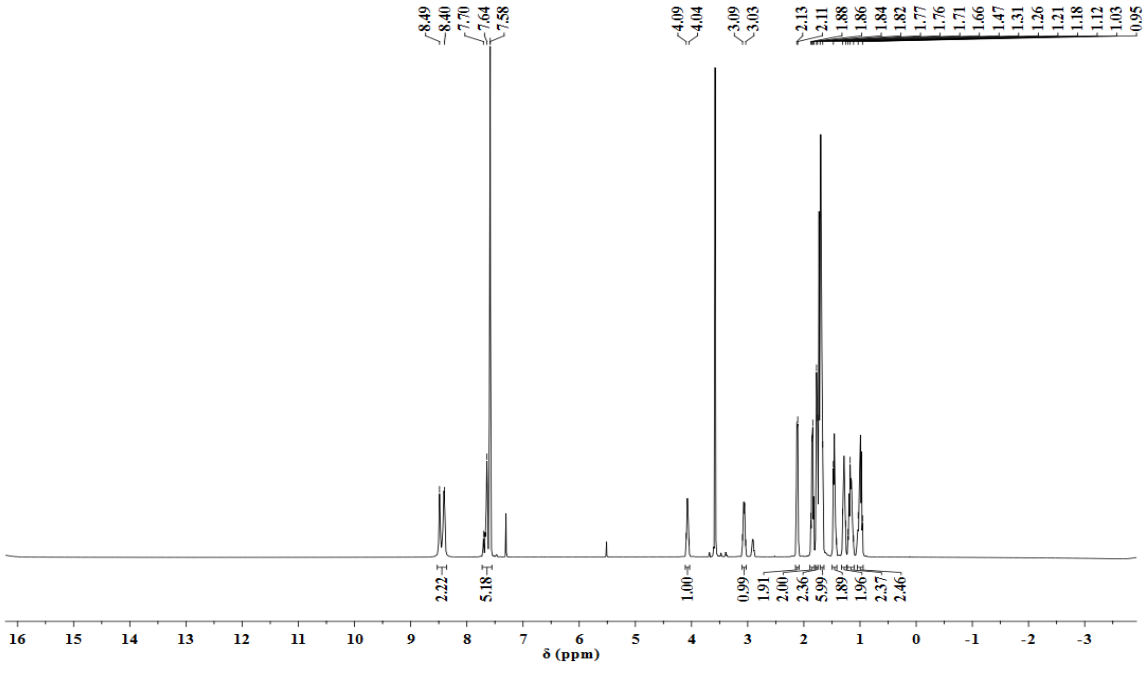

Figure 4.23. ^{1}H NMR spectrum of amidinium-BF_4 salt in THF-d_8 solution.

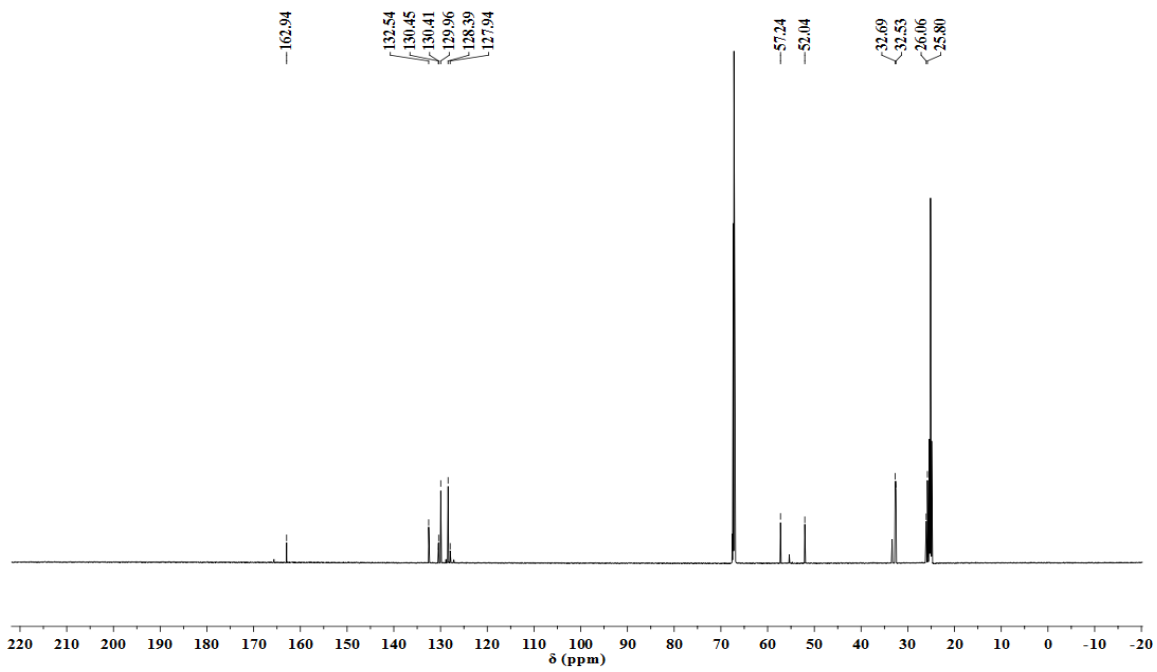

Figure 4.24. ^{13}C NMR spectrum of amidinium-BF_4 salt in THF-d_8 solution.

4.4.3.7 Reduction of [(Cy-xantphos)Ni($^{13}CO_2$)]amidinium complex

(Cy-xantphos)Ni(0) (0.021 g, 0.032 mmol) was dissolved in 0.6 mL of C_6D_6 solution and transferred to a J-young tube. This was degassed by freeze-pump-thaw cycles after which 1 atm of $^{13}CO_2$ was added into the tube leading to an immediate color change. In a 20-mL scintillation vial, amidinium-BF_4 salt (0.010 g, 0.032 mmol) was dissolved in 0.4 mL of THF-d_8 and transferred into the tube. This was analyzed after 1 h, 24 h and 48 h. ^1H NMR spectrum showed slightly broadened peaks. ^{13}C NMR (176 MHz, C_6D_6) δ (ppm) 200.24 (NiCO, t, J = 29.4 Hz), 171.35 (s), 156.04 (s), 133.18 (s), 132.29 (s), 129.26 (s), 128.54 (d, J = 6.9 Hz), 125.22 (s), 35.54 (s), 30.66 (s), 29.83 (s), 28.94 (s), 27.70 (s), 27.70 (s), 27.48 (s), 26.80 (s), 26.07 (s). $^{31}P\{^1H\}$ NMR (161 MHz, THF-d_8, 85% H_3PO_4): δ (ppm) 15.92.

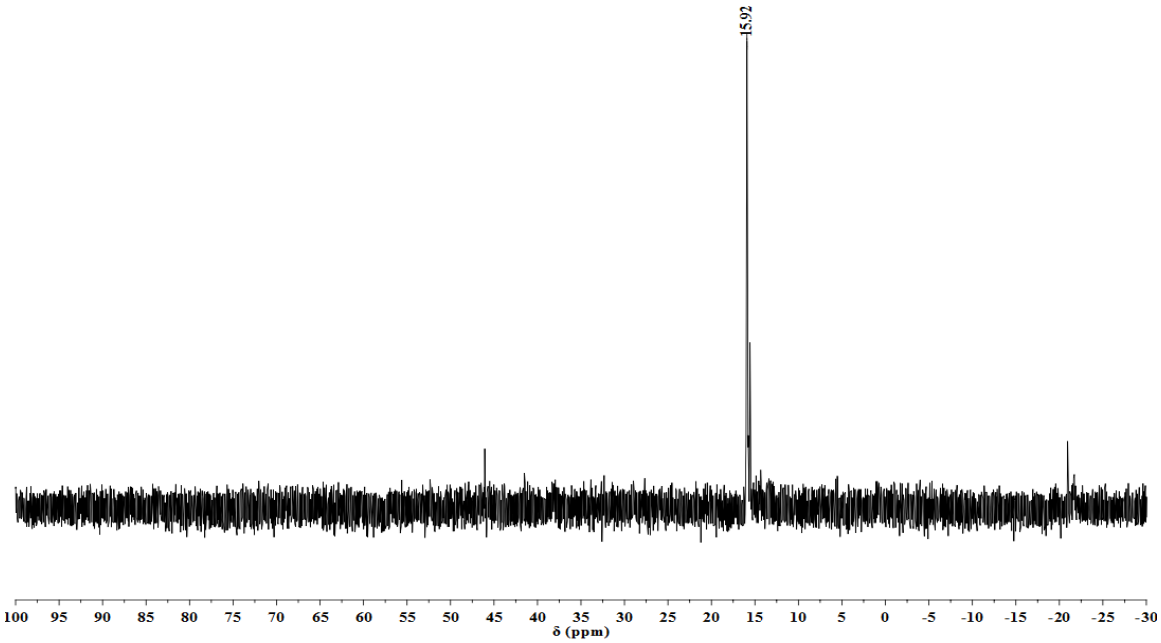

Figure 4.25. ^{31}P NMR spectrum of [(Cy-xantphos)Ni($^{13}CO_2$)]amidinium mixture after reduction.

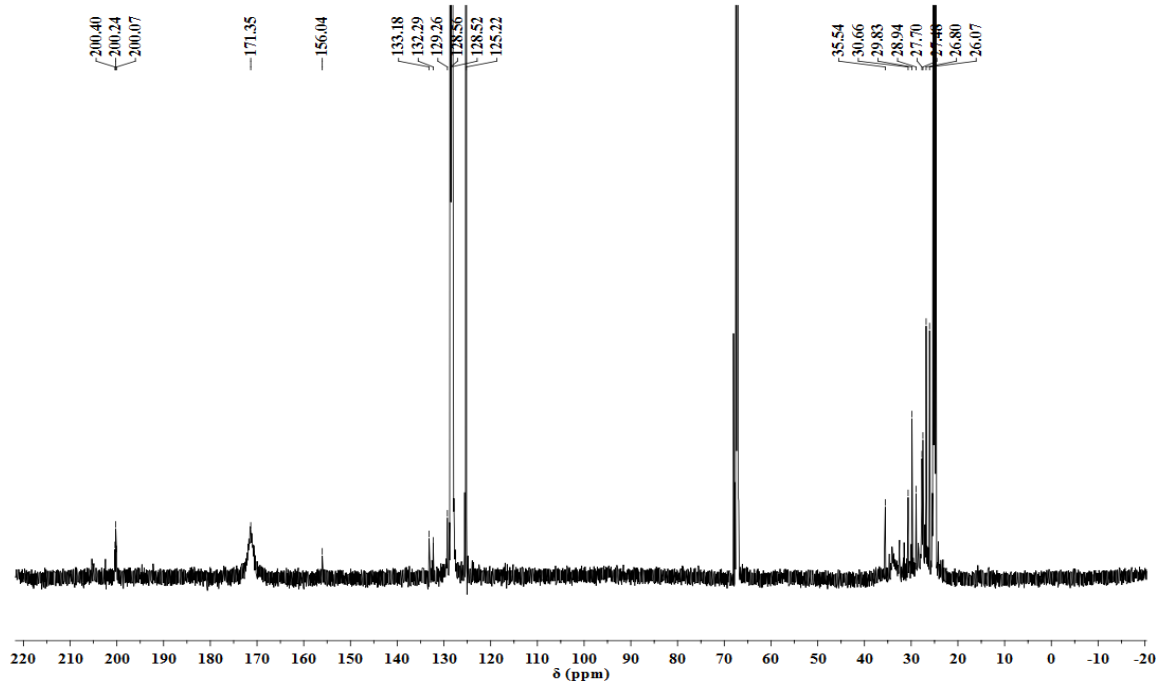

Figure 4.26. ^{13}C NMR spectrum of [(Cy-xantphos)Ni($^{13}CO_2$)]amidinium mixture after reduction.

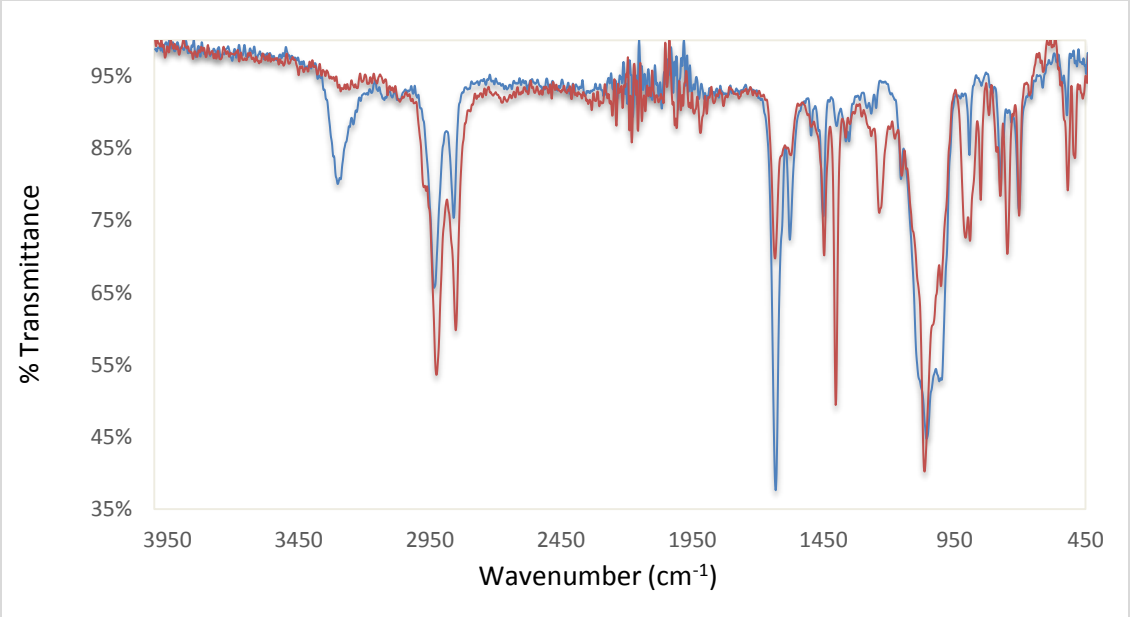

Figure 4.27. IR spectrum of amidinium-BF_4 before reaction (blue trace) and [(Cy-xantphos)Ni($^{13}CO_2$)]amidinium mixture after reduction (red trace).

4.4.3.8 Procedure for the reduction of (Cy-xantphos)Ni($^{13}CO_2$) in presence of $Mg(OTf)_2$

(Cy-xantphos)Ni($^{13}CO_2$) was prepared as earlier described. To a solution of this complex in THF was added a solution of 1 equivalent of $Mg(OTf)_2$ in THF. It was stirred for 1 hour. A solution of 1 equivalent of KC_8 in THF was added to this mixture while stirring at room temperature. After complete addition, the mixture was set to stir overnight. The mixture was filtered through Celite, and solvent evaporated to dryness to give the product.

4.4.4 X-ray Diffraction Studies

A suitable crystal of complex **8** from a THF solution at -35 ^oC was selected and mounted on Bruker APEX-II CCD diffractometer. The crystal was kept at 100(2) K during data collection. Using Olex2,[78] the structure was solved with ShelXT[79] structure solution

program using Intrinsic Phasing and refined with ShelXL[80] refinement package using Least Squares minimisation.

Crystal Data for $C_{44.5}H_{64}Cl_{0.5}NiO_{3.5}P_2$ (*M* =793.33 g/mol), (**8**): orthorhombic, space group Pbca (no. 61), *a* = 12.5369(16) Å, *b* = 16.5870(19) Å, *c* = 40.334(5) Å, *V* = 8387.4(18) Å^3, *Z* = 8, *T* = 100(2) K, μ(MoKα) = 0.610 mm^{-1}, *Dcalc* = 1.257 g/cm^3, 122505 reflections measured (4.546° ≤ 2Θ ≤ 61.016°), 12789 unique (R_{int} = 0.1181, R_{sigma} = 0.0605) which were used in all calculations. The final R_1 was 0.0474 (I > 2σ(I)) and wR_2 was 0.1147 (all data).

Crystals of **6** grown from a DCM solution layered with Et_2O and kept at -35 °C was selected and analyzed in the same way as for **8** above.

Crystal Data for $C_{39}H_{56}Cl_2NiOP_2$ (*M* =732.38 g/mol), (**6**): tetragonal, space group I-4 (no. 82), *a* = 22.820(3) Å, *c* = 14.415(2) Å, *V* = 7507(2) Å^3, *Z* = 8, *T* = 100.01 K, μ(MoKα) = 0.774 mm^{-1}, *Dcalc* = 1.296 g/cm^3, 37446 reflections measured (4.89° ≤ 2Θ ≤ 60.99°), 11401 unique (R_{int} = 0.0508, R_{sigma} = 0.0566) which were used in all calculations. The final R_1 was 0.0358 (I > 2σ(I)) and wR_2 was 0.0778 (all data).

4.5 REFERENCES

1. Arakawa, H.; Aresta, M.; Armor, J. N.; Barteau, M. A.; Beckman, E. J.; Bell, A. T.; Bercaw, J. E.; Creutz, C.; Dinjus, E.; Dixon, D. A., Catalysis research of relevance to carbon management: progress, challenges, and opportunities. *Chem. Rev.* **2001,** *101*, 953-996.

2. Peters, M.; Köhler, B.; Kuckshinrichs, W.; Leitner, W.; Markewitz, P.; Müller, T. E., Chemical technologies for exploiting and recycling carbon dioxide into the value chain. *ChemSusChem.* **2011,** *4*, 1216-1240.

3. Appel, A. M.; Bercaw, J. E.; Bocarsly, A. B.; Dobbek, H.; DuBois, D. L.; Dupuis, M.; Ferry, J. G.; Fujita, E.; Hille, R.; Kenis, P. J., Frontiers, opportunities, and challenges in biochemical and chemical catalysis of CO_2 fixation. *Chem. Rev.* **2013,** *113*, 6621-6658.

4. Aresta, M., *Carbon dioxide as chemical feedstock*. John Wiley & Sons: 2010.

5. Laitar, D. S.; Müller, P.; Sadighi, J. P., Efficient Homogeneous Catalysis in the Reduction of CO_2 to CO. *J. Am. Chem. Soc.* **2005,** *127*, 17196-17197.

6. Wu, L.; Liu, Q.; Jackstell, R.; Beller, M., Recent Progress in Carbon Dioxide Reduction Using Homogeneous Catalysts. In *Carbon Dioxide and Organometallics*, Springer: 2015; pp 279-304.

7. Qiao, J.; Liu, Y.; Hong, F.; Zhang, J., A review of catalysts for the electroreduction of carbon dioxide to produce low-carbon fuels. *Chem. Soc. Rev.* **2014,** *43*, 631-675.

8. Benson, E. E.; Kubiak, C. P.; Sathrum, A. J.; Smieja, J. M., Electrocatalytic and homogeneous approaches to conversion of CO_2 to liquid fuels. *Chem. Soc. Rev.* **2009,** *38*, 89-99.

9. Schneider, J.; Jia, H.; Kobiro, K.; Cabelli, D. E.; Muckerman, J. T.; Fujita, E., Nickel(II) macrocycles: highly efficient electrocatalysts for the selective reduction of CO_2 to CO. *Energy Environ. Sci.* **2012,** *5*, 9502-9510.

10. Costentin, C.; Drouet, S.; Robert, M.; Savéant, J.-M., A local proton source enhances CO_2 electroreduction to CO by a molecular Fe catalyst. *Science* **2012,** *338*, 90-94.

11. Wang, W.-H.; Himeda, Y.; Muckerman, J. T.; Manbeck, G. F.; Fujita, E., CO_2 hydrogenation to formate and methanol as an alternative to photo-and electrochemical CO_2 reduction. *Chem. Rev.* **2015,** *115*, 12936-12973.

12. Cokoja, M.; Bruckmeier, C.; Rieger, B.; Herrmann, W. A.; Kuehn, F. E., Transformation of carbon dioxide with homogeneous transition-metal catalysts: a molecular solution to a global challenge? *Angew. Chem. Int. Ed.* **2011,** *50*, 8510-8537.

13. Amatore, C.; Jutand, A.; Khalil, F.; Nielsen, M. F., Carbon dioxide as a C1 building block. Mechanism of palladium-catalyzed carboxylation of aromatic halides. *J. Am. Chem. Soc.* **1992,** *114*, 7076-7085.

14. Leitner, W., Carbon dioxide as a raw material: the synthesis of formic acid and its derivatives from CO_2. *Angew. Chem. Int. Ed. Eng.* **1995,** *34*, 2207-2221.

15. Leitner, W., The coordination chemistry of carbon dioxide and its relevance for catalysis: a critical survey. *Coord. Chem. Rev.* **1996,** *153*, 257-284.

16. Jia, C.; Kitamura, T.; Fujiwara, Y., Catalytic functionalization of arenes and alkanes via C−H bond activation. *Acc. Chem. Res.* **2001,** *34*, 633-639.

17. Aresta, M.; Dibenedetto, A., The contribution of the utilization option to reducing the CO_2 atmospheric loading: research needed to overcome existing barriers for a full exploitation of the potential of the CO_2 use. Elsevier: 2004.

18. Sakakura, T.; Choi, J.-C.; Yasuda, H., Transformation of carbon dioxide. *Chem. Rev.* **2007,** *107*, 2365-2387.

19. Aresta, M.; Dibenedetto, A., Utilisation of CO_2 as a chemical feedstock: opportunities and challenges. *Dalton Trans.* **2007,** 2975-2992.

20. Riduan, S. N.; Zhang, Y., Recent developments in carbon dioxide utilization under mild conditions. *Dalton Trans.* **2010,** *39*, 3347-3357.

21. Mikkelsen, M.; Jørgensen, M.; Krebs, F. C., The teraton challenge. A review of fixation and transformation of carbon dioxide. *Energy Environ. Sci.* **2010,** *3*, 43-81.

22. Li, Y.; Cui, X.; Dong, K.; Junge, K.; Beller, M., Utilization of CO_2 as a C_1 building block for catalytic methylation reactions. *ACS Catal.* **2017,** *7*, 1077-1086.

23. Behr, A., Carbon Dioxide as an Alternative C1 Synthetic Unit: Activation by Transition-Metal Complexes. *Angew. Chem. Int. Ed. Eng.* **1988,** *27*, 661-678.

24. Gibson, D. H., The organometallic chemistry of carbon dioxide. *Chem. Rev.* **1996,** *96*, 2063-2096.

25. Gibson, D. H., Carbon dioxide coordination chemistry: metal complexes and surface-bound species. What relationships? *Coord. Chem. Rev.* **1999,** *185*, 335-355.

26. Yin, X.; Moss, J. R., Recent developments in the activation of carbon dioxide by metal complexes. *Coord. Chem. Rev.* **1999,** *181*, 27-59.

27. Palmer, D. A.; Van Eldik, R., The chemistry of metal carbonato and carbon dioxide complexes. *Chem. Rev.* **1983,** *83*, 651-731.

28. Mondal, B.; Song, J.; Neese, F.; Ye, S., Bio-inspired mechanistic insights into CO_2 reduction. *Curr. Opin. Chem. Biol.* **2015,** *25*, 103-109.

29. Can, M.; Armstrong, F. A.; Ragsdale, S. W., Structure, function, and mechanism of the nickel metalloenzymes, CO dehydrogenase, and acetyl-CoA synthase. *Chem. Rev.* **2014,** *114*, 4149-4174.

30. Jeoung, J.-H.; Dobbek, H., Carbon dioxide activation at the Ni, Fe-cluster of anaerobic carbon monoxide dehydrogenase. *Science* **2007,** *318*, 1461-1464.

31. Doukov, T. I.; Iverson, T. M.; Seravalli, J.; Ragsdale, S. W.; Drennan, C. L., A Ni-Fe-Cu center in a bifunctional carbon monoxide dehydrogenase/acetyl-CoA synthase. *Science* **2002,** *298*, 567-572.

32. Darnault, C.; Volbeda, A.; Kim, E. J.; Legrand, P.; Vernède, X.; Lindahl, P. A.; Fontecilla-Camps, J. C., Ni-Zn-[Fe_4-S_4] and Ni-Ni-[Fe_4-S_4] clusters in closed and open α subunits of acetyl-CoA synthase/carbon monoxide dehydrogenase. *Nat. Struct. Molecul. Biol.* **2003,** *10*, 271.

33. Gong, W.; Hao, B.; Wei, Z.; Ferguson, D. J.; Tallant, T.; Krzycki, J. A.; Chan, M. K., Structure of the $\alpha_2\varepsilon_2$ Ni-dependent CO dehydrogenase component of the Methanosarcina barkeri acetyl-CoA decarbonylase/synthase complex. *Proc. Nat. Acad. Sci.* **2008,** *105*, 9558-9563.

34. Fesseler, J.; Jeoung, J. H.; Dobbek, H., How the [$NiFe_4S_4$] cluster of CO dehydrogenase activates CO_2 and NCO−. *Angew. Chem. Int. Ed.* **2015,** *54*, 8560-8564.

35. Schneck, F.; Ahrens, J.; Finger, M.; Stückl, A. C.; Würtele, C.; Schwarzer, D.; Schneider, S., The elusive abnormal CO_2 insertion enabled by metal-ligand cooperative photochemical selectivity inversion. *Nature commun.* **2018,** *9*, 1161.

36. Yoo, C.; Kim, J.; Lee, Y., Synthesis and Reactivity of Nickel(II) Hydroxycarbonyl Species, NiCOOH-κ C. *Organometallics* **2013,** *32*, 7195-7203.

37. Kim, Y.-E.; Kim, J.; Lee, Y., Formation of a nickel carbon dioxide adduct and its transformation mediated by a Lewis acid. *Chemical Commun.* **2014,** *50*, 11458-11461.

38. Kim, Y.-E.; Oh, S.; Kim, S.; Kim, O.; Kim, J.; Han, S. W.; Lee, Y., Phosphinite-Ni(0) Mediated Formation of a Phosphide-Ni(II)-OCOOMe Species via Uncommon Metal–Ligand Cooperation. *J. Am. Chem. Soc.* **2015,** *137*, 4280-4283.

39. Yoo, C.; Ajitha, M. J.; Jung, Y.; Lee, Y., Mechanistic Study on C–C Bond Formation of a Nickel(I) Monocarbonyl Species with Alkyl Iodides: Experimental and Computational Investigations. *Organometallics* **2015,** *34*, 4305-4311.

40. Yoo, C.; Lee, Y., Formation of a tetranickel octacarbonyl cluster from the CO_2 reaction of a zero-valent nickel monocarbonyl species. *Inorg. Chem. Front.* **2016,** *3*, 849-855.

41. Yoo, C.; Lee, Y., AT-Shaped Nickel(I) Metalloradical Species. *Angew. Chem. Int. Ed.* **2017,** *56*, 9502-9506.

42. Yoo, C.; Lee, Y., Carbon dioxide binding at a Ni/Fe center: synthesis and characterization of Ni(η^1-CO_2-κC) and Ni-μ-CO_2-κ C: κ^2O,O′-Fe. *Chem. Sci.* **2017,** *8*, 600-605.

43. Yoo, C.; Oh, S.; Kim, J.; Lee, Y., Transmethylation of a four-coordinate nickel(I) monocarbonyl species with methyl iodide. *Chem. Sci.* **2014,** *5*, 3853-3858.

44. Yoo, C.; Kim, Y.-E.; Lee, Y., Selective Transformation of CO_2 to CO at a Single Nickel Center. *Acc. Chem. Res.* **2018,** *51*, 1144-1152.

45. Sahoo, D.; Yoo, C.; Lee, Y., Direct CO_2 addition to a Ni(0)–CO species allows the selective generation of a Nickel(II) carboxylate with expulsion of CO. *J. Am. Chem. Soc.* **2018,** *140*, 2179-2185.

46. Seravalli, J.; Kumar, M.; Lu, W.-P.; Ragsdale, S. W., Mechanism of carbon monoxide oxidation by the carbon monoxide dehydrogenase/acetyl-CoA synthase from Clostridium thermoaceticum: kinetic characterization of the intermediates. *Biochemistry* **1997,** *36*, 11241-11251.

47. Chen, J.; Huang, S.; Seravalli, J.; Gutzman, H.; Swartz, D. J.; Ragsdale, S. W.; Bagley, K. A., Infrared studies of carbon monoxide binding to carbon monoxide dehydrogenase/acetyl-CoA synthase from Moorella thermoacetica. *Biochemistry* **2003,** *42*, 14822-14830.

48. Amara, P.; Mouesca, J.-M.; Volbeda, A.; Fontecilla-Camps, J. C., Carbon Monoxide Dehydrogenase Reaction Mechanism: A Likely Case of Abnormal CO_2 Insertion to a $Ni{-}H^-$ Bond. *Inorg. Chem.* **2011,** *50*, 1868-1878.

49. Aresta, M.; Nobile, C. F.; Albano, V. G.; Forni, E.; Manassero, M., New nickel–carbon dioxide complex: synthesis, properties, and crystallographic characterization of (carbon dioxide)-bis(tricyclohexylphosphine)nickel. *J. Chem. Soc., Chem. Commun.* **1975,** 636-637.

50. Anderson, J. S.; Iluc, V. M.; Hillhouse, G. L., Reactions of CO_2 and CS_2 with 1,2-Bis(di-*tert*-butylphosphino)ethane Complexes of Nickel(0) and Nickel(I). *Inorg. Chem.* **2010,** *49*, 10203-10207.

51. Kamer, P. C.; Van Leeuwen, P. W.; Reek, J. N., Wide bite angle diphosphines: Xantphos ligands in transition metal complexes and catalysis. *Acc. Chem. Res.* **2001,** *34*, 895-904.

52. Birkholz, M.-N.; Freixa, Z.; van Leeuwen, P. W., Bite angle effects of diphosphines in C–C and C–X bond forming cross coupling reactions. *Chem. Soc. Rev.* **2009,** *38*, 1099-1118.

53. Paul, C.; ávan Leeuwen, P. W., Effect of the bite angle of diphosphine ligands on activity and selectivity in the nickel-catalysed hydrocyanation of styrene. *J. Chem. Soc., Chem. Commun.* **1995,** 2177-2178.

54. Goertz, W.; Kamer, P. C.; van Leeuwen, P. W.; Vogt, D., Application of chelating diphosphine ligands in thenickel-catalysed hydrocyanation of alk-l-enes and ω-unsaturatedfatty acid esters. *Chem. Commun.* **1997,** 1521-1522.

55. Boele, M. K.; van der Veen, L.; Kamer, P. J.; van Leeuwen, P. N., Electronic effects in the nickel-catalysed hydrocyanation of styrene applying chelating phosphorus ligands with large bite angles. *J. Chem. Soc., Dalton Trans.* **1998,** 2981-2988.

56. Goertz, W.; Kamer, P. C.; van Leeuwen, P. W.; Vogt, D., Asymmetric Nickel-Catalyzed Hydrocyanation of Vinylarenes by Applying Homochiral Xantphos Ligands. *Chem. Eur. J., Eur. J.* **2001,** 1614-1618.

57. Hirata, Y.; Tanaka, M.; Yada, A.; Nakao, Y.; Hiyama, T., Alkynylcyanation of alkynes and dienes catalyzed by nickel. *Tetrahedron* **2009,** *65*, 5037-5050.

58. Yamamoto, T.; Yamakawa, T., Nickel-Catalyzed Vinylation of Aryl Chlorides and Bromides with Vinyl ZnBr·MgBrCl. *J. Org. Chem.* **2009,** *74*, 3603-3605.

59. Mora, G.; Van Zutphen, S.; Klemps, C.; Ricard, L.; Jean, Y.; Le Floch, P., Synthesis, X-ray, and electronic structures of a new nickel dibromide complex. Activity in the regioselective catalyzed dimerization of ethylene into 1-butene. *Inorg. Chem.* **2007,** *46*, 10365-10371.

60. Kumar, P.; Prescher, S.; Louie, J., A serendipitous discovery: Nickel catalyst for the cycloaddition of diynes with unactivated nitriles. *Angew. Chem. Int. Ed.* **2011,** *50*, 10694-10698.

61. Staudaher, N. D.; Stolley, R. M.; Louie, J., Synthesis, mechanism of formation, and catalytic activity of Xantphos nickel π-complexes. *Chem. Commun.* **2014,** *50*, 15577-15580.

62. Jegat, C.; Fouassier, M.; Tranquille, M.; Mascetti, J.; Tommasi, I.; Aresta, M.; Ingold, F.; Dedieu, A., Carbon dioxide coordination chemistry. 3. Vibrational, NMR, theoretical studies of (carbon dioxide) bis(tricyclohexylphosphine)nickel. *Inorg. Chem.* **1993,** *32*, 1279-1289.

63. Aresta, M.; Dibenedetto, A.; Quaranta, E., CO_2 Coordination to Metal Centres: Modes of Bonding and Reactivity. In *Reaction Mechanisms in Carbon Dioxide Conversion*, Springer: 2016; pp 35-69.

64. Bianchini, C.; Mealli, C.; Meli, A.; Sabat, M., Metal-promoted transformation of carbon dioxide into carbon monoxide. X-ray crystal structure of the nickel-carbonate complex $[O{=}PPh_2CH_2C(CH_3)(CH_2PPh_2)_2]Ni(O_2CO).0.5H_2O.C_6H_6$. *Inorg. Chem.* **1984,** *23*, 2731-2732.

65. Reinking, M. K.; Ni, J.; Fanwick, P. E.; Kubiak, C. P., Carbon dioxide chemistry of a binuclear iridium(0) complex. Rapid and reversible oxygen atom transfer from carbonate. *J. Am. Chem. Soc.* **1989,** *111*, 6459-6461.

66. Mastrorilli, P.; Moro, G.; Nobile, C. F.; Latronico, M., Carbon dioxide-transition metal complexes. IV. New Ni(0)-CO_2 complexes with chelating diphosphines: influence of P-Ni-P angle on complex stabilities. *Inorg. Chim. Acta* **1992,** *192*, 189-193.

67. Dewar, M. J.; Thiel, W., Ground states of molecules. 39. MNDO results for molecules containing hydrogen, carbon, nitrogen, and oxygen. *J. Am. Chem. Soc.* **1977,** *99*, 4907-4917.

68. Fontaine, F. G.; Courtemanche, M. A.; Légaré, M. A., Transition-Metal-Free Catalytic Reduction of Carbon Dioxide. *Chem. Eur. J.* **2014,** *20*, 2990-2996.

69. Gambarotta, S.; Arena, F.; Floriani, C.; Zanazzi, P. F., Carbon dioxide fixation: bifunctional complexes containing acidic and basic sites working as reversible carriers. *J. Am. Chem. Soc.* **1982,** *104*, 5082-5092.

70. Schmeier, T. J.; Dobereiner, G. E.; Crabtree, R. H.; Hazari, N., Secondary Coordination Sphere Interactions Facilitate the Insertion Step in an Iridium(III)CO_2 Reduction Catalyst. *J. Am. Chem. Soc.* **2011,** *133*, 9274-9277.

71. Miller, A. J. M.; Labinger, J. A.; Bercaw, J. E., Trialkylborane-Assisted CO_2 Reduction by Late Transition Metal Hydrides. *Organometallics* **2011,** *30*, 4308-4314.

72. Pornet, J.; Miginiac, L., Behavior of phenylic, saturated, and allylic organometallics towards carbodiimides. *Bull. Soc. Chim. Fr.* **1974,** (5-6, Pt.2), 994-8.

73. Fachinetti, G.; Floriani, C.; Chiesi-Villa, A.; Guastini, C., Carbon dioxide activation. Deoxygenation and disproportionation of carbon dioxide promoted by bis (cyclopentadienyl)titanium and-zirconium derivatives. A novel bonding mode of the carbonato and a trimer of the zirconyl unit. *J. Am. Chem. Soc.* **1979,** *101*, 1767-1775.

74. Herskovitz, T.; Guggenberger, L. J., Carbon dioxide coordination chemistry. The structure and some chemistry of the novel carbon dioxide addition product chlorobis (carbon dioxide)tris(trimethylphosphine)iridium. *J. Am. Chem. Soc.* **1976,** *98*, 1615-1616.

75. Chatt, J.; Kubota, M.; Leigh, G. J.; March, F. C.; Mason, R.; Yarrow, D. J., A possible carbon dioxide complex of molybdenum and its rearrangement product di-μ-carbonato-bis{carbonyltris(dimethylphenylphosphine)molybdenum}: X-ray crystal structure. *J. Chem. Soc., Chem. Commun.* **1974,** 1033-1034.

76. Song, J.; Klein, E. L.; Neese, F.; Ye, S., The mechanism of homogeneous CO_2 reduction by Ni(cyclam): Product selectivity, concerted proton–electron transfer and C–O bond cleavage. *Inorg. Chem.* **2014,** *53*, 7500-7507.

77. Fulmer, G. R.; Miller, A. J.; Sherden, N. H.; Gottlieb, H. E.; Nudelman, A.; Stoltz, B. M.; Bercaw, J. E.; Goldberg, K. I., NMR chemical shifts of trace impurities: common laboratory solvents, organics, and gases in deuterated solvents relevant to the organometallic chemist. *Organometallics* **2010,** *29*, 2176-2179.

78. Dolomanov, O. V.; Bourhis, L. J.; Gildea, R. J.; Howard, J. A.; Puschmann, H., OLEX2: a complete structure solution, refinement and analysis program. *J. Appl. Crystallogr.* **2009,** *42*, 339-341.

79. Sheldrick, G. M., SHELXT - integrated space-group and crystal-structure determination. *Acta Crystallogr. A Found Adv* **2015,** *71*, 3-8.

80. Sheldrick, G. M., Crystal structure refinement with SHELXL. *Acta Crystallogr. C Struct. Chem.* **2015,** *71*, 3-8.

CHAPTER 5. CONCLUSIONS AND FUTURE OUTLOOK

This thesis presents the design, synthesis, modification and characterization of new ligand frameworks. These ligands have been applied in complex formation and coordination studies with CO and CO_2. From a commercially available bis(4-*tert*-butylphenyl)amine, substituted acridone can be synthesized. The obtained acridone can then be converted into functionalized acridone- or acridine-based ligand frameworks.

Presented herein is the synthesis of acridone from bis(4-*tert*-butylphenyl)amine via directed metalation using in-situ-formed carbamate as a removable directing group,[1] followed by closing of the central six-membered ring using phenyl chloroformate. This method leads to formation of substituted acridones bearing an alkyl side chain that would undergo dealkylation under the strong acid conditions used in several current available synthetic methods.[2] When converted to *ortho*-dibrominated substrate, the resulting dibromoacridone, is a versatile synthon that can be converted to numerous ligand frameworks via cross-coupling reactions or directed *ortho*-metalation reactions. Also included in this chapter is the synthesis of different *ortho*-substituted acridones and their applications in complex formation reactions. Even though the data obtained point to possible interactions of the ligands with the transition metals in these synthesis, attempts to isolate and characterize any resulting complexes were not successful.

The dibromoacridone can be easily converted to dibromoacridine which provides a new route to synthesis of a rigid tridentate PNP-acridine that eliminates the requirement of pre-functionalized substrates. The activated C-9 position of this ligand makes it possible to replace the chloride with nucleophiles such as alkoxy and aryloxy groups to give

(MeO)PNP-acridine and (ArO)PNP-acridine respectively. One-electron reduction of (ArO)PNP-acridine leads to formation of a radical anion as confirmed by EPR spectroscopy. Cyclic voltammetry of (ArO)PNP-acridine shows that it undergoes a reversible redox process. Both the (MeO)PNP-acridine and (ArO)PNP-acridine react with Ni(II) and Co(II) chlorides to form the corresponding complexes. Reduction of [(ArO)PNP-acridine]$Ni^{II}Cl_2$ and subsequent exposure to CO_2 leads to possible formation of a carbonate as judged by ^{13}C NMR spectroscopy. Reduction of cobalt complexes followed by exposure to CO leads to formation of dicarbonyl complexes.

For comparison, as well as in pursuit of developing a catalytic system that can transform CO_2 as a C_1 building unit in C-C bond formation, also presented herein is the synthesis and application of (Cy-xantphos)Ni complexes in CO_2 activation. The treatment of (Cy-xantphos)Ni(CO_2) complex with different Lewis acids followed by reduction and subsequent exposure to CO_2, produces what on comparison to the independently synthesized (Cy-xantphos)Ni$(CO)_2$ complex, appears to be (Cy-xantphos)nickel carbonyl complexes instead of the insertion products.

Future Outlook

In light of the observations made from the ligand synthesis as well as the applications of their complexes in coordination and activation of CO and CO_2, a few variations could offer informative comparisons. We have showed that it is possible to install dialkylphosphino groups at the 4- and 5-positions of the acridine ring. We have also showed that the C-9 position could be functionalized by reaction of the 9-Cl component with nucleophiles. Also showed is the ease with which acridone can be converted to

acridine, including those that already have functional groups installed at the *ortho* positions to the nitrogen like 4,5-di-*p*-tolyl-2,7-di-*tert*-butyl-9-chloroacridine. Therefore, structural modifications like functionalization of 2,7-di-*tert*-butyl-4,5-bis(diisopropylphosphino)-9-chloroacridine with a methoxy or aryloxy group at its C-9 position then comparing the reactivity of CO and CO_2 with its low-valent complexes to those discussed in this thesis could be important in structure and bonding comparison. It would be especially interesting to see how changes in donor ability of the phosphines affect the structure and bonding in the cobalt complexes formed. Other variations could include changing the appendage at the C-9 position and monitoring how that affects the reactivity at the nitrogen donor atom.

More interesting will be to find out whether this ligand can be converted into one that is applicable in homogenous electrocatalysis. Its ability to undergo a reversible redox process if coupled with a functional group that could possibly participate in hydrogen bonding like morpholine groups in the 2,7-di-*tert*-butyl-4,5-dimorpholinoacridone, could lead to a suitable framework for an electrocatalyst ligand. A ligand with such a framework might be able to support the PCET processes that are necessary to convert CO_2 to hydrocarbons or even to alcohols.[3]

Before diverting to acridine-based ligands and applications of their complexes in small molecules activation, we had set out to synthesize and study the reactivity of complexes based on acridone ligands. We successfully synthesized different variations of functionalized acridone ligand frameworks, however attempts to form complexes were not fruitful. However, in 2017 Lee and co-workers showed the functionalization and complexes of a ligand with as similar framework constrain as the acridone framework (Scheme 5.1).[4]

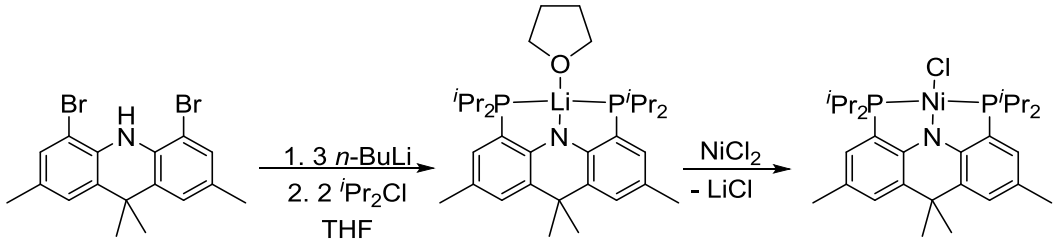

Scheme 5.1. Synthesis of 4,5-bis(diisopropylphosphino)-2,7,9,9-tetramethyl-9*H*-acridin-10-ide and its nickel complex formation.

Installation of the phosphino substituents at the 4- and 5-positions enabled the ligand to interact with transition metals and bring the metal within a bonding distance to the nitrogen, leading to a successful formation of the respective complexes. Similarly, Grubbs and co-workers showed that treatment of 1,8-bis(diisopropylphosphino)anthracene with ((chlorobis(cyclooctene)iridium dimer), $[IrCl(COE)_2]_2$ in toluene at reflux leads to formation of the iridium complex.[5] It is therefore possible that installation of phosphino substituents at the 4- and 5-positions on acridone would lead to successful formation of complexes. An alternative to solving the difficulty in complexes formation would be to install a linker at the 4- and 5-positions so that the bond lengths of the ligand pendant arms could be extended in order to hold the incoming transition metal at a suitable bonding distance to the nitrogen. For example, placing a protecting group on the nitrogen, followed by halogen-metal exchange then treatment with DMF should provide a 4,5-dicarboxaldehyde substituted intermediate. A condensation reaction of this intermediate with primary amines followed by deprotection should provide a neutral ligand.

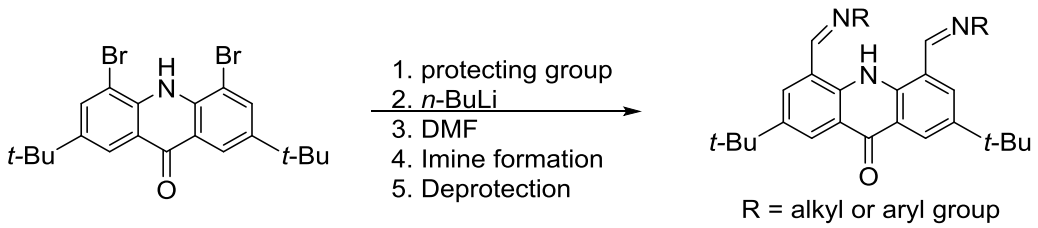

Scheme 5.2. Acridone modification through installation of a -CH linker.

It is also possible to install a -CH_2 linker via bromomethylation. The obtained intermediate can then undergo nucleophilic reactions especially with chlorophosphines to form the corresponding anionic PNP ligands.

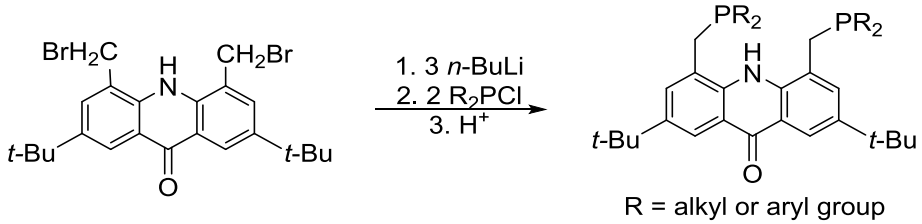

Scheme 5.3. Acridone modification through installation of a –CH_2 linker followed by phosphine substituents.

Successful synthesis of these ligand frameworks and their respective complexes should provide a point of comparison for reactivity studies to those observed with acridine- and Cy-xantphos-based complexes. It would be especially interesting to determine whether the flexibility in the pendant arms will lead to different CO_2 binding modes and how that affects the reactivity of the CO_2 adducts formed. An equally interesting study will be to determine whether the formed complexes undergo tautomerization and interconvert between the acridone and hydroxyacridine frameworks and how that affects the reactivity of the complexes.

5.1 REFERENCES

1. Katritzky, A. R.; Fan, W.-Q.; Akutagawa, K., Carbon dioxide: a reagent for the simultaneous protection of nucleophilic centres and the activation of alternative locations to electrophilic attack.: Part III1. A new synthetic method for the ortho-subttitution of *N*-monoalkylanilines. *Tetrahedron* **1986,** *42*, 4027-4034.

2. Zhou, W.; Yang, Y.; Liu, Y.; Deng, G.-J., Copper-catalyzed C-C bond cleavage and intramolecular cyclization: an approach toward acridones. *Green Chem.* **2013,** *15*, 76-80.

3. Benson, E. E.; Kubiak, C. P.; Sathrum, A. J.; Smieja, J. M., Electrocatalytic and homogeneous approaches to conversion of CO_2 to liquid fuels. *Chem. Soc. Rev.* **2009,** *38*, 89-99.

4. Yoo, C.; Lee, Y., AT-Shaped Nickel(I) Metalloradical Species. *Angew. Chem. Int. Ed.* **2017,** *56*, 9502-9506.

5. Romero, P. E.; Whited, M. T.; Grubbs, R. H., Multiple C-H Activations of Methyl tert-Butyl Ether at Pincer Iridium Complexes: Synthesis and Thermolysis of Ir(I) Fischer Carbenes[1]. *Organometallics.* **2008,** *27*, 3422-3429.

APPENDIX A. SYNTHESIS AND REACTIVITY STUDIES OF ANIONIC PNP COMPLEXES

A.1 Background

Pincer-type PNP ligands based on bis(*ortho*-phosphinoaryl)amine substructure of the form N-H [PN(H)P, **1**] or N-R [PN(Me)P, **2**] contains both hard amido donor as well as soft phosphine donors.[1-3] Since the pioneering work by Fryzuk[1] in these types of ligand frameworks, a variety of related ligands have been synthesized.[4] Ligands of this framework prefer tridentate, anionic, *mer*-PNP binding mode to late transition metals, and normally form complexes through N-H or N-C bond cleavage.[3] **1** and **2** form complexes with group 10 metals through oxidative addition to the zerovalent metal centers.[3]

Ligand **1** does not have as rigid a framework as that of PNP-acridine. But due to the uni-negative nature of the nitrogen donor atom in PN(H)P,[1] it is capable of forming robust complexes. We were therefore interested in investigating the reactivity of its Ni, Cu, Pd and main group metal complexes with N_2, CO, CO_2 etc. After the first report on catalytic conversion of N_2 to NH_3 at ambient temperature in 2003 by Schrock and Yandulov using a Mo-N_2 complex of a triamidoamine ligand,[5-8] a number of complexes bearing the PNP-type pincer ligand framework have been shown to be effective catalysts in conversion of N_2 to NH_3.[9-11] Peters and coworkers reported the conversion of N_2 to NH_3 catalyzed by Fe pincer complexes at a very low temperature.[12-14] Many effective N_2 fixation complexes are based on Mo and Fe even though [$CoH(N_2)(PPh_3)_3$] was the first reported transition metal-dinitrogen complex directly derived from N_2.[15-20] Cobalt is not only abundant and cheap, but it has been shown to bind dinitrogen and in some cases afford the transformation of N_2

under mild conditions.[20-26] In light of these observations, we were interested in part in the study of N_2 transformation using cobalt amido pincer complexes.

A.2 Results and Discussion

Ligand **1** was obtained via stepwise reaction starting with bromination of bis(4-*tert*-butylphenyl)amine followed by halogen-metal exchange and finally phosphination using $ClPPh_2$.[27-28] Ligand **2** was prepared as a neutral N-donor ligand for comparison starting with *N*-methylation of bis(4-*tert*-butylphenyl)amine [27] then following similar procedure as with **1**. Cobalt and palladium complexes of **1** were then prepared in good yields from the respective metal precursors (Scheme A1).

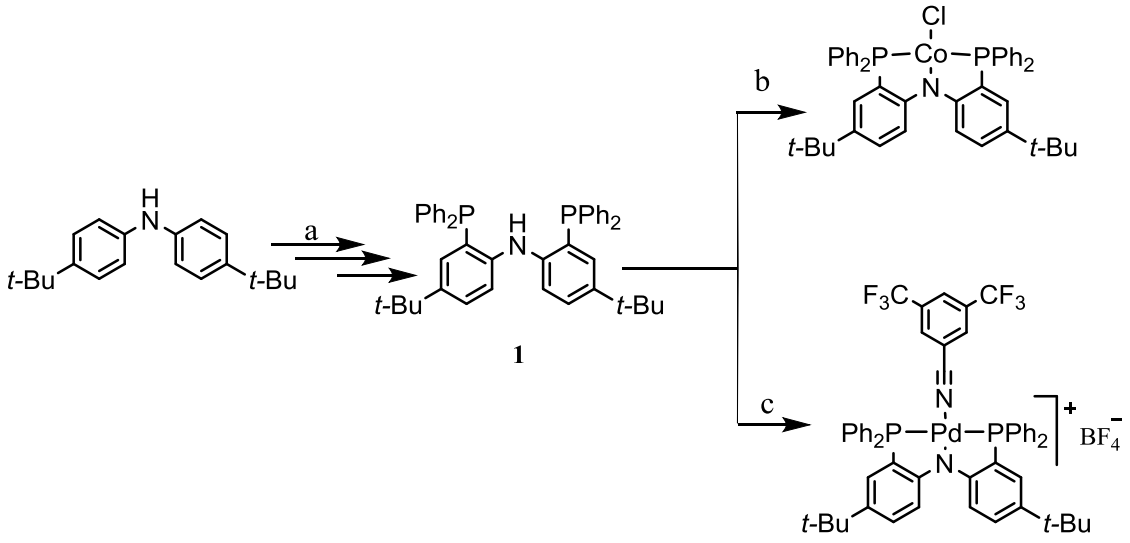

Conditions: a. (i) NBS, DMF (ii) *n*-BuLi (iii) $ClPPh_2$ b. *n*-BuLi then $CoCl_2$ or $CoCl_2$ then KO^tBu
c. (i) $Pd(OAc)_2$ (ii) brine (iii) $AgBF_4$ (iv) $(CF_3)_2C_6H_3CN$

App Scheme A.1. Synthesis of PN(H)P (**1**) and its cobalt and palladium complexes.

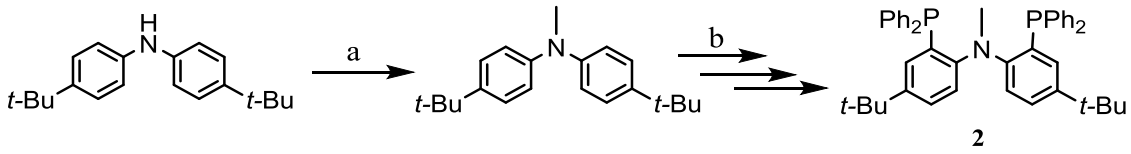

Conditions: a. (i) MeI, K_2CO_3 b. (i) Br_2, AcOH (ii) *n*-BuLi (iii) $ClPPh_2$

App Scheme A.2. Synthesis of PN(Me)P ligand (**2**).

The reduction of the cobalt complex using sodium naphthalenide or KC_8 under nitrogen at room temperature does not lead to a dinitrogen complex. However, reaction of the cobalt complex with diethylzinc or triethylaluminum show conversion of a paramagnetic complex into one with more diamagnetic properties as reflected by a better resolved ^{1}H NMR spectrum.

A.2.1 Reactivity studies of (PNP)NiH

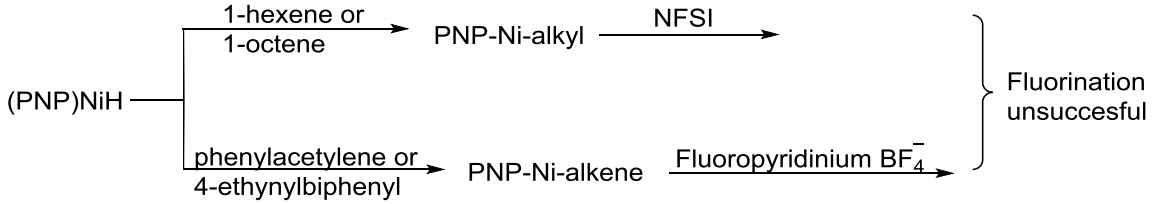

App Scheme A.3. Reactivity of (PNP)NiH with alkenes and subsequent fluorination studies.

Insertion of $Ni(COD)_2$ into the N-H bond is fast and takes place with liberation of free COD to form (PNP)NiH.[29] The hydride resonance appears as a triplet at δ -18.5 ppm in the ^{1}H NMR spectrum. This reaction however leads to formation of two products as can be seen from the existence of two phosphorus signals in the ^{31}P NMR spectrum at δ 27.4 and 32.7 ppm. At the beginning, the products are in a nearly 1:1 ratio, but as time goes by there is an 8-fold increase in the intensity of the product with a resonance at δ 32.7 ppm. This could be as a result of the addition of the liberated COD to the Ni-H bond to form a

(PNP)Ni-cyclooctene complex. Similar reactivity was observed before by Liang and coworkers in formation of [Ph-PNP]Ni(η^1-C_8H_{13}).[29]

(PNP)NiH reacts with linear alkenes like 1-hexene or 1-octene to form the respective (PNP)Ni-alkyls.[29-30] The reaction with 1-hexene produces a major product with a resonance at δ 26.8 ppm in the ^{31}P NMR spectrum. This chemical shift value is very close to the one observed by Liang and coworkers for their amido (PNP)NiH reaction with alkene to form [Ph-PNP]Ni(*n*-hexyl).[30] The ^{1}H NMR shows the disappearance of Ni-H peak while the nickel bound CH_2 appears as a triplet at δ 1.13 ppm and the CH_3 as a triplet at δ 0.76 ppm. Attempts to synthesize fluoro alkyls from these substrates however did not give any positive results. For comparison, fluorination of styrene using the cationic palladium complex [(PNP)Pd^+]BF_4^- was attempted which nevertheless gave negative results.

Due to these unpleasant observations, our interest drifted towards synthesis of low nuclearity copper(I) complex. The reactivity of this complex with CO or CO_2 would be of great interest due to the exceptional role of copper as the only metal that can reduce CO_2 to either CO or hydrocarbons in the electrocatlytic reduction of CO_2.[31] Insights into structure, bonding and reactivity of Cu-CO or Cu-CO_2 complexes could be useful inputs to molecular-level mechanistic understanding of the active sites of the copper-based complexes and contribute towards design of a more selective copper catalyst.[32-36] The copper complex is obtained from the reaction of **1** with mesitylcopper in benzene (App Scheme A4). However, solid-state analysis reveals a dicopper diamond core, Cu_2-N_2 stucture (App Figure A1), that is incapable of acting as a catalyst towards CO or CO2.

A related solid-state structure was obtained from analysis of the resulting product of reaction between mesitylcopper and (^{t}Bu$_2$-PNP)H.[37] As expected, the ^{31}P NMR shows phosphorus in very different chemical environments with phosphorus resonance of **3** coming up at δ -11.2 ppm compared to δ -33.9 ppm in [(^{t}Bu$_2$-PNP)Cu]$_2$. The Cu•••Cu distances in both cases are almost identical with 2.676 Å in **3** and 2.624 Å in the solid-state structure of [(^{t}Bu$_2$-PNP)Cu]$_2$. The P-Cu-P bond angles are 132.93^o and 137.69^o as compared to 127.79^o and 131.39^o in **3**.[37]

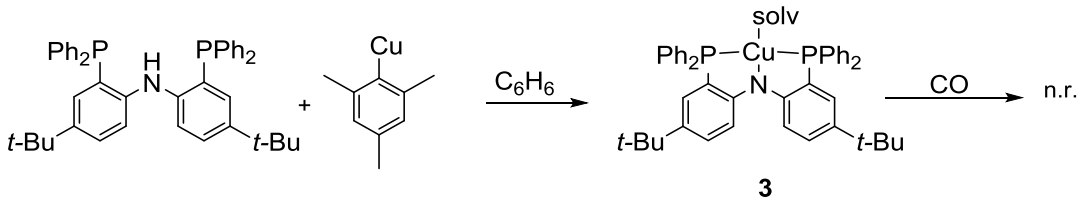

App Scheme A.4. Synthesis of (PNP)Cu complex and exposure to CO.

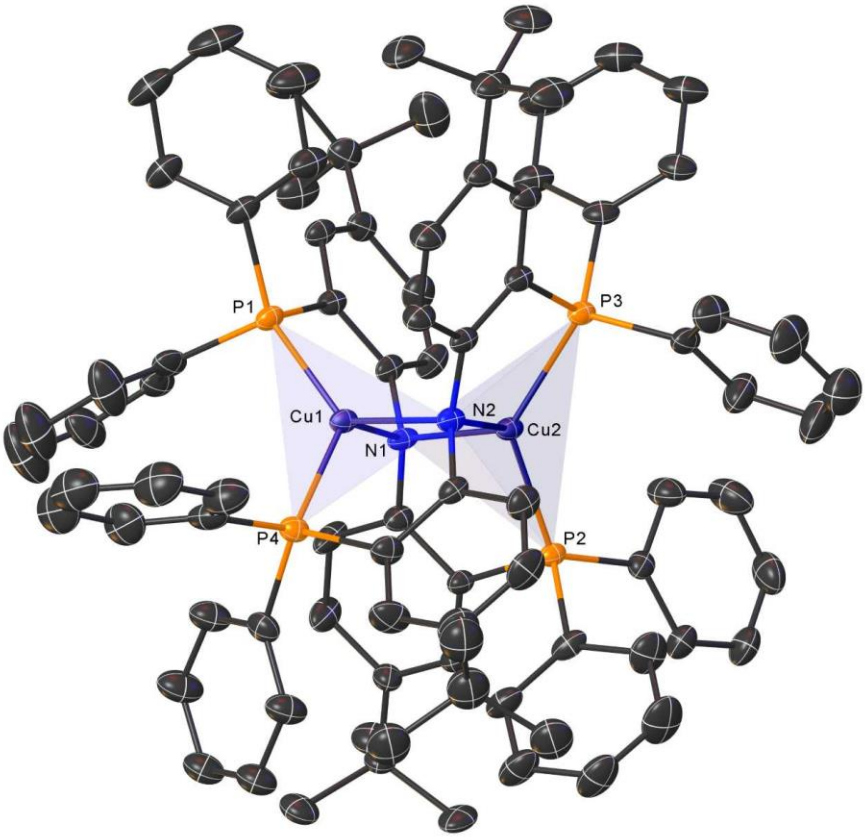

App Figure A.1. Solid-state structure of (PNP)Cu.

H atoms omitted for clarity with selected interatomic distances (Å) and angles (°): Cu••••Cu, 2.676; P1-Cu1-P2, 127.79; P1-Cu2-P2, 131.39.

A.3 Concluding Remarks

Observations of dimer formation in synthesis of (PNP)Cu complex synthesis is a reiteration of the role that ligand backbone strain and steric hindrance play in rearrangements around metal center. Changing from alkyl phosphorus to aryl phosphorus substituents do not alter much the type of copper complexes obtained in the reaction of PN(H)P with mesitylcopper. In keeping with the current literature evidence,[38] for a successful synthesis of PNP-Co(N_2) complexes, the substituents on the phosphorus might need to be alkyl groups.

A.4 Experimental

A.4.1 General Considerations

All reactions, unless otherwise stated, were carried out in an MBraun inert atmosphere (nitrogen) glovebox, or in a resealable glassware on a Schlenk line under argon atmosphere. Glassware and magnetic stir bars were dried in a ventilated oven at 160 °C and were allowed to cool under vacuum. Molecular sieves (Alfa Aesar) and Celite (EMD 545) were dried under vacuum for at least twelve hours at 160°C.

^{1}H NMR spectra were obtained using a Varian Vx 400 MHz or Varian Mercury 300 (300.323 MHz for ^{1}H) spectrometer and ^{13}C NMR spectra were obtained using either Avance IIIHD 500 spectrometer, or Bruker Avance IIIHD 700 spectrometer. ^{1}H and ^{13}C NMR chemical shifts are referenced with respect to solvent signals and are reported relative to tetramethylsilane.[39] Elemental analyses were performed by Atlantic Microlab, Inc. in Norcross, GA. Infrared spectra were collected from neat and liquid samples using a Bruker Alpha-P FT-IR spectrometer equipped with an attenuated total reflection (ATR) platinum diamond reflector accessory. Air and moisture sensitive samples were exposed to air as briefly as possible prior to data collection.

A.4.2 Materials and Methods

Tetrahydrofuran (EMD Millipore Omnisolv), hexanes (EMD Millipore Omnisolv), diethyl ether (EMD Millipore Omnisolv) and toluene (EMD Millipore Omnisolv) were sparged with ultra-high purity argon (NexAir) for 30 min prior to first use, and dried using an MBraun solvent purification system. These solvents were further dried over sodium benzophenone ketyl, degassed by successive freeze–pump–thaw cycles and then transferred under vacuum to an oven-dried resealable flask. Dichloromethane (EMD

Millipore Omnisolv), acetonitrile (EMD HPLC) were each stirred over calcium hydride (Alfa Aesar) in a sealed flask for at least twelve hours and degassed by several freeze-pump-thaw cycles, then vacuum-transferred to a resealable Sclenk flasks. These solvents were then stored over 3Å molecular sieves (Alfa-Aesar) in the glovebox. Methanol (BDH), acetone (BDH), ethyl acetate (BDH) and hexanes used in benchtop work were used as received.

Dichloromethane-d_2 (Cambridge Isotope Laboratories) and acetonitrile-d_3 were dried by stirring overnight over calcium hydride for at least twelve hours, degassed by several successive freeze–pump–thaw cycles. They were then transferred under vacuum to an oven-dried resealable flasks and stored in the glovebox. Benzene-d_6 and Tetrahydrofuran-d_8 (Cambridge Isotope Laboratories) were dried over sodium benzophenone ketyl, degassed by successive freeze–pump–thaw cycles and transferred under vacuum to an oven-dried resealable flask and stored in the glovebox. D_2O (Cambridge Isotope Laboratories), sodium *tert*-butoxide (TCI America), sodium hydroxide (EMD), anhydrous $MgSO_4$ (AlfaAesar), HCl (BDH), $NaHCO_3$ (BDH), benzophenone (Alfa-Aesar), calcium hydride (Alfa-Aesar), acetic acid (Alfa-Aesar), nitrogen (NexAir), and argon (both industrial and ultra-high purity grades, NexAir) were used as received.

Bis(4-*tert*-butylphenyl)amine (TCI), *n*-BuLi and *t*-BuLi (Sigma Aldrich), bromine (Alfa Aesar), dimethylformamide (EMD), $Pd(OAc)_2$ (STREM), Me_3Al (Sigma Aldrich), $CoCl_2$ (Sigma Aldrich), NBS (Sigma Aldrich), $ClPPh_2$ (TCI), Diethylzinc (Acros, 1M in hexanes), $Ni(COD)_2$ (Strem), mesitylcopper (Sigma Aldrich), carbon monoxide (GT&S Inc.), Carbon dioxide (NexAir), 1-hexene (Sigma Aldrich), 1-octene (Sigma Aldrich), NFSI (Sigma Aldrich), Fluoropyridinium tetrafluoroborate (Sigma Aldrich), methyl iodide

(Sigma Aldrich), K_2CO_3 (Sigma Aldrich), $AgBF_4$ (Alfa-Aesar), 2,4,6-trifluorobenzonitrile (Sigma Aldrich) were all used as received.

A.4.3 Experimental Procedure

A.4.3.1 Bis(2-bromo-4-*tert*-butylphenyl)amine

Method A: To a 250-mL Strauss flask was added (2.00 g, 7.11 mmol) of bis(4-*tert*-butylphenyl)amine followed by 50 mL of acetic acid to dissolve. The solution was cooled to 5 ^oC, then (0.74 mL, 14 mmol) of bromine was added. The cooling bath was removed and the mixture left to stir overnight. The reaction formed an off-white precipitate which was filtered off and dried over vacuum. The crude product was recrystallized from hot hexanes to give (1.75 g. 56%) of pure product.[27-28]

Method B: In a round bottom flask, bis(4-*tert*-butylphenyl)amine (1.018 g, 3.620 mmol) was added. To this was added 11 mL of DMF and stirred to dissolve then wrapped with aluminum foil. *N*-bromosuccinimide (1.293 g, 7.265 mmol) in 2 mL of DMF was added dropwise over 10 min while stirring. The mixture, red in color, was left to stir for 3 hours at room temperature in the dark. To this green mixture was added 30 mL of H_2O and then extracted using dichloromethane (3 x 5 mL). The combined organic layers were washed with H_2O (2 x 15 mL), then dried using anhydrous $MgSO_4$. The solvent was evaporated to dryness. The crude was taken up in 10 mL of dichloromethane and filtered through Celite/silica bed (5 g each). The obtained filtrate was again filtered through 3 g of Celite and 7 g of silica. The light pink solution was evaporated to dryness resulting to a pinkish-red solid. The solid was washed with 5 mL of cold methanol resulting to white solid (1.213 g, 76%). ^1H NMR (400 MHz, $CDCl_3$) δ (ppm) 7.58 – 7.55 (m, 2H), 7.22 – 7.21 (m, 4H), 6.27 (s, 1H), 1.30 (s, 18H). ^{13}C NMR (176 MHz, $CDCl_3$) δ (ppm) 145.82 (s),

137.89 (s), 130.17 (s), 125.21 (s), 117.72 (s), 114.08 (s), 34.43 (s), 31.46 (s). Anal. Calcd for $C_{20}H_{25}Br_2N$: C, 54.69; H, 5.74; N, 3.19. Found: C, 54.90; H, 5.74; N, 3.25.

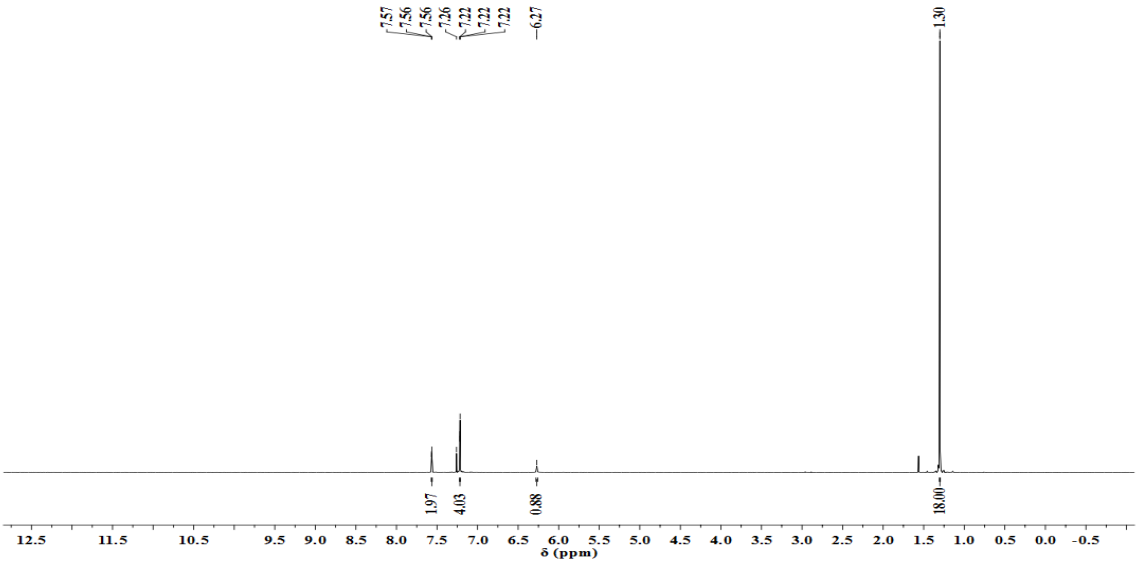

App Figure A.2. ^{1}H NMR spectrum of bis(2-bromo-4-*tert*-butylphenyl)amine in $CDCl_3$ solution.

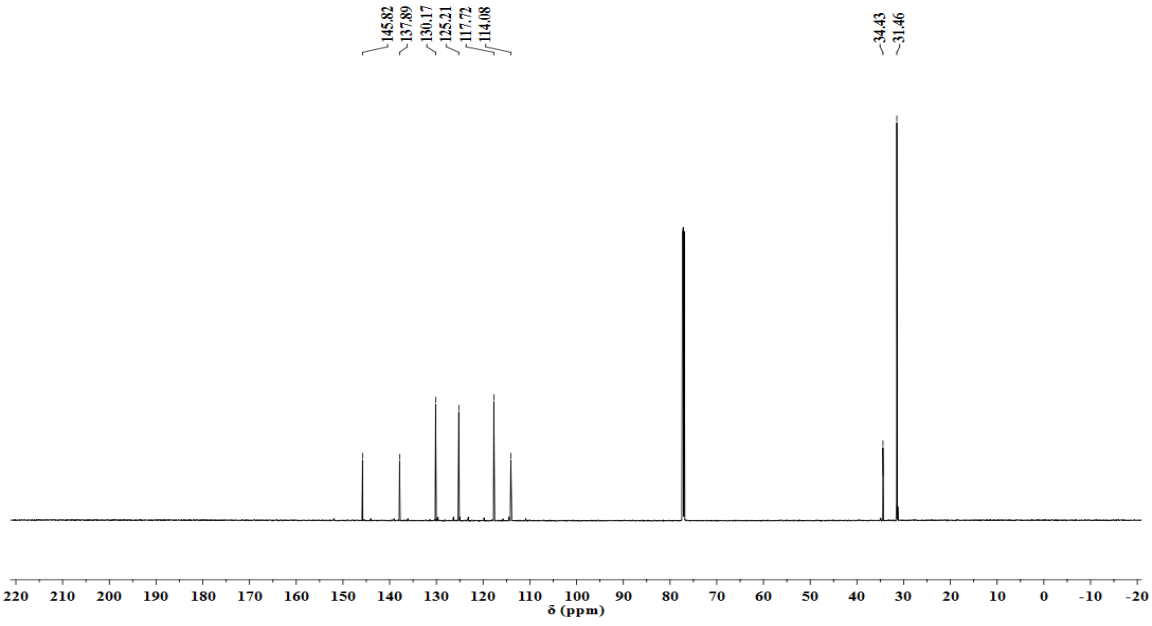

App Figure A.3. ^{13}C NMR spectrum of bis(2-bromo-4-*tert*-butylphenyl)amine in $CDCl_3$ solution.

A.4.3.2 *N*-Methyl-4,4'-di-*tert*-butyldiphenylamine

Protocol adapted from Fan et al.[27] To a 250-mL Schlenk flask under nitrogen was added (1.01 g, 3.58 mmol) of bis(4-*tert*-butylphenyl)amine and (1.48 g, 10.7 mmol) of K_2CO_3. Acetonitrile (7 mL) was added to dissolve followed by methyl iodide (0.9 mL, 14 mmol). The mixture was stirred at 86 ^oC for 24 hours. After cooling down to room temperature, 36 mL of H_2O was added to the mixture then extracted using diethyl ether (2 x 18 mL). The combined organic phases were dried using anhydrous $MgSO_4$, filtered over Celite and solvent evaporated to dryness. The crude was taken up in 5 mL of diethyl ether and let to cool to -15 ^oC for 30 min. The white solid formed was filtered and dried over vacuum to give (1.06 g, 95%) of pure product. ^1H NMR (300 MHz, $CDCl_3$) δ (ppm) 7.28 (d, *J* = 8.8 Hz, 4H), 6.95 (d, *J* = 8.8 Hz, 4H), 3.29 (s, 3H), 1.32 (s, 18H). ^{13}C NMR (176 MHz, $CDCl_3$) δ (ppm) 146.74 (s), 143.87 (s), 126.06 (s), 119.94 (s), 40.37 (s), 34.25 (s), 31.62 (s). Anal. Calcd for $C_{21}H_{29}N$: C, 85.37; H, 9.89; N, 4.74. Found: C, 85.36; H, 9.69; N, 4.72.

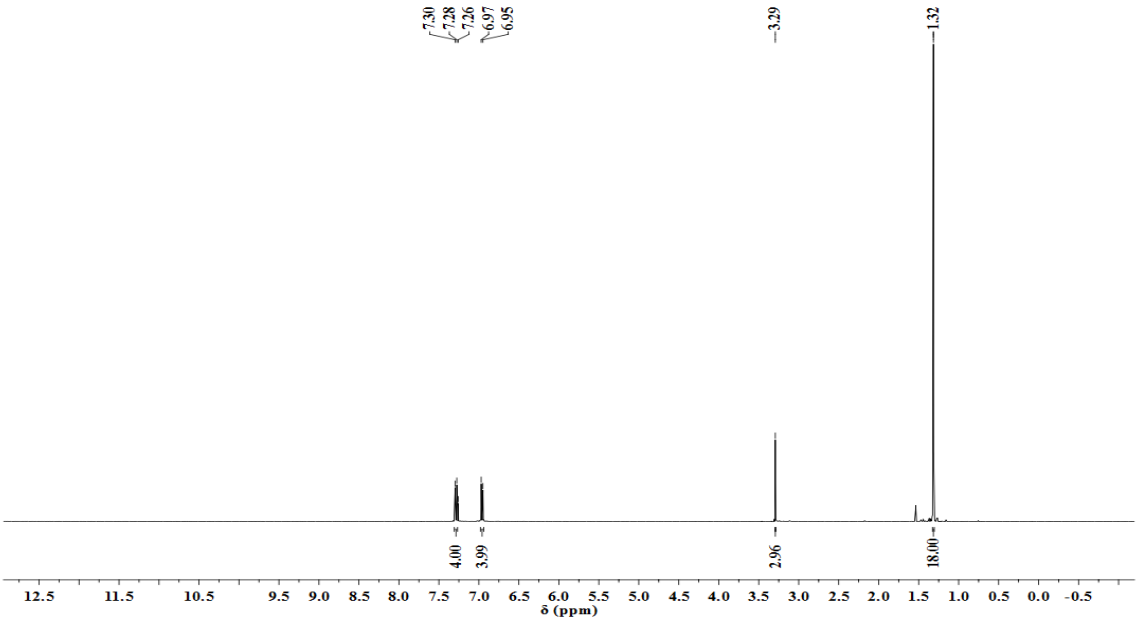

App Figure A.4. ^1H NMR spectrum of *N*-methyl-4,4'-di-*tert*-butyldiphenylamine in $CDCl_3$ solution.

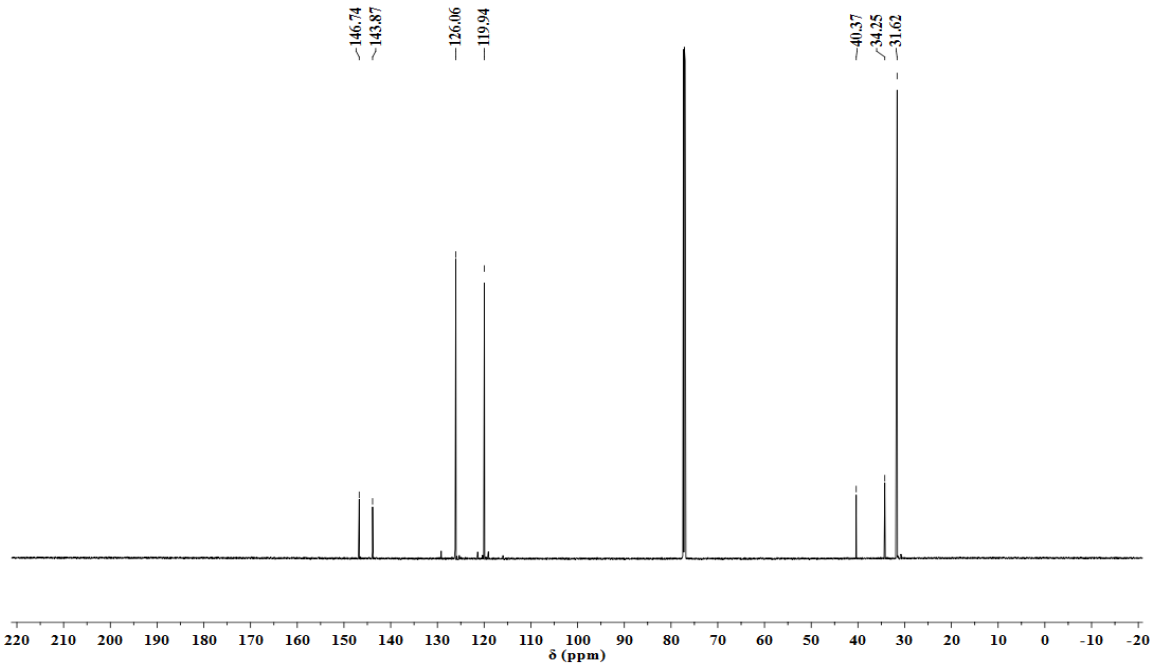

App Figure A.5. ^{13}C NMR spectrum of *N*-methyl-4,4'-di-*tert*-butyldiphenylamine in $CDCl_3$ solution.

A.4.3.3 <u>*N*-Methyl-2,2'-dibromo-4,4'-di-*tert*-butyldiphenylamine</u>

Into a round bottom flask, *N*-methyl-4,4'-di-*tert*-butyldiphenylamine (0.13 g, 0.43 mmol) was added. To this was added 2.5 mL of DMF and stirred to dissolve. It was then wrapped with aluminum foil. *N*-bromosuccinimide (0.151 g, 0.851 mmol) in 0.3 mL of DMF was added dropwise over 10 min while stirring. The mixture, green in color, was left to stir for 3 hours at room temperature in the dark. To this green mixture was added 2.5 mL of cold H_2O and then extracted using dichloromethane (3 x 2 mL). The combined organic layers were washed with H_2O (2 x 2.5 mL), then dried using anhydrous $MgSO_4$. The solvent was evaporated to dryness. The crude was taken up in 2 mL of dichloromethane and filtered through Celite/silica bed (2.5 g each). The obtained filtrate (light brown in color) was evaporated to dryness resulting into an oily reddish-brown crude product. Cold methanol (2.5 ml) was added to precipitate out the solid and placed in the freezer overnight.

It was filtered and washed with 2 mL of cold methanol resulting to a white solid (0.15 g, 77%). ^{1}H NMR (400 MHz, $CDCl_3$) δ (ppm) 7.55 (d, *J* = 2.2 Hz, 2H), 7.23 (dd, *J* = 8.4, 2.3 Hz, 2H), 6.92 (d, *J* = 8.4 Hz, 2H), 3.19 (s, 3H), 1.29 (s, 18H). ^{13}C NMR (176 MHz, $CDCl_3$) δ (ppm) 148.07 (s), 146.25 (s), 131.40 (s), 125.12 (s), 123.32 (s), 120.11 (s), 41.54 (s), 34.44 (s), 31.42 (s). Anal. Calcd for $C_{21}H_{27}Br_2N$: C, 55.65; H, 6.00; N, 3.09. Found: C, 55.57; H, 5.87; N, 3.11.

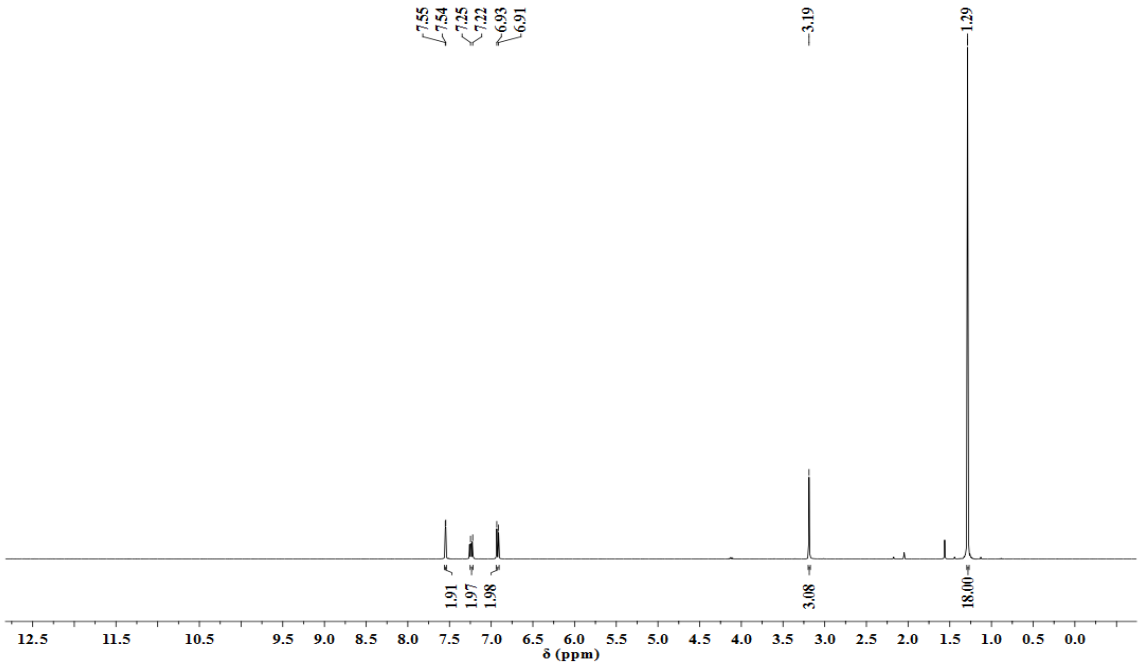

App Figure A.6. ^{1}H NMR spectrum of *N*-methyl-2,2'-dibromo-4,4'-di-*tert*-butyldiphenylamine in $CDCl_3$ solution.

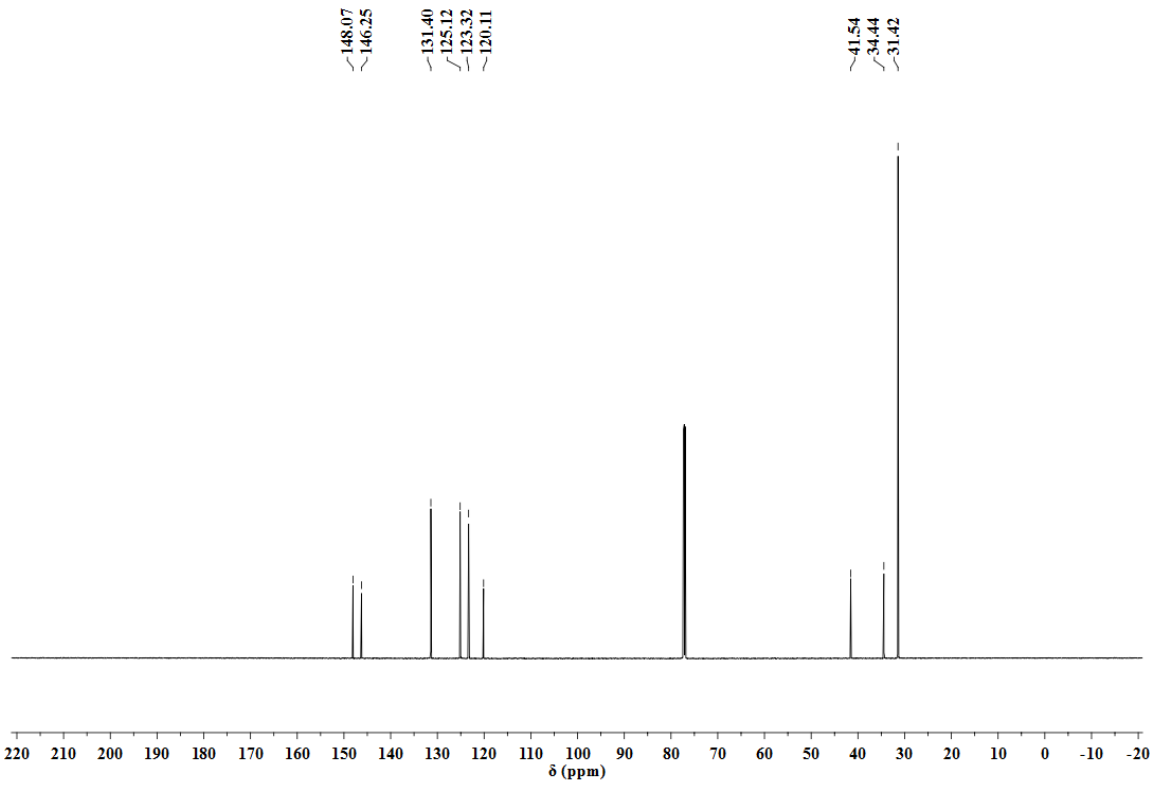

App Figure A.7. ^{13}C NMR spectrum of *N*-methyl-2,2'-dibromo-4,4'-di-*tert*-butyldiphenylamine in $CDCl_3$ solution.

A.4.3.4 <u>*N*-Methyl-bis(2-diphenylphosphino)-4,4'-di-*tert*-butylphenylamine</u>

Adapted from Fan et al.[27] To a 100-mL Schlenk flask containing (0.200 g, 0.440 mmol) of *N*-methyl-2,2'-dibromo-4,4'-di-*tert*-butyldiphenylamine under argon was added 5 mL of diethyl ether to dissolve. This solution was cooled to -35 ^{o}C after which a solution of *n*-BuLi in hexanes (2.5 M, 0.24 mL, 0.59 mmol) was added dropwise over 5 min while stirring. The cooling bath was removed and the reaction mixture stirred at room temperature overnight. The reaction mixture was cooled down to -35 ^{o}C again before addition of chlorodiphenylphosphine (0.11 mL, 0.59 mmol) dropwise while stirring. The cooling bath was removed and the reaction mixture stirred at room temperature for another 12 hours. The reaction mixture with some white suspension was pumped down to dryness after which 2.5 mL of toluene was added and the resulting precipitate filtered off over

Celite. The filtrate was pumped down to dryness resulting into an oily crude product. To this crude product was added 2 mL of cold pentane and set to stand in the freezer at -35 °C overnight yielding clear to white crystals. The crystals were filtered off and washed with 2 x 2 mL of cold pentane. They were dried under vacuum to give a white solid (0.131 g, 45%). ^{1}H NMR (400 MHz, C_6D_6) δ (ppm) 7.50-7.46 (m, 8H), 7.36 (q, *J* = 2.4 Hz, 2H), 7.07-7.01 (m, 12H), 6.97 (dd, *J* = 2.4, 8.4 Hz, 2H), 6.83 (dt, *J* = 2.4 Hz, 2H), 3.11 (s, 3H), 1.09 (s, 18H). ^{31}P{^{1}H} NMR (161 MHz, C_6D_6, 85% H_3PO_4): δ (ppm) -16.74. ^{13}C{^{1}H} NMR (176 MHz, CD_2Cl_2): δ (ppm) 154.53 (t, C_{Ar}), 145.82 (C_{Ar}), 139.60, 139.55 (dd, C_{Ar}), 135.31 (C_{Ar}), 133.91 (t, C_{Ar}), 128.89 (C_{Ar}), 128.40 (t, C_{Ar}), 128.29 (C_{Ar}), 126.90 (C_{Ar}), 122.86 (t, C_{Ar}), 45.50 (N(*C*H$_3$)), 34.45 (*C*(CH$_3$)), 31.24 (C(*C*H$_3$)). Anal. Cald for $C_{45}H_{47}NP_2$: C, 81.42; H, 7.14; N, 2.11. Found: C, 81.29; H, 7.11; N, 2.17.

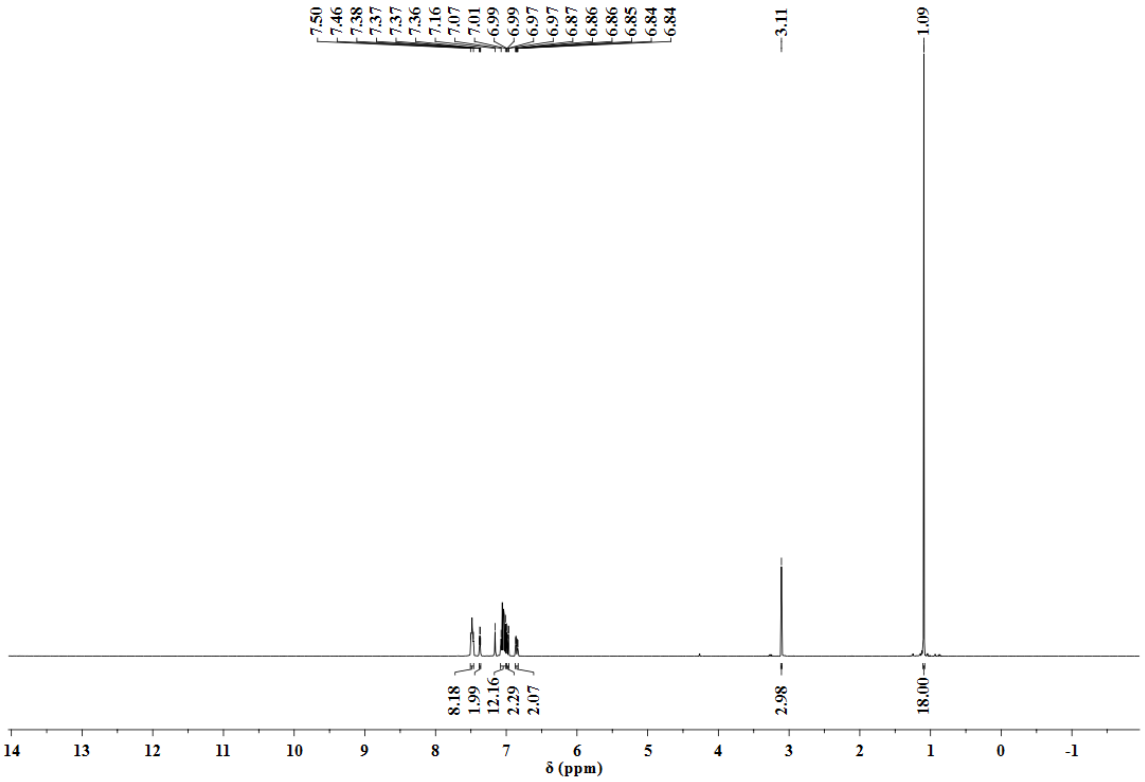

App Figure A.8. ^{1}H NMR spectrum of *N*-methyl-bis(2-diphenylphosphino)-4,4'-di-*tert*-butylphenylamine in C_6D_6 solution.

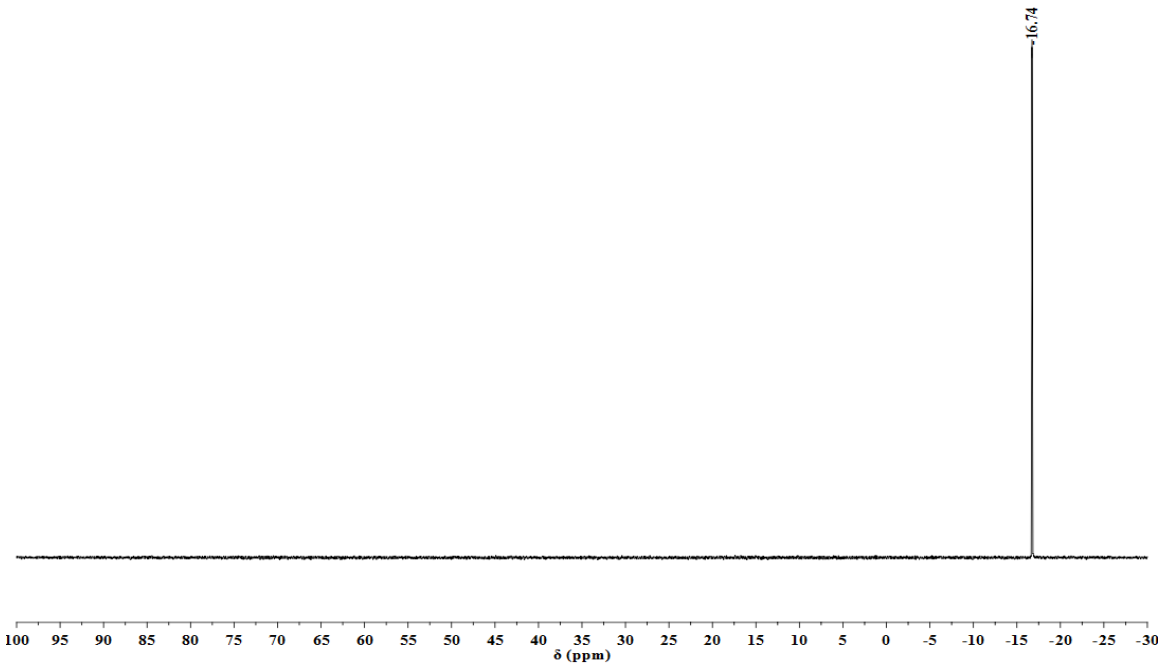

App Figure A.9. ^{31}P NMR spectrum of *N*-methyl-bis(2-diphenylphosphino)-4,4'-di-*tert*-butylphenylamine in C_6D_6 solution.

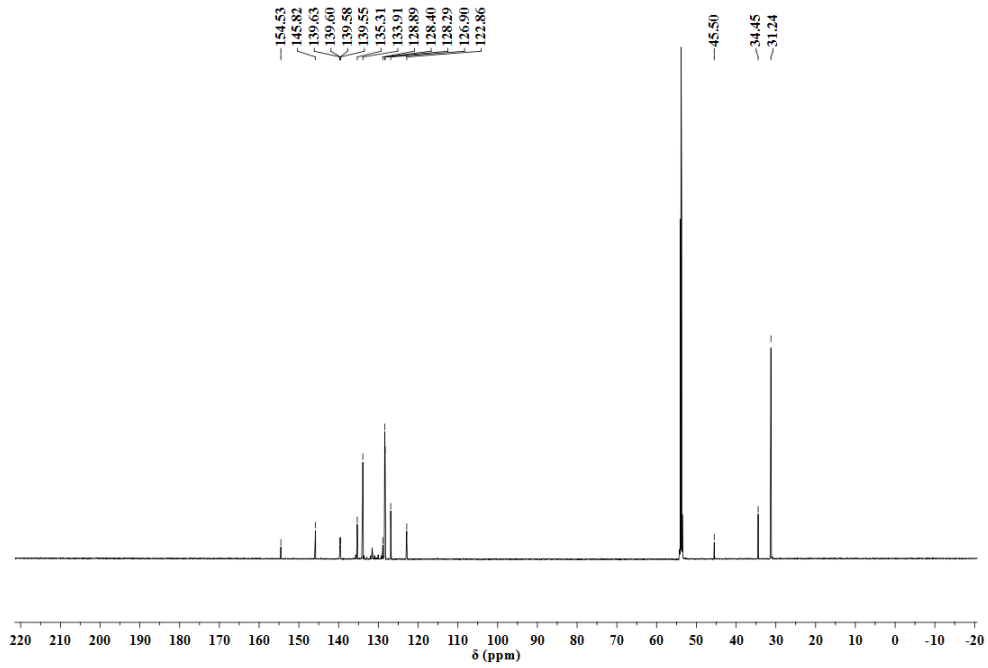

App Figure A.10. ^{13}C NMR spectrum of *N*-methyl-bis(2-diphenylphosphino)-4,4'-di-*tert*-butylphenylamine in CD_2Cl_2 solution.

A.4.3.5 Bis(4-(*tert*-butyl)-2-(diphenylphosphino)phenyl)amine

Into a 250-mL Schlenk flask fitted with a stir-bar was added (2.11 g, 0.481 mmol) of bis(2-bromo-4-*tert*-butylphenyl)amine. To this was added 80 mL of diethyl ether and cooled to -35 ^{o}C. Under argon, a solution of *n*-BuLi in hexanes (2.5 M, 5.9 mL, 1.5 mmol) was added dropwise over 15 min while stirring. The cooling bath was removed and the mixture set to stir at room temperature for 3 hours. The yellowish mixture with white suspension was cooled back to -35 ^{o}C before adding (2.6 mL, 1.5 mmol) of chlorodiphenylphosphine dropwise over 15 min while stirring. The cooling bath was removed and the reaction set to warm up to room temperature overnight while stirring. To this mixture was added 2 mL of concentrated HCl and stirred for 2 hours. The mixture was extracted three times with 10 mL of diethyl ether. The combined organic layers were washed water (3 x 10 mL), dried using anhydrous $MgSO_4$ then filtered over Celite. The solvent was removed under vacuum to give an off-white solid which was then washed with cold ethanol. The solid was recrystallized from 50% CH_2Cl_2/ethanol mixture to give a white solid (1.78 g, 57%). ^{1}H NMR (400 MHz, CD_2Cl_2) δ 7.37-7.29 (m, 12H), 7.23-7.19 (m, 10H), 7.07 (dd, *J* = 8.5, 4.9 Hz, 2H), 6.80 (dd, *J* = 5.1, 2.4 Hz, 2H), 6.54 (t, *J* = 5.4 Hz, 1H), 1.09 (s, 18H). ^{13}C{^{1}H} NMR (176 MHz, CD_2Cl_2): δ (ppm) 144.78 (C_{Ar}), 144.66 (C_{Ar}), 144.33 (C_{Ar}), 136.58 (d, C_{Ar}), 134.10 (C_{Ar}), 134.05 (d, C_{Ar}), 131.63 (C_{Ar}), 129.08 (C_{Ar}), 128.85 (t, C_{Ar}), 127.12 (C_{Ar}), 125.73 (C_{Ar}), 118.02 (C_{Ar}), 34.48 ($C(CH_3)$), 31.32 ($C(CH_3)$). ^{31}P{^{1}H} NMR (161 MHz, C_6D_6, 85% H_3PO_4): δ (ppm) -18.93. IR (cm^{-1}): 3302 (N-*H*), 3070-2861.57 (C-H sp^2). Anal. Calc for $C_{44}H_{45}NP_2$: C, 81.33; H, 6.98; N, 2.16. Found: C, 81.29; H, 6.93; N, 2.23.

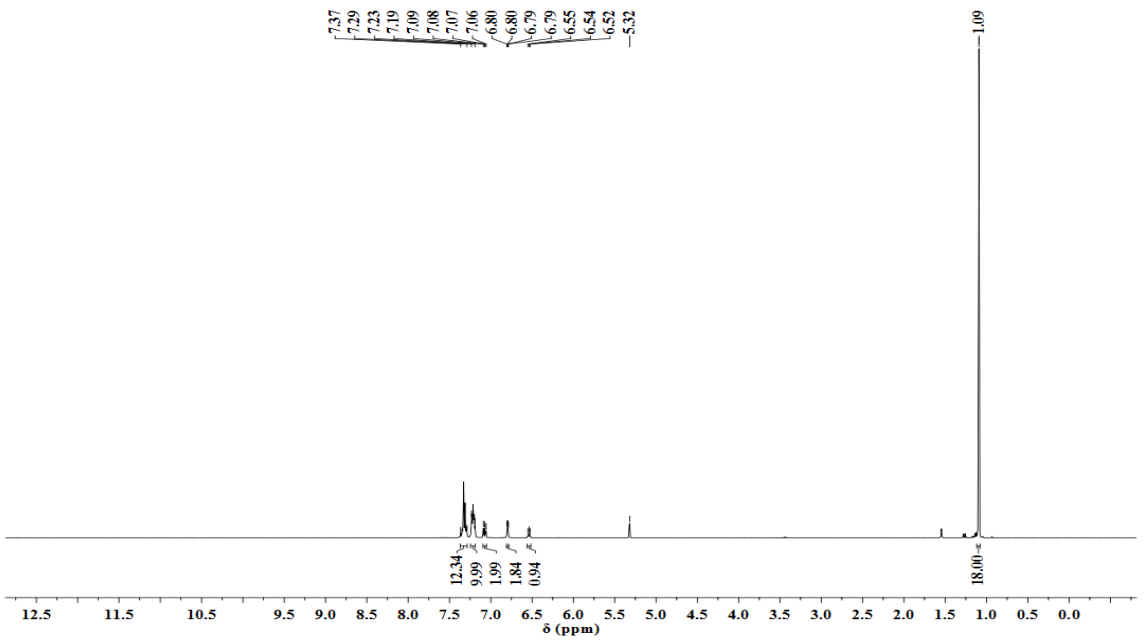

App Figure A.11. ^{1}H NMR spectrum of bis(4-(*tert*-butyl)-2-(diphenylphosphino)phenyl) amine in CD_2Cl_2 solution.

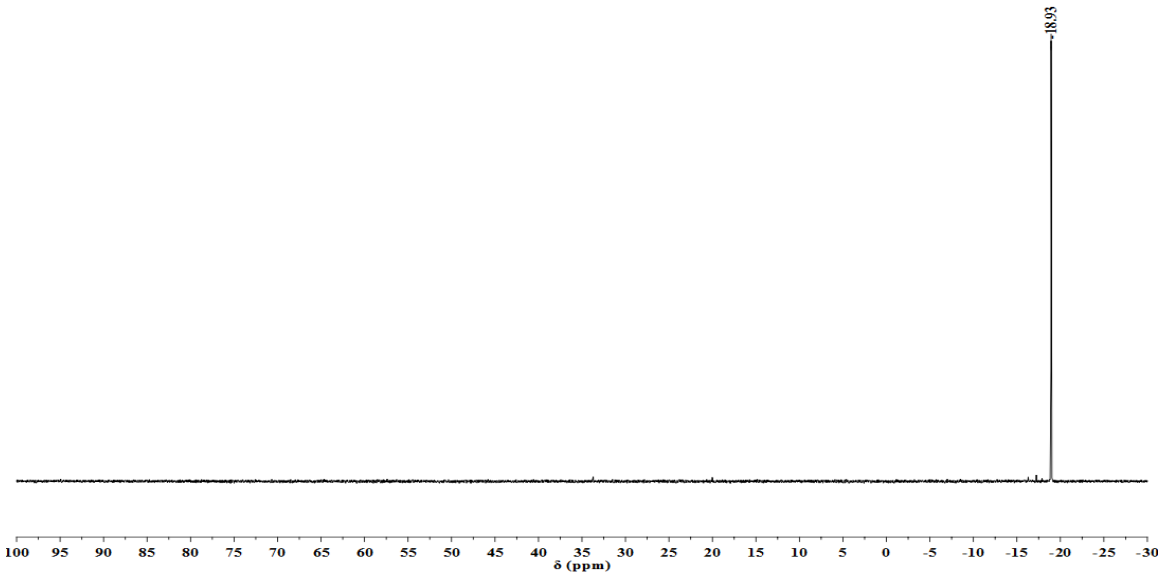

App Figure A.12. ^{31}P NMR spectrum of bis(4-(*tert*-butyl)-2-(diphenylphosphino)phenyl) amine in CD_2Cl_2 solution.

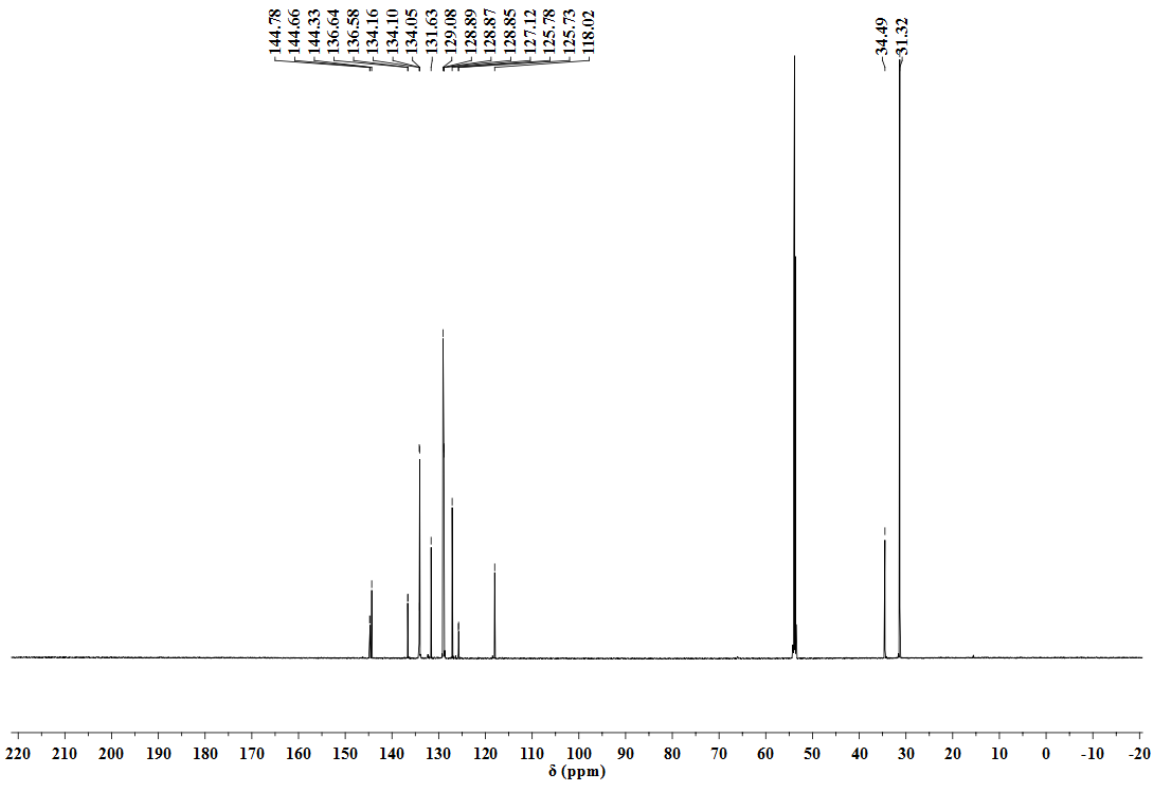

App Figure A.13. ^{13}C NMR spectrum of bis(4-(*tert*-butyl)-2-(diphenylphosphino) phenyl)amine in CD_2Cl_2 solution.

A.4.3.6 [Bis(4-(*tert*-butyl)-2-(diphenylphosphino)phenyl)amido]Pd(II) acetate

Adapted from Davidson et al.[3] Into a 20-mL scintillation vial was added bis(4-(*tert*-butyl)-2-(diphenylphosphino)phenyl)amine (0.305 g, 0.469 mmol) and palladium(II) acetate (0.112, 0.493 mmol). To this mixture was added 3 mL of toluene to dissolve. This purpleish-brown solution was set to stir at room temperature for 12 hours after which the solvent was removed under vacuum. The resulting solid was recrystallized from 50% CH_2Cl_2/diethyl ether mixture to give a purple solid (0.334 g, 87%). ^1H NMR (400 MHz, C_6D_6) δ (ppm) 8.03 (dd, *J* = 12.3, 6.0 Hz, 8H), 7.73 (dt, *J* = 8.8, 2.8 Hz, 2H), 7.29 (td, *J* = 5.6, 2.0 Hz, 2H), 7.12 (d, *J* = 7.6 Hz, 2H), 7.07-7.00 (m, 17H), 1.95 (s, 3H), 1.13 (s, 18H). $^{31}P\{^1H\}$ NMR (161 MHz, C_6D_6, 85% H_3PO_4): δ (ppm) 29.4.

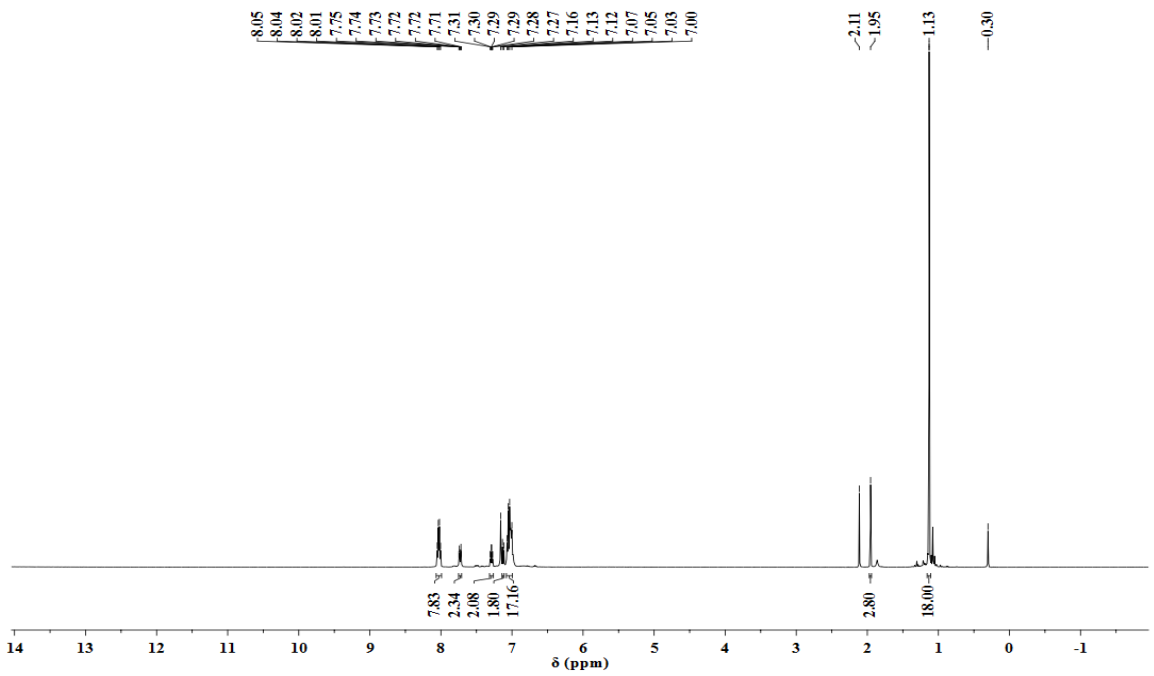

App Figure A.14. ^{1}H NMR spectrum of [bis(4-(*tert*-butyl)-2-(diphenylphosphino)phenyl)amido]Pd(II) acetate in C_6D_6 solution.

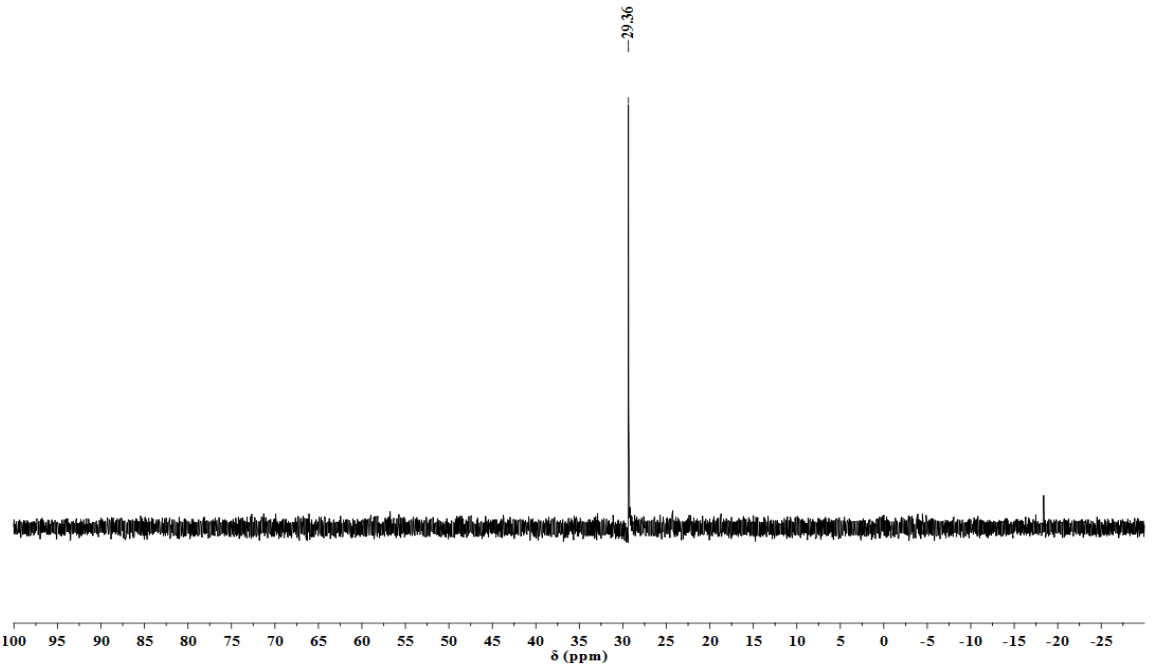

App Figure A.15. ^{31}P NMR spectrum of [bis(4-(*tert*-butyl)-2-(diphenylphosphino)phenyl)amido]Pd(II) acetate in C_6D_6 solution.

Acetate exchange for chloride was achieved by dissolving the resulting [bis(4-(*tert*-butyl)-2-(diphenylphosphino)phenyl)amido]Pd(II) acetate in 2.5 mL of dichloromethane. To this solution was added 2.5 mL of brine and stirred at room temperature for 1 hour. The mixture was extracted twice using 2.5 mL of CH_2Cl_2. The combined organic layers were dried using anhydrous $MgSO_4$ then filtered over Celite. The resulting purple solid was dried overnight under vacuum to give (0.311 g, 96%). ^{1}H NMR (400 MHz, C_6D_6) δ (ppm) 7.97-7.92 (m, 8H), 7.84 (dt, *J* = 8.9, 2.8 Hz, 2H), 7.29 (td, *J* = 5.8, 2.3 Hz, 2H), 7.07 (dd, *J* = 8.9, 2.4 Hz, 2H), 6.98-6.96 (m, 12H), 1.14 (s, 18H). ^{31}P{^{1}H} NMR (161 MHz, C_6D_6, 85% H_3PO_4): δ (ppm) 30.01.

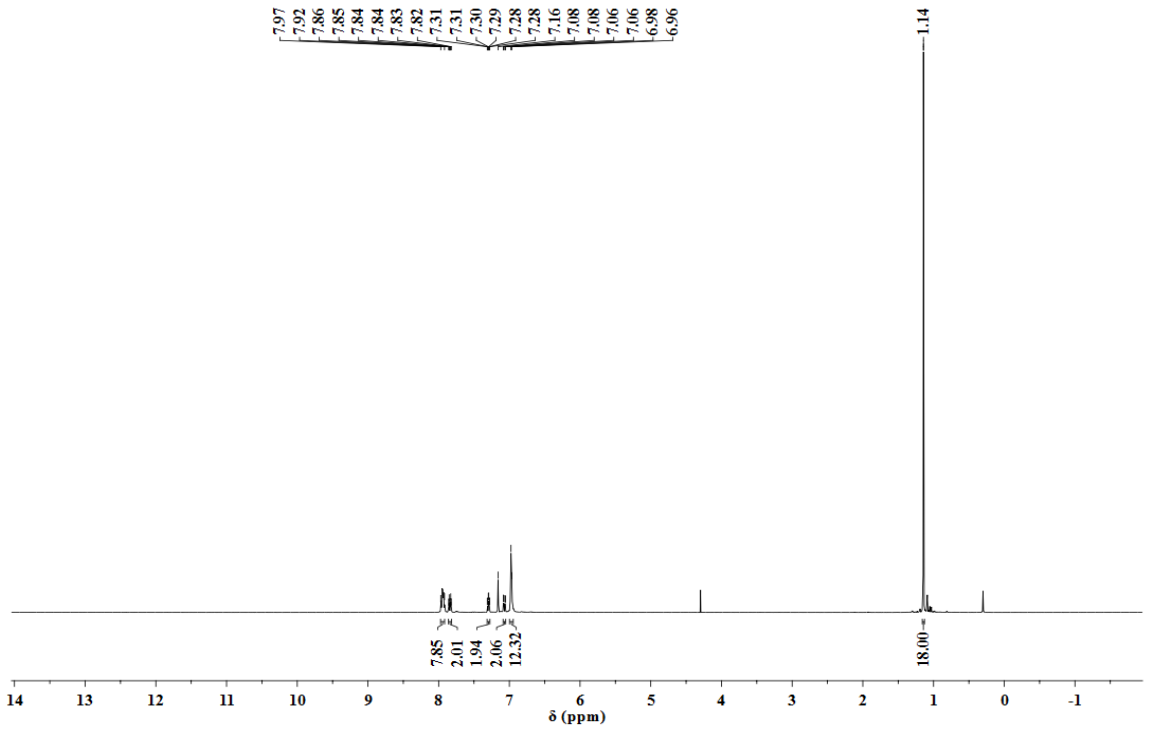

App Figure A.16. ^{1}H NMR spectrum of [bis(4-(*tert*-butyl)-2-(diphenylphosphino)phenyl)amido]Pd(II) chloride in C_6D_6 solution.

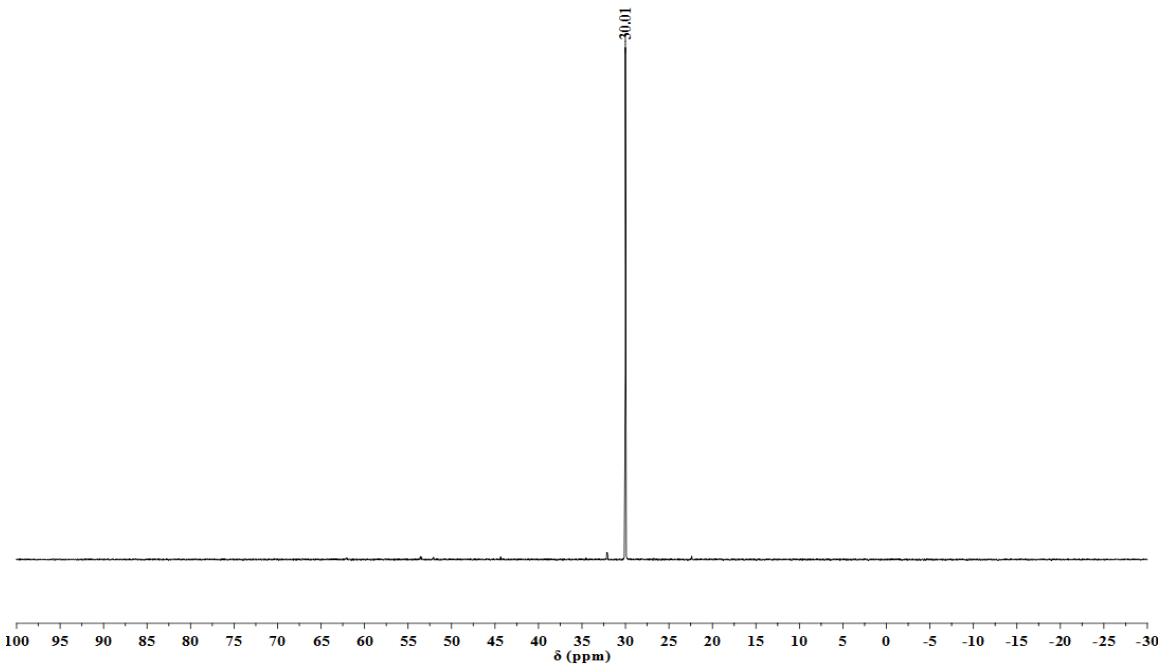

App Figure A.17. ^{31}P NMR spectrum of [bis(4-(*tert*-butyl)-2-(diphenylphosphino)phenyl)amido]Pd(II) chloride in C_6D_6 solution.

A.4.3.7 [Bis(4-(tert-butyl)-2-(diphenylphosphino)phenyl)amido]cobalt chloride

Method A. Adapted from Lagaditis et al.[40] Into a 20-mL scintillation vial, (0.118 g, 0.182 mmol) of bis(4-(*tert*-butyl)-2-(diphenylphosphino)phenyl)amine was added followed by cobalt(II) chloride. To this mixture was added 3 mL of THF and the reaction set to stir at room temperature for 48 hours. A solution of KO^{t}Bu (0.025 g, 0.220 mmol) in 2.2mL of THF was added to the reaction mixture and stirred for 1 hour. This was then filtered and the solvent removed under vacuum. The resulting solid was dissolved in 2 mL of toluene, layered with 1 mL of pentane and put in the freezer to recrystallize. Green crystals obtained were filtered off and dried under vacuum to give the product (0.102 g, 75% yield).

Method B. Adapted from Liang et al.[41] To a 100-mL Schlenk flask was added bis(4-(*tert*-butyl)-2-(diphenylphosphino)phenyl)amine (0.208 g, 0.320 mmol) followed by 8 mL of THF to dissolve. This solution was cooled down to -35 ^{o}C after which a solution of *n*-BuLi in hexanes (0.21 mL, 0.51 mmol) was added dropwise over 5 min while stirring. The mixture was warmed to room temperature and stirred for 2 hours. Into another flask, cobalt(II) chloride (0.042 g, 0.320 mmol) was dissolved in 5 mL of THF. The lithium amide salt at -35 ^{o}C was added dropwise to the cobalt chloride solution at -35 ^{o}C while stirring. The reaction was left to warm up to room temperature while stirring for 22 hours. Solvent was removed under vacuum and the crude taken in toluene, then filtered off over Celite. The filtrate was pumped down to dryness to give green solid which was washed with pentane then filtered off and dried to give the product as a green solid (0.147 g, 62% yield). Comparison of the IR spectra of the product and that of the starting ligand shows disappearance of the N-H peak (3303 cm^{-1}).

A.4.3.8 [Bis(4-(*tert*-butyl)-2-(diphenylphosphino)phenyl)amido]copper(I)

Mesitylcopper (0.017 g, 0.093 mmol) and (0.055 g, 0.085 mmol) of bis(4-(*tert*-butyl)-2-(diphenylphosphino)phenyl)amine were placed into a 20-mL scintillation vial. To this was added 2 mL of benzene to dissolve and stirred at room temperature overnight. The solvent was evaporated under vacuum to dryness to give a yellow solid. This was then washed with cold 2 mL of cold pentane to give bright yellow powder (0.058 g, 95%). ^{1}H NMR (400 MHz, C_6D_6) δ (ppm) 7.62 (s, 2H), 7.34 (s, 2H), 7.16 (s, 4H), 6.92 (s, 18H), 1.18 (s, 18H). $^{31}P\{^{1}H\}$ NMR (161 MHz, C_6D_6, 85% H_3PO_4): δ (ppm) -12.5.

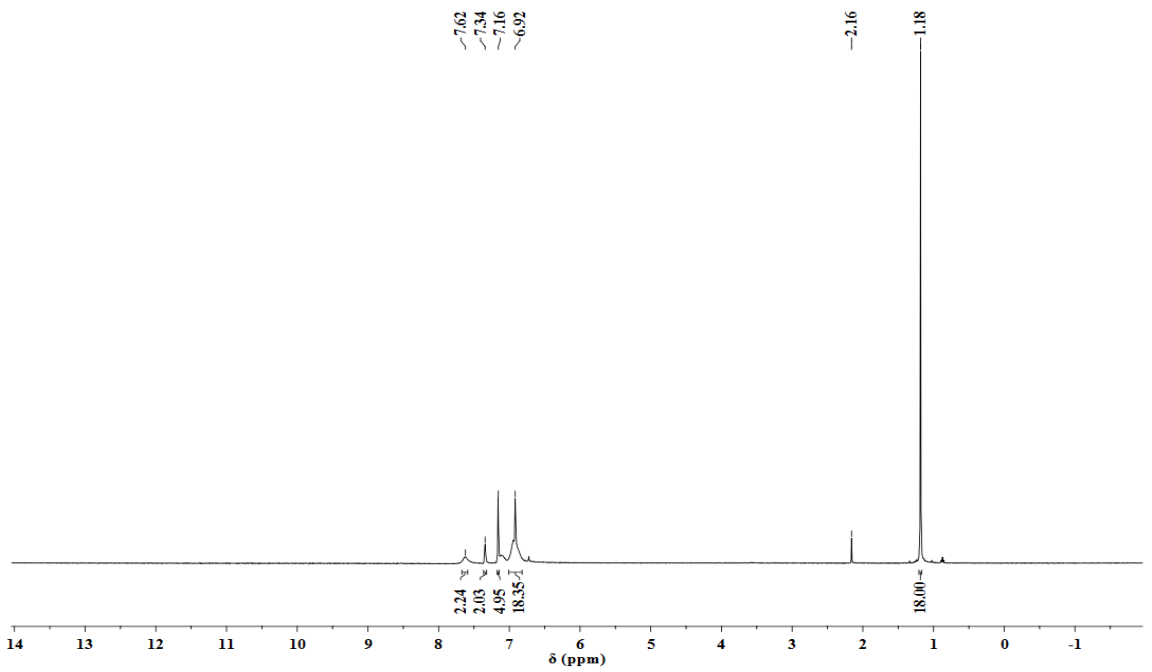

App Figure A.18. ^{1}H NMR spectrum of [bis(4-(*tert*-butyl)-2-(diphenylphosphino) phenyl)amine]copper(I) in C_6D_6 solution.

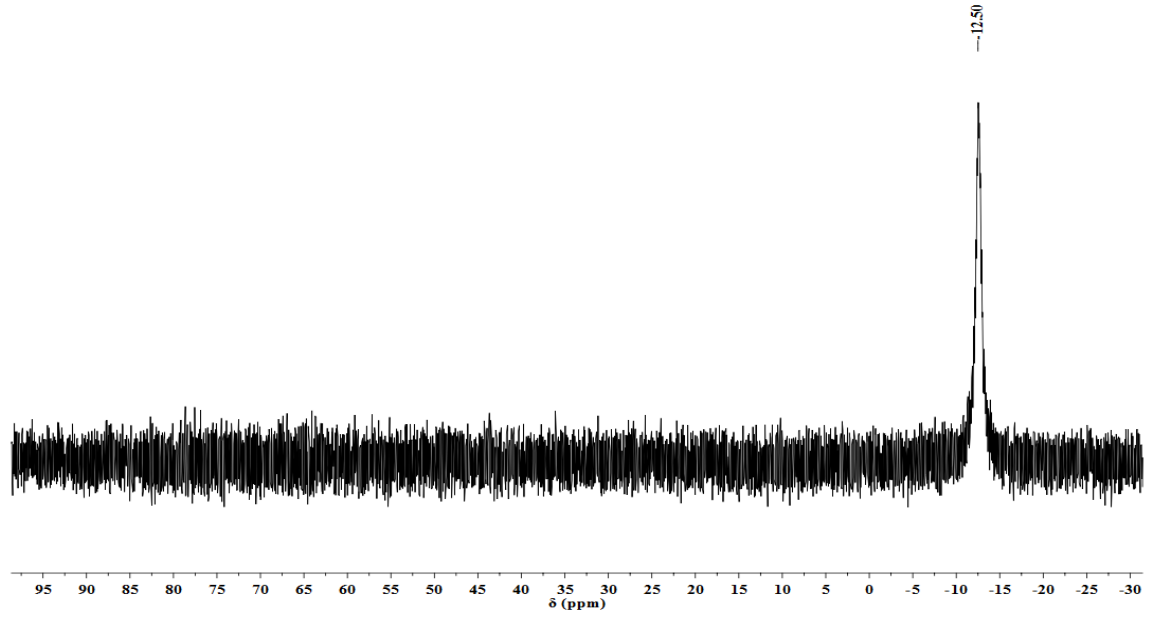

App Figure A.19. ^{31}P NMR spectrum of [bis(4-(*tert*-butyl)-2-(diphenylphosphino) phenyl)amine]copper(I) in C_6D_6 solution.

A.4.3.9 [Bis(4-(*tert*-butyl)-2-(diphenylphosphino)phenyl)amido]nickel hydride

Into a 20-mL scintillation vial containing a solution of $Ni(COD)_2$ (0.013 g, 0.047 mmol) in 1 mL of THF was added a solution of bis(4-(*tert*-butyl)-2-(diphenylphosphino)phenyl)amine (0.03 g, 0.05 mmol) in 1 mL of THF dropwise while stirring at room temperature. The solution turned brown immediately. It was stirred for 10 min and then solvent removed under vacuum, and the product taken up in C_6D_6 for NMR. ^{1}H NMR (400 MHz, C_6D_6) δ (ppm) 7.88 (d, *J* = 9.9 Hz, 2H), 7.77 (d, *J* = 5.6 Hz, 6H), 7.39 (m, 2H), 7.23 (s, 2H), 7.19-7.14 (m, 5H), 6.99-6.91 (m, 14H), 5.58 (s, 5H), 2.21 (s, 16H), 1.21 (s, 18H), 1.09 (s, 6H), -18.50 (t, 1H). ^{31}P{^{1}H} NMR (161 MHz, C_6D_6, 85% H_3PO_4): δ (ppm) 32.76, 27.43.

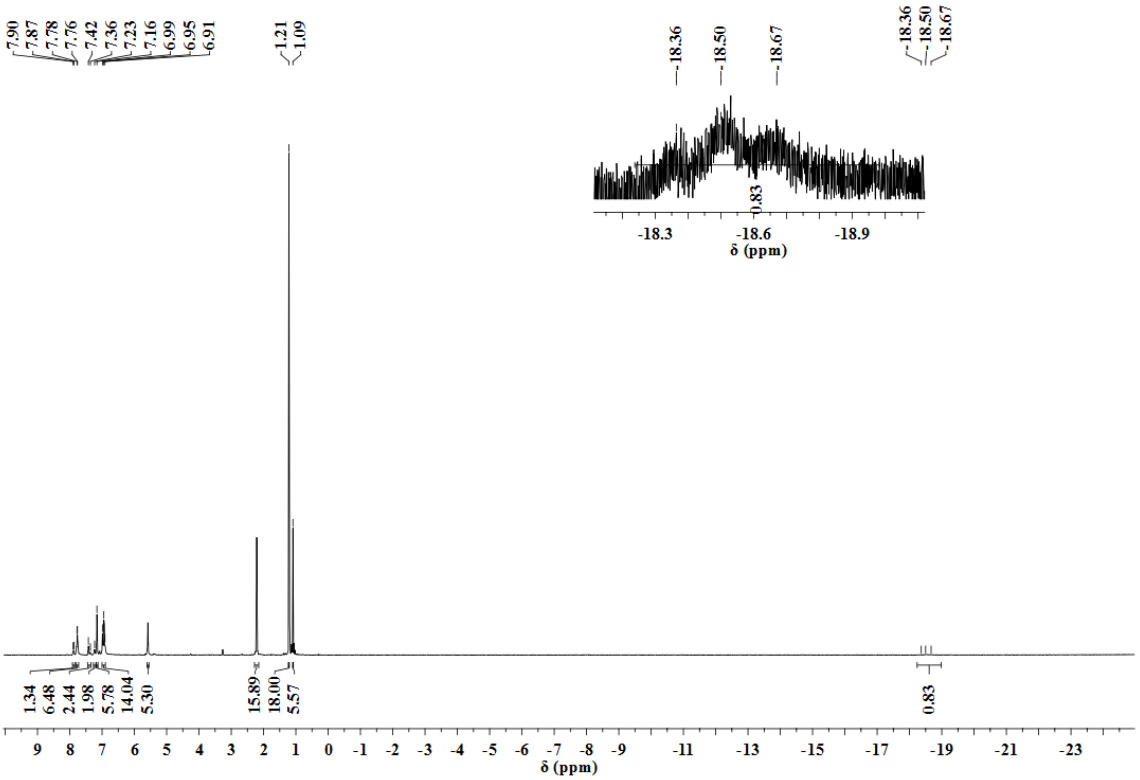

App Figure A.20. ^{1}H NMR spectrum of [bis(4-(*tert*-butyl)-2-(diphenylphosphino)phenyl)amido]NiH in C_6D_6 solution.

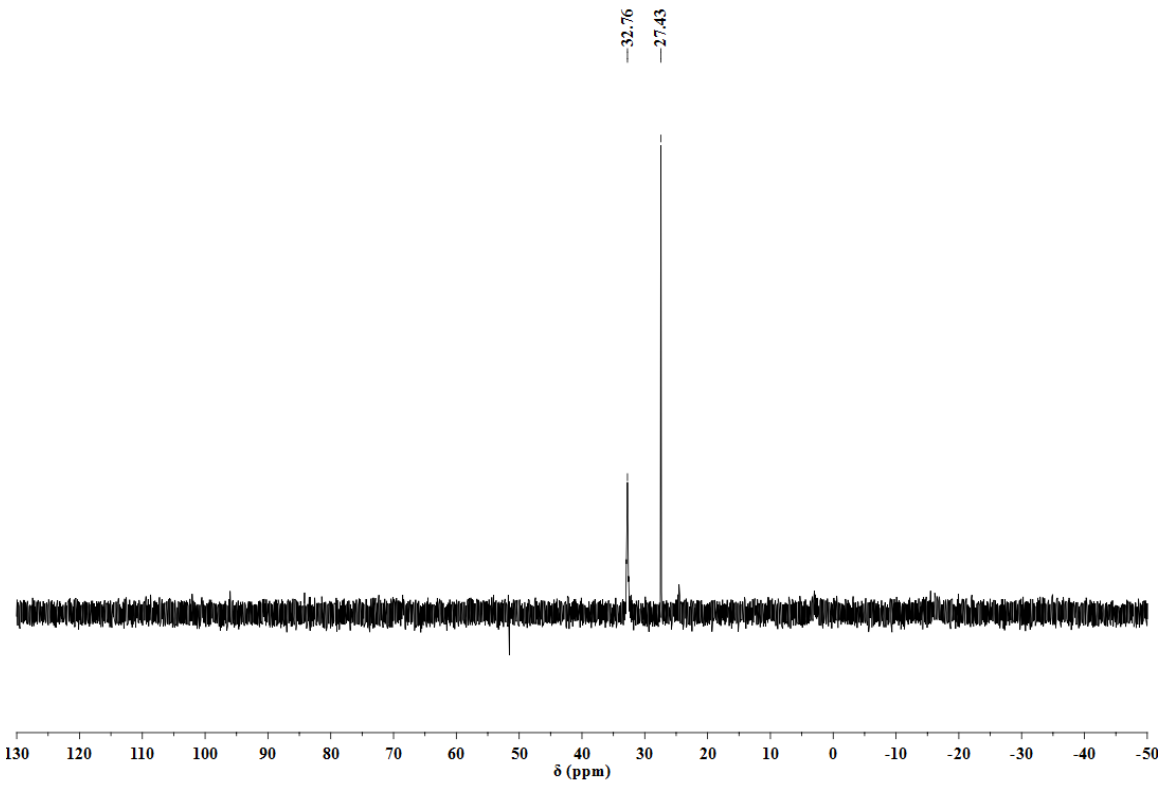

App Figure A.21. ^{31}P NMR spectrum of [bis(4-(*tert*-butyl)-2-(diphenylphosphino)phenyl)amido]NiH in C_6D_6 solution.

A.4.3.10 [PNP]Ni(*n*-hexyl).

To a 20-mL scintillation vial containing bis(4-(*tert*-butyl)-2-(diphenylphosphino)phenyl)amine (0.01 g, 0.02 mmol), $Ni(COD)_2$ (0.004 g, 0.015 mmol) and 1-hexene (30 µL, 0.233 mmol) were added 1 mL of benzene. The resulting light brown reaction mixture was stirred at room temperature for 24 hours while being monitored by ^1H NMR and $^{31}P\{^1H\}$ NMR spectroscopy. ^1H NMR (400 MHz, C_6D_6) δ (ppm) 7.88-7.79 (m, 10H), 7.38 (td, *J* = 2.4 Hz, 2H), 7.11 (dd, *J* = 2.4 Hz, 2H), 7.06 – 7.04 (m, 13H), 1.19 (s, 18H), 1.13 (t, 3H), 0.76 (t, 3H).

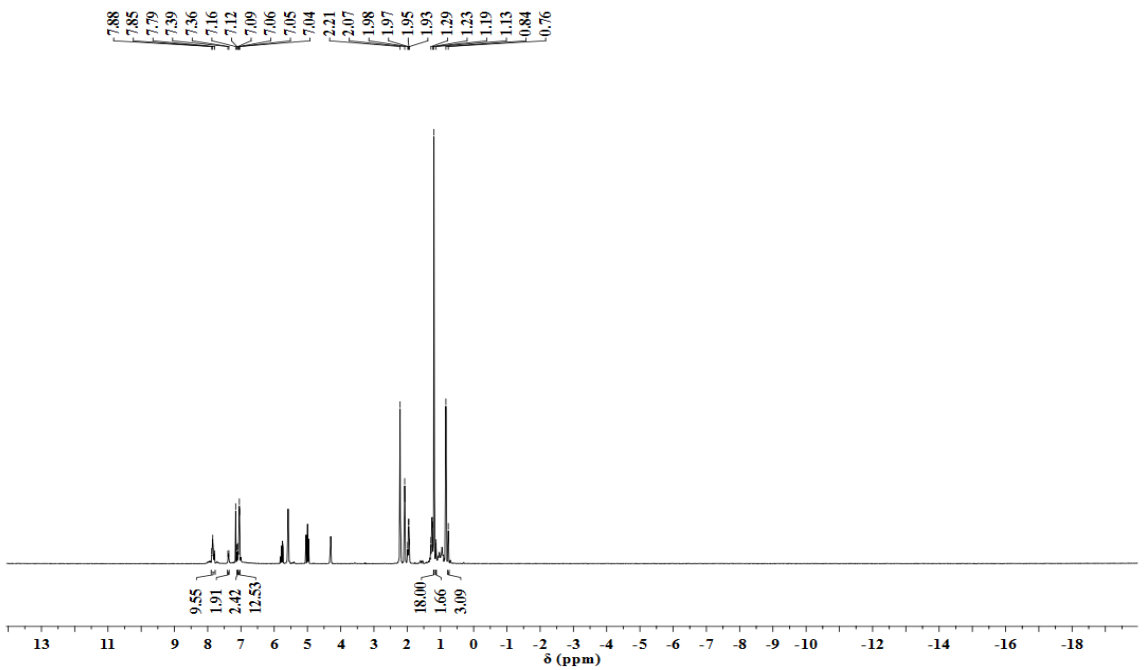

App Figure A.22. ^{1}H NMR spectrum of [bis(4-(*tert*-butyl)-2-(diphenylphosphino)phenyl)amido]Ni(*n*-hexyl) in C_6D_6 solution.

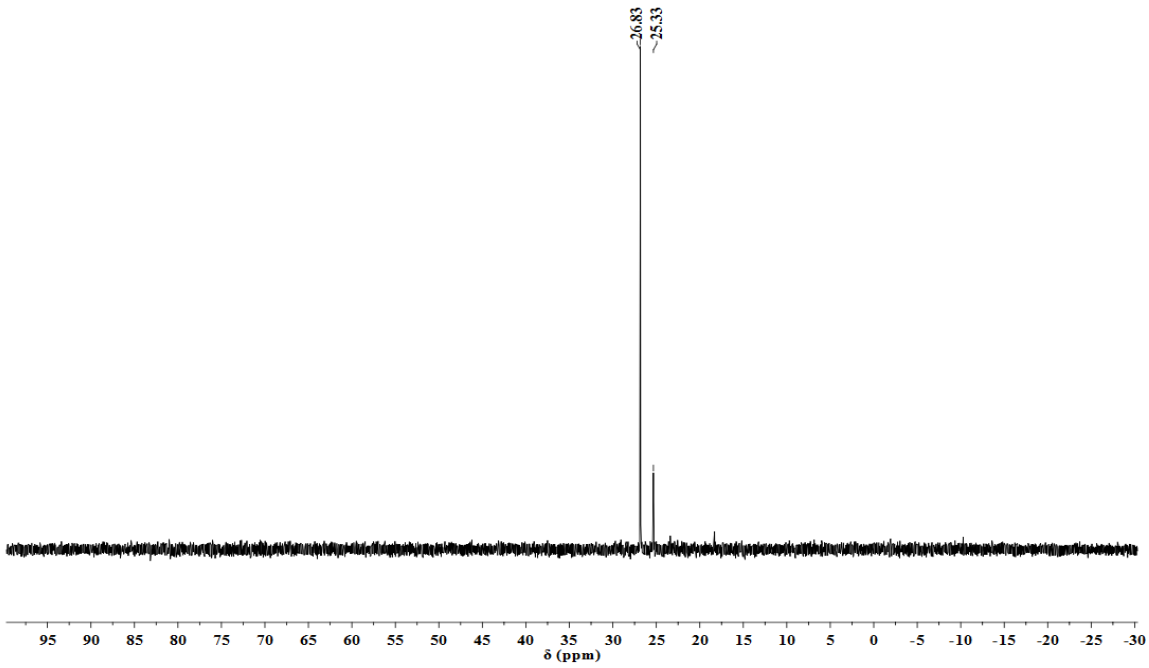

App Figure A.23. ^{31}P NMR spectrum of [bis(4-(*tert*-butyl)-2-(diphenylphosphino)phenyl)amido]Ni(*n*-hexyl) in C_6D_6 solution.

A.5 REFERENCES

1. Fryzuk, M. D.; MacNeil, P. A.; Rettig, S. J.; Secco, A. S.; Trotter, J., Tridentate amidophosphine derivatives of the nickel triad: synthesis, characterization, and reactivity of nickel(II), palladium(II), and platinum(II) amide complexes. *Organometallics* **1982,** *1,* 918-930.

2. Fryzuk, M. D.; Montgomery, C. D., Amides of the platinum group metals. *Coord. Chem. Rev.* **1989,** *95,* 1-40.

3. Ozerov, O. V.; Guo, C.; Fan, L.; Foxman, B. M., Oxidative addition of N−C and N−H bonds to zerovalent nickel, palladium, and platinum. *Organometallics* **2004,** *23,* 5573-5580.

4. Venkanna, G. T.; Tammineni, S.; Arman, H. D.; Tonzetich, Z. J., Synthesis, characterization, and catalytic activity of nickel(II) alkyl complexes supported by pyrrole–diphosphine ligands. *Organometallics* **2013,** *32,* 4656-4663.

5. Yandulov, D. V.; Schrock, R. R., Catalytic reduction of dinitrogen to ammonia at a single molybdenum center. *Science* **2003,** *301,* 76-78.

6. Ritleng, V.; Yandulov, D. V.; Weare, W. W.; Schrock, R. R.; Hock, A. S.; Davis, W. M., Molybdenum triamidoamine complexes that contain hexa-*tert*-butylterphenyl, hexamethylterphenyl, or *p*-bromohexaisopropylterphenyl substituents. An examination of some catalyst variations for the catalytic reduction of dinitrogen. *J. Am. Chem. Soc.* **2004,** *126,* 6150-6163.

7. Schrock, R. R., Catalytic reduction of dinitrogen to ammonia at a single molybdenum center. *Acc. Chem. Res.* **2005,** *38,* 955-962.

8. Schrock, R. R., Catalytic reduction of dinitrogen to ammonia by molybdenum: theory versus experiment. *Angew. Chem. Int. Ed.* **2008,** *47,* 5512-5522.

9. Tanaka, H.; Arashiba, K.; Kuriyama, S.; Sasada, A.; Nakajima, K.; Yoshizawa, K.; Nishibayashi, Y., Unique behaviour of dinitrogen-bridged dimolybdenum complexes bearing pincer ligand towards catalytic formation of ammonia. *Nature commun.* **2014,** *5,* 3737.

10. Kuriyama, S.; Arashiba, K.; Nakajima, K.; Tanaka, H.; Kamaru, N.; Yoshizawa, K.; Nishibayashi, Y., Catalytic formation of ammonia from molecular dinitrogen by use of dinitrogen-bridged dimolybdenum–dinitrogen complexes bearing PNP-pincer ligands: remarkable effect of substituent at PNP-pincer ligand. *J. Am. Chem. Soc.* **2014,** *136,* 9719-9731.

11. Arashiba, K.; Miyake, Y.; Nishibayashi, Y., A molybdenum complex bearing PNP-type pincer ligands leads to the catalytic reduction of dinitrogen into ammonia. *Nature chem.* **2011,** *3,* 120.

12. Ung, G.; Peters, J. C., Low-Temperature N_2 Binding to Two-Coordinate L_2Fe^0 Enables Reductive Trapping of $L_2FeN_2^-$ and NH_3 Generation. *Angew. Chem. Int. Ed.* **2015,** *54*, 532-535.

13. Anderson, J. S.; Rittle, J.; Peters, J. C., Catalytic conversion of nitrogen to ammonia by an iron model complex. *Nature* **2013,** *501*, 84.

14. Creutz, S. E.; Peters, J. C., Catalytic reduction of N_2 to NH_3 by an Fe–N_2 complex featuring a C-atom anchor. *J. Am. Chem. Soc.* **2014,** *136*, 1105-1115.

15. MacLeod, K. C.; Holland, P. L., Recent developments in the homogeneous reduction of dinitrogen by molybdenum and iron. *Nature Chem.* **2013,** *5*, 559.

16. Yamamoto, A.; Kitazume, S.; Pu, L.; Ikeda, S., Study of the fixation of nitrogen. Isolation of tris(triphenylphosphine)cobalt complex co-ordinated with molecular nitrogen. *Chem. Commun. (London)* **1967,** 79-80.

17. Sacco, A.; Rossi, M., Hydride and nitrogen complexes of cobalt. *Chem. Commun. (London)* **1967,** 316-316.

18. Misono, A.; Uchida, Y.; Saito, T., Preparation of a Cobalt Complex Coordinated by Molecular Nitrogen and Triphenylphosphine. *Bull. Chem. Soc. Jap.* **1967,** *40*, 700-700.

19. Davis, B. R.; Payne, N. C.; Ibers, J. C., Geometry of coordinated molecular nitrogen. Structure of $Co(H)(N_2)(PPh_3)_3$. *J. Am. Chem. Soc.* **1969,** *91*, 1240-1241.

20. Yamamoto, A.; Miura, Y.; Ito, T.; Chen, H. L.; Iri, K.; Ozawa, F.; Miki, K.; Sei, T.; Tanaka, N.; Kasai, N., Preparation, X-ray molecular structure determination, and chemical properties of dinitrogen-coordinated cobalt complexes containing triphenylphosphine ligands and alkali metal or magnesium. Protonation of the coordinated dinitrogen to ammonia and hydrazine. *Organometallics* **1983,** *2*, 1429-1436.

21. Bullock, R. M., *Catalysis without precious metals*. John Wiley & Sons: 2011.

22. Pellissier, H.; Clavier, H., Enantioselective cobalt-catalyzed transformations. *Chem. Rev.* **2014,** *114*, 2775-2823.

23. Cahiez, G. r.; Moyeux, A., Cobalt-catalyzed cross-coupling reactions. *Chem. Rev.* **2010,** *110*, 1435-1462.

24. Friedfeld, M. R.; Shevlin, M.; Hoyt, J. M.; Krska, S. W.; Tudge, M. T.; Chirik, P. J., Cobalt precursors for high-throughput discovery of base metal asymmetric alkene hydrogenation catalysts. *Science* **2013,** *342*, 1076-1080.

25. Betley, T. A.; Peters, J. C., Dinitrogen chemistry from trigonally coordinated iron and cobalt platforms. *J. Am. Chem. Soc.* **2003,** *125*, 10782-10783.

26. Imayoshi, R.; Tanaka, H.; Matsuo, Y.; Yuki, M.; Nakajima, K.; Yoshizawa, K.; Nishibayashi, Y., Cobalt-Catalyzed Transformation of Molecular Dinitrogen into Silylamine under Ambient Reaction Conditions. *Chem. Eur. J.* **2015,** *21*, 8905-8909.

27. Fan, L.; Yang, L.; Guo, C.; Foxman, B. M.; Ozerov, O. V., N−C Cleavage in Pincer PNP Complexes of Palladium. *Organometallics* **2004,** *23*, 4778-4787.

28. Dodds, D. L.; Boele, M. D.; van Strijdonck, G. P.; de Vries, J. G.; van Leeuwen, P. W.; Kamer, P. C., Design, testing and kinetic analysis of bulky monodentate phosphorus ligands in the Mizoroki–Heck reaction. *Eur. J. Inorg. Chem.* **2012,** *2012*, 1660-1671.

29. Liang, L.-C.; Chien, P.-S.; Lee, P.-Y., Phosphorus and olefin substituent effects on the insertion chemistry of nickel(II) hydride complexes containing amido diphosphine ligands. *Organometallics* **2008,** *27*, 3082-3093.

30. Liang, L.-C.; Chien, P.-S.; Lin, J.-M.; Huang, M.-H.; Huang, Y.-L.; Liao, J.-H., Amido pincer complexes of nickel(II): Synthesis, structure, and reactivity. *Organometallics* **2006,** *25*, 1399-1411.

31. Azuma, M.; Hashimoto, K.; Hiramoto, M.; Watanabe, M.; Sakata, T., Carbon dioxide reduction at low temperature on various metal electrodes. *J. Electroanalyt. Chem. Interfac. Electrochem.* **1989,** *260*, 441-445.

32. Li, C. W.; Kanan, M. W., CO_2 reduction at low overpotential on Cu electrodes resulting from the reduction of thick Cu_2O films. *J. Am. Chem. Soc.* **2012,** *134*, 7231-7234.

33. Chen, Y.; Kanan, M. W., Tin oxide dependence of the CO_2 reduction efficiency on tin electrodes and enhanced activity for tin/tin oxide thin-film catalysts. *J. Am. Chem. Soc.* **2012,** *134*, 1986-1989.

34. Feng, X.; Jiang, K.; Fan, S.; Kanan, M. W., Grain-boundary-dependent CO_2 electroreduction activity. *J. Am. Chem. Soc.* **2015,** *137*, 4606-4609.

35. Lu, Q.; Rosen, J.; Zhou, Y.; Hutchings, G. S.; Kimmel, Y. C.; Chen, J. G.; Jiao, F., A selective and efficient electrocatalyst for carbon dioxide reduction. *Nature commun.* **2014,** *5*, 3242.

36. Lee, C. H.; Kanan, M. W., Controlling H^+ vs CO_2 reduction selectivity on Pb electrodes. *ACS Catal.* **2014,** *5*, 465-469.

37. Harkins, S. B.; Mankad, N. P.; Miller, A. J.; Szilagyi, R. K.; Peters, J. C., Probing the Electronic Structures of $[Cu_2(\mu\text{-}XR_2)]^{n+}$ Diamond Cores as a Function of the Bridging X Atom (X= N or P) and Charge (n = 0, 1, 2). *J. Am. Chem. Soc.* **2008,** *130*, 3478-3485.

38. Kuriyama, S.; Arashiba, K.; Tanaka, H.; Matsuo, Y.; Nakajima, K.; Yoshizawa, K.; Nishibayashi, Y., Direct transformation of molecular dinitrogen into ammonia catalyzed by cobalt dinitrogen complexes bearing anionic PNP pincer ligands. *Angew. Chem. Int. Ed.* **2016,** *55*, 14291-14295.

39. Fulmer, G. R.; Miller, A. J.; Sherden, N. H.; Gottlieb, H. E.; Nudelman, A.; Stoltz, B. M.; Bercaw, J. E.; Goldberg, K. I., NMR chemical shifts of trace impurities: common laboratory solvents, organics, and gases in deuterated solvents relevant to the organometallic chemist. *Organometallics* **2010,** *29*, 2176-2179.

40. Lagaditis, P. O.; Schluschaß, B.; Demeshko, S.; Würtele, C.; Schneider, S., Square-Planar Cobalt(III) Pincer Complex. *Inorg. Chem.* **2016,** *55*, 4529-4536.

41. Liang, L.-C.; Lin, J.-M.; Hung, C.-H., Nickel(II) complexes of bis(2-diphenylphosphinophenyl)amide. *Organometallics* **2003,** *22*, 3007-3009.

APPENDIX B. COLLABORATOR CONTRIBUTIONS

Chapter 2: Acridone Synthesis and Application in Complex Formation

Dr. John Bacsa of Emory and Georgia Tech X-Ray Crystallography Center collected and solved the X-ray diffraction data.

Chapter 3: New Synthesis of acridine-based ligands, Complex formation, Characterization and Reactivity Studies

Dr. John Bacsa of Emory and Georgia Tech X-Ray Crystallography Center collected and solved the X-ray diffraction data.

Chapter 4: Complexes of Cy-xantphos, their Characterization, and Application in CO2 Fixation

Dr. John Bacsa of Emory and Georgia Tech X-Ray Crystallography Center collected and solved the X-ray diffraction data.

VITA

Kevin O. Omolo

Kevin O. Omolo was born in Kenya where he received his primary education at Mabinju Primary School and secondary education at St. Mary's School Yala. He then came to the United States of America and joined the University of Central Arkansas in the spring of 2008 for his bachelor's degree. He transferred to Hendrix College in Conway, Arkansas in the fall of 2008 to continue with his studies. He participated in undergraduate research in the lab of Dr. Liz Gron studying the 'Interactions of H_2S with rat liver microsomes.' He received a Bachelor of Arts degree in Chemistry and Politics in 2011. He joined the Georgia Institute of Technology in Atlanta, Georgia in 2013 where he attended graduate school and conducted graduate research under the advisement of Professor Joseph P. Sadighi. He obtained his Ph.D. in Inorganic Chemistry in 2019.